University of Pisa
Scuola di Dottorato in Ingegneria “Leonardo da Vinci”

Corso di Dottorato in
Sicurezza Industriale e Nucleare

Tesi di Dottorato di Ricerca

Severe Accident Phenomenology Analyses and Fission Gas Release for Advanced Nuclear Reactors

Anno 2012

Autore: G. Mazzini

Relatori:

Prof. F. Oriolo

Prof. Sandro Paci

Prof. N. Cerullo

Dr. Ing. A. Manfredini

Grazie al sostegno della mia famiglia,

Grazie al sostegno dei miei amici

Grazie alla mia "quasi" moglie,

Tre anni sono volati!

RINGRAZIAMENTI

Ringrazio tutti coloro che mi hanno aiutato; grazie dei momenti sereni e felici. In particolare vorrei ringraziare tutti i miei relatori.

Inoltre vorrei ricordare anche il Prof. Ambrosini, il Prof. Forasassi, il Gruppo del Cubetto (Nicola, Daniele, Mariana, ecc.), compresi tutti i ragazzi che sono passati di lì e che ora sono a giro per il mondo, gli amici di Genova (Dr. Ing Lomonaco, Riccardo, ecc.), i miei colleghi di Dottorato e gli amici che mi hanno sopportato in tutto questo lungo cammino.

Vorrei esprimere un particolare gratitudine ad Edison, in particolar modo l'Ing Serracane e alla Dr.sa Battaglino, per aver finanziato questo lungo lavoro durato tre anni sullo sviluppo di un argomento molto interessante ai fini della cultura nucleare italiana.

Infine vorrei anche ringraziare ANSALDO Nucleare e Westinghouse, in particolar modo il Dr. Saiu, la Dr.sa Frogheri e il Dr. Scobel per il loro supporto e per il loro aiuto, soprattutto con i loro consigli tecnici. Un caloroso ringraziamento va anche ai ragazzi di RSE (in particolare Ada e Sonia) che mi hanno aiuto a metter a fuoco alcuni problemi sugli aerosol e la chimica dello iodio.

ABSTRACT

The aim of this work is to set-up a methodology for qualifying models able to simulate the progression of a severe accident (SA), evaluating the related Source Term, in a III Generation nuclear power plant (NPP), as AP1000 and EPR.

The present Ph.D. thesis is articulated in 3 different parts.

The first part refers to the status of the art on the SA phenomenology and on the Lumped Parameter Codes involved in the analyses. In particular, the core relocation, hydrogen production, FP release and transport are addressed along with the models involved in MELCOR 1.8.5 and in ASTECv20 rev.2 [7].

The second part of the work is focused on the analyses of tests carried out in the PHEBUS scaled facility and on the ability of code models to follow the progression of the test scenarios. In this way, the problems of the qualification of the user and of the codes to be used for the analyses have been addressed. In particular, the attention is devoted to PHEBUS FP programme, which comprised five integral experiments on severe accidents, dealing with fuel degradation, hydrogen production, fission product release, transport and behaviour in the containment. The first version of the FPT1 nodalization was based on the ISP46 simulation, considering only the containment behavior, in order to acquire sensibility on ASTEC and MELCOR codes performances. The methodology developed for the analysis of the FPT1 test [20] was also useful in order to prepare the basis of FPT2 and FPT3 nodalizations for the ASTECv2.0 rev.2 and MELCOR 1.8.5 codes. The attention is particularly focused on the FPT3 test, proposed as an international benchmark , organized by IRSN in the framework of SARNET 2 network. In this way, the experience needed to evaluate the SA phenomenology in III+ Generation Power Plant has been acquired.

The third part of the thesis concerns SA sequence analyses of AP1000 plant. AP1000 plant, as well known, presents new passive and simplified design safety concepts. Thanks to courtesy, help and suggestions of “ANSALDO Nucleare” and Westinghouse, the analyses of different severe accident scenarios have been performed. The sequences simulated in the analyses have been selected on the basis of the AP1000 PSA. The SA analyses were carried out taking into account the

experience of DIMNP on the simulation of the TMI phase 1 and 2 accident, as well as the results of simulations of severe accidents on different nuclear plants, such as TEMELIN or IRIS. The analyses carried out using MELCOR concern the phenomena occurring in the LB-LOCA PSA dominant sequence and in SBO sequences, considering also some additional failures or systems unavailability to maximize the consequences of the sequence. The analyses of the SBO sequences are also in relation with the Fukushima accident, in order to outline the robustness of AP1000 during a similar event.

ACRONYMS LIST

ADS – Automatic Depressurization System

ALARA –As Low As Reasonably Achievable

ALWR – Advance Light Water Reactor

AOV – Air-Operated Valve

ATWS – Anticipated Transient Without Scram

BWR – Boiling Water Reactor

CCI – Core/Concrete Interactions

CO – Carbon Monoxide

CO2 – Carbon Dioxide

CH4 – Methane

CV – Check Valves

CVCS – Chemical and Volume Control System

DBA – Design-Basis Accident

DCH – Direct Containment Heating

EPR – European Pressurize Reactor

ECCS – Emergency Core Cooling System

EPRI – Electric Power Research Institute

ESF – Engineered Safety Features

EUR – European Utility Requiems

FP – Fission Product

FSAR – Final Safety Analysis Report

H2 – Hydrogen

IAEA – International Atomic Energy Agency

IRWST – Incontainment Refueling Water Storage Tank

LBLOCA – Large Break Loss of Coolant Accident

LOCA – Loss of Coolant Accident

LOOP – Loss of Offsite Power

LRF – Large Release Frequency

LWR – Light Water Reactor

MAAP – Modular Accident Analysis Program

MOV – Motor Operated Valve

MFW – Main Feed Water

NPP – Nuclear Power Plant

PAR – passive autocatalytic recombiners

PMS – Protection and safety Monitoring System

PRA – Probabilistic Risk Assessment

PRHR – Passive Residual Heat Removal

PSA – Probabilistic Safe Assessment

PWR – Pressurize Water Reactor

RAI – Request for Additional Information

RCP – Reactor Coolant Pump

RIA – Reactivity Initiated Accident

RHR – Residual Heat Removal

RNS – Normal Residual Heat Removal System

SA – Severe Accident

SAMG – Severe Accident Management Guidance

SARNET – Severe Accident Research NETwork

SBLOCA – Small Break Loss of Coolant Accident

SBO – Station Black Out

SIS – Safety Injection System

TMI – Three Mile Island

URD – Requirements Document

US – United States

US-NRC – United States – Nuclear Regulatory Commission

CONTENTS

LIST OF FIGURES

INTRODUCTION

The aim of this work is to contribute to qualify a model in order to simulate the progression of a severe accident (SA), evaluating the Source Term during SA scenarios for a III Generation nuclear power plant (NPP), as AP1000 and EPR.

The present Ph.D. thesis is articulated in 3 different parts. The first part is a status of the art on the SA phenomenology [1] [2] and on the Lumped Parameter Codes [3] involved in the analyses. In particular, the core relocation, Hydrogen production [1] [2] [4], FP release [1] and transport [1] [5] are addressed along with the models involved in MELCOR 1.8.5 [6] and in ASTECv20 rev.2 [7]. Moreover the analyses will focus on the results obtained from the scaled facility tests and the available data related to plant accidents. In particular the data obtained from the SA occurred at TMI [8] or Fukushima [9] [10] are rather lacking; in fact, they are affected from the loss of the instrumentation due to the propagation of the SA sequence.

Severe accidents [1] [2] in nuclear power plants (NPPs) are unlikely events but with serious consequences, as shown by the accident that recently occurred in the Fukushima Daiichi NPPs [11] [12]. The research on SA started originally in the seventies with initial risk assessment studies and later on with experimental programs, development of numerical simulation codes, and Level 2 Probabilistic Safety Assessments (PSA2) [13]. A huge amount of research and development was performed in the last thirty years in the international framework. This was pushed forward by the two accidents that occurred at Three Mile Island (TMI-2) [8] Pressurized Water Reactor (PWR) and at Chernobyl RBMK reactor in Ukraine. Large progress has been reached in recent years on the understanding of SA phenomena, but several issues still need research activities to reduce uncertainties and consolidate the accident management plans.

Consideration of beyond [1] [2] design basis accidents at nuclear power plants is an essential component of the defence in depth approach used for assuring nuclear safety. The probability of occurrence of a beyond design basis accident is very low, but such an accident may lead to significant consequences resulting from the degradation of nuclear fuel. A beyond design basis accident comprises accident conditions more severe than design basis accidents, and may or may

not involve core degradation. i. e. a SA. The severe accident therefore refers to an event with an extremely low probability of occurrence (usually lower than 10^{-5} per reactor per year for internal events), thanks to the preventive measures implemented by design and by operators, but causing significant damage to the reactor core, with more or less complete core meltdown and finally possible serious consequences in case of release of radioactive products into the environment.

Severe accidents are generally caused by failure of the reactor cooling system, which prevents proper removal of residual power from the core, and by multiple faults, arising from equipment and/or human error, including the failure of safety procedures. A series of complex phenomena occur, according to various scenarios and depending on the initial conditions of the accident and on the operator actions. If the reactor core remains uncovered by water for an extended period of time (typically a few hours), nuclear fuel progressively overheats due to residual power. Steam initiates an exothermic oxidation of zircaloy fuel cladding, resulting in substantial production of hydrogen and thermal power. Additionally, chemical reactions between fuel and its cladding produce low-melting-point eutectics, resulting in relocation of molten materials (called "corium") in the core. The fuel first releases the most volatile fission products, then the semi-volatile ones. Progressively, a corium pool forms in the core and progresses towards the lower head of the vessel. When it reaches water remaining there, this is vaporized and corium is at least partially fragmented and forms a debris bed. During core degradation, standby supplies of water can be delivered to the reactor coolant system. Reflooding a degraded core is a complex phenomenon which may enable the accident progression to be slowed down or halted under certain conditions. In contrast, reflooding may also increase hydrogen production and cause further release of fission products.

Hydrogen produced by core degradation is released into the containment, where it burns on contact with oxygen, provoking a pressure and temperature spike which may damage the containment building. For all modes of containment rupture, the release of fission products into the environment depends on the conditions affecting their transfer within the primary circuit. The transfer of fission products depends primarily on their physical and chemical properties, i.e. whether they are gases or aerosols and their chemical form. Iodine and Ruthenium behaviour requires particular attention, given their complexity and their significant short-term radiological impact. Regarding longer-term accident consequences, particular attention must also be paid to caesium releases.

After TMI 2 accident [9], the safety authorities asked for new NPP requirements for events beyond the Design Basis Accidents (DBAs). The US-NRC (United States – Nuclear Regulatory Commission) expects that new reactor plant designs (as AP1000, etc.) will achieve a higher standard of severe accident safety performances than previous designs. In this respect, US-NRC [13] has developed guidance and goals to accommodate events that are beyond the design basis of the plant. Similar guidelines were already adopted in Europe with EUR requirements [14]. The new reactors should assure a significant reduction of the risk associated with the use of nuclear energy, also avoiding the necessity" of the emergency evacuation plan. All this received new impulse from the Fukushima accidents. In particular new challenges have been evidenced from this lesson [11] [12].

In the present work, a comprehensive set of insights on the behaviour of the Generation III plants during beyond design basis and severe accidents has been obtained; this is outlined in the second Part of the thesis.

The main phenomena that may occur and their expected timing and severity are identified, in the perspective of severe accident management. The insights have been obtained using appropriate analysis tools. Other inputs were also used, such as the results of research on severe accidents and from engineering judgement. In developing these insights, consideration was given to uncertainties in severe accident models and in the assumptions made. The major motivation is to reduce the remaining uncertainties on the possibility of cooling structures and materials during SA, either in core or in vessel lower head or in the reactor cavity, in order to limit the progression of the accident. This could be achieved by water injection, either by ensuring corium retention within the vessel or at least slowing down core meltdown progression and limiting the flow rates of corium release into the cavity. The current PSA 2 [13] studies show very large uncertainties in the results of the core reflooding phase. For the issue of in-vessel retention in principle two different aspects have to be considered: the probability for reflooding systems to begin operation in due time, and the status or degree of core damage.

Typically the reference data are partial and incomplete due to the low frequency of SA. The research in this field and the progress of the models tend to overcome this situation with the data obtained in scaled test facilities. In particular, the attention is devoted to PHEBUS FP programme [3] [15], which comprised five integral experiments on severe accidents, dealing with fuel

degradation, hydrogen production, fission product release, transport and behaviour in the containment. It was undertaken by the French Nuclear Safety Institute (IRSN), in close collaboration with the European Commission, using the experimental facilities of the "Commissariat à l'Energie Atomique" at the Research Centre of Cadarache (France). Also an extensive collaboration was promoted amongst international partners from Europe, North America and the Far East. The overall aim of the PHEBUS FP programme [15] was to investigate the key phenomena involved in LWR SA sequences, through a series of in-pile integral experiments. In particular the investigation of the PHEBUS FPT tests program is important in order to qualify the models of the codes as ASTEC and MELCOR. The facility provided prototypic reactor conditions which allowed the study of basic phenomena governing release, transport, deposition and retention of the fission products. The PHEBUS program is composed from several tests; the present work analyzes the FPT1 [16], FPT2 [17] and FPT3 [18] tests.

The set up of the nodalization [19] of the PHEBUS facility for the simulation of the abovementioned tests is based on the experience earned at DIMNP [20] [21] during several years of analyses on the phenomenology of the thermal-hydraulic and aerosol behavior in vessel, primary circuit and containment. Many benchmarks were performed in order to evaluate the capability of the users and the codes to simulate the phenomenology involved in a severe accident. The first version of the FPT1 nodalization was based on the ISP46 [22] simulation, considering only the containment behavior, in order to acquire a sensibility on ASTEC and MELCOR codes performances. The methodology developed for the analysis of the FPT1 test [20] [21] [21] was also needed in order to prepare the basis of FPT2 and FPT3 nodalizations for the ASTECv2.0 rev.2 [7] and MELCOR 1.8.5 [6] codes. The attention is particularly focused on the FPT3 test, proposed as an international benchmark 18], organized by IRSN in the framework of SARNET 2 network [3]. However other important key for this part is the analysis of FPT2 test, closed to FPT3 except for the burn-up, bundle power and the control rod material. In particular the comparison focuses on the Iodine chemistry in the presence of different amount of Silver in the 3 tests, central topic for the estimation of a Source term.

The aim of this part of the work is to give an overview on the phenomena and on the ability of code models to follow the progression of the test scenarios. In this way, the experience needed to evaluate the phenomenology in III+ Generation Power Plant has been acquired. In fact, one of the

main goal of the work is to set-up a methodology for qualifying the models of SA analyses in III+ generation reactors; in this way, the problems of the qualification of the user and of the codes to be used for the analyses have been addressed.

The third part of the thesis concerns SA sequence analyses of AP1000 plant. AP1000 plant, as well known, presents new passive and simplified design safety concepts. Thanks to courtesy, help and suggestions of "ANSALDO Nucleare" and Westinghouse [25], the analyses of different severe accident scenarios on the AP1000 plant have been performed. The sequences have been selected on the basis of the AP1000 PRA to determine how the risk associated with the design relates to the US-NRC's goals of less than 10^{-4}/yr for core damage frequency (CDF)[13] [26] and less than 10^{-6}/yr for large release frequency (LRF). The AP1000 PRA evidences also that EUR's [14] requirements are satisfied, because EUR fixes the abovementioned goals to less than 10^{-5}/yr for CDF and less than $10^{-6/}$yr for LRF.

The Westinghouse Advanced Passive PWR AP1000 [13] is a 1117 MWe pressurized water reactor (PWR) closely based on the AP600 design. The AP1000 maintains the AP600 design configuration, characterised by proven components and licensing basis by limiting the changes to the AP600 design to as few as possible. The AP1000 design includes advanced passive safety with a significant reduction and a simplification of the internal structures, pipes and components. The experience of over 35 years of operating PWR plants is reversed inside the philosophy of passive systems operation during an accident. As evolution of previous reactors generations (Gen. I, II and III), the AP1000 is designed to achieve a high safety and performance (one of goals of ALWR). Practically the safety features rely on natural driving forces such as pressurized gas, gravity flow, natural circulation flow, and convection. Safety systems do not use active components (such as pumps, fans or diesel generators) and are designed to operate without safety-grade support systems (such as AC power, component cooling water, service water, etc.). The consequence is that in the AP1000 plant the number and complexity of operator actions required to control the safety systems are minimized; the approach is to eliminate operator action rather than automate it.

A nodalization of AP1000 for the MELCOR 1.8.5 code [6] has been set up and qualified against RELAP predictions of a DBA sequence. Also the modelling of the core structures has been improved trough this comparison. The results give to us a useful tool for the evaluation of the phenomena taking place during a SA.

The SA analyses were carried out taking into account the experience of DIMNP on the simulation of the TMI phase 1 and 2 accident [8], as well as the results of simulations of severe accidents on different nuclear plants, such as TEMELIN or IRIS [27]. Moreover the experience in using MELCOR code was upgraded with the PHEBUS FPT1 analysis [16] [20] [21], in particular with respect to the containment behaviour. The choose of MELCOR 1.8.5 is due to the capability of correctly simulating the AP1000 core with respect to the latest versions of this code. In particular, the use of the last version MELCOR 2.1 [25] to simulate the AP1000 could originate problems, due to the more complex model in order to simulate the relocation phenomena of the core melt in the vessel lower head.

The analyses carried out using MELCOR concern the phenomena occurring in a PSA dominant sequence [13] and in SBO sequences [11], considering also some additional failures or systems unavailability to maximize the consequences of the sequence. The aim of this part, as already said, is to set-up a qualified model of the AP1000 plant, to provide an overview on the main phenomena occurring in SA sequences and on the ability of this new NPP to prevent and manage possible severe accidents. In particular the attention is focused on the SBO sequence, also in relation with the Fukushima accident, in order to outline the robustness of AP1000 during a similar event.

Reference

[1] SARNET2/ENENIII, “Materials of Short Course on Severe Accident analyses Phenomenology, January 2011

[2] F. Oriolo, “Fenomeni e modelli per incidenti severi”, Corso introduttivo su SA, Genova, 2011

[3] T. Haste, P. Giordano, L. Herranz, N. Girault, R. Dubourg, J.-C. Sabroux, L. Cantrel, D. Bottomley, F. Parozzi, A. Auvinen, S. Dickinson, J.-C. Lamy, G. Weber, T. Albiol, “SARNET integrated European Severe Accident Research—Conclusions in the source term area”, Nuclear Engineering and Design 239 (2009) 3116–3131, 18 September 2009

[4] P. Hofmann, “Current knowledge on core degradation phenomena, a review”, Journal of Nuclear Materials 270 (1999) 194±211, 16 November 1998

[5] L. Z. Waldmann, On the motion of spherical particles in non-homogeneous gases, *Rarefied Gas Dynamics*, Academic Press, New York (1961).

[6] R. Gauntt et al. MELCOR Computer Code Manuals Vol. 2: Reference manual, Version 1.8.6, September 2005 - NUREG/CR-6119, Vol. 2, Rev.3 SAND2005-5713 - Sandia National Laboratories.

[7] J. P. Van Dorsselaere et al. The ASTEC integral code for severe accident simulation, *Nucl. Technology* – NT-3-0846, vol.165, March.

[8] A. Manfredini, "OECD/CSNI – Alternative TMI-2 Scenario Benchmark", DINMP – University of Pisa, Pisa, 2001

[9] http://www.iaea.org

[10] http://www.tepco.co.jp/en/index-e.html

[11] F. D'Auria, G. Galassi, P. Pla, M. Adorni," THE FUKUSHIMA EVENT: THE OUTLINE AND THE TECHNOLOGICAL BACKGROUND", GRNSPG (Nuclear Research Group, San Piero a Grado), Pisa

[12] INPO, "Special Report on the Nuclear Accident at the Fukushima Daiichi Nuclear Power Station", November 2011, special report

[13] US-NRC, "Final Safety Evaluation Report Related to Certification of the AP1000 Standard Design", *NUREG-1793*, 2006

[14] EUR, "European Utility Requirements for LWR Nuclear Power Plants", April 2001

[15] P. von der Hardt, A. V. Jones, C. Lecomte and A. Tattegrain, Nuclear Safety Research: The Phebus FP Severe Accident Experimental Programme, *Nuclear Safety*, vol 35(2), July-December 1994, pp 187-205.

[16] D. Jacquemain, S. Bourdon, A. de Braemaeker and M. Barrachin, FPT1 Final Report (Final version) IPSN/DRS/SEA/PEPF report SEA1/00, IP/00/479, December 2000.

[17] Greogoire, et ali., "FPT2 Final Report (Final version)", IRSN. N° PH-PF: DOCUMENT Phébus PF, IP/08/579, Febbrary 2008.

[18] A. Bieliauskas, T. Haste, "SPECIFICATIONS OF SARNET2 PHEBUS FPT3 BENCHMARK", IRSN, DPAM-SEMIC-2011-057, 5/07/2011

[19] A. Kontautas, E. Urbonavicious. Analysis of aerosol deposition in PHEBUS containment during FPT-1 experiment, *Nucl. Engineering and Design* – vol 239 (2009), pp 1267-1274.

[20] A.Manfredini, G. Mazzini "Analysis of the Physics of Severe Accidents in Advanced Light Water Reactors", 29th UIT National Heat Transfer Conference 2010, Torino, Giugno, 2011

[21] A.Manfredini, G. Mazzini "Analysis of the Phenomena Occuring in the PHEBUS During the FPT1 Test Using MELCOR and ASTEC", 29th UIT National Heat Transfer Conference 2010, Torino, Giugno, 2011

[22] T. Haste, Specification of International Standard Problem ISP-46 (Phebus FPT1), Revision 0, IPSN Note Technique SEMAR 01/91, November 2001. A. C.

[23] Luis E. Herranz, Mònica Vela-Garcìa, Joan Fontanet, Claudia Lòpez del Prà, "Experimental interpretation and code validation based on the PHEBUS-FP programme: Lessons learnt from the analysis of the containment scenario of FPT1 and FPT2 tests", Nuclear Engineering and Design 237 (2007) 2210–2218, 22 March 2007

[24] T. Haste, F. Payot, C. Dominguez, Ph. March, B. Simondi-Teisseire, M. Steinbrück**, "**Study of boron behavior in the primary circuit of water reactors under severe accident conditions: A comparison of Phebus FPT3 results with other recent integral and separate-effects data", Nuclear Engineering and Design, 2011

[25] ANSALDO Nucleare and Westinghouse private communications

[26] NUREG-1560, Volume 1, "Individual Plant Examination Program: Perspectives on Reactor Safety and Plant Performance," Part 1.

[27] A. Del Nevo, A. Manfredini, F. Oriolo, S. Paci, "Integrated Analysis for a Small Break Loca in the IRIS Reactor Using Melcor and Relap5 Codes" *5th International Conference on Nuclear Option in Countries with Small and Medium Electricity Grids* - Dubrovnik, Croatia, May 16-20, 2004.

PART I: SA PHENOMENOLOGY AND MODELS USED IN THE STUDY

1 GENERAL DESCRIPTION OF SA PHENOMENOLOGY

1.1 Overview

The Reactor Safety Study (WASH 1400)[1], published in 1975, was the first major study in the world on the progression and consequences of a set of hypothetical accidents that could lead to core melt in a nuclear power plant, and sometimes to the release of a significant quantities of fission products outside of containment.

The results of this study led to some re-examination of US safety philosophy, but it was until the TMI-2 accident in 1979 that not serious consideration was given by the US-NRC to the problem of dealing with these severe accidents. Until TMI-2 [8] the technical basis for nuclear power plant safety was limited to design basis accidents. Events beyond those considered in the design basis envelope were thought incredible. This means that they have a sufficiently low probability of occurrence and therefore it is unnecessary to demonstrate that such events could lead to consequences acceptable for the health and safety of the public. Thus, accidents beyond the design basis were completely ignored by licensing process. To put it in a different and modern terminology, the generally accepted view was that the probability versus consequences curve had a long indeterminable tail, in the low-probability, high-consequences portion of the spectrum.).

In the TMI accident, a core uncovery resulted from a stuck open valve, PORV, and the operator's interference with the high pressure safety injection. The situation was turned round by activating the safety injection and re-flooding the core. The extent of damage is illustrated in Figure 1.1. The TMI core practically starts with the assembly degradation, candling and cracking of the fuel (a) and the sequence progresses with the large molten of portions of the assembly in the center and in the top of the core starting with a pool formation (b). The progression of the core damage are increased with the formation of a central pool in the core and a debrise bed on the top of the core (c), until the lower crust of the pool is cracked and the molten material fall down trough the lower support plate into the lower head (d). In particular, the quantity of debris mass found in the lower plenum area was about 20 tons. This accident also demonstrated the significance of the hydrogen production and burning phenomena.

A wide variety of other types of small leaks with failure or disabling of the emergency cooling systems would lead to core uncovery and TMI-like behaviour, that is, severe core damage at elevated primary system pressure. Similar behavior can also be obtained from postulated station blackout events (loss of all on-site and off-site power), where the secondary and primary sides boil dry with steam released through the safety relief valves. This occurred recently at Fukushima. This accident is adding to the list of the main accidents in nuclear facilities and will be one of the most referenced accidents, as Chernobyl and Three Miles Island (TMI). The Fukushima nuclear facilities [3][4] were damaged by a magnitude 9 earthquake on March 11, 2011. The BWR plants on the site, even though not designed for such earthquake magnitude, were not directly affected by the earthquake. Anyway, serious secondary effects followed, including the loss of external power, a significant tsunami and a series of strong aftershocks. In particular at Fukushima plants the tsunami caused to a complete Station Black-Out (SBO), including diesel generators, with stop of about all Emergency Core Cooling Systems (ECCS) after nearly 1 hour since the earthquake. The reactors were isolated, without the possibility to remove the decay heat power. The units 1, 2, 3 went in severe conditions, with partial melt of the core and release of Fission Products (FP) in the Containment of MARK I type.

The core uncovery can also occur at low pressure. Typically this would involve a large system leak (Large Break Loss of Coolant Accident) and failure of the ECCS to perform as designed. These sequences are called low pressure scenarios. Of course, high pressure scenarios can revert to low pressure scenarios by depressurization. To this aim, the Boiling Water Reactors have an ADS and Pressurized Water Reactors have the manually operated PORV.

The description of the SA scenario is usually subdevided in 2 main parts: In Vessel Phenomena and Ex Vessel Phenomena, characterized also by different timing in the evolution of the scenario. A brief description of the involved phenomena is given hereafter:

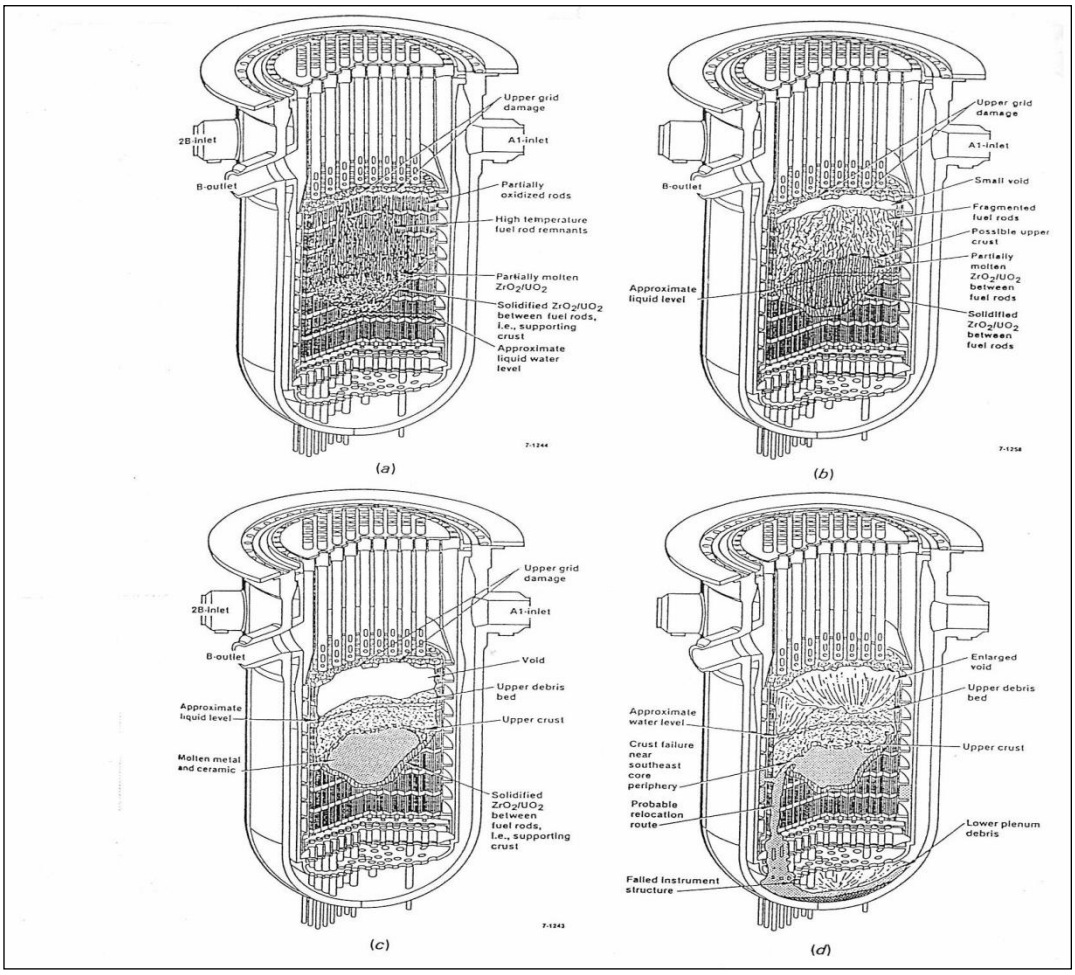

Figure 1.1 TMI Core Degradetion phase [1]

- **<u>In Vessel Phenomena</u>**

  - **Blow-down:** Loss of coolant through break or relief valves. May be rapid or slow. May occur at high pressure or with loss of pressure.

  - **Uncovery:** The water mixture level in the reactor vessel falls below the top of the active fuel.

  - **Boil-off:** Liquid level gradually drops as decay heat vaporizes water and loss of coolant occurs through break or relief valves.

  - **Heat-up:** Core is at least partially uncovered. Zircaloy-steam reaction produces hydrogen and heat. Cladding fails, releasing volatile fission products which

migrate and deposit in primary system circuit and/or escape to the containment with steam.

- **Early Phase:** It refers to the initial stages of core damage, including cladding oxidation and swelling (ballooning), which reduces the flow area; the melting and relocation of mainly metallic materials of fuel bundles, like grid spacers and control rods, can also occur.

- **Core Damage:** The fuel assemblies are deformed by mechanical fracturing, or by liquefaction due to material interactions or melting.

- **Flowering**: Process controlling the beginning of the melt flow down, due to non homogeneous azimuthal temperature distribution and/or oxidation extent in the clad circumferential section; this causes stresses up to the cladding rupture produced by axial cracks formed along the hottest side of the clad tube and depending upon the ZrO2 layer strength.

- **Candling**: Process concerning the eutectic melt, occurring after local failure of the cladding, in form of rivulets or droplets, depending on the height of the liquefied column, the geometry of the breach, and the pressure drop between the rod inner and the system; this downward film typically refreezes during its relocation path along the surface of the rod.

- **Core Melt:** The reactor core overheats and this leads to significant melting or liquefaction of the core and structural materials (this mixture is also called corium).

- **Degraded Core:** An advanced state of core damage in which the original fuel bundle geometry has been substantially lost, due to molten relocation.

- **Core Melt/Slump:** Bulk of core is uncovered; core melt drops/fragments and begins to fall into the water pool in vessel bottom. **Fission product migration through primary circuit** and to containment can be significant for more volatile fission products.

- **Small scale steam explosions** in vessel due to water-corium interaction are probable, while large ones are unlikely but possible.
- **Melt through** Pressure vessel fails due to the attack of molten coriumto the bottom head and corium drops into the reactor cavity.

- **Ex Vessel Phenomena**
  - **Core quenching:** the molten debris fallen into the reactor cavity boils off whatever water is there. If sufficient water is present, the core would be cooled and solidified, but could subsequently re-melt.
  - **Core dispersion:** Steam explosions may also occur at this time as the molten corium falls onto water in the reactor cavity. This can disperse fuel material, create radioactive aerosols, and increase the rate of heat transfer to the containment atmosphere.
  - **Molten Core-Concrete Interaction:** The molten corium attacks the concrete basement, proceeds to penetrate it, and creates a cauldron that releases aerosols and gases, with containment pressure increase.

1.2 Core Melt and Relocation Models

The interaction among the various core materials (Zry with SS and Inconel spacer grids, Al_20_3 in Zry cladding of B_4C/Al_20_3 control rods with Zry, $Zr0_2$ and $U0_2$) involves a lot of metallurgical phenomena as temperature increases (Figure 1.2). The major processes interesting the fuel from a general point of view during the core damage progression include three different relocation mechanisms:

- candling and re-solidification of molten and liquefied material along the external surface of the rods;
- falling on a previously solidified crust of fuel pellets and fragmented core materials and formation of a debris bed;

- growing of molten material trapped in the crust, and consequent crust breaking, with corium falling in the lower plenum

When portions of the clad reach temperatures between 1473÷1673 °K (Figure 1.3), control rods, burnable poison rods and structural material can form a low temperature liquid phase. The grids that hold the fuel together also melt at around 1400° C, as the control rods passing through the fuel. This liquefied material may relocate and form local blockage which could restrict flow and cause accelerate heat up of the core. The molten material is itself held up by the blockages. This material is still generating heat, and there is a tendency for it to move down through the core, growing in volume.

The second temperature regime is between 2033÷2273 °K. If the zircaloy clad has not been oxidised, then it will melt at about 2030 °K and relocate downward along the fuel rod. If a sufficient oxide layer has formed on the external cladding surface, then the relocation of the zircaloy will be prevented because the oxide layer remains solid until the core reaches higher temperatures ($Zr0_2$ melting point is 2973 °K), or until the oxide layer fails mechanically, or until the layer is dissolved by molten zircaloy.

At higher temperatures (2879÷3123 °K), UO_2, $Zr0_2$ and the $(U,Zr)O_2$ solid solutions will start to melt. Dissolution of $Zr0_2$ layer by molten Zry is a potential competitive mechanism of UO_2 liquefaction during this phase. The internal cladding oxidation as a consequence of steam penetration into the rod gap after the clad rupture (due to ballooning), can prevent molten Zry from dissolving UO_2.

At higher temperatures (~3000 °K), the UO_2 and the $Zr0_2$ layers melt [5], forming eutectics with higher oxygen concentration which, due to the higher temperature, can dissolve other eutectics and metals.

The material rewetting during its falling in liquid water is very important, because the fast steam production can significantly influence the oxidation in the hot core regions (especially if steam starvation conditions have occurred before).

The relocation mechanism obviously involves a global geometric reconfiguration of the core. The flow area reduction in the lower regions of the core limits the coolant flow-rate in the core

channels, and this can create a steam starved situation. In the case of total channel blockage, the unavailability of steam could stop the H_2 production. The relocation mechanism, taking away metallic Zircaloy from high temperature core regions, is effective in limiting the temperature escalation, and then the fast H_2 generation by autocatalytic oxidation.

The mass of molten material will eventually reach the bottom core support plate and will be held there for a period of time until that core plate also fails due to mechanical and thermal loads. As illustrated in Figure 1.2, the lower part of the vessel may still contain a pool of water, notwithstanding the high temperature existing in the upper part.

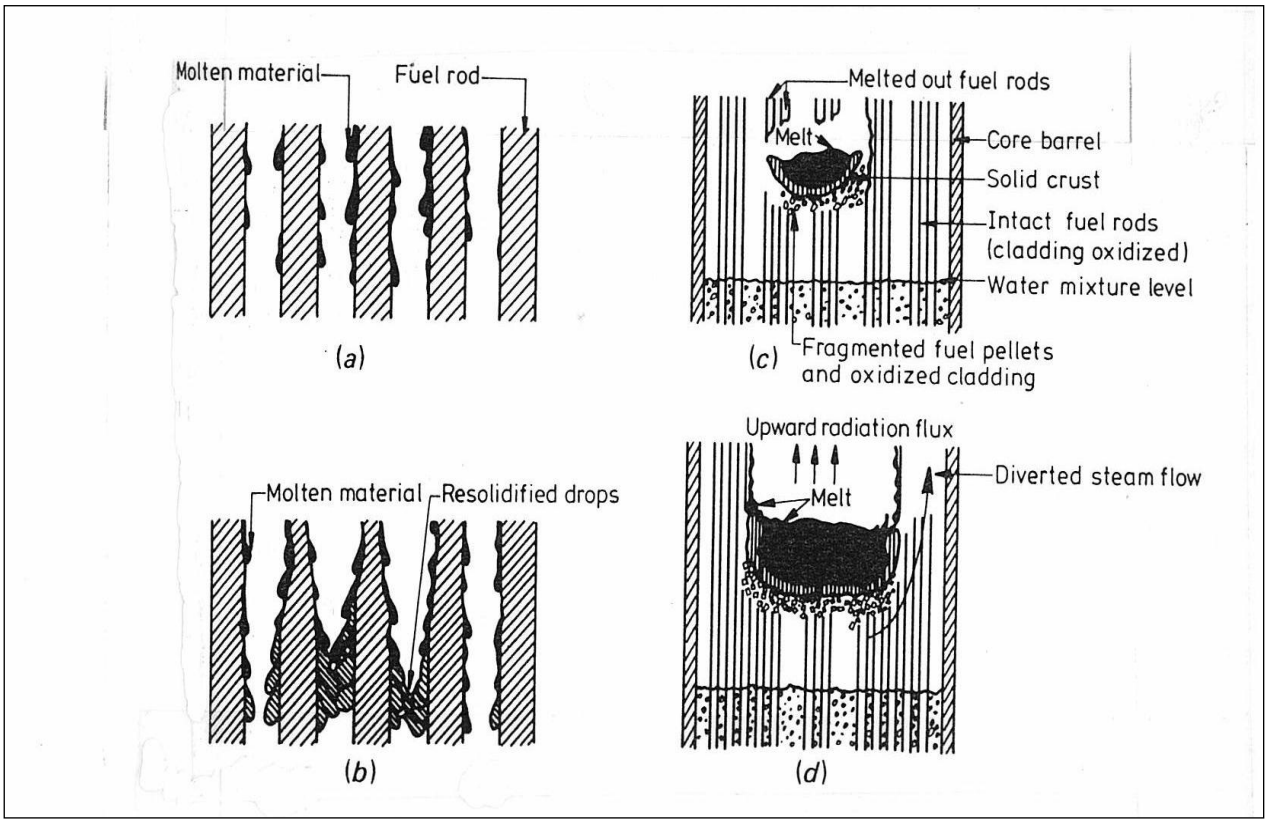

Figure 1.2 Example of the progression of the molten phenomena inside a core [1]

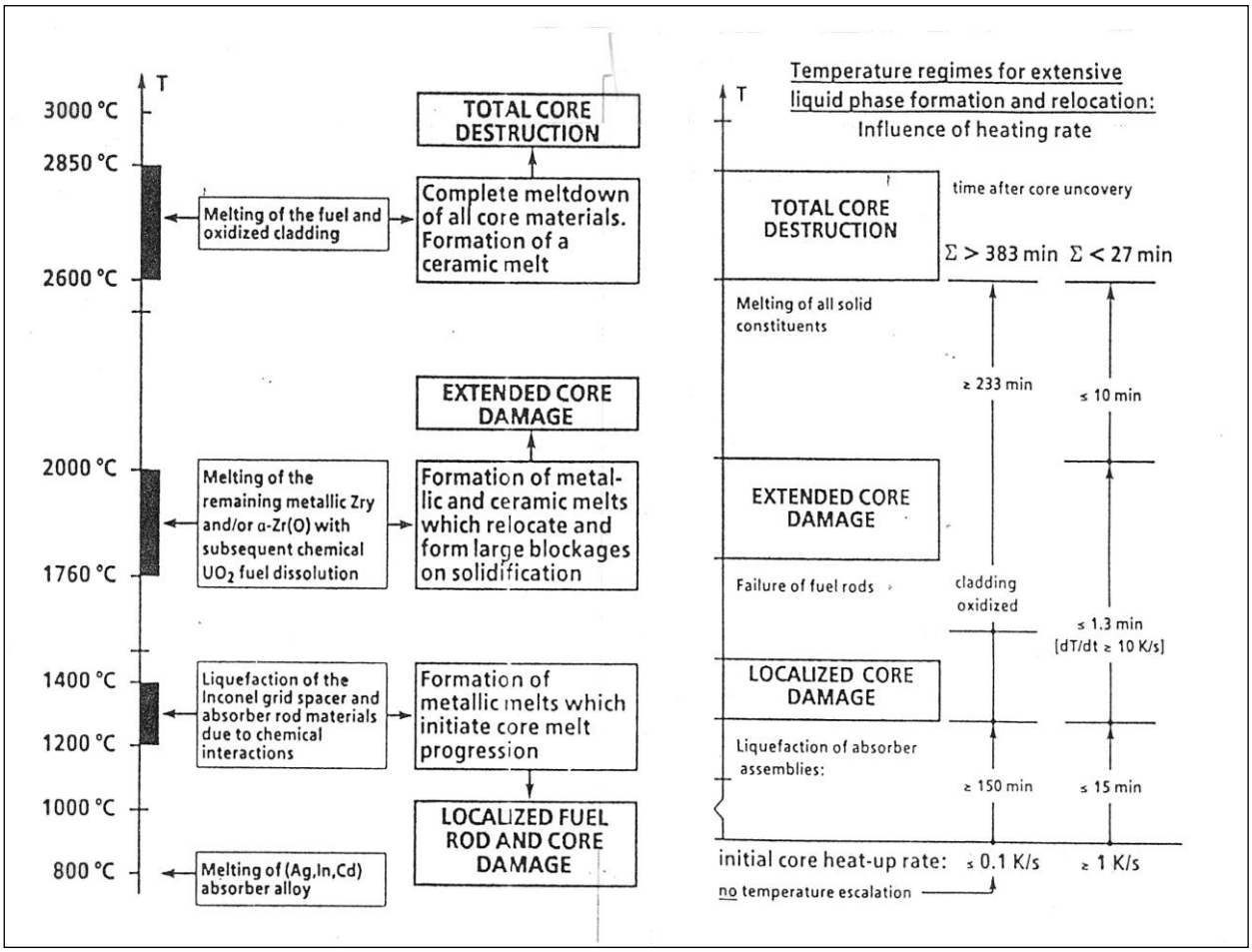

Figure 1.3 Schematic tree of the core degradation as a function of the temperature [1]

1.3 Cladding Ballooning

The Cladding Balloning is taken into account in the design of fuel for LWR [6], and it has been shown the blockages by the ballooning effect of up to 90% can be coped with heat-up progression. The radiative thermal exchange becomes the major heat transfer mechanism between reactor core and internals.

For low pressure accident sequences, the Zircaloy cladding starts to balloon and rupture once the core temperature reaches 1000 to 1200 K (Figure 1.4). In that case, the timing and temperature of ballooning and rupture depend on the internal pressure of the fuel rods (including any fission gases that may be released into the gap), and the mechanical characteristics of the cladding material. For high pressure accident sequences, due to the collapse of cladding onto the fuel at lower temperatures, the failure of Zircaloy cladding may be delayed until the core temperature increases

above 1500 K. Even though the cladding does not fail mechanically in that case, chemical interactions between the Zircaloy cladding and other core materials can cause local failures of the cladding due to the formation of low melting temperature alloys.

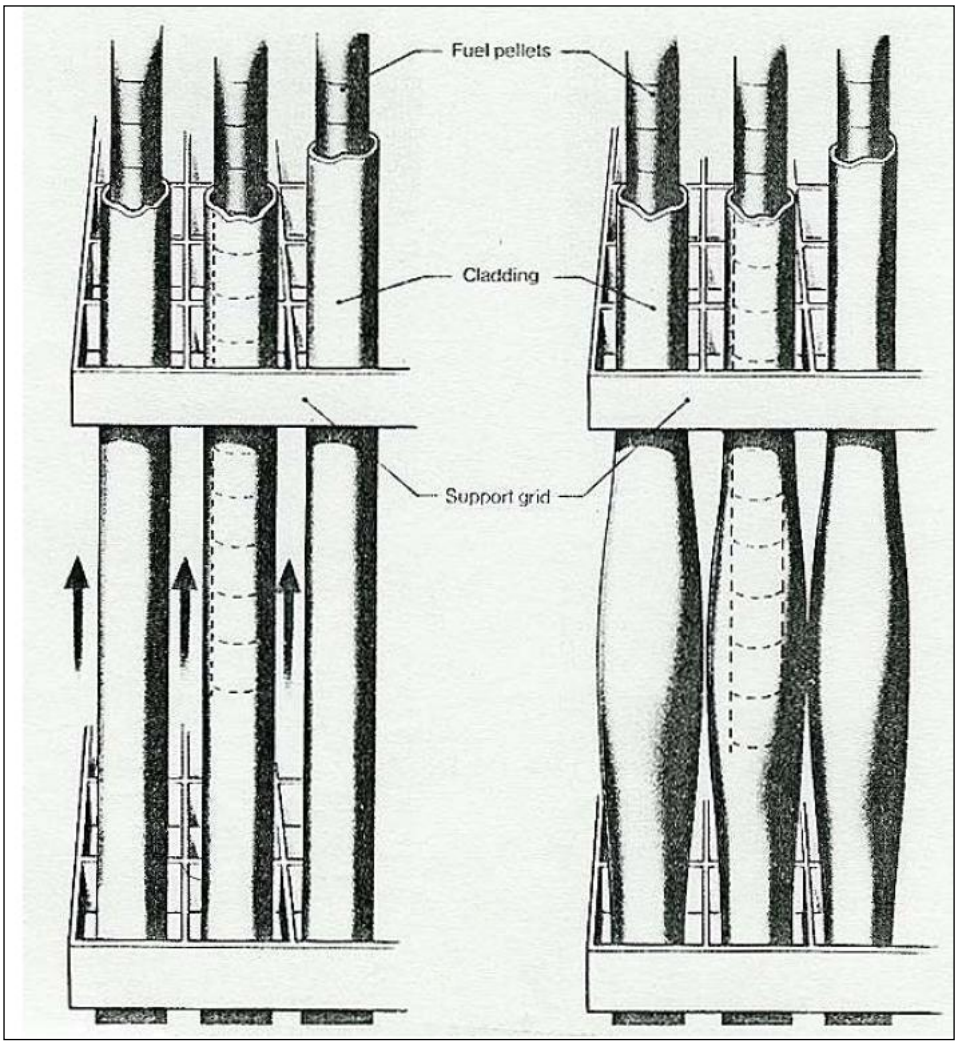

Figure 1.4 Clad ballooning can lead to flow obstruction and fuel damage.[7]

At this stage of core damage, the most significant consequences of cladding ballooning and rupture is the release of fission products, the exposure of the inner surface of the cladding to steam, and changes in the relocation of fuel rod materials later in the transient. Ballooning and rupture may also alter subsequent flow patterns in the core, particular when the deformation is extensive.

1.4 Hydrogen Production

If the temperature continues to rise above 1300 K the zircaloy cladding begins to interact with water or steam, with a strongly exothermic reaction [6]:

$$Zr + H_2O \rightarrow ZrO_2 + 2H_2$$

The energy released during the reaction is given by the following relationship:

$$\Delta H = a - bT$$

where:

- a is 6.774 x 10^7 (J/kg)
- b is 244.9 J/(kg*K)
- T is temperature (K).

The reaction rate, governed by oxygen diffusion through the $Zr0_2$ layer, has a typical parabolic temperature dependence, with a rapid increase at roughly 1650 K, connected with the oxide cracking and consequent enhanced oxygen diffusion in the layer, and with the tetragonal to cubic phase transition of $Zr0_2$.

Iron also oxides exothermically in an oxidizing environment by the reaction:

$$3Fe + 4H_2O \rightarrow Fe_3O_4 + 4H_2$$

As the fuel temperature continues to increase, a temperature is reached (~1400°C) at which the first signs of melting of material in the core begin to be observed. The melting process is very complex and occurs most rapidly in the regions of the core that have had the highest neutron flux, and therefore have the highest concentration of fission products, whose decay is causing the heating.

In principle, there are several possible sources of hydrogen [7], [8] in the course of a severe accident (Figure 1.5):

- zirconium-steam reaction (zircaloy oxidation),

- boron carbide – steam reaction,
- uranium-steam reaction,
- steel-steam reaction,
- molten core-concrete interaction, water radiolysis and Al/Zn corrosion.

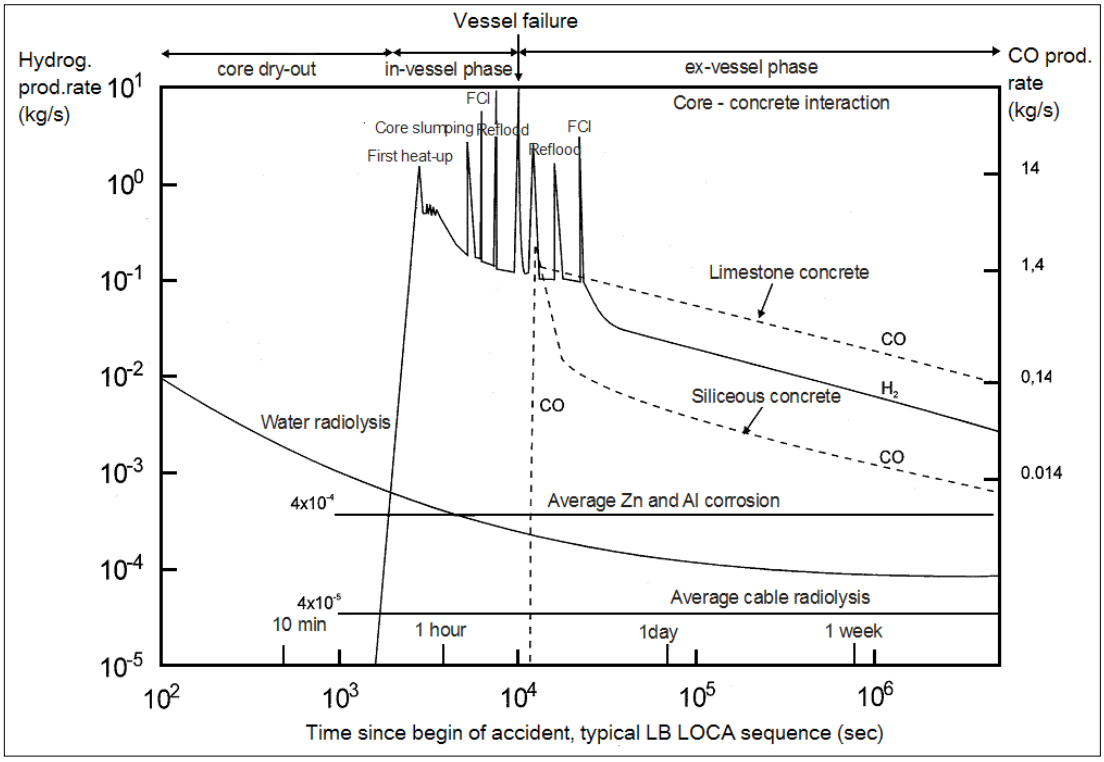

Figure 1.5 Typical hydrogen production rates during a SA [6]

Table 1.1 and Table 1.2 give an idea of the most important chemical reactions taking place in the vessel and of the amounts of materials that could react, producing hydrogen able to escape from the primary system and deflagrate in the containment or in the cavity.

Chemical reaction	Energy release	Mol.Weight
$Zr + 2\ H_2O \rightarrow ZrO_2 + 2\ H_2$	$\Delta H = 64$ MJ/kg $_{Zr}$	91 g/mol
$2\ Fe + 3\ H_2O \rightarrow Fe_2O_3 + 3\ H_2$	Not significant	56 g/mol
$B_4C + 8\ H_2O \rightarrow 2\ B_2O_3 + CO_2 + 8\ H_2$	$\Delta H = 15$ MJ/kg $_{B4C}$	56 g/mol

Table 1.1 Principal reactions involved in a Core Degradation sequence for Hydrogen production [6]

Component	Fuel Ass.	Canister	Absorber	Absorber	Hydrog.
Reactor type	Zr (kg)	Zr (kg)	Fe (kg)	B_4C (kg)	H_2 (kg)
French PWR 900 MW	20,000	--	300	--	900
Konvoi PWR 1300 MW	32,000	--	500	--	1,400
BWR-72 1300 MW	39,000	36,000	15,000	1,200	4,500

Table 1.2 Structural material quantity example [6]

1.5 Aerosols and FP Gas Releases

During normal operation in a LWR [6], fission gases form in the grains of UO_2. These atoms of gas either diffuse towards the grain boundaries, or collect into inter-granular bubbles, slowing down their rate of migration towards the grain boundaries. The bubbles may then dissolve under the influence of fission spikes, phenomena that speed up the rate at which gas is supplied to the grain boundaries. Once on the grain surface (mainly by atomic diffusion, but also by bubble migration), the fission gases accumulate to a point where they coalesce to form larger bubbles and fill the boundaries. These bubbles are then capable of moving into the free volume of the rod.

During the accident, the gas populations can be classified into four categories [9]:

- Gas atoms dissolved in the matrix,
- Intra-granular gas bubbles with little mobility,
- Gas accumulated in the grain boundaries,

- Gas released in the upper plenum of the fuel rod.

Their release is governed by a number of mechanisms [6]. The first release phase (often referred to as the "burst release") corresponds to the release of gases accumulated in the inter-granular spaces. The fraction already released in the rod plenum during normal irradiation must also be taken into account; it ranges from a few percent to 10% depending on the burn-up, the irradiation power and the fuel type. Such releases occur at the beginning of the temperature rise at around 1000°C, though sometimes at lower temperature for high burn-up fuels. The second phase concerns the release of intra-granular gases via a thermally-activated diffusion process which begins with dissolved atoms. The gas trapped in the intra-granular bubbles is the last to be released, which generally occurs when the fuel melts. Also with the FP gas release, the FP vapour are released as consequence of high temperature due to the melting of the fuel. In particular semi-volatile or low-volatile materials as Silver are released in as vapour when the temperature of the fuel rises up 2000K.

It is important to correctly quantify the respective fractions of these four gas populations when modelling gas releases, which depend on their radial position in the pellet (different temperatures, microstructure on the periphery, etc.) and the fuel type (heterogeneous MOX fuels have a higher inter-granular fraction). It is also important to point out that these fractions depend on the radioactive half-life of the gases; the short-lived gases decay and do not contribute to the source term. This effect is mainly beneficial for LOCA- or RIA-type accidents as the total gas inventory is generally released during a severe accident.

It is generally accepted that the release of fission products follows a two-phase process: initially the fission products in solution in the matrix (or the precipitates when the solubility limit has been reached) diffuse towards the grain boundaries, and then a 2^{nd} mechanism of mass vaporization transfers the fission products from the grain surface outside of the fuel matrix. This mechanism also involves a number of physical and chemical aspects: potential formation of defined compounds (CsI, molybdates, zirconates, and uranates of caesium, barium, strontium, etc.), or the oxidation or reduction of precipitates by steam and/or hydrogen. These chemical reactions have a significant impact on the volatility of some elements. The basic high temperature thermodynamic parameters governing the formation and destruction of these species are currently poorly understood; this is a problem when it determines the mechanistic model of these processes.

When releases outside the fuel matrix, potential chemical interactions with the cladding and/or the core structural elements can also reduce the volatility of some elements through the formation of more refractory species. Last of all, once released from the core, a significant fraction of the fission products condenses in the colder areas of the upper core structures, before even reaching the primary cooling system or the containment. This is especially true for the low-volatile fission products.

Qualitatively speaking [6], the main physical parameters influencing the release of fission products are as follows:

- The temperature is the main parameter, at least until the loss of the core geometry.
- The oxidizing-reducing conditions have a significant impact. The release kinetics of volatile fission products is particularly accelerated under oxidizing conditions. Furthermore, the overall release of certain fission products is very sensitive to the oxygen potential. For example, the release of Mo increases in steam, whereas that of Ru can be very high in air. Conversely, the release of Ba (as for Sr, Rh, La, Ce, Eu and Np) increases under reducing conditions.
- The interactions with the cladding and/or the structural elements can play a major role. For example, the presence of tin in the cladding delays the emission of the volatile elements tellurium and antimony. Barium significantly contributes to the decay heat (via its daughter product 140La) and is also partially trapped in both the cladding (probably due to the formation of zirconates) and the structural steels.
- The burn-up accentuates releases, increasing both the kinetics of volatile fission products and the release rate of low-volatile species such as Nb, Ru, La, Ce and Np.
- The fuel type also seems to have a significant impact: MOX releases tend to be higher than those of UO2. This phenomenon is probably related to its heterogeneous microstructure, with the presence of plutonium-rich agglomerates where the local burn-up can be very high.

- The state of the fuel during in-vessel degradation has a significant influence: the transition from a “degraded rod” geometry to a “debris bed” geometry also involves an increase in releases due to the higher surface-to-volume ratio. Conversely, the transition from a debris bed to a molten pool slows down the release of fission products as a solid crust forms on the surface of the molten pool.

1.6 Aerosols and FP gas transport

During a severe accident in a nuclear power plant [6], fission products , actinides and structural materials are released as gases or vapours from the degrading core into the RCS. These are then swept, in general, by a steam-hydrogen gas mixture towards the breach in the RCS. A number of important physical and chemical processes occur between release from the core and the RCS breach into the containment (or into the auxiliary building in the case of a containment-bypass sequence). The physical effects (Figure 1.6) involve primarily aerosol physics and dynamics.

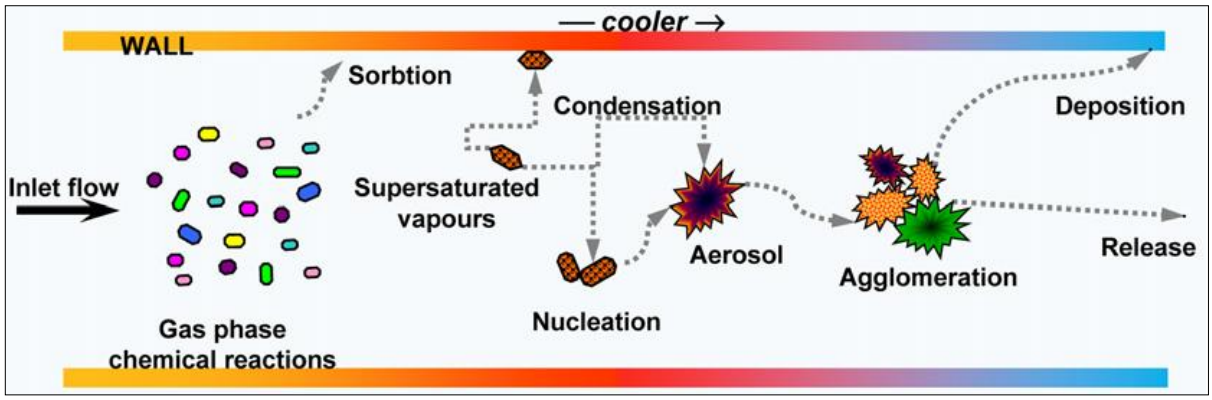

Figure 1.6 Aerosol transport phenomena

In the following, a brief review will be given on the physical basis and the basic theory for the internal aerosol processes and the particle motion mechanisms.

Gas-to-particle conversion occurs as physical or chemical processes generate a supersaturated vapour in the gas phase. In severe accidents the basic physical process that leads to super-saturation is cooling. The metastable vapor state relaxes to equilibrium via two distinct routes: i) the generation of new particles, called nuclei or embryos, via a process known as homogeneous nucleation; ii) the growth of existing particles, via a process known as condensation or heterogeneous nucleation.

Other processes induce changes in the aerosol properties across the volume boundaries. There are several mechanisms driving particle motions, like gravitational settling, Brownian diffusion, inertial motion, phoretic forces, etc. They are strongly influenced by the aerosol particle sizes. Indeed, two are the primary quantities of interest that characterize the source term: the chemical composition of the particles and the particle size distribution. Typically, in the RCS or in the containment the various nuclides reside in particles of less than 1 μm in diameter, characterized by a poly-disperse size distribution [10]. In the RCS and the containment, the aerosol size distribution is broad, i.e. the particle diameters span over several orders of magnitude, from a few nanometers to more than 1 μm.

References

[1] F. Oriolo, "Fenomeni e modelli per incidenti severi!, Corso introduttivo su SA, Genova, 2011

[2] A. Manfredini, "OECD/CSNI – Alternative TMI-2 Scenario Benchmark", DINMP – University of Pisa, Pisa, 2001

[3] F. D'Auria, G. Galassi, P. Pla, M. Adorni," THE FUKUSHIMA EVENT: THE OUTLINE AND THE TECHNOLOGICAL BACKGROUND", GRNSPG (Nuclear Research Group, San Piero a Grado, Pisa, 2011

[4] INPO, "Special Report on the Nuclear Accident at the Fukushima Daiichi Nuclear Power Station", November 2011, special report

[5] P. Hofmann, "Current knowledge on core degradation phenomena, a review", Journal of Nuclear Materials 270 (1999) 194±211, 16 November 1998

[6] SARNET2/ENENIII, "Materials of Short Course on Severe Accident analyses Phenomenology, January 2011

[7] M. Ragheb, "Clad Ballooning Accident", 12/13/2010

[8] T. Haste, F. Payot, C. Dominguez, Ph. March, B. Simondi-Teisseire, M. Steinbrück, "Study of boron behaviour in the primary circuit of water reactors under severe accident conditions: A comparison of Phebus FPT3 results with other recent integral and separate-effects data", Nuclear Engineering and Design 246 (2012) 147– 156, 8 August 2011

[9] T. Haste, P. Giordano, L. Herranz, N. Girault, R. Dubourg, J.-C. Sabroux, L. Cantrel, D. Bottomley, F. Parozzi, A. Auvinen, S. Dickinson, J.-C. Lamy, G. Weber, T. Albiol, "SARNET integrated European Severe Accident Research—Conclusions in the source term area", Nuclear Engineering and Design 239 (2009) 3116–3131, 18 September 2009

[10] R. Frutos, D. Gido, G. Henneges, P. Schmuck, "Calculation of fission product behaviour in an advanced containment in case of a severe accident", Nuclear Engineering and Design 202 (2000) 173–178, 18 April 2000

2 CODES DESCRIPTION AND QUALIFICATION METHODOLOGY

2.1 Introduction on Lumped Parameter Code

Lumped-parameter (LP) codes describe a NPP containment [1] as a network of control volumes (sometimes called "cells" or "zones"), connected with junctions (sometimes called "vents" or "flow paths"). The number of control volumes in containment simulations typically lies in the range of 10 to 100. Control volumes contain so-called "heat structures": these include all the structures such as walls, pipes, platforms, equipment, etc … These structures are referred as "heat structures" because in the modelling of heat and mass transfer in lumped-parameter codes, they act basically as heat reservoirs and provide surfaces for steam condensation. Since only scalar equations are solved in LP models, control volumes are repositories of mass and energy, but do not contain information of momentum direction.

Junctions between control volumes connect fictions "control points" within each volume. Junctions are not repositories of mass or energy, and do not contain heat structures. The mass flow rate in junctions is determined solving various forms of one-dimensional momentum equations. Generally in LP codes, connections between control points are only modelled via a single flow path, so that no simultaneous counter flow is possible. Turbulence effects are not modelled at all, but its influence might be taken into account via flow-loss coefficients in the momentum equation.

Lumped-parameter codes were devised basically to enable predictions of so-called thermal-hydraulic accident conditions in the containment (that is, pressure, atmosphere temperature, and temperatures of structures). In principle, each control volume should correspond to an actual containment compartment. Thus, their volumes range from a few cubic meters up to a few hundreds cubic meters.

However, lumped-parameter codes are also used sometimes to model the non-homogeneous atmosphere in large compartments (e.g. in the dome region of a large containment). This is achieved by subdividing large volumes into smaller control volumes, and connecting them with "fictius" junctions (fictius, because they do not exist as such in the containment). The cross-section area of these junctions is equal to the area of the dividing surface between the connected volumes. The

direction of the flow is implicitly defined by the spatial arrangement of the zero-dimensional control points. i.e. the convection paths are predetermined, or at least restricted, by the user due to the chosen subdivision of compartments into control volumes (this subdivision is usually referred to as "nodalisation"). The flow rate between control volumes may be adjusted by prescribing the values of flow-loss coefficients. In principle, this should not prevent accurate simulations of thermal-hydraulic conditions (pressure and temperature). However, as the control volumes are not repositories of momentum, the simulation of inertial effects is not possible. Thus, this approach is in principle possible for transients where buoyancy effects are dominant, whereas the simulation of transients where inertial effects are dominant is questionable. Also, the resulting flow (both in the cases of buoyant and inertial dominant effects) could be very much dependent on the (subjective) subdivision of the compartments into smaller control volumes.

The more used lumped-parameter codes (listed in alphabetical order) in the modelling of containment thermo-hydraulics and hydrogen and aerosol distribution are:

- ASTEC (i.e. the module CPA – Containment Part of ASTEC), which is being developed jointly by the Gesellschaft für Anlagen- und Reaktorsicherheit – GRS (Germany) and the Institut de Radioprotection et de Sûreté Nucléaire – IRSN (France);
- MELCOR (i.e. the module that deals with the containment), which is being developed by Sandia National Laboratories (USA);

2.2 ASTEC v2.0 rev 2 Code General Description

The aim of the ASTEC code [7] is to simulate an entire severe accident sequence from the initiating event up to the release of radioactive elements out of the containment. The applications are:

- Source term determination studies,
- Probabilistic Safety Assessment level 2 (PSA-2) studies,
- Accident management studies,
- Physical analyses of experiments to improve the understanding of SA phenomenology.

The code has been set-up with the following requirements: sufficient validation to cover the main physical phenomena; account for safety systems and procedures; user-friendly to easily perform sensitivity analyses; equipped with tools for pre-processing, on-line visualisation, and post-processing; fast running code.

While ASTEC V1 played a central role in SARNET, thus progressively becoming the reference European integral severe accident code, IRSN and GRS launched in parallel, since 2007, the development of the ASTEC V2 series. As ASTEC V1 in SARNET, the ASTEC V2 series shall continue playing a central role in SARNET 2, thus confirming its status of reference European integral SA analyses code.

The version V2.0 was released in June 2009. As concerns the physical modelling, the two major evolutions with respect to the V1.3-rev2 version (Figure 2.1) are:

- on one hand, the replacement of the DIVA module by the ICARE module (directly issued from the mechanistic ICARE2 code) to deal with the in-vessel core degradation,
- on the other hand, a significant evolution of the MEDICIS capabilities to allow the application of ASTEC V2 to the Gen-III EPR reactors, in particular thanks to a dedicated core catcher modelling.

In addition to these two major evolutions, most of the other physical modules (CESAR, CPA, IODE, …) have been also improved. In particular, concerning the user tools to analyse and interpret code results, the ASTEC V2.0 version includes additional couplings to JADE, ATLAS and SUNSET tools, respectively for pre-processing (and on-line visualisation), post-processing and uncertainty analyses.

As said before, the code has been developed with the aim to have a fast running simulation of the total SA sequence in LWR, from the initiating event up to the possible FP release to the environment. The modules (Figure 2.2) of the version ASTEC V2.0 rev 2 used in this analysis are:

- CESAR for RCS two-phase thermal hydraulics during the front-end phase and the degradation phase;

- DIVA for core degradation including late phase phenomena (molten pool, corium slump to lower head, corium in lower head) and vessel failure;
- ICARE: this model simulates the progression of the core degradation and hydrogen production,
- ELSA for release of FP from fuel rods and debris and of materials from control rods, using a semi-empirical approach;
- SOPHAEROS for FP vapour and aerosol transport in RCS;
- CPA for multi-compartment containment simulation, including thermal-hydraulics, hydrogen combustion, and aerosol and FP behaviour.
- IODE, which can model in detail the Iodine and Ruthenium behaviour in the containment and sump
- MEDICS, comprising:
  - RUPUICUV for corium discharge from vessel to cavity with cavity pressurisation and potential direct containment heating;
  - SYNSIT model to simulate the system involved to simulate a Nuclear Power Plant (as valves, sprays, …)
  - CORIUM for molten core-corium interaction in the cavity;

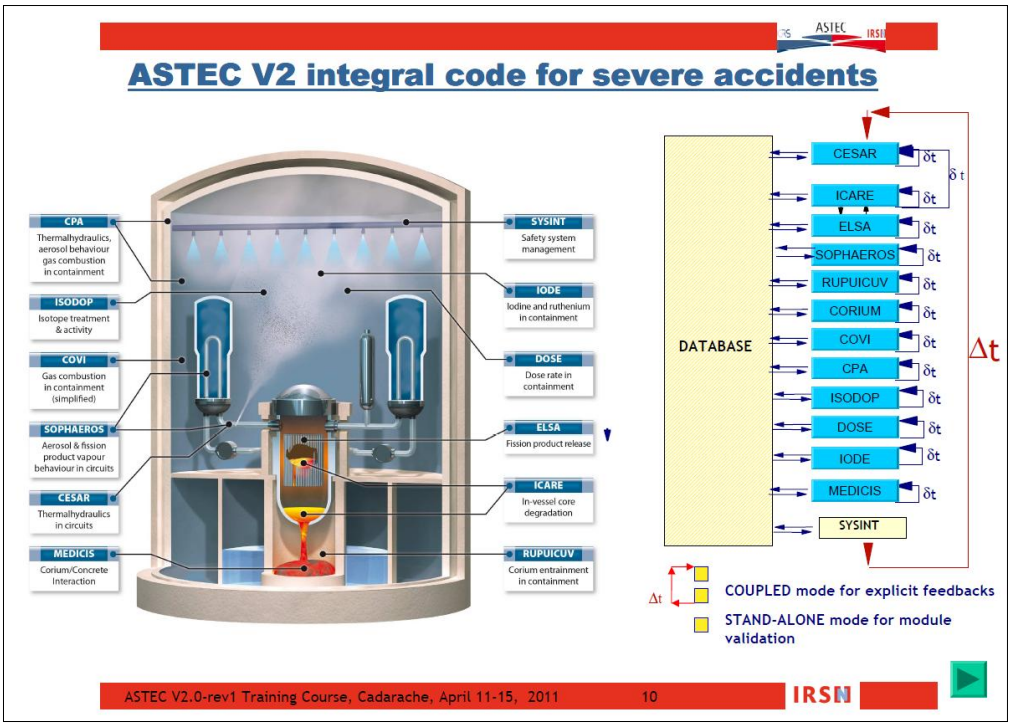

Figure 2.1 ASTEC code costitutive modules

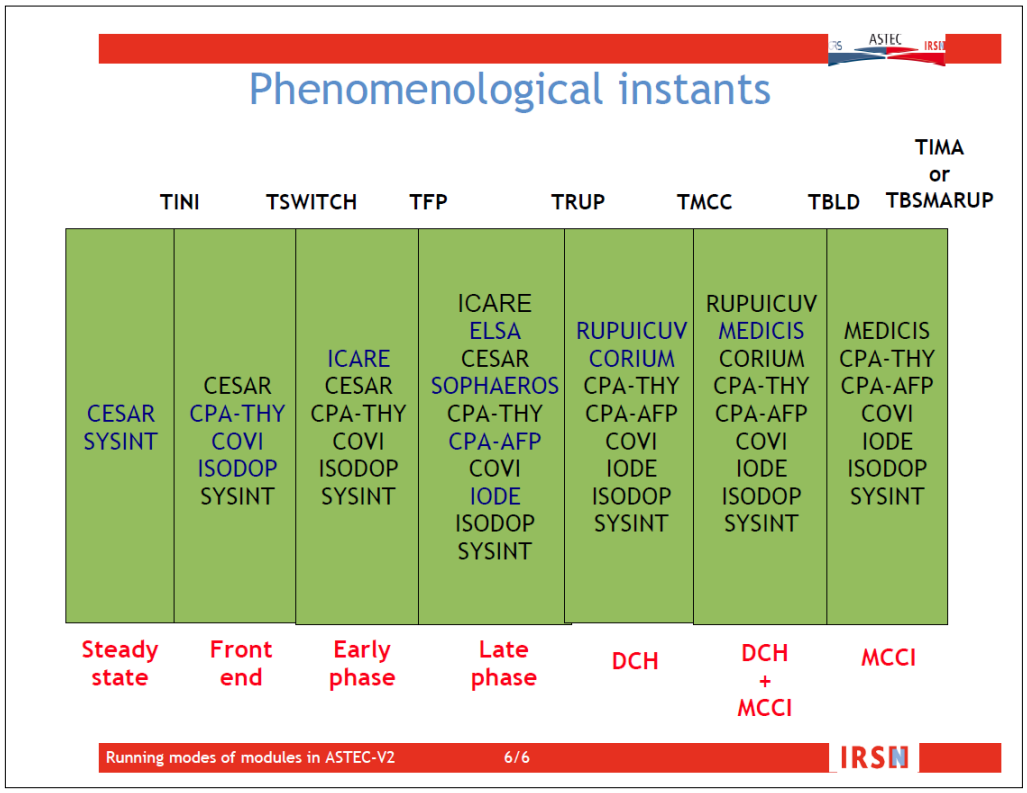

Figure 2.2 Schematic view of the ASTEC modules involved in the progression of SA

2.3 MELCOR Code General Description

MELCOR is a second generation plant risk assessment tool, successor to the Source Term Code Package [3]. The code has been under development since 1982; the following discussion refers mainly to version 1.8.5, released in October 2000.

The whole spectrum of severe accident phenomena is treated, including reactor coolant system and containment thermal-hydraulic response, core heat-up, degradation and relocation, and FP release and transport, in a unified framework for both BWR and PWR reactors. Thermal-hydraulic behaviour is modelled in MELCOR in terms of control volumes and flow paths. MELCOR is especially designed to facilitate sensitivity and uncertainty analyses. MELCOR is a fully integrated, engineering-level computer code able to model the progression of severe accidents in LWR nuclear power plants. It is being developed at SNL for the U.S.N.R.C [6]. Thermal-hydraulic behaviour is modelled in MELCOR in terms of control volumes and flow paths. All hydrodynamic material (and its energy) resides in control volumes. Hydrodynamic material includes the coolant and non-condensable gases. These materials are assumed to separate under the influence of gravity within a

control volume to form a pool beneath and an atmosphere above. Each control volume is characterised by a single pressure and two temperatures, one for the pool and one for the atmosphere. The control volumes are connected by flow paths through which materials may move without residence time, driven by a momentum equation. Based on the elevations of the pool surfaces in the connected control volumes relative to the junctions, both pool and atmosphere may pass through each flow path. Appropriate hydrostatic head terms are included in the momentum equation for the flow paths, allowing calculation of natural circulation.

MELCOR calculates both the release and transport behaviour of fission products and control rod materials. It tracks the masses of these materials by grouping them into classes. Each material class represents a group of one or more elements or compounds with similar physical properties. Each class has its own set of values of parameters, such as release coefficients and vapour pressure. Three different options are available in MELCOR for the simulation of radio-nuclides release from the fuel due to fuel heat-up. The reference calculation uses the CORSOR model with default values for release rate coefficients and the surface-to-volume ratio (but the surface-to-volume ratio can be corrected by the user trough particular sensitivity coefficent). The aerosol dynamics portion of MELCOR is based on the MAEROS computer program, except for the condensation model. MAEROS is a multi-component aerosol dynamics code which evaluates the dynamic particle size distribution of each component. Each component contains one or more MELCOR classes that share the same particle size distribution. Thus components contain classes and classes contain elements and compounds. The particles diameter range is subdivided in a user defined number of sections. Both agglomeration and deposition effects are included in MAEROS. Agglomeration of aerosols by Brownian motion, gravity, and turbulence are accounted for. The deposition processes which are modelled in MAEROS are: gravity, Brownian diffusion, thermo-phoresis, and diffusion-phoresis. The code is not able to model deposition of aerosols by inertia in tube bends and at obstacles. Also hygroscopic effects and the Kelvin effect, which may play an important role for aerosol behaviour in saturated or nearly saturated conditions, are not modelled in MELCOR. Aerosols and vapours can deposit directly on surfaces such as heat structures and water pools. In addition, aerosols can agglomerate and settle. The aerosol deposited on the various surfaces cannot be re-suspended. If a water film drains from a heat structure to the pool in the associated control volume, fission products deposited on that surface are relocated with the water. Depending on the vapour pressure of a particular material class, the released materials may exist as aerosols and/or vapours. If the vapour

mass in the atmosphere is greater than the saturation value, the excess vapour mass condenses. The condensation on existing aerosols is mass transfer limited and the excess vapour mass is converted into new aerosols with the smallest possible diameter within the user-defined diameter ranges. Aerosols and vapours are transported between control volumes by bulk fluid flow of the atmosphere and of the pool, assuming zero slip. In addition, aerosols may settle from a control volume to a lower situated control volume in absence of bulk flow.

The MELCOR COR-package calculates the thermal response of the core and lower plenum structures, including the portion of the lower head directly beneath the core. In addition, the relocation of core materials during melting, slumping, and debris formation are modelled. Fuel pellets, cladding, grid spacers, canister walls, other core structures (e.g. control rods), and particulate debris are modelled separately with individual cells. Cells are the basic nodalisation units in the COR-package. All important heat transfer processes are modelled in each COR cell. Thermal radiation within a cell and between different cells in both axial and radial direction is accounted for, as well as radiation to boundary structures. Radiation to a liquid pool and to steam is also included. Radial conduction across the fuel cladding gap and axial conduction between cells is modelled. Convection to the control volume fluids is simulated for a wide range of fluid conditions and structure surface temperatures, including nucleate and film boiling. Oxidation of Zircaloy and steel is modelled for both the limiting cases of solid state diffusion of oxygen through the oxide layer and gaseous diffusion of steam or oxygen through the mixture. The core degradation model treats eutectic reactions, dissolution reactions, candling of molten core materials and the formation and relocation of particulate debris.

Other physical models and individual code modifications have been performed: a coupled calculation of the core degradation phases, the saturation curve of elemental Cadmium has been added , as well as the input cards for the simulation of the chemical reaction between I and Cs.

As for ASTEC, several new code versions have been released: MELCOR 1.8.6, MELCOR 2.0 and MELCOR 2.1. Each version is characterized from substantial modification and implementation of the models. In particular the COR and RN packages are modified with more complex and innovative models passing from version 1.8.5 to version 1.8.6. An important change in syntax has been done passing from 1.8.6 to 2.0 version;this implies that the input of the code is totally changed in the card description and form. Also other models are corrected, in particular from V 2.0 to V 2.1.

2.4 Relocation Model Description

As already said, the ICARE module of ASTEC V2 code [7] is in charge of the in-vessel core degradation simulation. It computes the behaviour of in-vessel structures, the formation and the evolution of liquid and solid mixtures, the thermal-hydraulics for water, steam and non-condensable gases, and chemical reactions between materials. Early phase corresponds to the first degradation phase of the accident; it covers the initial thermal-hydraulic phase (heat-up phase before any material movement) as well as the first step of the loss of geometry phase This phase is identified as a "Rod-like Geometry" configuration, even if it does not concern exclusively the rods, but also the shrouds, the spacer grids, etc. Standard physical models (gap, creep, oxidation models, ...) are used in this phase, just taking into account the true "deformed" geometry. Molten materials can only be relocated through the hydraulic channels, via magma or debris.

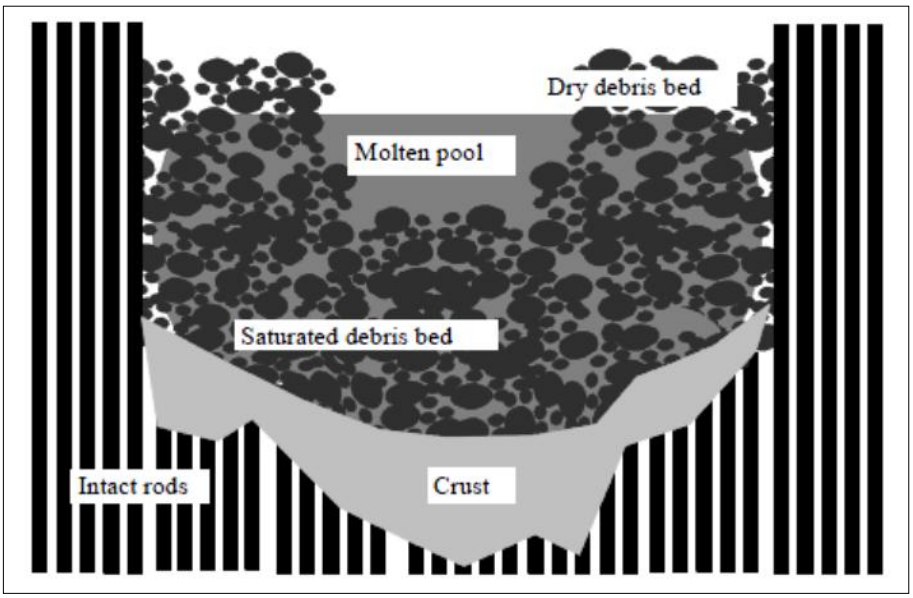

Figure 2.3 Typical configuration of a degraded core

The late phase (Figure 2.3) corresponds to advanced core degradation,involving debris and possible molten pool and/or crust formation. Specific models (porous media approach, axial radiation in cavities, ...) are activated dynamically.

The final stages of core degradation involve substantial melting and material relocation. The governing phenomena of this late melt progression are still not well understood, in particular the reflooding of a degraded core. Models have been developed in the ICARE module to take into

account the dynamics of molten pool formation, its growth inside the debris bed and the progression of the melt inside the core. With these models, it is possible to study the thermal and mechanical behaviour of the debris bed, to predict the amount of melt that may be released into the lower plenum and to investigate any possibility of cooling the materials to stop melt progression.

The MELCOR COR [6] package calculates the thermal response of the core and lower-plenum structures, including the portion of the lower head directly beneath the core; COR models the relocation of core materials during melting, slumping, and debris formation. Multiple structures are modeled as separate components within a single core cell. Intact components include fuel pellets, cladding, PWR and BWR core baffles, and other structures such as control rods or blades. Particulate debris is also modeled as a possible component within a core cell as well as molten pools.

All important heat transfer processes are modeled in each COR cell. Thermal radiation within a cell and between cells in both the axial and radial directions is calculated, as well as radiation to boundary structures (e.g., the core shroud or upper plenum, which are modelled by the Heat Structure package) from the outer and upper COR cells. Radiation to a liquid pool (or to the lower head, if a pool is absent) and to steam is also included. Heat transfer within fuel pellets and across the fuel cladding gap is evaluated. Axial conduction between segments of components in adjacent cells is modeled, as is radial conduction within core plates and within debris beds that are not interrupted by BWR canister walls. Intracell conduction is calculated between particulate debris and other components with which it is in intimate contact. An option is available to include radial conduction between the core and radial boundary heat structures. An analytical model for axial conduction is applied within structures that are partially covered with a liquid pool. Convection to the control volume fluids is modeled for a wide range of fluid conditions and structure surface temperatures, including nucleate and film boiling.

Each of these components may be composed of several materials (e.g., Zircaloy and ZrO2 in the cladding), which are maintained in thermal equilibrium. Oxidation of Zircaloy and steel is modeled as limited by both solid-state diffusion of oxygen through the oxide layer and gaseous diffusion of steam or oxygen through the mixture. The reaction of B4C with steam is also modeled.

The core degradation model treats eutectic liquefaction and dissolution reactions, candling of molten core materials (i.e., downward flow and refreezing), local blockages formed from refrozen materials, formation and heat transfer from convecting molten pools, and the formation and relocation of particulate debris. Geometric variables (e.g., cell surface areas and volumes) are updated for changing core geometry.

2.5 Investigations of Hydrogen Combustion in Containment

For hydrogen distribution [1], the purposes of the investigations of hydrogen combustion in nuclear power plants are:

- to understand the mechanisms of hydrogen combustion from basic physical principles,
- to develop models able to predict the hydrogen combustion in the containment of an actual plant during a severe accident.

As for hydrogen distribution, in the field of nuclear engineering research, investigations of hydrogen combustion consist mostly in the analysis of experiments performed in experimental facilities with suitable computer codes. The differences between experimental and calculation results are then analyzed, in order to:

- detect eventual deficiencies of the models in the code that are the main cause of the discrepancies (i.e., incorrect physical assumptions on which the models are based),
- correct the model (or better propose corrections to code developers).

Simulations are sometimes performed of accident scenarios in ALWR, for which there is no corresponding experimental results. These simulations cannot be classified as investigations of hydrogen combustion, as they do not fulfill any of the two purposes stated above. They may be considered as applications of theoretical investigations, which are of course valuable.

The models used in computer codes may use different levels of detail, solving the transport equations of fluid mechanics on different spatial scales. As in the field of containment atmosphere modeling, two types of codes are basically used in the simulation of hydrogen combustion: Lumped-Parameter (LP) codes and Computational Fluid Dynamics (CFD) codes.

2.6 Release Models

2.6.1 CORSOR Models

As already said, MELCOR [6] calculates the release and transport of FPs and control rod materials in the primary circuit and in the containment. It tracks the masses of these materials by grouping them into classes. Each class represents a group of one or more elements or compounds with similar physical properties. In MELCOR the release of the radio-nuclides is evaluated by the RN (Radio Nuclide) package, which uses the CORSOR models.

The FPs are grouped together in around 10 volatility categories. The variation of the N_i concentration of each group is given by a simple analytical expression, associated with a release rate K:

$$\frac{dN_i}{dt} = -K \cdot N_i \tag{1}$$

where:

$$N_i = N_{i,0} \cdot e^{-K \cdot t} \tag{3}$$

The release (R) at each instant (t) is thus given by the expression:

$$R = 1 - \frac{N_i}{N_{i,0}} = 1 - e^{-K \cdot t} \tag{4}$$

The release rate K depends on the fuel temperature. Two mathematical formulations of K have been established, respectively, within the CORSOR and CORSOR-M models.

The original CORSOR model calculates K according to the following expression:

$$K = A_i \cdot e^{B_i \cdot T} \tag{5}$$

where A_i and B_i are the constants determined experimentally for each FP category and adjusted in different temperature ranges, and T is the temperature. The CORSOR-M model calculates K according to an Arrhenius-type expression:

$$K = K_0 \cdot e^{\frac{Q}{R \cdot T}} \quad (6)$$

where K_0 and Q are constants resulting from adjustments to experimental results. The A_i, B_i, K_0, and Q constant coefficients were mainly established on the basis of SASCHA and HI/VIexperiments for both types of model.

A third model (CORSOR-BOOTH) was implemented with the aim of improving the physical representation of the phenomena. It is based on the diffusion of atoms in solids according the classical Fick's law:

$$\frac{\partial C}{\partial t} = D \cdot \nabla^2 C \quad (7)$$

where C represents the FP concentration at a given point in the fuel and at a given instant, and D is the diffusion coefficient of the species considered in the fuel. To simplify this expression, the Booth hypothesis consists of assuming that the fuel is made up of spherical grains with radius "a" and considering that the concentration is nil on the surface of the grain, that is the release is complete as soon as the FPs reach the grain boundaries. Variations in the released fraction Fr(t) as a function of time can thus be described by:

$$Fr(t) = 6 \cdot \left[\frac{D \cdot t}{\pi \cdot a^2} \right]^{1/2} - 3 \cdot \frac{D \cdot t}{a^2} \text{ for } \frac{D \cdot t}{a^2} \leq \frac{1}{\pi^2} \quad (8)$$

$$Fr(t) = 1 - \frac{6}{\pi^2} \cdot e^{\left[-\frac{\pi^2 D \cdot t}{a^2} \right]} \text{ for } \frac{D \cdot t}{a^2} > \frac{1}{\pi^2} \quad (9)$$

with:

$$D = D_0 \cdot e^{-\frac{Q}{R \cdot T}} \quad (10)$$

D_0: pre-exponential term of the Arrhenius law

Q: activation energy

R: perfect gas constant

The coefficients D_0 and Q are established on the basis of the HI/VI and HEVA/VERCORS experiments.

The CORSOR-BOOTH model contains low and high burn-up options, while CORSOR and CORSOR-M release rates can be modified in function of the component surface-to-volume ratio as compared to a base value, derived from the experimental data on which CORSOR is based.

Release of radio-nuclides can occur from the core fuel (with nonradioactive releases from other core structures), from the fuel-cladding gap and from corium material in the cavity. The radio-nuclides residing in the fuel (simulated in COR package) are assumed to be in elemental form and therefore not to have associated molecular mass.

2.6.2 Semi mechanistic Models of the ASTEC Computer Code

In the case of ASTEC [7], ELSA model deals with all FP elements and actinides taken into account in the inventory ASTEC module ISODOP. Such initial inventory has to be set in the code input. On the basis of measured and expected similarities in physico-chemical behavior for release from solid fuel, the FPs have been grouped into categories (such an approach is used also in MELCOR code). The categories are characterized mainly by the volatility of the element:

- highly volatile: Xe, Kr, I, Br, Cs, Rb, Cu, Se, Te, Sb, Ag. The releases of these so-called volatile FP are governed by the diffusion mechanism in the fuel grain, according to an improved Booth model in which the diffusion coefficient is a function of the fuel stoichiometry (as well as of the temperature and grain size). This coefficient is the same for all these FPs, with the exception of Sb and Te for which a release delay is applied to take into account their retention in the cladding, as long as the latter is not oxidized completely.
- semi-volatile: Ba, Ru, Sr, La, Eu, Ce, Mo – So-called semi-volatile FP releases are governed by the mass transfer induced by their vaporization at the grain boundaries. The steam pressures are tabulated by thermodynamic correlations implemented in the sobrutines GEMINI2 (Sr, Ru, Ba, and La) or FACT (Mo, Ce, Eu). It is the same mass transfer mechanism that is then applied to all the FPs released from the molten pool.
- low-volatile: Rh, Pd, Tc, Nb, Zr, Np, Pu, Nd, Pm, Gd, Tb, Dy, Ho, Er, Tm, Yb, Pr, Am, Cm, Sm, U, Zn, As, Cd, Sn, Ga, Ge, In,Y – Nonvolatile FP releases are governed by the vaporization of UO_2 when it becomes over-stoichiometric and oxidizes until UO_3 forms.

ELSA is based on a semi-empirical approach and models only the principal mechanism governing the release in each of these categories. Also a model for the release of FP and SM from in-vessel molten pools has been developed, completing the release treatment in a severely degraded-core configuration. It is to be noted that the model for the release of FPs and SMs from a molten pool is active in this analysis, having selected the magma option in DIVA and the Decanting/Candling option.

2.7 Transport Model of Aerosol and Gases

The aerosol dynamics portion of both MELCOR and ASTEC codes (SOPHAEROS and CPA) is based on the MAEROS computer program, except for the condensation model. MAEROS is a multi-component aerosol dynamics code which evaluates the dynamic particle size distribution of each component. Each component contains one or more classes that share the same particle size distribution. Thus components contain classes and classes contain elements and compounds. The particles diameter range is subdivided in a user defined number of sections. Both agglomeration and deposition effects are included in MAEROS. Agglomeration of aerosols by Brownian motion, gravity, and turbulence are accounted for. The deposition processes which are modelled in MAEROS are gravity, Brownian diffusion, thermo-phoresis, and diffusion-phoresis.

Practically the transport of the aerosol particle (divided in size and element classes) uses the same models in both codes. The two main differences are in the boundary conditions that are given from the thermo hydraulics energy, mass and momentum balances and in the chemistry. The SOPHAEROS models of ASTEC take into account a more detailed chemistry with a lot of chemical species caracteristics on the MDB (Material Data Base) integrated in the code. Also MELCOR has a chemical module, but much more analytic and simplified than ASTEC. Practically the correct use of the model depends from the sensibility of the user, which can choose the point where the reactions are generated. The model is based on the mole fraction and it is characterized from the definition of new material classes with respect to the original 16, in order to simulate chemical species as AgI and CsI.

Of the above-mentioned natural depletion processes, gravitational deposition is often the dominant mechanism for large control volumes such as those typically used to simulate the containment, although phoretic effects may be significant in some cases (e.g., diffusion-phoresis

during water condensation). When water condenses on a surface, composition gradients will exist in the adjacent gas phase which affects aerosol deposition on the surface. Two related mechanisms produce these gradients. First, a net molar flux of gas toward the condensing surface will exist, and this net flux, commonly called the Stefan flow, will tend to move aerosol particles with it. Second, differences in the momentum transferred by molecular impacts on opposite sides of the particle will tend to drive the particle in the direction of decreasing concentration of the heavier constituent. When the non-condensable gas is heavier than steam, as in air-steam mixtures, the differential molecular impact effect opposes the Stefan flow (which dominates the net result); the effects are in the same direction if the non-condensable gas is lighter than steam. The Waldmann model is used to calculate the particle diffusion-phoretic deposition velocity as soon as steam condensation flux exists. This model is based on the Stefan velocity with a correction factor, based on a theoretical approach. which is consistent with the free molecular regime and leads to a deposition velocity independent from the particle size class.

The mass transfer rate limitation is a function of the diffusion mass transfer coefficient, which is calculated at a heat structure boundary surface whenever the surface is exposed to the atmosphere of its boundary volume. Different models are developed in ASTEC and MELCOR codes to evaluate the condensation mass transfer onto heat structures. In MELCOR the mass transfer coefficient is related to the atmosphere Nusselt number through a heat and mass transfer analogy and is calculated by a Sherwood number correlation involving Nusselt, Prandtl, and Schmidt numbers [6]. On the other side, ASTEC code employs the Stephan's law [7]:

$$G_{tot} = \frac{\beta p}{R_D T (1 - n_0)} \ln \frac{p - p_{DS}(T_f)}{p - p_0} \tag{11}$$

$$T = \frac{1}{2}(T_z - T_f) \tag{12}$$

$$\beta = \frac{\alpha}{\rho c_p} \left(\frac{D \rho c_p}{\lambda} \right)^{1-n} \tag{13}$$

Where:

α	Convective heat transfer coefficient	$\frac{W}{m^2 \cdot K}$
n_0	Droplet mass fraction	$\div$
p	Partial pressure	*Pa*
$p_{DS}(Tf)$	Steam partial pressure at wall surface	*Pa*
p_D	Steam partial pressure in zone	*Pa*
T_Z	Zone temperature	*K*
T_f	Water temperature	*K*
T_S	Surface temperature	*K*
D	Diffusion coefficient of steam at temperature T	m^2/s
c_p	Average heat capacity of gas mixture at T	$\frac{W}{ka \cdot K}$
λ	Average heat conductivity of gas mixture at T	$\frac{W}{m \cdot K}$
ρ	Average density of gas mixture at temperature T	kg/m^3
N	Exponent calculated	$\div$

2.8 The Problem of Code Models Qualification

The problem of the correctness of SA simulation by computer codes is based on the models implemented and on the sensibility of the user to understand the evolution of a SA scenario. Very similar nodalizations done for the same code, with the same initial and boundary conditions, could give different results. In particular MELCOR results depend from the interpretation of the phenomena and the choices to try to simulate them; it allows the user to take few decisions, as the characterization of the components and the setup of the models with corrective and sensitivity factors. Also ASTEC has a lot of features for modifying the models outputs, as limits or switches and corrective factors applied to modules options.

Therefore, the first important step is to prepare the user to the use of the codes with the experience obtained in this sector. In particular, the methodology developed for the knowledge of the codes' models is based on the reference experimental results obtained in experimental facilities and on the analyses of accidents as TMI or Fukushima. This is essential to gain insights about the robustness of the design and in providing knoledge-informed input to pre- and post-certification activities.

In the present work, for investigating the capability of the two codes (in particular with respect to core degradation, FP transport in the circuit and aerosol deposition in the containment) we have performed simulations of FPT sequences [5] considering as initial and boundary conditions in input the experimental data for steam inlet in test sections, temperatures of each element of test section, circuit and containment vessel and power of bundle. The main goal of these analyses is the validation of the most important models for the simulation of the behaviour of PWR under severe accident conditions and their interactions with the models describing aerosol dynamics. This experience will highlight the most important phenomena from a safety point of view, that could be significant in the SA evolution in the II and III Generation NPP. For example, the choice of the control rod absorber material can determinate a different source term in the containmentThe combination experience derived from PSA of level 1 (Appendix 1), as starting point for the reconstruction of a scenarios' family, and from evaluations of the main SA phenomenologies in the PHEBUS tests should allow to acquire a qualitative idea of the phenomenology involved in SA analyses of AP1000 plant.

2.9 General Observations of the Problem of the Scaling Facility

The problem of the scaling facility is due to complex phenomena, reference data and knowledge in the SA phenomenology. As described in the introduction, the most relevant accidents which gave information on the phenomenology and the source term in the nuclear power plant are TMI [3], Chernobyl and Fukushima [7]. Chernobyl is useful only for the source term, but this information is stricthly related to the characteristics of the sequence and to the type of plant. In the case of TMI and Fukushima, they give a lot of data able to characterize SA in LWR. The problem for Fukushima accident is the short time from the occurring date (11/03/2011); the accident is under analyses and

needs more investigation to understand completely the lesson on the various aspects of the phenomenology.

In order to predict and to prevent severe accidents in LWR, in the world and in particular in Europe few scaling tests have been performed in order to upgrade the knowledge of the phenomenology and to improve the capability of the SA codes as MELCOR [6] [7] and RELAP/SCDAP [8]. In particular it is important to understand the physics and the chemistry of the aerosol release and transport, in order to estimate the source term and the related doses in case of release to the environment.

The chemistry and the physics of SA are very complex and one must keep in consideration a lot of variables in order to set-up an adequate model for each particular aspect to simulate. For example, in the case of coree release, we should take into account the fuel crystalline microstructure, the dislocation ad relocation phenomena, gas diffusion in the fuel matrix, fuel temperature distribution, etc. . These models, based on a rigorous and theoretic approach, are also heavy from the computational point of view. The solution is often to use semi-empirical models calibrated on the basis of experimental tests, as PHEBUS and QUENCH programs [9].

2.10 Chemistry Aspects

Problems of chemistry are often present for the evaluation of FP aerosol and gas releases [1], also due to their interaction with the structural materials; the following phenomena shall be mentioned in this respect:

- The effect of oxidizing conditions on release of fission products from the reactor core and their transport in the primary circuit (especially the behavior of the highly radiotoxic ruthenium under air ingress conditions);
- iodine forms released in reducing or oxidizing conditions and theirtransport in the primary circuit;
- control rod aerosol release (Ag–In–Cd) that affects iodine transport in the primary circuit;

- fission product release during containment by-pass sequences (especially in the cases of steam generator tube rupture (SGTR));
- aerosol remobilization from the primary circuit;
- iodine/ruthenium behavior in the containment, especially for what concerns the volatile fractions in the atmosphere.

Trying to solve these problems, the work was organized through a number of technical circles, each focusing on a specific issue, which helped to bring experimentalists and modelers closer together. In addition, strong cooperation was established with major international projects such as PHEBUS FP [10] the International Source Term Project (ISTP), the International Science and Technology Centre (ISTC), and OECD/NEA through the THAI and Behavior of Iodine (BIP) iodine chemistry projects in the framework of SARNET network [11]. The studies covered definition and performance of experiments, joint interpretation of new and existing data, formulation and improvement of computer models, particularly in the case of ASTEC code.

The main objective was to predict the Iodine behavior in a reactor coolant system (RCS) under severe accident transient conditions. Iodine was indeed the only fission product element, except for noble gases, observed in the PHEBUS FP tests [10] in gaseous form in the containment. There is an indication that the largest part in FPT3 [9], and smaller fractions in the other tests, came as volatile iodine directly from the primary circuit. Therefore, present work on PHEBUS mainly concerned analysis of the iodine experimental results in the primary circuit in terms of iodine retention, gaseous iodine fraction and iodine vapor speciation. The primary circuit in PHEBUS tests is characterized by gas temperatures reaching nearly 1600 °C at its entrance and cooling down to 150 °C at its outlet, just before entering into the containment. The main phenomena arising in the RCS are chemical transformation of vapors, vapor condensation on structures as well as nucleation into aerosols or onto aerosols, aerosol agglomeration and deposition due to thermo-phoresis. Earlier work was essentially based on applications of a standard fission product (FP) transport code, SOPHAEROS (part of ASTEC). These calculations could reproduce some important aspects of the first two PHEBUS tests, FPT0 and FPT1 (principally vapor/aerosol behavior and total retention in the primary circuit). Nevertheless, significant disagreements with experimental results were identified, for example in the FP deposition in the vertical hot leg and in the steam generator.

Another important aspect to be considered in this framework is the vaporization of metallic elements from the Ag–In–Cd control rods [11] and their interaction with the Iodine released and the amount and nature of the species transported for the following reasons:

- First, except maybe for uranium, the silver and indium release is the main contributor in terms of mass to the aerosols present along the reactor coolant system. Thus, it may affect the aerosol deposition modelling through the density and the size of the aerosols formed.
- Secondly, silver, indium and cadmium are very reactive with iodine which is a major contributor to the source term, at least for the evaluation of doses at short times. Kinetic release and the chemical composition through the RCS of these elements are therefore of primary[12] importance [11] to evaluate the gaseous fraction of iodine reaching the containment.

2.11 Main Uncertainties in FP Transport and Deposition

Aerosol phenomena during postulated severe accidents [11] have been extensively investigated worldwide and a reasonable level of understanding has been achieved. The models in currently used, integral safety codes can be considered mature enough, provided that the thermal–hydraulic conditions are adequately defined via the interface between the respective modules in the code. Nevertheless, EURSAFE highlighted some remaining issues that needed further investigation [10]. These are retention in complex structures such as the steam generator during an SGTR containment by-pass sequence, leakage through cracks in concrete walls of an over-pressurised containment and remobilization of fission product deposits in the primary circuit, either as vapors (re-vaporisation) or aerosols (re-suspension). EURSAFE noted the absence of any adequate treatment of these aspects in the methods used for evaluating the releases to the environment, and the potential of these processes to modify the source term. Cooperative studies were included in SARNET to address these points. In SARNET framework, progress has been achieved in understanding and modelling of these aerosol phenomena, which can result either in a reduction (i.e., SGTR by-pass sequences and cracked concrete containments) or in an increase (i.e., re-vaporisation and re-suspension) of the potential source term to environment.

References

[1] SARNET2/ENENIII, "Materials of Short Course on Severe Accident analyses Phenomenology, jennuary 2011

[2] J. P. Van Dorsselaere et al. The ASTEC integral code for severe accident simulation, *Nucl. Technology* – NT-3-0846, vol.165, March. 2010

[3] A. Manfredini, "OECD/CSNI – Alternative TMI-2 Scenario Benchmark", DINMP – University of Pisa, Pisa.

[4] R. Gauntt et al. MELCOR Computer Code Manuals Vol. 2: Reference manual, Version 1.8.6, September 2005 - NUREG/CR-6119, Vol. 2, Rev.3 SAND2005-5713 - Sandia National Laboratories.

[5] P. von der Hardt, A. V. Jones, C. Lecomte and A. Tattegrain, Nuclear Safety Research: The Phebus FP Severe Accident Experimental Programme, *Nuclear Safety*, vol 35(2), July-December 1994, pp 187-205.

[6] US-NRC, "Final Safety Evaluation Report Related to Certification of the AP1000 Standard Design", *NUREG-1793*, 2006

[7] INPO, "Special Report on the Nuclear Accident at the Fukushima Daiichi Nuclear Power Station", November 2011, special report

[8] C. Allison, "RELAP5 Mod 3.4 Input Deck Manual", 2010 Innovative Systems Software, LLC, 2010

[9] T. Haste, F. Payot, C. Dominguez, Ph. March, B. Simondi-Teisseire, M. Steinbrück, "Study of boron behavior in the primary circuit of water reactors under severe accident conditions: A comparison of Phebus FPT3 results with other recent integral and separate-effects data", Nuclear Engineering and Design 246 (2012) 147– 156, 8 August 201

[10] R. Frutos, D. Gido, G. Henneges, P. Schmuck, "Calculation of fission product behavior in an advanced containment in case of a severe accident", Nuclear Engineering and Design 202 (2000) 173–178, 18 April 2000

[11] T. Haste, P. Giordano, L. Herranz, N. Girault, R. Dubourg, J.-C. Sabroux, L. Cantrel, D. Bottomley, F. Parozzi, A. Auvinen, S. Dickinson, J.-C. Lamy, G. Weber, T. Albiol,

"SARNET integrated European Severe Accident Research—Conclusions in the source term area", Nuclear Engineering and Design 239 (2009) 3116–3131, 18 September 2011

[12] P. Hofmann, "Current knowledge on core degradation phenomena, a review", Journal of Nuclear Materials 270 (1999) 194±211, 16 November 1998

PART II: PHEBUS FPT TESTS ANALYSES

3 PHEBUS FPT PROGRAM DESCRIPTION

3.1 The PHEBUS Facility

The ongoing PHEBUS FP programme [1] is the centre of an international co-operation investigating, through a series of integral in-pile experiments, key-phenomena involved in the progression of postulated severe accidents in light water reactors (LWRs). The dedicated PHEBUS facility offers the capability to study the degradation of real core material, from the early phase of cladding oxidation and hydrogen production up to the late phase of melt progression and molten pool formation. The subsequent release of fission products (FPs) and structural materials is also experimentally studied, including their physicochemical interactions, their transport in the cooling system, and their deposition in the containment. The re-volatilisation of iodine due to radiochemical effects in the water of the sump and the amount of low-volatility FPs and transuranium elements reaching the containment are receiving a special interest, as large uncertainties related to their modelling subsist.

FPT-0 and FPT-1 [2] [3] (Figure 3.1), the first experiments of the programme performed in December 1993 and July 1996 respectively, have demonstrated that the PHEBUS FP facility is capable of successfully attaining the above-mentioned objectives. They reached very advanced states of degradation, comparable to what was observed in TMI 2, and generated a wealth of results on FP behaviour. The resulting database has been—and will be—applied to develop and validate the computer codes used to assess the safety of the currently operating plants and to check the efficiency of accident management procedures. They will also support the design of future plants having the capability to confine core melt-down accidents within their containments.

In the PHEBUS facility [3] conditions similar to those waited in a real plant in case of severe accidents are reproduced, allowing for an in depth investigation of the basic phenomena that determine the release, transport, deposition and retention of FPs. These phenomena take place in the core region, in the primary circuit and in the containment system and involve a strong coupling between thermal-hydraulics and chemical/physical processes determining nuclear aerosol behaviour.

The facility provides a reduced-scale representation of the core, the primary circuit (with the steam generator) and of the containment system of a nuclear plant (Figure 3.2), allowing for a detailed analysis of the prototypical conditions expected during a severe accidental sequence. The test train is located in a loop crossing the central part of the PHEBUS driver core which supplies the nuclear power.

In experiments FPT0, FPT1, FPT2 [4] and FPT3 [5] [6], the fuel rods were 1.12 m long with a 1 m long fissile zone (total mass of UO_2 about 11kg), were held in place by two Zircaloy spacer grids and arranged in a 5x5 square lattice with a pitch of 12.6 mm, without the four corner rod. In the next paragraphs it is described each part of the facility, in particular focusing on the parts nodalized in the simulations with ASTEC [7] and MELCOR codes [8].

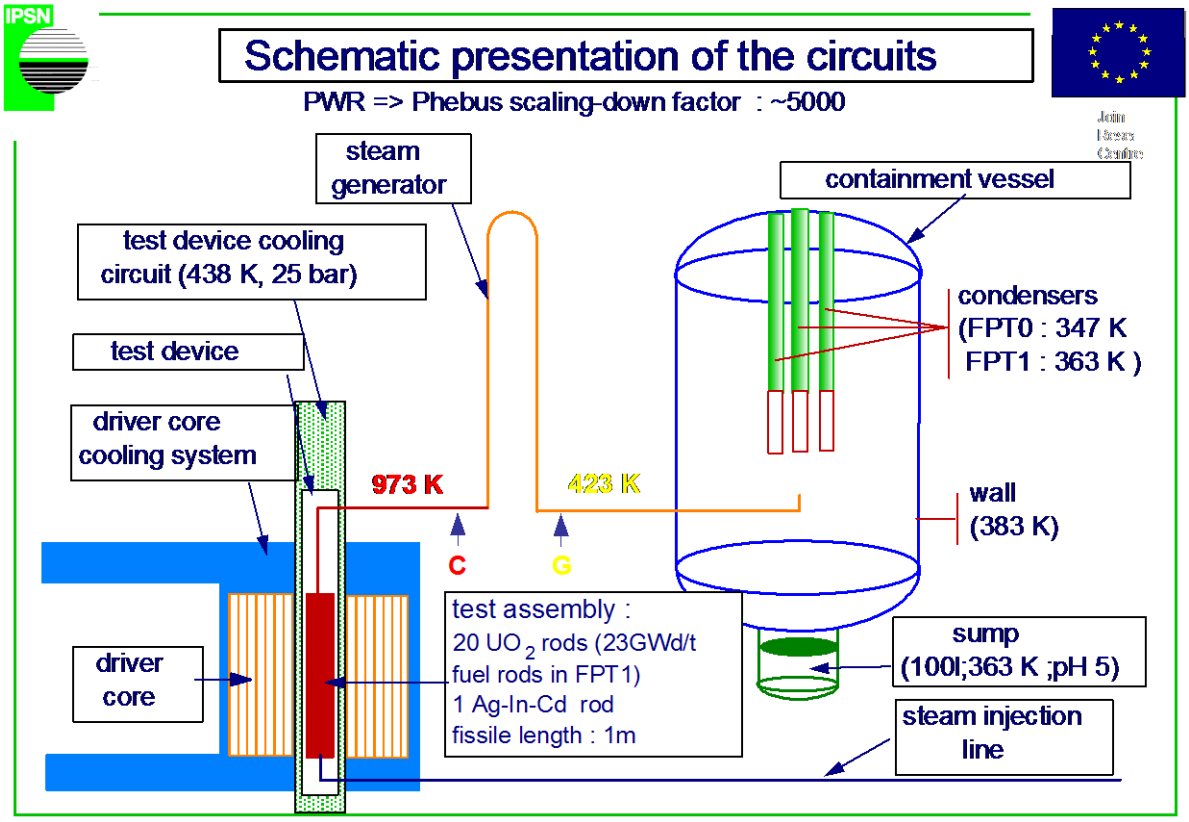

Figure 3.1 Sketch of PHEBUS test apparatus for FPT0 and FPT1

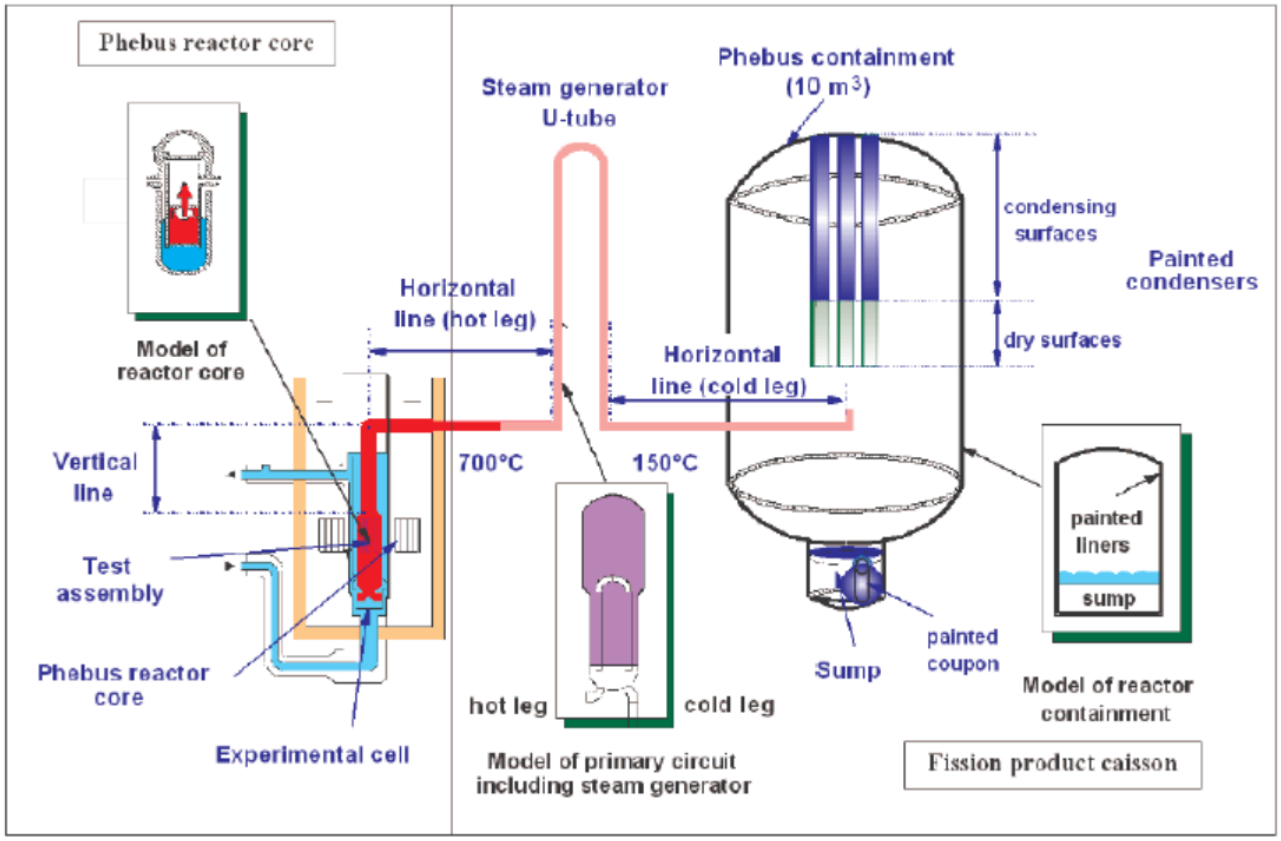

Figure 3.2 Sketch of the PHEBUS experimental facility

3.2 The Bundle

The PHEBUS test bundles [3] [4] [5] (Figure 3.3 and Figure 3.4) contain 18 fuel rods (UO2) previously irradiated at different burn-up (see successive paragraph 1.5 for a detailed description). Two fresh instrumented fuel rods were also introduced into the bundle and an absorber control rod. The test bundle was surrounded by an insulating zirconia shroud with an inner circular ThO2 layer (ZrO2 in FPT0), an external ZrO2 layer and a pressure tube of Inconel coated on the internal face by flame-sprayed dense ZrO2. These three annular structures were separated by two gaps under cold conditions. The outer pressure tube was cooled by an independent pressurised cooling circuit, with a high mass flow of water at a temperature of 438 K. The rods were cooled by a measured gaseous flow of steam imposed at the entrance.

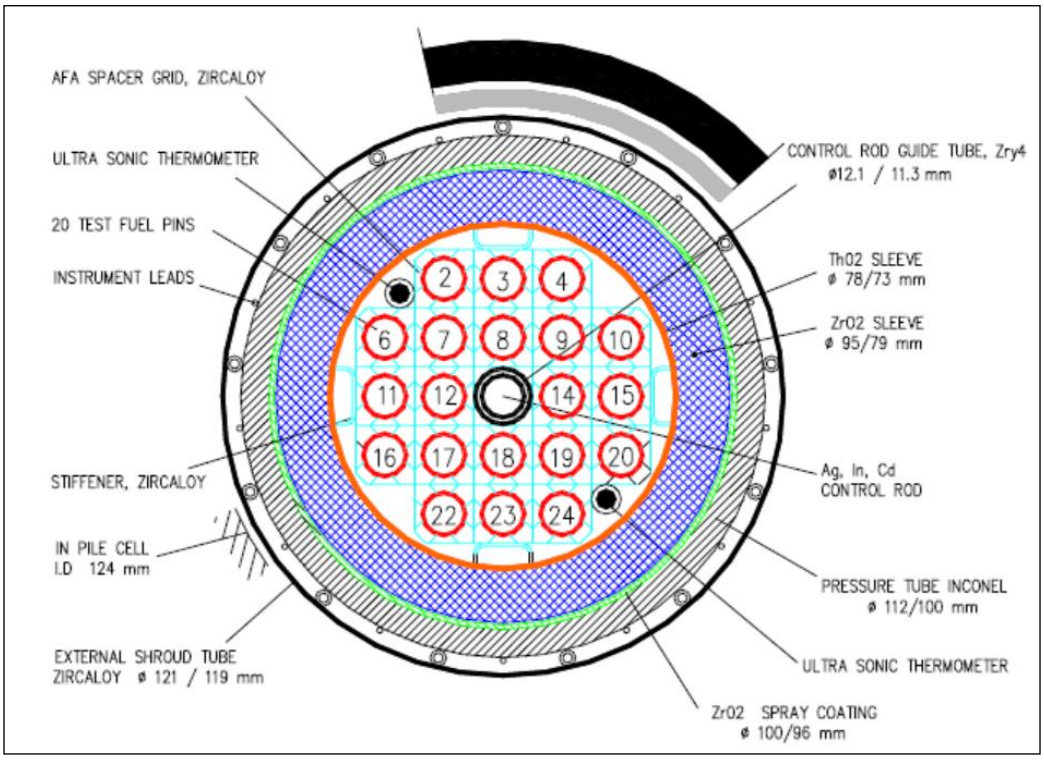

Figure 3.3 PHEBUS facility: the fuel bundle for FPT0-1-2

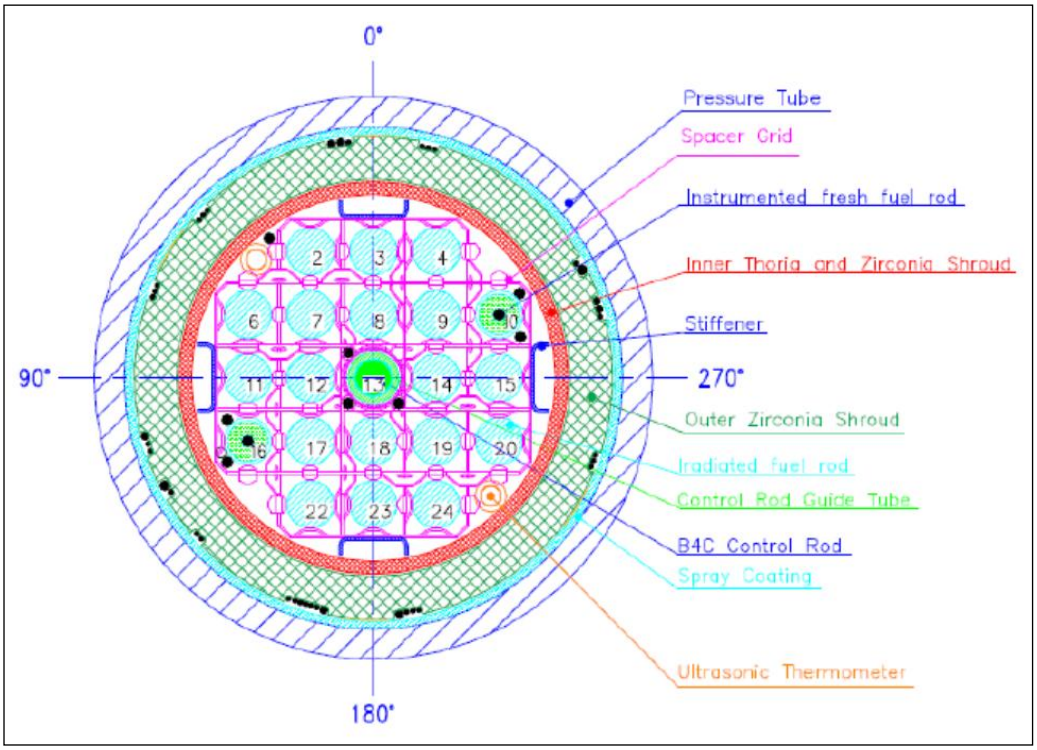

Figure 3.4 PHEBUS facility: the fuel bundle for FPT3

3.3 The Circuit

The circuit of the PHEBUS test facility is a simulation line of the primary circuit of 900 MWe PWR plant. It is divided in 4 sections [2] [4] [5]: Test Section, Hot Leg Line, Steam Generator and Cold Leg line. The gases and aerosols released from the fuel bundle during the degradation phase are conveyed through experimental lines up to the CV. The experimental lines are composed of:

- a vertical line directly above the test bundle (vertical line, ~3m high, internal diameter 0.073m reducing in steps to 0.048m and then to 0.03m), where the gas temperature drops to 970 K; it leads to a horizontal line (isothermal at 970 K) with a length of 9m and an internal diameter of 0.03m; both lines simulate conditions in the hot leg of a PWR primary circuit (Figure 3.5),
- the vertical steam generator U-tube (~4m high with an internal diameter of 0.02m), with pipe walls maintained at 420 K (Figure 3.6),
- a horizontal line (at 420 K and ~4m long with an internal diameter of 0.03m), simulating conditions in the cold leg of a PWR primary circuit, leading to the CV.

The vertical line is composed of the upper plenum and the riser. The bottom part (0.2 m length) of the upper plenum is unheated, while the remainder part of the vertical line is at a temperature of 700°C. In FPT1 [3], a section of the liner in the temperature controlled part of the vertical line was made of stainless steel, while Inconel 600 was used in the other part; this allows to study the differences in deposition on these materials. The horizontal line simulating conditions in the hot leg is made of Inconel-600 and its temperature is regulated to 700°C. Also the steam generator U-tube is made of Inconel-600; its walls are maintained at 150°C during the test, i.e. above the conditions for steam saturation at the test pressure. The outlet of the U tube and the horizontal line simulating conditions in the cold leg are made of stainless-steel (AISI 304L) and are maintained at 150°C.

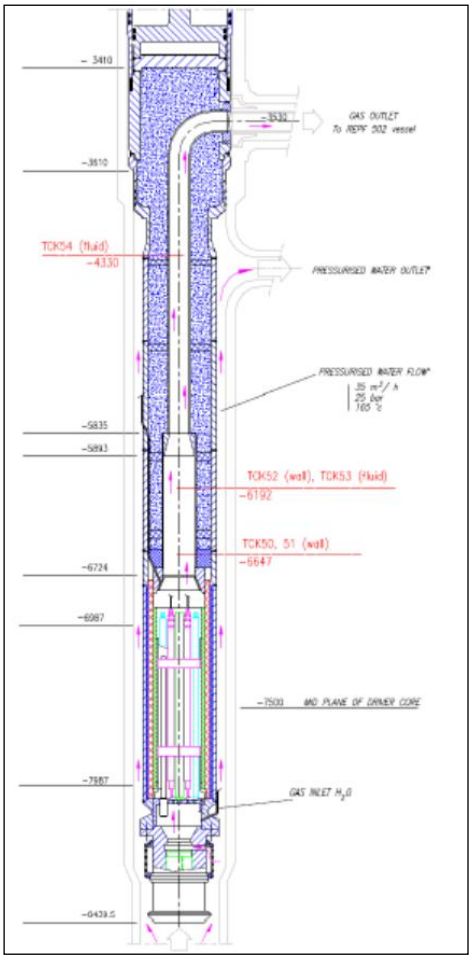

Figure 3.5 FPT3 PHEBUS facility: the test section

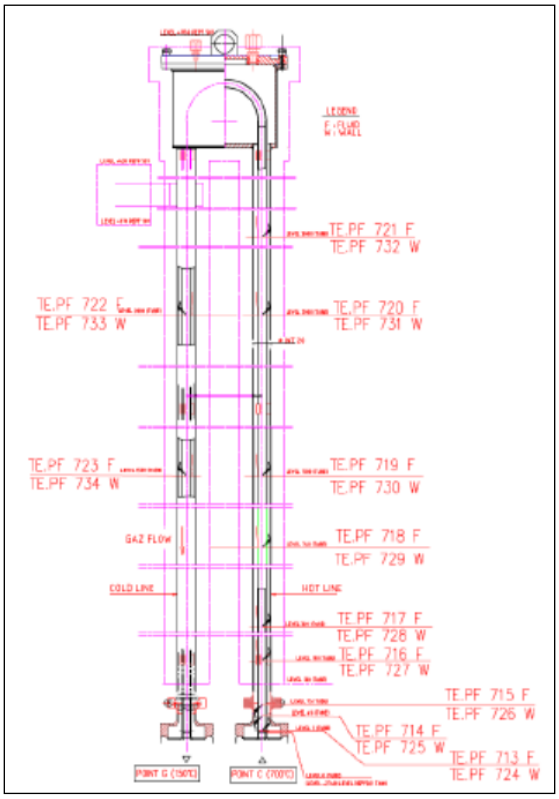

Figure 3.6 FPT3 PHEBUS facility: the SG U tube

3.4 The Containment

The containment of the Phebus facility is a cylindrical vessel (5 m height, 1.8 m external diameter) with 10 m^3 free volumes (Figure 3.7). The volumetric scale factor corresponds to the ratio between the mass of the core of a 900 MW(e) PWR and the mass of the fuel element employed in the PHEBUS tests, i.e. about 5000:1 as volume scale [1]. The aim is to preserve the concentration of the fission products, with respect to the situation expected in the actual containment system. The containment has cylindrical form with rounded bottom and top; the walls of the containment are made of AISI 316L grade stainless steel. The top vault is equipped with a group of three condensers, which are designed to control heat transfer and steam condensation, and thus simulate the cold structures of a reactor building.

Condensation heat transfer onto containment walls is simulated with three vertical condensers, each divided into two zones whose superficial temperature can be adequately controlled. The lower part of each condenser is kept dry by heaters and contains equipment to collect condensate from the upper cooled part. When the collection device is full, the condensate is sequentially drained into the sump. During the FPT0 and FPT1 [2] [3] experiments the values of the temperature imposed to the condensers allowed for condensation only in the upper part of the three structures. The surface of the three condensers is covered with epoxy paint, which is a possible trap for molecular iodine and for the formation of iodine organic compounds. The cylindrical walls of the vessel are slightly superheated in order to avoid steam condensation and aerosol contamination. The lower part of the vessel is closed by an elliptic lid which allows for the formation of a 0.1 m^3 sump. The diameter of the sump is only 0.584 m in order to scale the actual exchange surface. The water of the sump can be recirculated in order to prevent a too much high increase of the temperature. A painted structure is finally submerged in the sump. A system of sprays can be actuated to wash the aerosols from the bottom of the vessel to the sump.

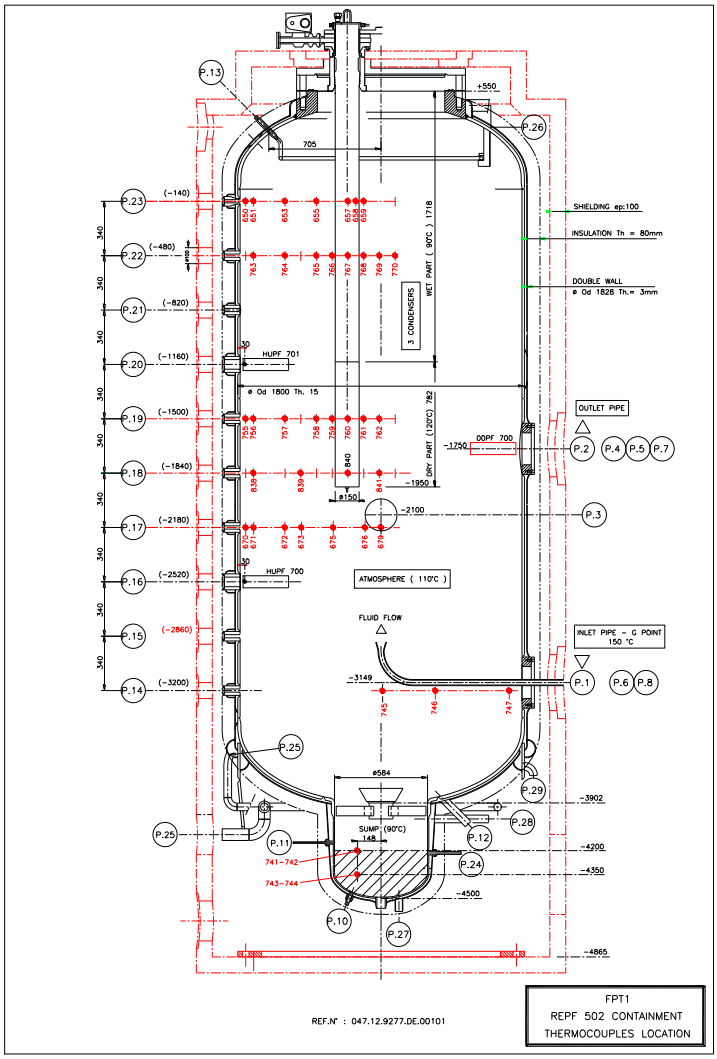

Figure 3.7 PHEBUSfacility: the containment vessel

3.5 General Description of the FPT 1 – 2 - 3

Really the FPT tests are five; only the first test FPT0 was performed using trace-irradiated fuel. For the rest of the matrix, irradiated fuel rods (~ 23 GWd/tU for FPT1 [2], ~ 32 GWd/tU for FPT2 [4] and ~ 24.5 GWd/tU for FPT3 [5]) were used. The FPT1 and FPT2 tests bundles (Figure 3.3 and Figure 3.4) contain 18 fuel rods (UO2) previously irradiated in the Belgian BR3 reactor, where they attained the rod average burn-indicated in the Table 3.1. Two fresh instrumented fuel rods were also introduced into the bundle as well as a Ag, In, Cd (AIC) absorber control rod (containing 80 wt.% silver, 15 wt.% indium and 5 wt.% cadmium). In the case of FPT3 the control rod is composed by Boron Carbide (B_4C).

Each experiment consisted of a re-irradiation period of approximately 7-9 days at a mean power of 205 kW (FPT1), 232 kW (FPT2) and 220 kW (FPT3), so as to generate the short-lived FP inventory. This pre-conditioning phase was followed by a 5 hour transient, during which steam at a pressure of ~2 bar was injected into the bundle with a flow rate varying between 0.5 and 2.2 g/s in the case of FPT1 [2] [3] and 0.5 g/s constant for FPT2 [4] and FPT3 [5], in order to evaluate steam starvation phenomena when the poor flow-rate of steam is used to create the respective mass of hydrogen. Meanwhile, the bundle nuclear power was progressively increased from 0, up to 34.4 kW for FPT1 [3], from 0, up to 52.5 kW for FPT2 [4] and from 0, up to 32.8 kW for FPT3 [5]. The power generated within the fuel rods produced the heat-up of the test bundle leading to bursting of the cladding, degradation of the control rod and relocation of the absorber material. As a consequence, cladding oxidation and hydrogen generation, melt relocation and accumulation, and release of FPs from bundle, structure and control rod materials take place. The temperature escalation started as the measured cladding temperature exceeded 1570°C and lasted for about 5 min in the upper part of the bundle. The temperature peak reached 2220°C at the elevation 700 mm. The maximum heating rate was ~15°C/s at elevation 800 mm. The total mass of hydrogen produced during the FPT1 [3] transient was ~96 g and 120 g for FPT2 [4] and FPT3 [5]. The onset of fuel movement probably occurred at the be-ginning of the heat-up phase. A second rapid heat-up at the bottom of the shroud, associated with a second fuel relocation, was detected ~2 min before the end of this phase of the test. This second temperature peak in the lower part of the shroud triggered reactor shut-down and the end of the “bundle degradation” phase of the test. A significant amount of FPs - more than 80 % of the initial bundle inventory of those most volatile - and bundle, structure and control rod materials were released. Releases were transported by the steam flow, through the experimental line to the containment vessel. The transient was terminated by core shut-down and the cooling of the bundle with steam for ~26 min.

In FPT3 the spacer grids were of ~0.043m heigth and were positioned at elevations 0.24 and 0.76m from the bottom of the fuel column. The two grids were linked to four Zircaloy stiffeners. The absorber rod in the centre of the bundle contained Ag-In-Cd [3] [4] in the first three tests and B_4C in FPT3 [5].

Test	Number of fresh + irradiated + absorber rods	Fuel Burnup (GWd/t U)	Bundle flow	Containment	Date of test
FPT0	20 + 0 + 1SIC*	Trace	Steam-rich	pH 5 non-evaporating sump	December 2, 1993
FPT1	2 + 18 + 1SIC	~23	Steam-rich	pH 5 non-evaporating sump	July 26, 1996
FPT2	2 + 18 + 1SIC	~32	Steam-poor with boric acid	pH 9 evaporating sump	October 12, 2000
FPT3	2 + 18 + 1B_4C	~24	Steam-poor	pH 5 evaporating sump	November 18, 2004
FPT4	Pre-formed debris bed; no absorber or metallic Zry	~38	Steam + H_2	-	July 22, 1999

*- SIC - Silver/Indium/Cadmium

Table 3.1 Summery of PHEBUS tests cases

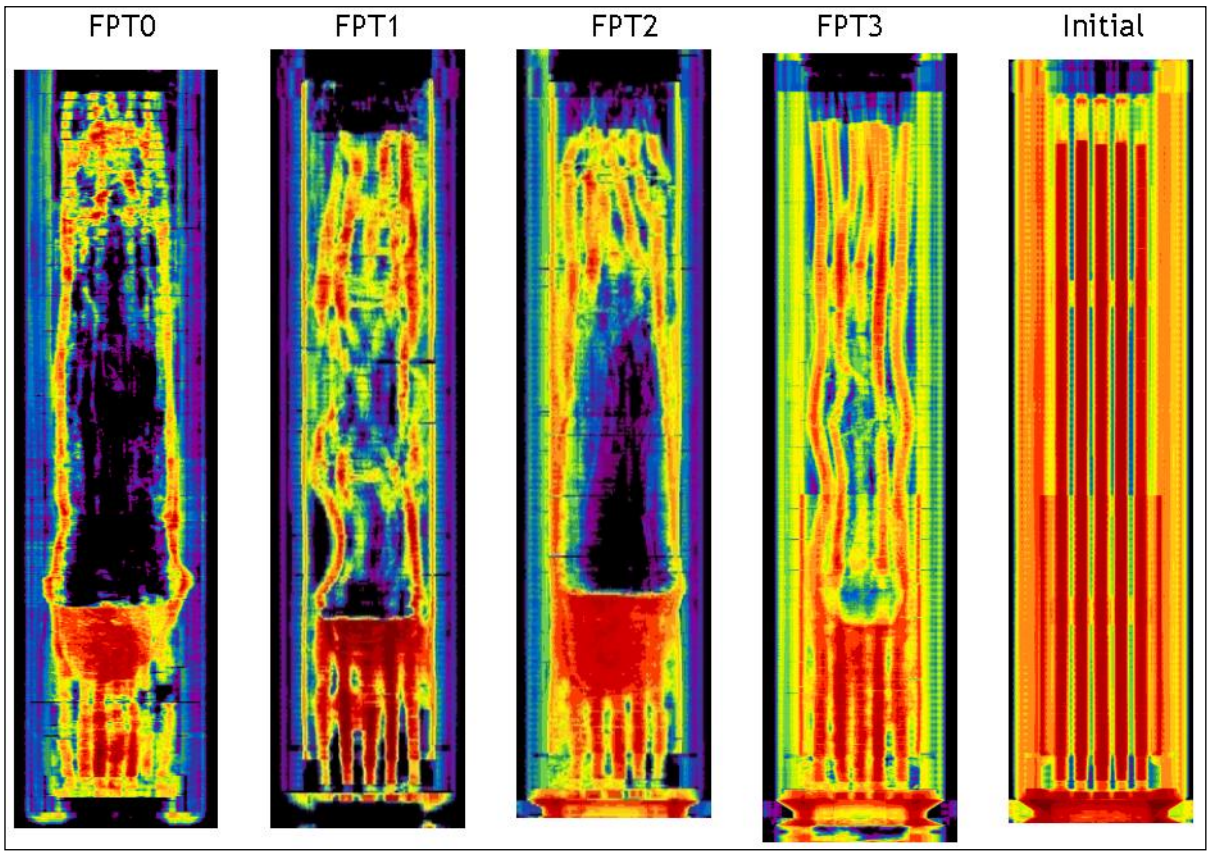

Figure 3.8 Thermography of each bundle before and after degradation phase

References

[1] P. von der Hardt, A. V. Jones, C. Lecomte and A. Tattegrain, Nuclear Safety Research: The Phebus FP Severe Accident Experimental Programme, *Nuclear Safety*, vol 35(2), July-December 1994, pp 187-205.

[2] D. Jacquemain, S. Bourdon, A. de Braemaeker and M. Barrachin, FPT1 Final Report (Final version) IPSN/DRS/SEA/PEPF report SEA1/00, IP/00/479, December 2000.

[3] T. Haste, Specification of International Standard Problem ISP-46 (Phebus FPT1), Revision 0, IPSN Note Technique SEMAR 01/91, November 2001.

[4] A. C. Greogoire, et ali., "FPT2 Final Report (Final version)", IRSN. N° PH-PF: DOCUMENT Phébus PF, IP/08/579, Febbrary 2008.

[5] A. Bieliauskas, T. Haste, "SPECIFICATIONS OF SARNET2 PHEBUS FPT3 BENCHMARK", IRSN, DPAM-SEMIC-2011-057, 5/07/2011

[6] T. Haste, F. Payot, C. Dominguez, Ph. March, B. Simondi-Teisseire, M. Steinbrück**,** **"**Study of boron behavior in the primary circuit of water reactors under severe accident conditions: A comparison of Phebus FPT3 results with other recent integral and separate-effects data", Nuclear Engineering and Design, 2011

[7] J. P. Van Dorsselaere et al. The ASTEC integral code for severe accident simulation, *Nucl. Technology* – NT-3-0846, vol.165, March. 2010

[8] R. Gauntt et al. MELCOR Computer Code Manuals Vol. 2: Reference manual, Version 1.8.6, September 2005 - NUREG/CR-6119, Vol. 2, Rev.3 SAND2005-5713 - Sandia National Laboratories.

4 PHEBUS FPT1 ANALYSES WITH ASTEC AND MELCOR CODES

4.1 Overview

The FPT1 sequence [1] simulates a severe accident with a steam inlet that represents the consequences of ECCS operation (until 4000 s). Following the failure of ECCS, the steam flow-rate decreases and melting of the bundle starts. Finally, an increase of steam injection flow-rate (after 10000 s since the beginning of the transient) takes place, due to the fall down of molten material with a strong evaporation of the water filling the vessel lower plenum. Steam, hydrogen and aerosols exiting the core bundle are forced to enter the test circuit simulating the upper plenum, the hot leg and the steam generator of a nuclear plant, before entering the Containment Vessel (CV) [2]. The initial containment humidity is 57.6 % and the initial temperature in the Containment Vessel (CV) is around 381 K. On the sump the temperature is around 363 K as the condensers wet part. The walls and the dry part of condensers have a temperature of 383 K in order to inhibit the condensation. Also, in order to prevent the hydrogen combustion with oxygen, the quantity of nitrogen is increased up to 95% of the atmosphere composition. In the containment, condensation occurred on the condensers up to 23000 s. The remaining non-condensed steam provided an average humidity ratio of about 60% in the containment for the aerosol phase. Almost no condensation occurred on containment surfaces other than on the wet part of condensers. The aerosol deposition with steam condensation (diffusion-phoresis) has occurred on the wet condenser surfaces up to 23000 s. Then aerosol sedimentation on the containment bottom by gravity has become the main aerosol deposition mechanism. Deposition on the other heat structures was negligible. The FPT1 is an important key test in order to understand the progression of a severe accident. The ISP46 experience [3] is used in several analyses and benchmarks in order to qualify the models present in the codes.

4.2 FPT1 Nodalizations

In order to define the capabilities of both codes to predict the thermodynamic behavior and aerosol transport phenomena during the FPT1 test, a similar nodalisation was set up for the simulation of the FPT1 test (Figure 4.1). This figure refers to the MELCOR [4] simulation, but core

and circuit are structured similarly in the case of ASTEC. The differences are on the definition of the thermal-hydraulic control volumes named Fluid Elements in the case of ASTEC [5]: ICARE creates some components as intersection of MESH distribution (10 vertical elements) with the 2 Fluid dynamic elements. The Core active length (approximately 1 m of height) is subdivided in 10 parts; with the bottom 3 other mesh rings used to simulate the fluid-dynamics at the inlet of the bundle. The components simulate the melting phenomena and the hydrogen production; also they are used to predict the ICARE boundary conditions. The coupling with CESARE predicts the thermo-hydraulic behavior of the Fluid Elements. Also the distribution of the power is important to simulate correctly the release of FP from the bundle.

The COR package of MELCOR allows a similar matrix with the difference that the fluid dynamic elements are 2 CVH with associated 22 COR nodes for active length, divided in 2 rings (11 axial nodes). These nodes are divided in materials proportional to the 21 rods.

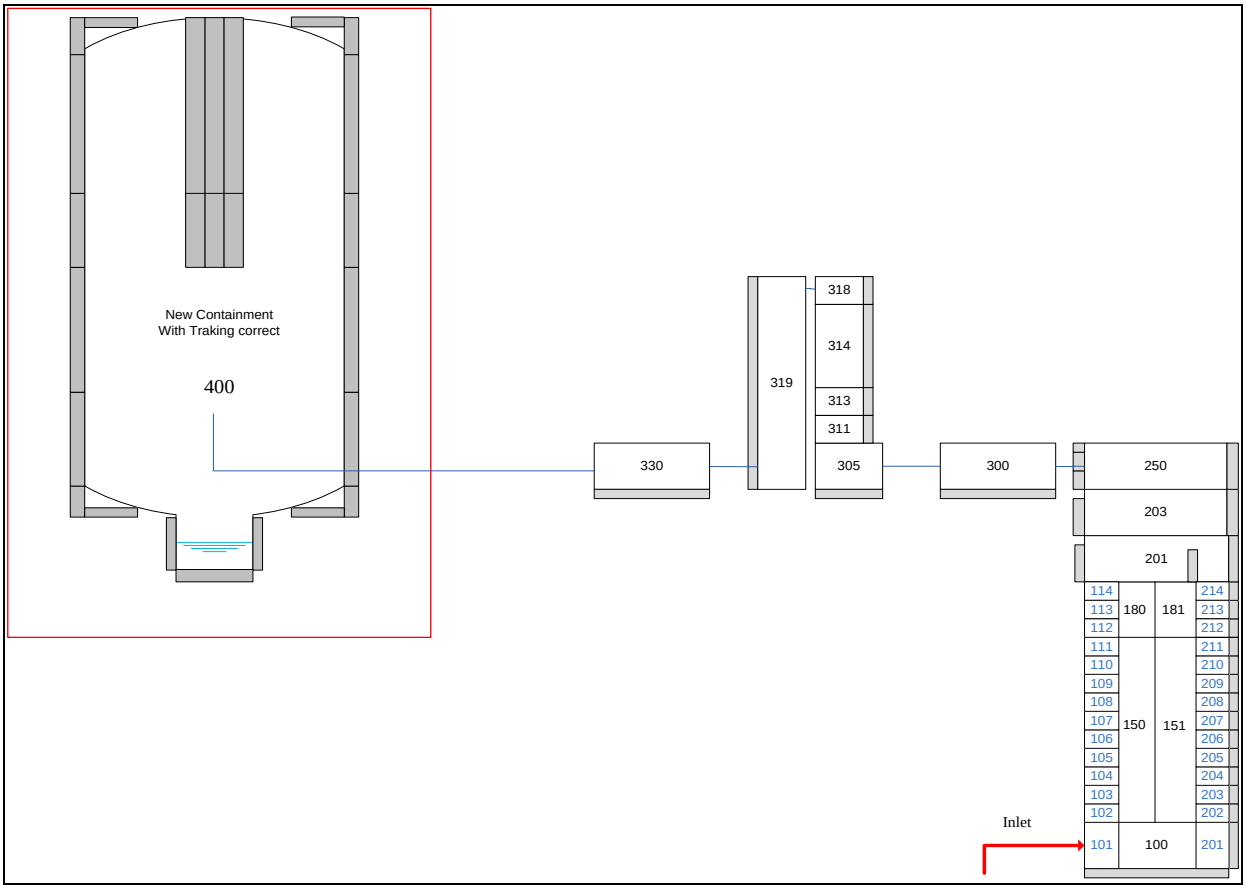

Figure 4.1 PHEBUS nodalization with MELCOR code

The nodalizations have been set-up on the basis of ISP 46 specifications [6] [7].

The boundary and initial conditions, imposed to simulate the evolution of the first part of the FPT1 test, are very important in order to define the sequence. In the present calculations the experimental steam, hydrogen and aerosols source rate, as measured at the containment inlet, are applied in order to eliminate the uncertainties related to aerosol deposition along the test circuit.

In order to define the capabilities of both codes to predict the CV thermodynamic behaviour and aerosol transport phenomena, also CV similar nodalisations were set up for the simulation of the FPT1 test (Figure 4.2):

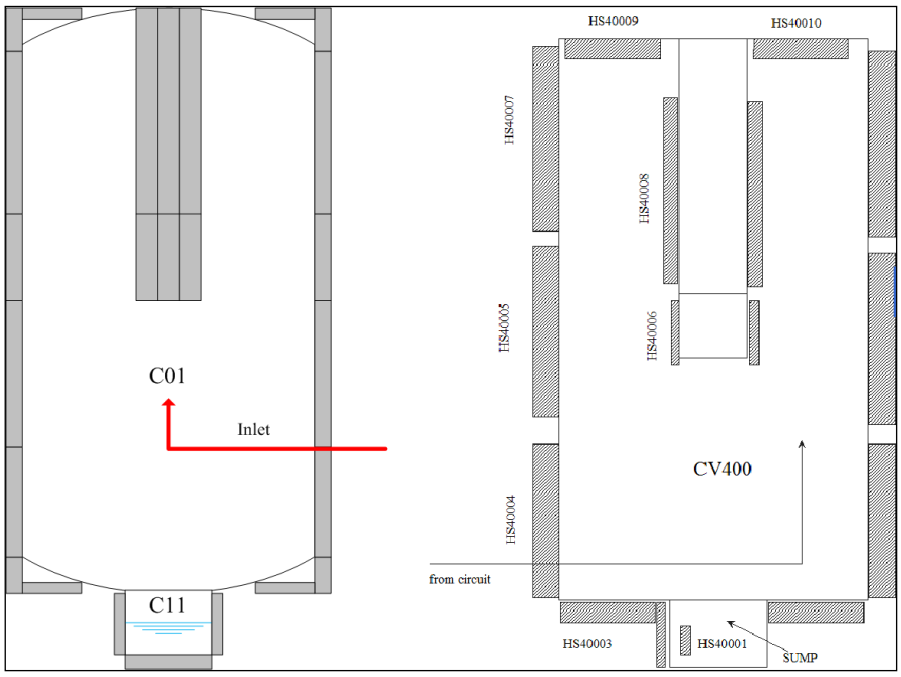

Figure 4.2 Containment Vessel nodalizations with ASTEC and MELCOR codes

Two control volumes are considered for the CV main volume and the sump respectively, linked by a junction flow-path. Care was devoted to the simulation of dry and wet heat structures, where steam and aerosols could condensate and settle.

A non-equilibrium model is applied in both codes for the simulation of the containment atmosphere and sump thermal-hydraulics. Condensation heat and mass transfer on the structures are also automatically accounted for, while the models for gravitational settling, diffusion-phoresis and thermo-phoresis are activated with similar physical parameters for the considered aerosols classes.

4.3 Validation and qualification process of FPT1 nodalizations

The choice of the FPT1 [1] in order to develop the nodalization for the analyses the FPT2 [8] and FPT3 [9] tests sequences is consequence of the experience earned in DINMP during several years of analyses on the SA phenomenology with respect to the thermo-hydraulics and aerosol behavior in vessel, primary circuit and containment. Many benchmarks were done in order to evaluate the capability of the users and the codes to follow the phenomenology involved in a severe accident. The first version of the FPT1 nodalization started from the ISP46 [6] [7] work analyzing only the containment behavior, in order to gain the first sensibility of the ASTEC and MELCOR codes performance.

The simulation starts with the release of steam, hydrogen and FP t from the pipe, which simulates the cold leg and enters in CV.

After that, progressive addition of the Circuit, from the Test Section to CV, as in the case of ISP46, was implemented. In this way, the investigation of the bundle degradation phenomena in this PHEBUS test was performed [10]. Practically we enter in SA complete analyses, with the evaluation of the models that simulate the release of FP aerosols and gas, hydrogen production from the chemical reactions of Zyrcaloy and other structural materials and the material relocation. This is the first step in order to obtain a version of the nodalization to be used in the analyses of FPT2 and FPT3, in order to have an idea of the capability of the codes to simulate SA transients.

4.4 Main Results Evidenced from the FPT1 Analyses

4.4.1 *Only Containment Main Results*

The thermodynamic and aerosol behaviours of the containment atmosphere during FPT1 [11], as predicted by MELCOR and ASTEC, are presented from Figure 4.3 to Figure 4.10. Both codes show evidence of an over-estimation of the atmosphere pressure (Figure 4.3) during the steaming phase.

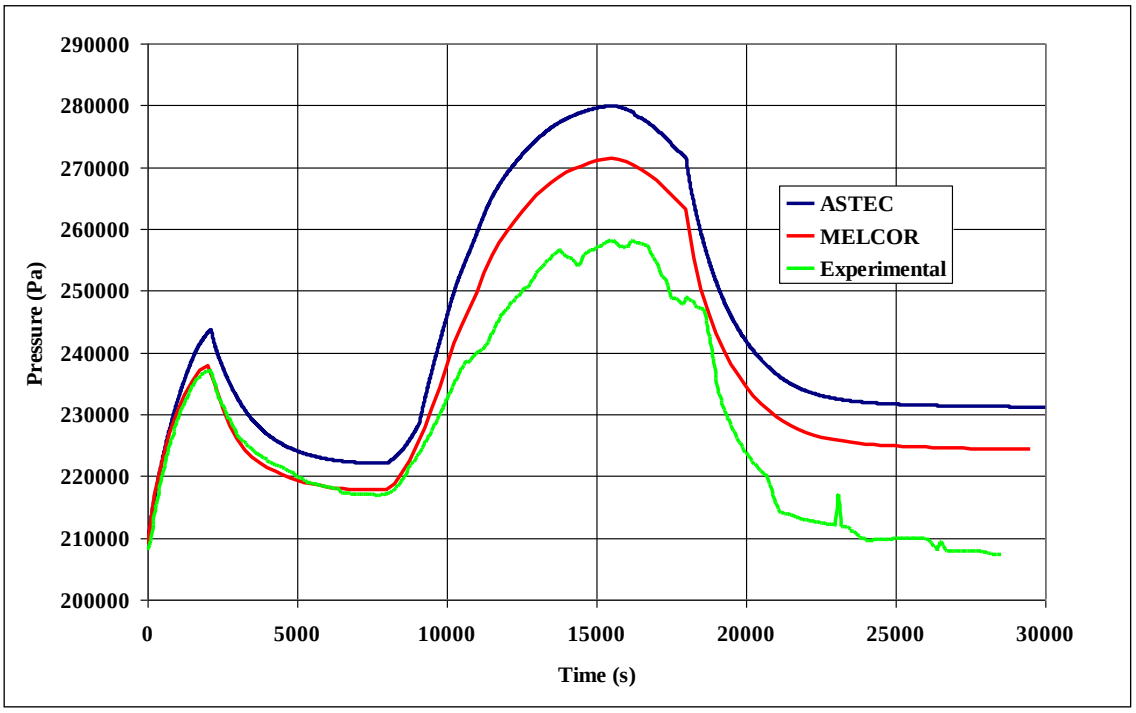

Figure 4.3 Containment atmosphere pressure

On the other side, Figure 4.4 shows a good agreement between the predicted values of the containment atmosphere temperature and the experimental data for both codes, even though ASTEC calculation results are slightly higher.

The overestimation of the atmosphere pressure can be explained by the larger values of the atmosphere relative humidity (Figure 4.5) if one eliminates the initial under-estimation of this parameter with respect to the experimental value; this is probably due to an insufficient condensation heat transfer onto wet condensers and in the lower sump. Condensation heat and mass transfer on containment heat structures is one of the most important thermal-hydraulic feature influencing aerosol dynamics and, in particular, the diffusio-phoresis towards cold structures.

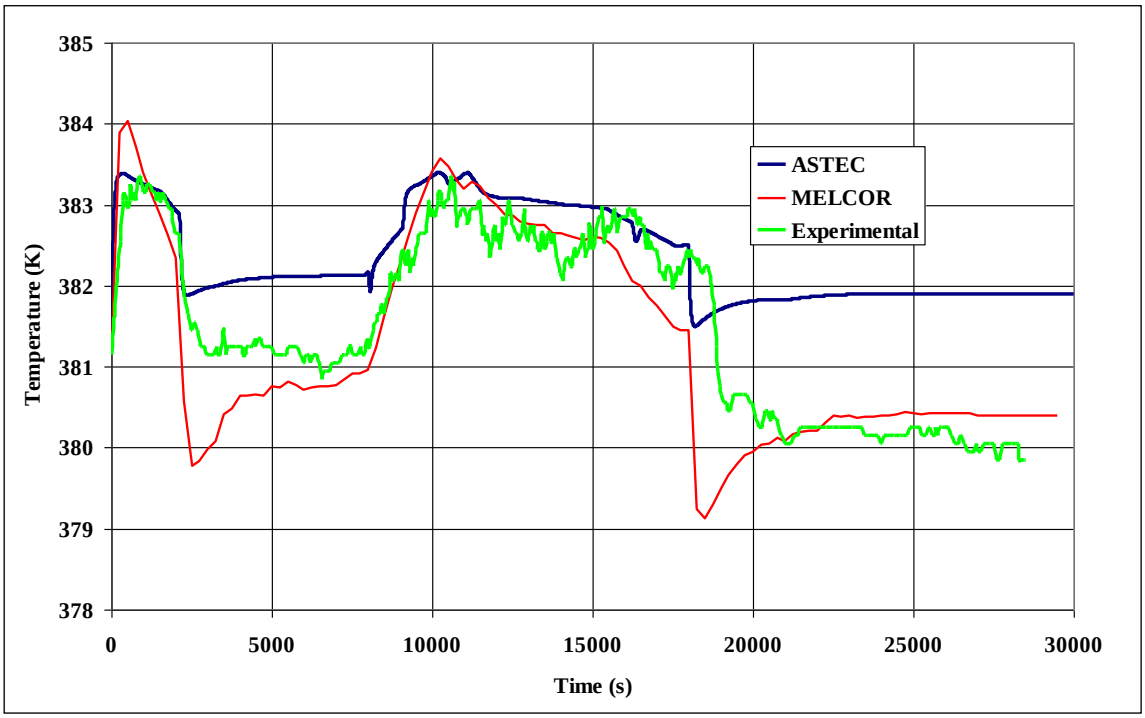

Figure 4.4 Containment atmosphere temperature

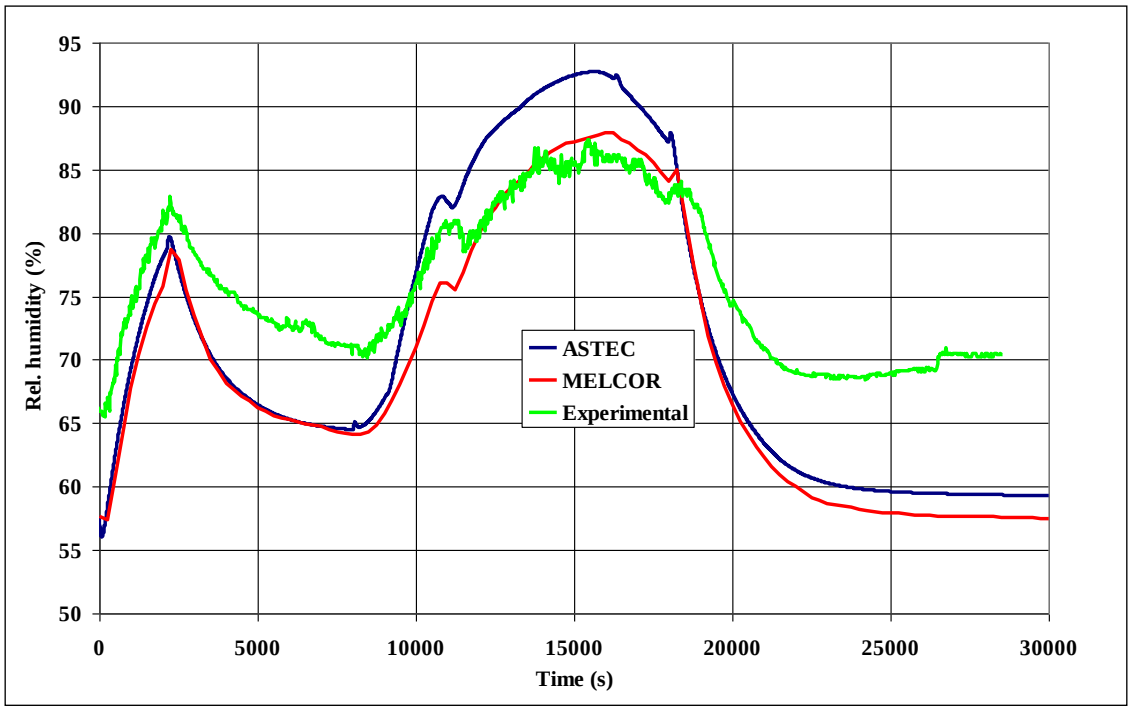

Figure 4.5 Containment relative humidity

Figure 4.6 shows that the ASTEC code predicts a slightly higher condensation on the wet condensers with respect to the total condensation flow-rate measured from condensate level sensor.

This can still be explained by the higher humidity (and therefore the higher steam partial pressure) predicted in the containment atmosphere. The MELCOR code instead predicts a slightly lower mass condensation rate onto the wet condensers, even though a very good qualitative agreement is shown.

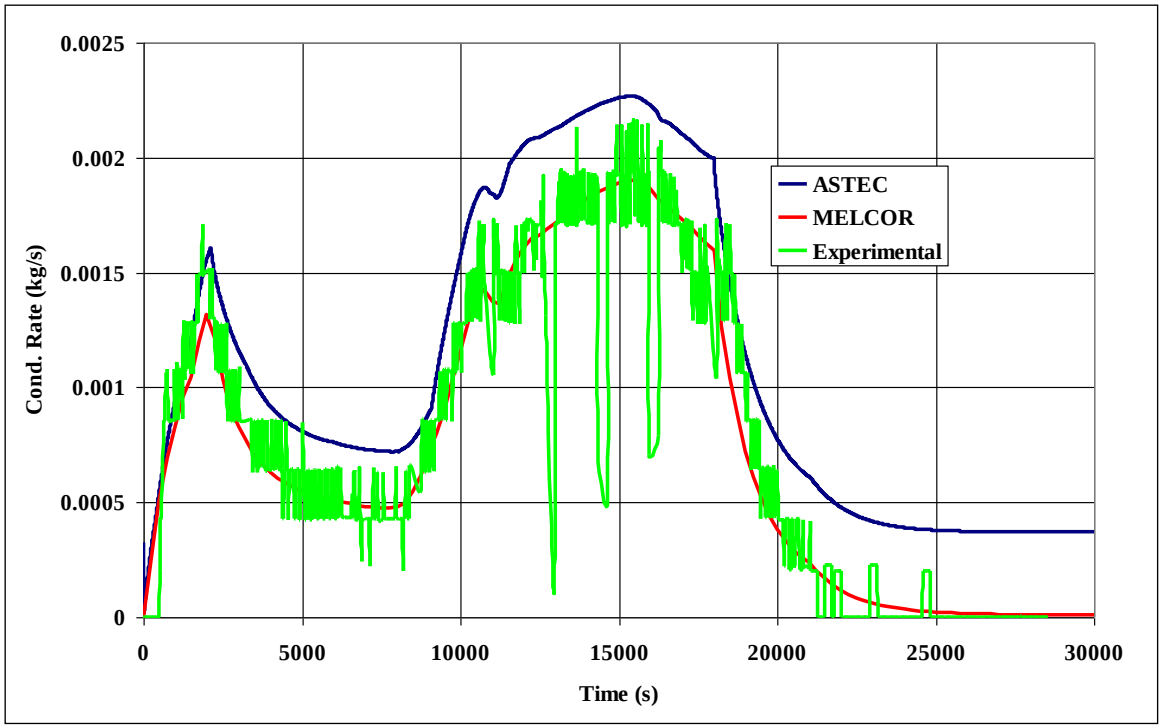

Figure 4.6 Condensation heat transfer on condensers

Concerning aerosols dynamics, the Figure 4.7 shows the total mass of aerosols suspended in the containment atmosphere during the experiment. The analysis of this variable shows that both MELCOR and ASTEC codes predict higher values with respect to the experimental evidence during the first phase of the test. During the first 15000 s of the transient, the aerosol deposition by diffusio-phoresis on the wet condensers is quit high and it is under-estimated by the codes. When the gravitational settling become the most important deposition mechanism, the predicted aerosol suspended mass shows a better agreement with experimental data.

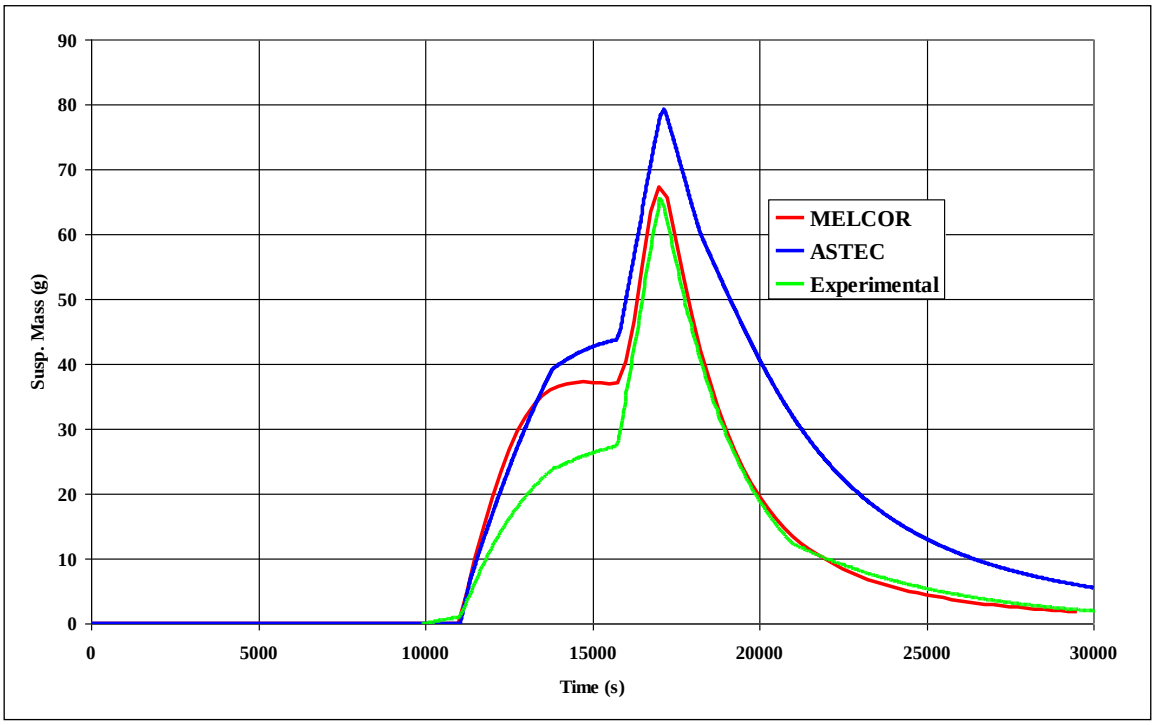

Figure 4.7 Total suspended aerosols mass

In Figure 4.8 the total amount of aerosols depositing onto the heat structures and in the lower sump of the containment vessel is presented as a function of time. As expected the MELCOR code predicts a larger overall deposition than ASTEC code. As the modelling of aerosol gravitation settling is the same, the difference in the deposition rate is due to the diffusion-phoretic mechanism. Despite the ASTEC code evaluates a larger condensation mass transfer to the wet condensers; the lower diffusion-phoresis is probably due to the larger atmosphere density that is predicted for the containment atmosphere. In the Waldmann model used by both codes in fact the diffusion velocity is inversely proportional to this density.

The amount of aerosols deposited onto the containment heat structures (basically on to the lower bottom elliptical shell) provides a clear evaluation of the relative importance of the two main deposition aerosols mechanisms. Figure 4.9 shows that almost 66% of the aerosols entering the PHEBUS containment vessel falls down due to gravitational settling.

Finally, Figure 4.10 shows the calculated mass of suspended Uranium aerosol vs the experimental data. Both ASTEC and MELCOR codes are able to capture aerosol concentration (actually ASTEC overestimates this quantity, but the trend is taken), proving their good capabilities

in the simulation of the main thermal-hydraulic phenomena taking place in a containment system following a severe accident, as well as the most important aerosol dynamics mechanisms.

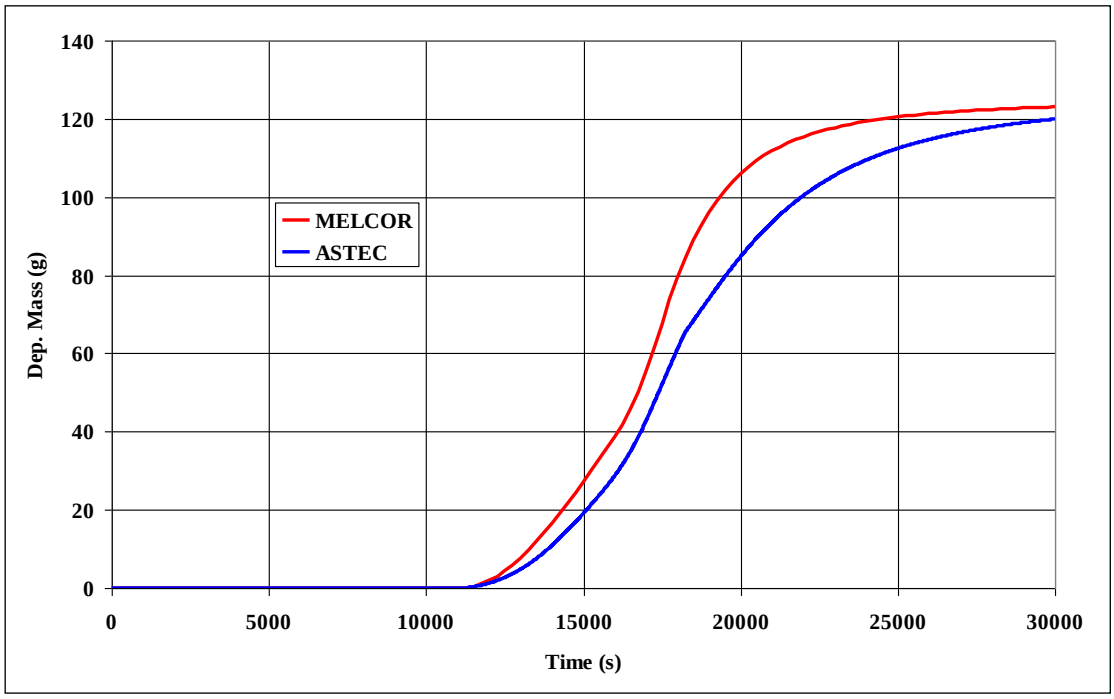

Figure 4.8 Total aerosols deposited mass

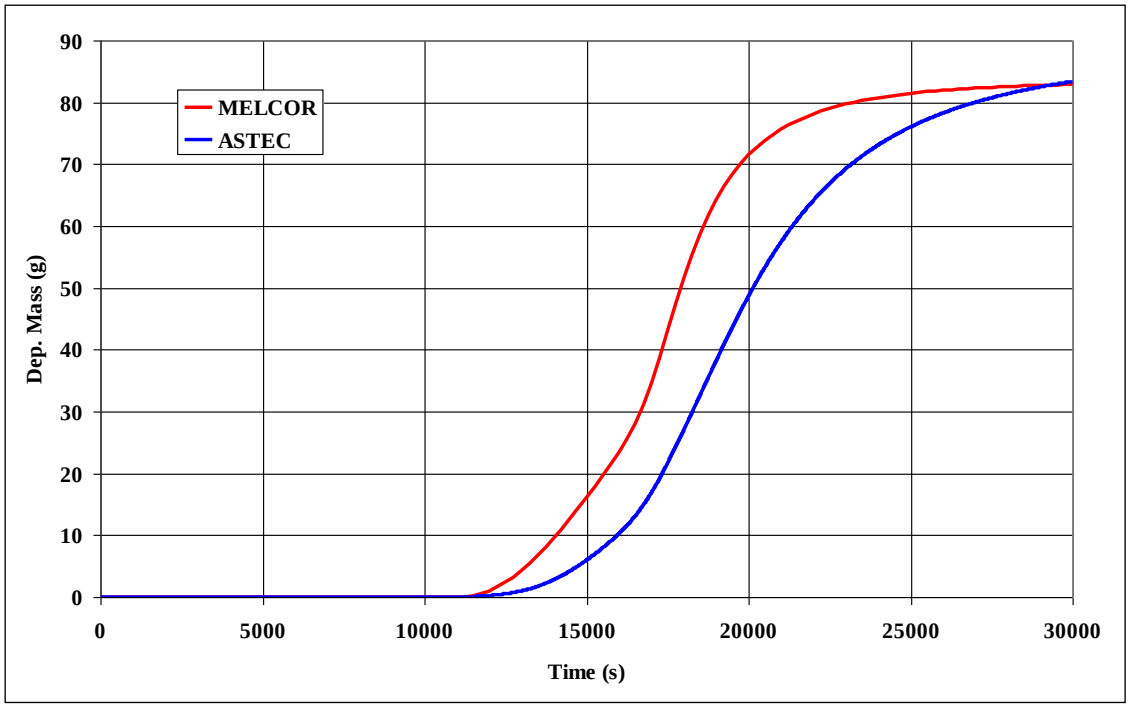

Figure 4.9 Mass of aerosols deposited on heat structures

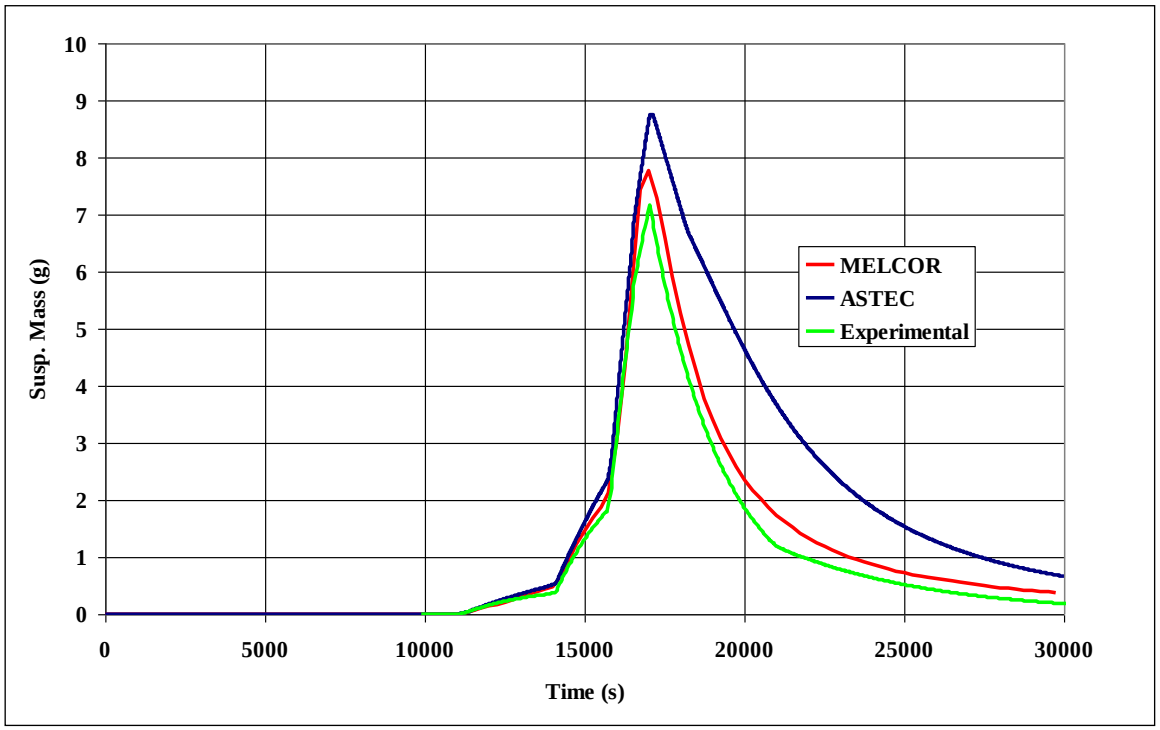

Figure 4.10 **Uranium aerosol suspended mass**

4.4.2 *Full Nodalization Main Results*

The main results of the FPT1 simulation [12] by MELCOR and ASTEC with the full nodalization are presented from Figure 4.3 to Figure 4.109.

The slight overestimation of the fuel temperature for both codes can be explained with the uncertainties of the measures, particularly near the relocation temperature point of the fuel and clad material (Figure 4.11 and Figure 4.12). Anyway, both codes are able to represent the mechanism of candling, relocation and pool formation, even if some differences are shown in the timing.

The general good agreement of the fuel temperature trends is due to the good modelling of the bundle power profile as a function of time, as well as of the axial and radial profiles. In particular the axial profile has the same mesh detail for both codes. Also sophisticated models are used in order to simulate the dynamics of the cladding failure and fuel degradation as function of the linear power.

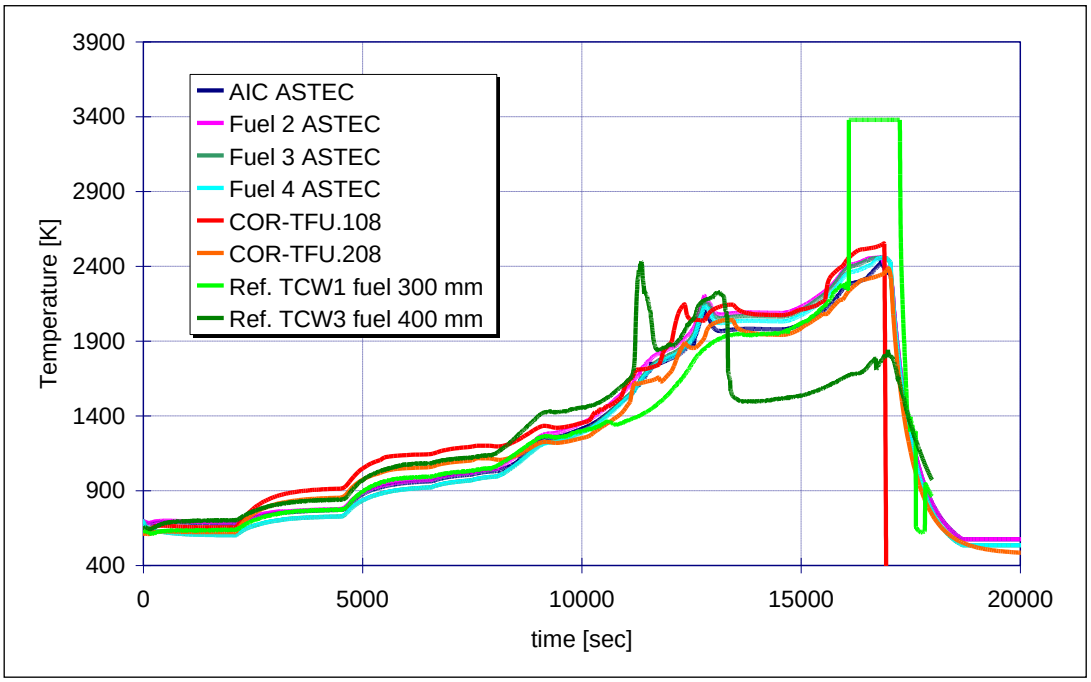

Figure 4.11 Fuel temperatures between 0.30 m and 0.40 m of active length

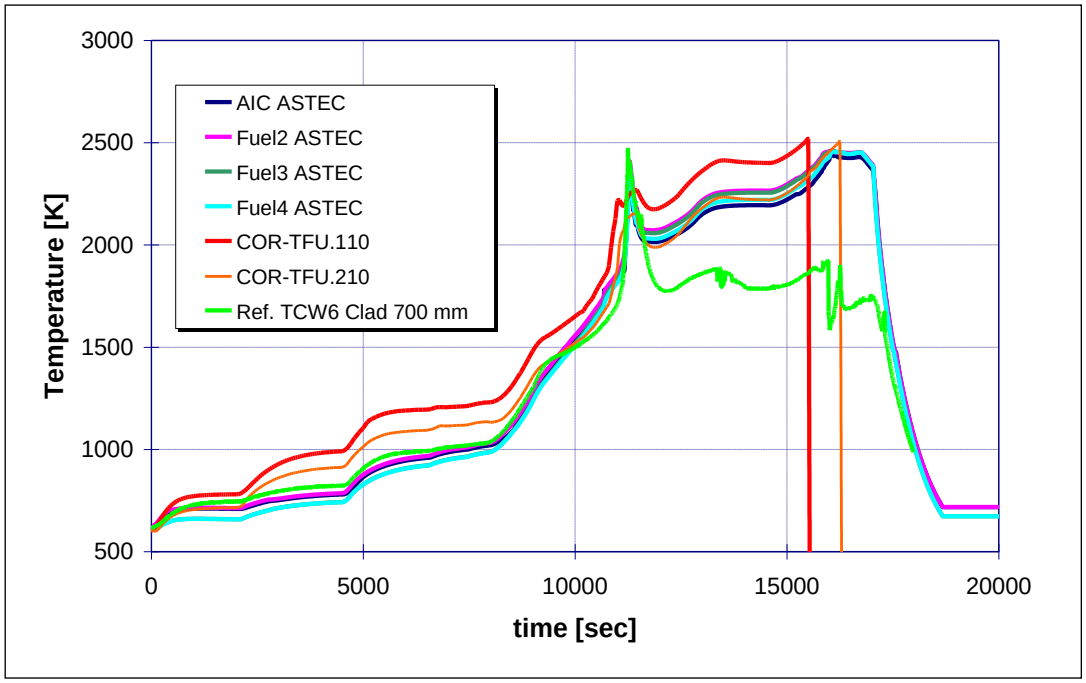

Figure 4.12 Fuel temperature between 0.60 m and 0.70 m of active length

In order to clarify the dynamics of the bundle phenomenology, a qualitative idea of the progression of the bundle degradation is presented in the figures 2.13 – 2.15. These figures show the test evolution from "rod like geometry" to late phase phenomena; the sequence is distributed in

3 sketches at 3 different times. In each figure, on the left there is a representative sketch extracted from ASTEC code in comparison (on the right) with the descriptive illustration found in FPT1 Final Report. ASTEC evidences behaviour similar to TMI, with the start of degradation from the Top of Active Fuel (TAF).

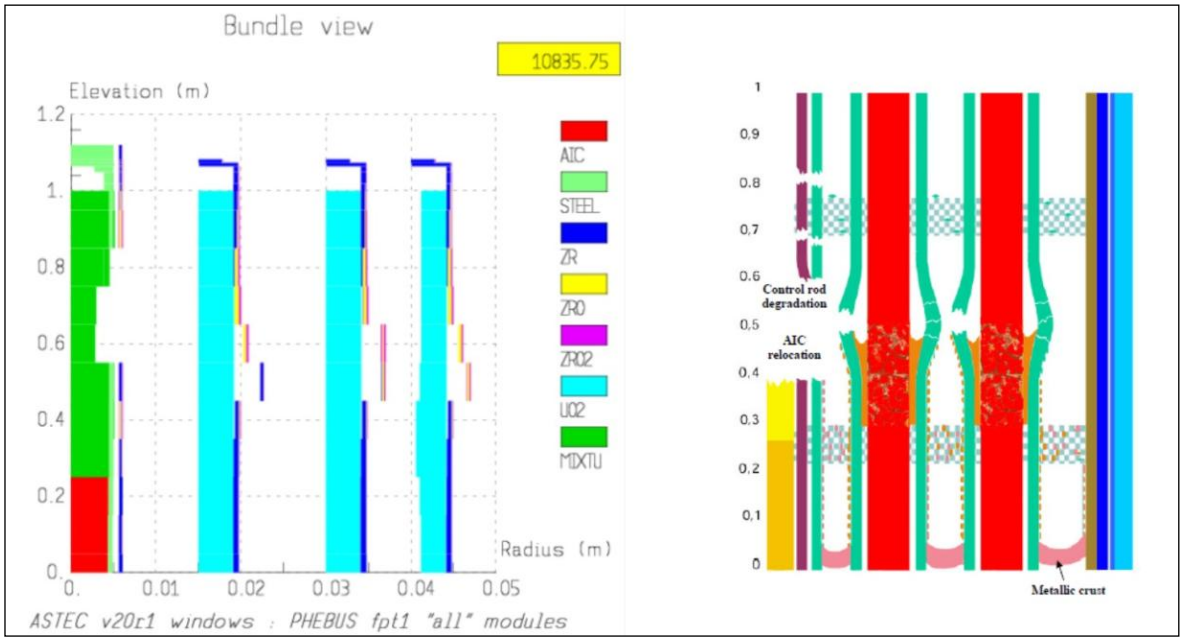

Figure 4.13 Bundle Sketches at ~11000 s

In the first figure (Figure 4.13) at 11000 s, the geometry is al most integral except for the Silver Indium and Cadmium rod (SIC) that starts the large relocation of the material in the bottom of the active length. In particular, the FP volatile release of the elements is concentrated in this period due to large damages of the claddings.

About an hour later, the high damage of the SIC is extended to the geometrical structure of bundle, allowing a large release of FP, not only volatile, but also the semi volatile ones. The candling becomes extended on the lower middle part of the rods, with some small relocation of fuel material (Figure 4.14).

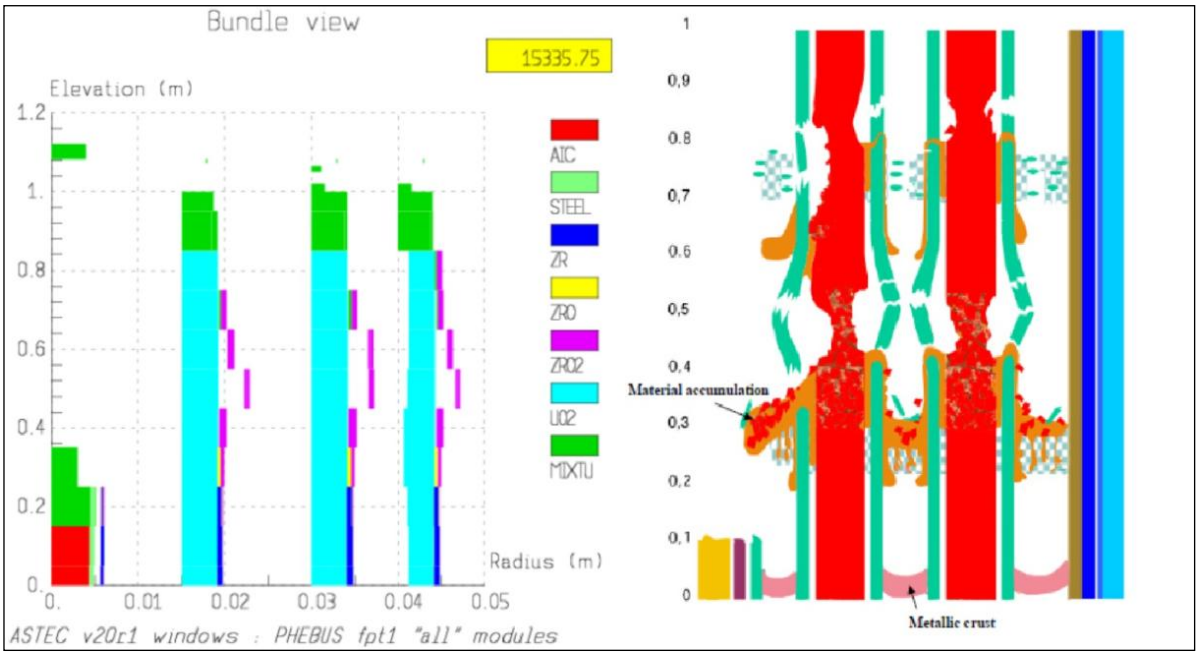

Figure 4.14 Bundle Sketches at ~15380 s

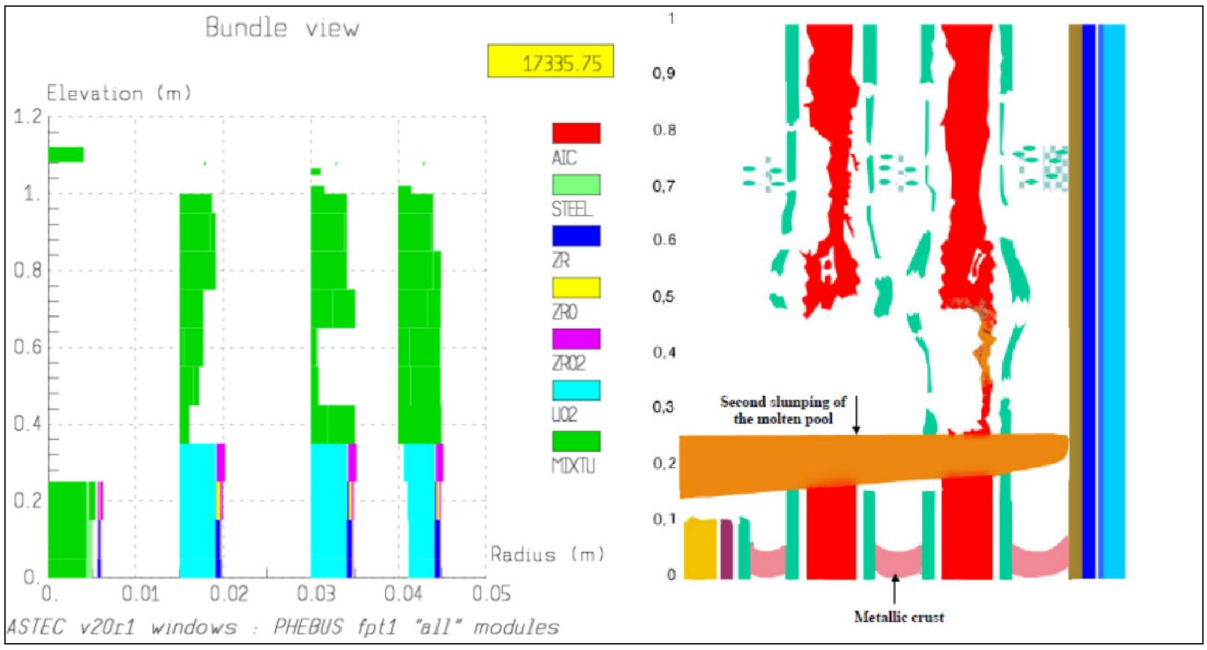

Figure 4.15 Bundle Sketches at ~17300 s

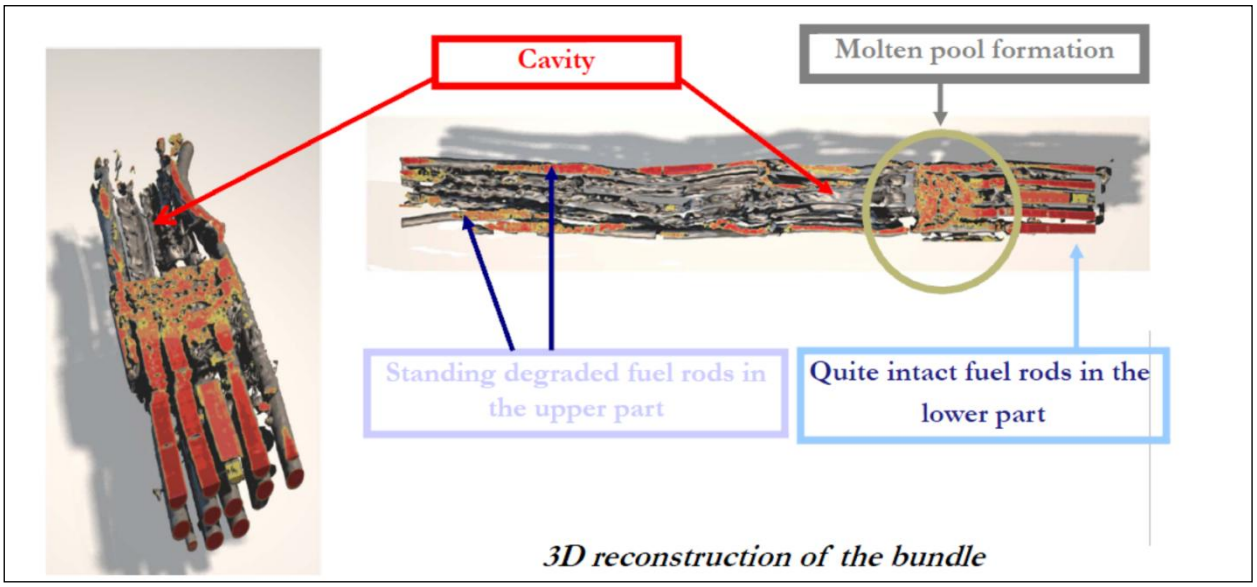

Figure 4.16 reconstruction of the bundle of FPT1 after degradation phase [1]

FP Element	References	ASTEC V2.0 R1	MELCOR 1.8.5
Nb_{95}	<1	0.03	16.65
Zr_{95}	<1	0.03	$1.37*10^{-04}$
Ba_{140}	<5	5.94	3.08
I_{131}	87(±4)	74.75	7.13
Te_{132}	83(±1)	73.06	100.0
La_{140}	<5	0.03	0.02
Cs_{137}	84(±0.8)	75.60	54.59
Mo_{99}	56(±4)	70.10	16.65
Ru_{103}	<5	1.96	$6.58*10^{-04}$
Ag_{110m}	15(±5)	74.32	45.16

Table 4.1 FP and molten material mass release fractions (in %)

Release (g)	References	ASTEC V2.0rev1	MELCOR 1.8.5
Bundle	206.51	260.21	59.15
Test Section and Circuit	75.81	141.94	26.70
Containment	130.7	118.27	32.45

Table 4.2 Mass distribution in FPT1 complete case

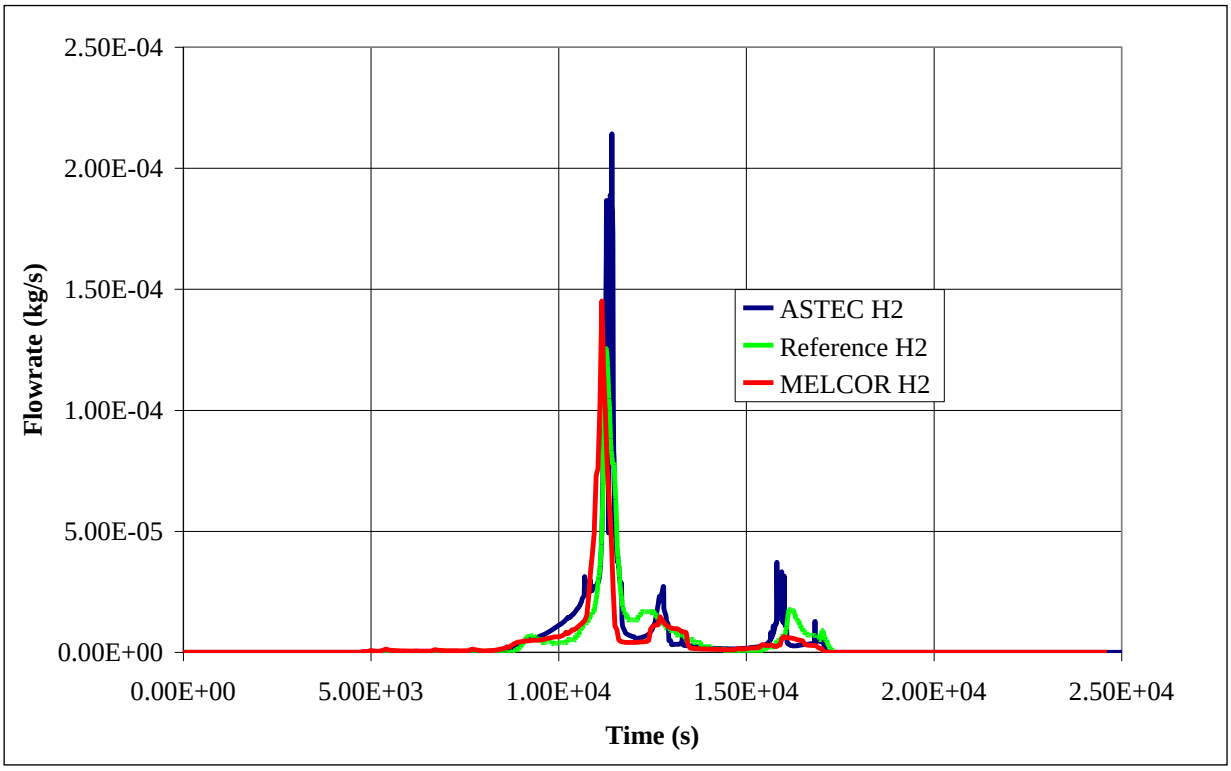

Figure 4.17 Hydrogen production rate

Finally, at 17300 s most of the bundle geometry is lost with a creation of a melt pool near 0.20 m from the BAF (Figure 4.15 and Figure 4.16). There is also the formation of a crust due to the relocation of material that inhibits the hydrogen production, as shown in Figure 4.17. The FP releases at the end of degradation phase of the bundle are reported in Table 4.1.

The ASTEC code is able to predict correct release factors for most of the elements.

The MELCOR code shows some discrepancies in the prediction of the FP releases, even though it gives good results in the prediction of the behaviour of the relocation phenomena and pool

formation, with correct hydrogen production rates. The subroutine CORSOR-BOOTH of MELCOR uses less complex models in comparison with ELSA subroutine of ASTEC; in particular, it cannot take into account the structural materials (SM) release, unless some sensitive factors are used in order to evaluate of the fraction of this material in comparison with FP. Moreover, MELCOR has not a model for aerosol release from the molten pool (ASTEC with MAGMA special features is able to simulate this phenomenon).

The thermal-hydraulics and aerosol dynamics inside the containment with the full nodalization is presented in the Figure 4.18 and Figure 4.19.

ASTEC over-estimates the atmosphere pressure (Figure 4.18) during the steaming phase. MELCOR calculation is in better agreement with the experiment, apart from an under-estimation of the first part of the curve.

Concerning aerosols dynamics, the Figure 4.19 shows the trends of total mass of aerosols suspended in the containment atmosphere. Both codes present a similar behaviour, taking into account the different release magnitudes (Table 4.2). Both codes show some discrepancies in the timing of the release of FP and SM, as highlighted in Figure 4.19; in particular ASTEC anticipates the release before 10000 s

Once the release of Aerosol is ceased, when the gravitational settling becomes the most important deposition mechanism, the predicted aerosol suspended mass shows a better agreement with experimental data. This is due to the fact that they use MAEROS to address this item and consider similar thermo-hydraulic results to calculate the diffusion and thermo-phoresis. As the modelling of aerosol gravitation settling is the same, the difference in the deposition rate is due to the diffusion-phoretic mechanism.

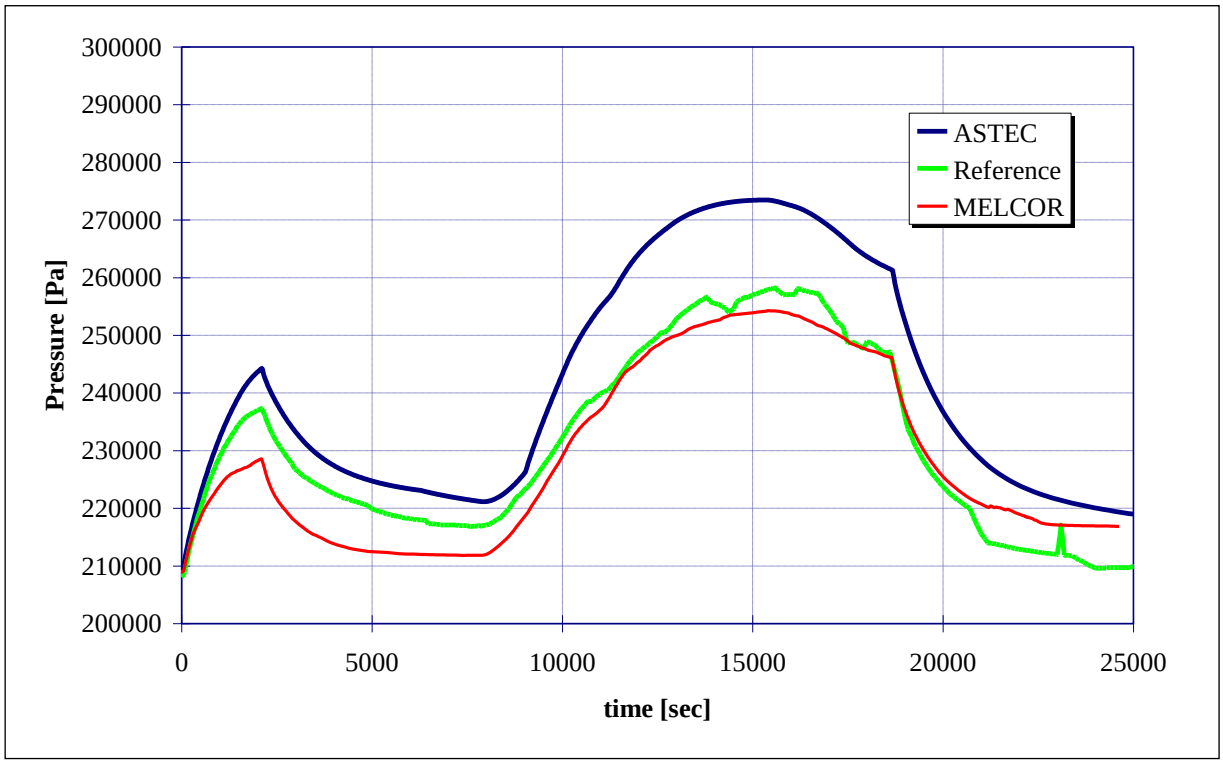

Figure 4.18 Containment atmosphere pressure

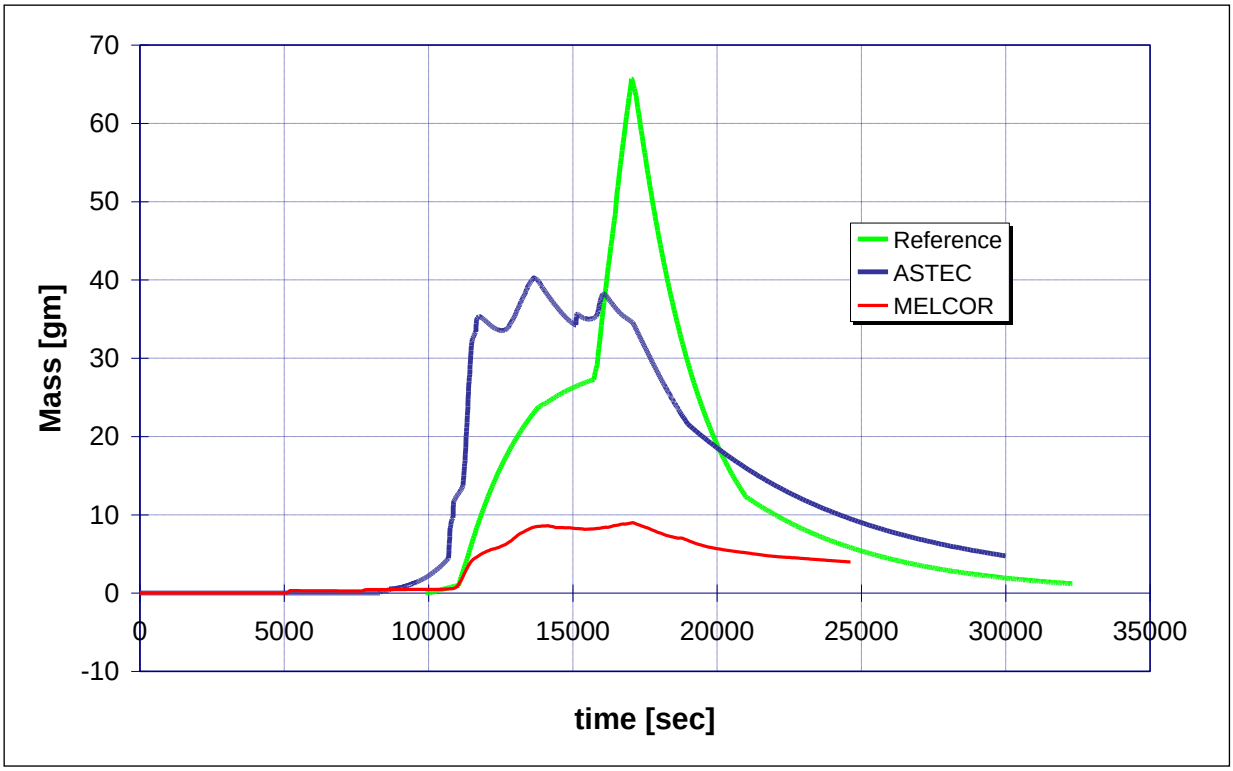

Figure 4.19 Total aerosols suspended mass

References

[1] D. Jacquemain, S. Bourdon, A. de Braemaeker and M. Barrachin, FPT1 Final Report (Final version) IPSN/DRS/SEA/PEPF report SEA1/00, IP/00/479, December 2000.

[2] A. Kontautas, E. Urbonavicious. Analysis of aerosol deposition in PHEBUS containment during FPT-1 experiment, *Nucl. Engineering and Design* – vol 239 (2009), pp 1267-1274.

[3] T. Haste, Specification of International Standard Problem ISP-46 (Phebus FPT1), Revision 0, IPSN Note Technique SEMAR 01/91, November 2001.

[4] R. Gauntt et al. MELCOR Computer Code Manuals Vol. 2: Reference manual, Version 1.8.6, September 2005 - NUREG/CR-6119, Vol. 2, Rev.3 SAND2005-5713 - Sandia National Laboratories.

[5] J. P. Van Dorsselaere et al. The ASTEC integral code for severe accident simulation, *Nucl. Technology* – NT-3-0846, vol.165, March 2010

[6] A. Manfredini, F. Oriolo, S. Paci," VALIDATION OF THE MELCOR V.1.8.5 CODE AGAINST THE FPT0 AND FPT1 PHEBUS EXPERIMENTAL TESTS", DIMNP, RL 932 (01), 2001

[7] A. Manfredini, F. Oriolo, S. Paci," DIMNP PRE TEST CALCULATIONS OF THE OECD/CSNI ISP-46 ON PHEBUS TEST FPT1 USING THE MELCOR V.1.8.5 COMPUTER CODE", DIMNP, DIMNP 006 (02), 2001, Paper presented at the Intermediate Comparison Workshop on "International Standard Problem 46" Aix-en Provence (F), 21 – 23 October 2002

[8] A. C. Greogoire, et ali., "FPT2 Final Report (Final version)", IRSN. N° PH-PF: DOCUMENT Phébus PF, IP/08/579, Febbrary 2008.

[9] A. Bieliauskas, T. Haste, "SPECIFICATIONS OF SARNET2 PHEBUS FPT3 BENCHMARK", IRSN, DPAM-SEMIC-2011-057, 5/07/2011

[10] Luis E. Herranz, Mònica Vela-Garcìa, Joan Fontanet, Claudia Lòpez del Prà, "Experimental interpretation and code validation based on the PHEBUS-FP programme: Lessons learnt from the analysis of the containment scenario of FPT1 and FPT2 tests", Nuclear Engineering and Design 237 (2007) 2210–2218, 22 March 2007

[11] G. Mazzini, A. Manfredini, Analysis of the Thermal-hydraulic and Aerosol Behaviour in the Phebus Containment Vessel During the FPT1 Test Using MELCOR and ASTEC Codes, *XXVIII Congresso UIT sulla Trasmissione del Calore*, Brescia (2010).

[12] A.Manfredini, G. Mazzini "Analysis of the Phenomena Occuring in the PHEBUS During the FPT1 Test Using MELCOR and ASTEC", 29th UIT National Heat Transfer Conference 2010, Torino, Giugno, 2011

5 PHEBUS FPT2 AND FPT3 ANALYSES

5.1 FPT2 and FPT3 Nodalizatios

As for FPT1, in order to define the capabilities of both codes to predict the thermodynamic behavior and aerosol transport phenomena during the FPT2 and FPT3 tests, a similar nodalisation was set up for the simulation of the tests (

Figure 5.1). The

Figure 5.1 refers to the MELCOR simulation, but core and circuit are structured similarly in the case of ASTEC. The Nodalizations were prepared for FPT3 Benchmark in the framework of SARNET 2 research program.

The Circuit is nodalized in a little bit different way. As for ISP46, the MELCOR Nodalization is characterized with a single Hot Leg. In the case of ASTEC, the Nodalization based on the Benchmark configuration has the Hot Leg divided in two parts.

Finally, it shall be noticed that also the distribution of the power is different among the various tests, because it is very important to simulate correctly the release of FP from the bundle.

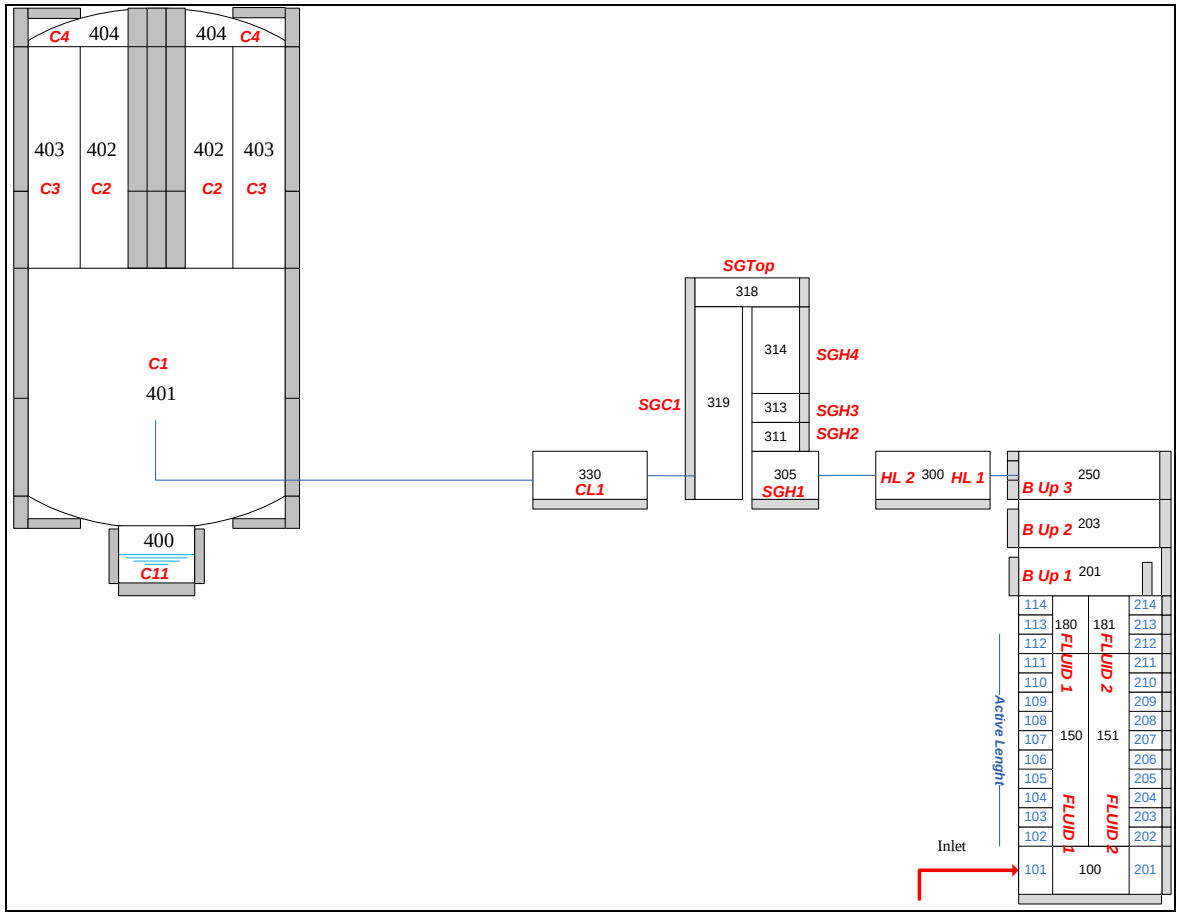

Figure 5.1 FPT2 and FPT3 Nodalizations

5.2 FPT2 and FPT3 Description

The fuel bundle burn-up, as already said, is one of the most important key in order to investigate the capability of the codes in the evaluation of FP releases. The irradiated fuel rods at different Burn-up, ~ 32 GWd/tU for FPT2 and ~ 24.5 GWd/tU for FPT3, have different FP mass inventories. Higher is the burn-up higher is the mass of each element and related isotopes present in the initial inventory. The data related to FPT2 and FPT3 are reported in Table 5.1.

As with most of the other PHEBUS experiments, FPT2 was conducted through three main phases:

- the fuel degradation phase during which the fuel bundle, with incorporated a silver/indium/cadmium control rod, was heated to a maximum of ~2500 ◦C; bundle

degradation occurred and fission products were released and transported through the primary circuit to the containment in a flow of steam/H_2;

- the aerosol phase, in which injection and depletion of aerosols governed the evolution of the source term in the containment; this period lasted for about 37 h;
- finally, the chemistry phase (about 48 h after the beginning of the test) which lasted about 50 h, during which the main focus was on the iodine evolution within the containment.

The airborne concentrations of various radio-nuclides (including ^{131}I) in the containment were monitored during the fuel degradation and subsequent aerosol phases.

After about 48 h (i.e. the start of the chemistry phase), the hemispherical bottom of the containment vessel was washed by recirculating sump water to transfer deposited aerosol into the sump, marking the end of the aerosol phase. Measurements of the airborne concentration of iodine then continued during the chemistry phase, which lasted for further 50 h. The containment sump was maintained at a pH of ~9 using a boric acid/borate buffer. The sump temperature was 90 ◦C during the aerosol phase, and was increased to 120 °C for the chemistry phase. The temperature of the containment atmosphere was maintained at 90 °C throughout the test, leading to a cycle of sump evaporation and condensation. The condensate descended to the sump via the walls and the painted condensers suspended in the vessel.

The main experimental observations on iodine behavior in the containment are summarized as follows:

- About 55% of the iodine inventory (Table 5.1) of the fuel bundle was released and transported to the containment vessel; mainly it was detected as aerosol, but a small gaseous fraction was detected during the fuel degradation/fission product release transient. There was no direct experimental evidence for the presence of gaseous iodine in the circuit.
- The gaseous iodine concentration decreased rapidly by about an order of magnitude from its initial peak, and then gradually increased throughout the aerosol phase. The concentration again fell rapidly at the start of the chemistry phase, and continued to fall

throughout the remainder of the test. The gaseous iodine was predominantly inorganic in nature, with organic species accounting for less than 30% of the total in all samples.

- Iodine in the sump was predominantly present in a soluble form. This contrasts with the behavior observed in the previous tests (FPT0 and FPT1) where the iodine in the sump was mainly in an insoluble form, most probably AgI formed by reaction with silver aerosol released from the control rods. An increase in the amount of insoluble iodine occurred during the chemistry phase, and in particular at the end of the test when the sump was cooled.

- The iodine activity measured on the vertical containment wall decreased gradually during the later part of the aerosol phase and throughout the chemistry phase. In contrast to FPT1, no strong decrease of the iodine activity from the painted condenser surfaces was observed; the results suggest an increase in the activity during the second half of the aerosol phase. A small decrease in the activity of several elements, including iodine, on the condenser was observed at the start of the chemistry phase and can probably be attributed to washing by the condensate flow. (Note: the low and decreasing, airborne iodine concentration during the chemistry phase occurred despite the increasing soluble iodine fraction in the sump.

In FPT3 (Table 5.1), iodine was almost totally released from the fuel bundle (about 87% of the initial bundle inventory), probably as a vapor/gas, considering the high temperatures reached in the fuel and the different chemistry of the control rod. In FPT2, the fraction of iodine released from the fuel bundle is slightly lower (about 73% of the initial bundle inventory; value estimated from deposits in the circuit and iodine injected in the containment). This difference could be attributed to the lower temperatures in the FPT2 upper rods of the fuel bundle compared with those of FPT3. Indeed, at this location, the lower temperatures throughout the degradation phase, in part attributed to the lower steam flow rate (2g/s in FPT0/FPT1 and 0.5g/s in FPT2and FPT3) lead to an important iodine retention fraction in FPT2, not observed in FPT1. The poor steam flow rates allow the steam starvation phenomena. All steam is used to produce hydrogen and the partial pressure of steam falls down in comparison with the incondensable partial pressure in the Circuit.

As for FPT2, in FPT3 during the fuel degradation phase the inlet steam flow rate injected at the bottom of the test train was set to 0.5 g/s, providing oxidizing conditions for fission product chemistry, while the bundle power was progressively increased up to 32.8 kW. The injected fluid was pure steam, with no additional substances such as boric acid or hydrogen. The pressure in the experimental circuit during the test was maintained roughly constant at ~ 2 bars.

One of the most important aspects of FPT2 is the control rod behavior. The interactions of Ag-In-Cd (SIC) control rod involve three stages:

1. SIC melting at T~1050 K. SIC relocates inside its cladding; this allows important interactions, due to the contact between Zr and SIC. The relocated material changes the local conductivity of the control rod.

2. Stainless Steel - Zr interaction at T~1500 K. It generates new alloys, with new properties and in particular brightness. The cladding starts to degrade in some parts where Zircaloy reacts with the steel generating new alloys. The control rod has a large plastic relocation and the gases are released (Helium gap).

3. SIC-Zr interaction at T > 1500 K: practically the Zyrcaloy of the control rod mixes with SIC materials. This reduces the production of hydrogen due to the dilution of Zr inside SIC. The silver is semi volatile and starts to be released in aerosol form.

After that, the guide tube fails very fast and Ag-In-SS-Zr melt relocates. Metallic melt freezes in the lower (colder) core areas. This generates a pool with a crust formation, typically associated with UO_2 and other FP mixed in this area. The pool, due to the large area and high temperature inside, releases Ag, In and Cd vapors and aerosols. This aerosol material could react with Ru and I forming salts. These salts successively are deposited in the Test Section, in the Primary Circuit and in CV. These phenomena are affected by large uncertainties and the codes have difficulties to simulate the related chemical and physical reactions and typically use semi-empirical methods.

The FPT3 bundle degradation phase consisted of two main periods. The first one, devoted to the thermal calibration of the bundle, lasted 7920 s. It consisted of two successive plateaus of core power, to 0.14 MW and then up to 0.38 MW. During this period, the bundle power was increased step by step from 0 to 3.02 kW. The steam flow rate was constant at 0.5 g/s. The second period was

the real temperature transient and degradation phase of the test, lasting from ~7920 to ~17370 seconds, in total for 9450 s. The degradation phase was specifically devoted to the release of fission products and bundle, structure and control rod materials (release of CO, CO_2 and CH_4 respectively), in order to study their transport and retention in the experimental circuit. During the degradation phase substantial hydrogen production was observed, particularly around 9800s at the zirconium oxidation peak, as well as fission product release. The thermal hydraulic conditions for the degradation phase were: constant steam flow rate set to 0.5 g/s and, a bundle power progressively increasing from 3.02 kW to 32.8 kW. The core power was progressively increased by successive ramps and plateaus from 0.38 MW to 4.51 MW. The power trends are shown in Figure 5.2 and Figure 5.3. Totally different relocation phenomena occurred in the SA progression, due to higher power and to a high Burn-up; this could be more dangerous in order to save the geometry of the reactor (Figure 5.4). It is clear in Figure 5.5 in comparison with Figure 5.6 that the FPT2 case is more degraded than FPT3, due to the difference of fuel temperatures.

Following the detection of a second temperature peak in the lower part of the bundle (shroud surface), the degradation phase was terminated by shutdown of the nuclear power at 17370 s, and the bundle was cooled in a steam flow of 0.5 g/s. At the end of this cooling phase the containment was isolated at 22500 s. The sequence of events in the bundle during the degradation phase is reflected in the thermal-hydraulic conditions in the circuit and in the containment. Moving along the circuit, the conditions of gas temperature, pressure and humidity in the horizontal line, hot leg, steam generator tube and cold leg are practically the same of FPT1.

For both tests the 37 hour aerosol phase started at about 22500 s and was dedicated to the analysis of aerosol deposition mechanisms in the containment (gravitational settling and wall deposition). This phase was conducted with containment thermal-hydraulic conditions identical to those of the degradation phase; condensation on the condensers ceased at 27660 s. During this phase, the sump temperature was maintained at 90°C, containment wall like containment bottom end-vault at 110°C, condenser wet part at 90°C and condenser dry part at 120°C. Throughout the aerosol phase, the containment humidity decreased from about 70% to about 55%.

In the case of FPT3 the absence of SIC material, replaced with B_4C, implies the impact of CO, CO_2, CH_4 and HBO_2 on FP behavior. This phenomenon could be expected for PWR B_4C control

rods and for BWR Control Blades. The interactions of B_4C control rods occur at T > 1500 K and involve four stages:

1. Stage 1: B_4C - Steinless Steel interaction at T ~1500 °K. Until this temperature the rods are practically integral due to the ceramic nature of B_4C. At this point the steel melt enters in contact with B_4C and the shape of the control rods starts to degrade.

2. Stage 2: (B_4C-Zr) - At T > 1500 K,the liquefaction and progressive candling of the metal material and Zr oxide on the B_4C material (that is al most integral) progressively reduce the thickness of the cladding metals, removing the protection of B_4C that starts to oxidaize.

3. Stage3: Control rod rupture and melt (B_4C – S.Steel-Zr) flow-down at T ~1600 K. The control rods fall down and the steam enters in contact with B_4C. Progressively, the amount of oxidation increases quickly.

4. Stage4: Oxidation of free standing B_4C by steam and related production of H_2, CO, CO_2 CH_4 and HBO_2. The HBO_2 (boric acid) could be dangerous because attacks the internal structuresand can increase the release of FP aerosols.

FPT2 Mass Inventory		FPT3 Mass Inventory	
Element	Mass (kg)	Element	Mass (kg)
Cu	2.0000E-25	Cu	1.78E-15
Zn	5.4000E-11	As	6.25E-07
Ga	1.4000E-08	Rb	2.75E-03
Ge	4.5000E-06	Nb	2.86E-06
As	8.2000E-07	Rh	2.93E-03
Se	4.8000E-04	In	1.31E-05
Br	1.8000E-04	I	1.19E-03
Kr	3.4000E-03	La	8.04E-03
Rb	3.5000E-03	Pm	3.03E-05
Sr	7.3000E-03	Tb	5.57E-06
Y	4.6000E-03	Tm	5.17E-09
Zr	3.4000E-02	Ra	1.15E-11
Nb	2.3000E-06	Th	1.44E-07
Mo	2.8000E-02	Pu	3.71E-02
Tc	7.0000E-03	Hg	3.48E-28
Ru	1.5000E-02	At	2.19E-25
Rh	3.7000E-03	Bk	4.72E-19
Pd	4.9000E-03	Ga	1.04E-08
Ag	2.5000E-04	Br	1.43E-04

Cd	2.4000E-04	Y	3.56E-03
In	1.6000E-05	Tc	5.45E-03
Sn	3.5000E-04	Ag	1.75E-04
Sb	6.5000E-05	Sb	4.73E-05
Te	3.6000E-03	Cs	1.60E-02
I	1.5000E-03	Pr	7.37E-03
Xe	4.1000E-02	Eu	3.95E-04
Cs	2.1000E-02	Ho	1.96E-07
Ba	1.4000E-02	Tl	1.12E-17
La	1.0000E-02	Re	6.10E-11
Ce	2.0000E-02	U	8.98E+00
Pr	9.5000E-03	Cm	7.84E-06
Nd	3.4000E-02	Bi	1.16E-15
Pm	8.1000E-05	Zn	5.13E-11
Sm	7.0000E-03	Se	3.74E-04
Eu	5.8000E-04	Sr	5.44E-03
Gd	2.9000E-04	Mo	2.16E-02
Tb	8.3000E-06	Pd	3.44E-03
Dy	4.5000E-06	Sn	2.59E-04
Ho	3.7000E-07	Xe	3.12E-02
Er	1.6000E-07	Ce	1.53E-02
Tm	8.7000E-09	Sm	5.46E-03
Yb	1.2000E-13	Dy	2.68E-06
Hg	1.7000E-28	Yb	8.31E-14
Tl	1.8000E-17	Ac	1.42E-12
Pb	6.1000E-11	Pa	7.78E-09
Bi	1.5000E-15	Am	9.57E-04
Po	2.1000E-16	Pb	5.43E-11
At	1.7000E-25	Rn	8.28E-17
Rn	6.0000E-17	Cf	1.01E-18
Fr	2.4000E-20	Ge	3.44E-06
Ra	7.0000E-12	Kr	2.60E-03
Ac	9.0000E-13	Zr	2.66E-02
Th	1.1000E-07	Ru	1.15E-02
Pa	5.6000E-09	Cd	1.68E-04
U	8.6000E+00	Te	2.73E-03
Np	1.5000E-03	Ba	1.14E-02
Pu	4.3000E-02	Nd	2.66E-02
Am	1.4000E-03	Gd	1.90E-04
Cm	1.0000E-05	Er	9.06E-08
		Po	4.22E-16
		Np	1.10E-03
		Fr	3.72E-20
		Es	1.27E-26

Table 5.1 FP mass Inventories in FPT2 and FPT3

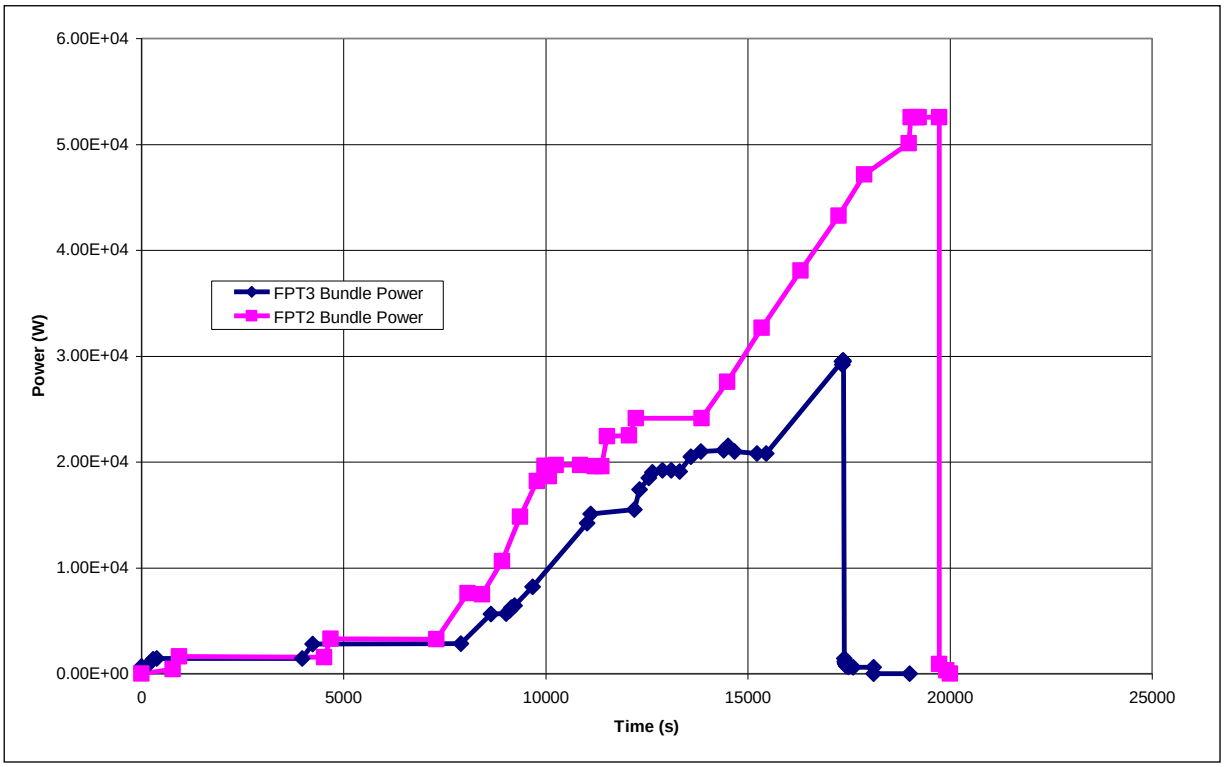

Figure 5.2 FPT2 and FPT3 Bundle power as function of time

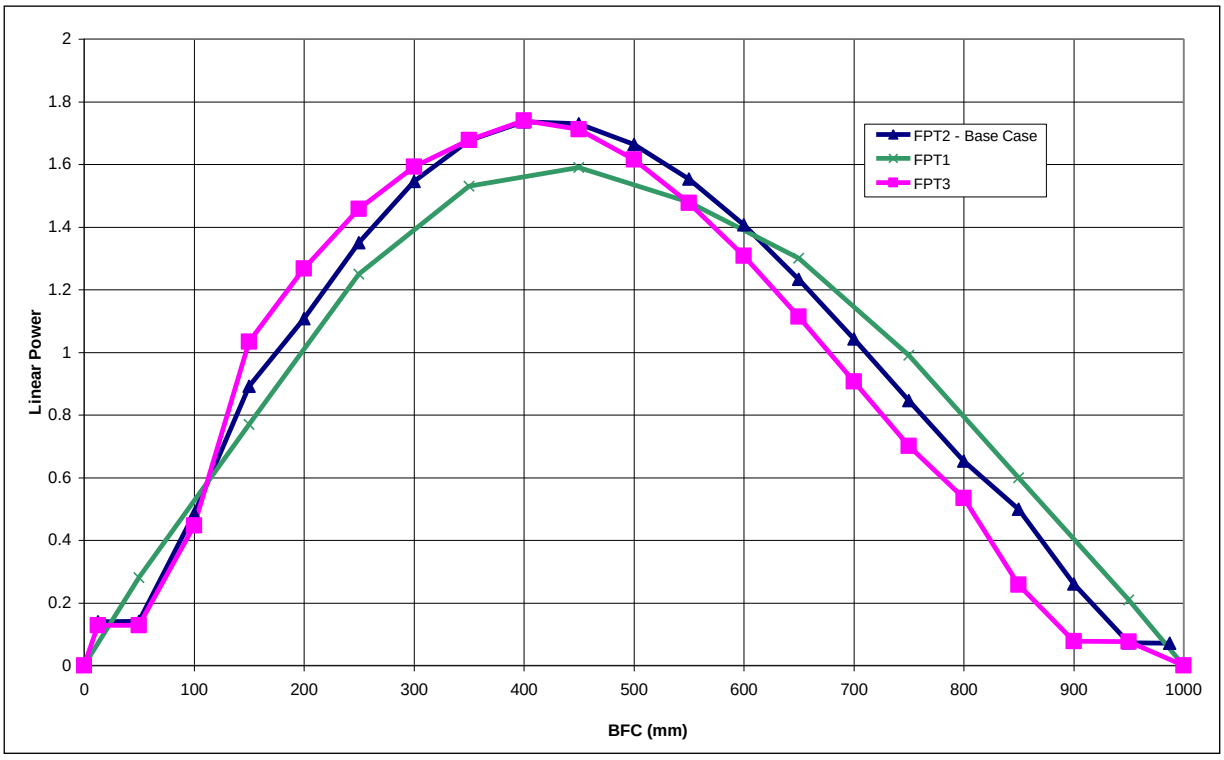

Figure 5.3 FPT1, FPT2 and FPT3 axial power profile

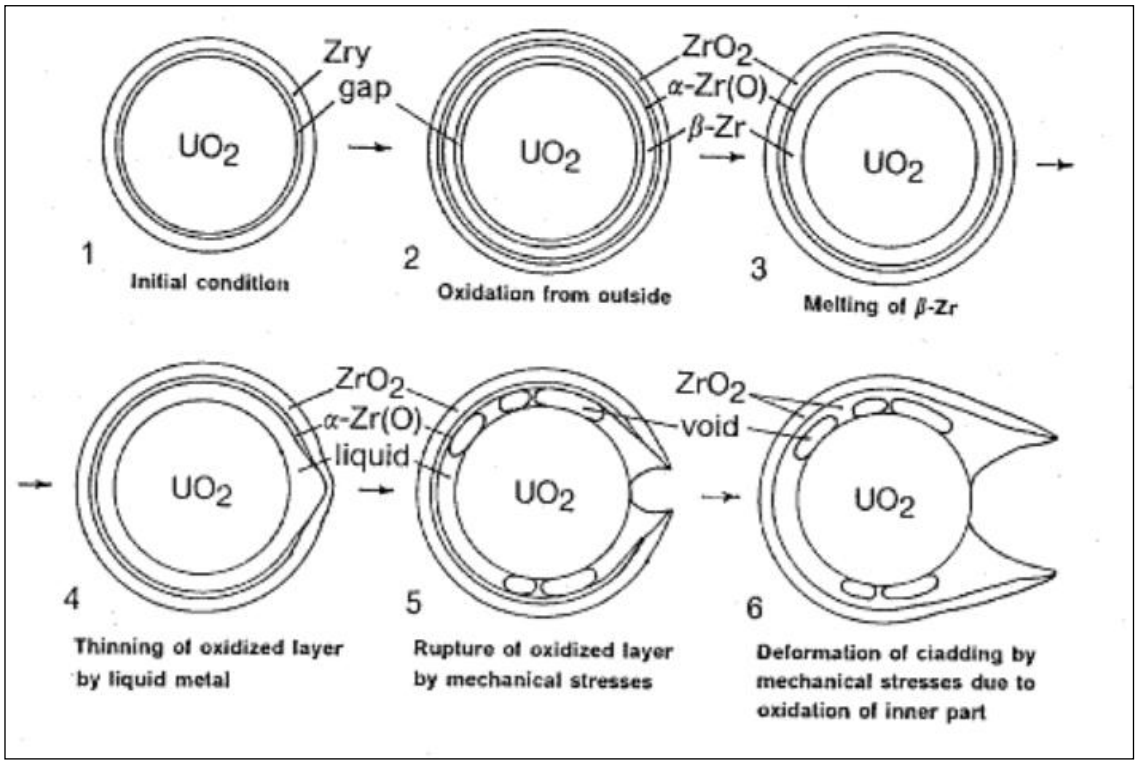

Figure 5.4 Progressive melt of the fuel

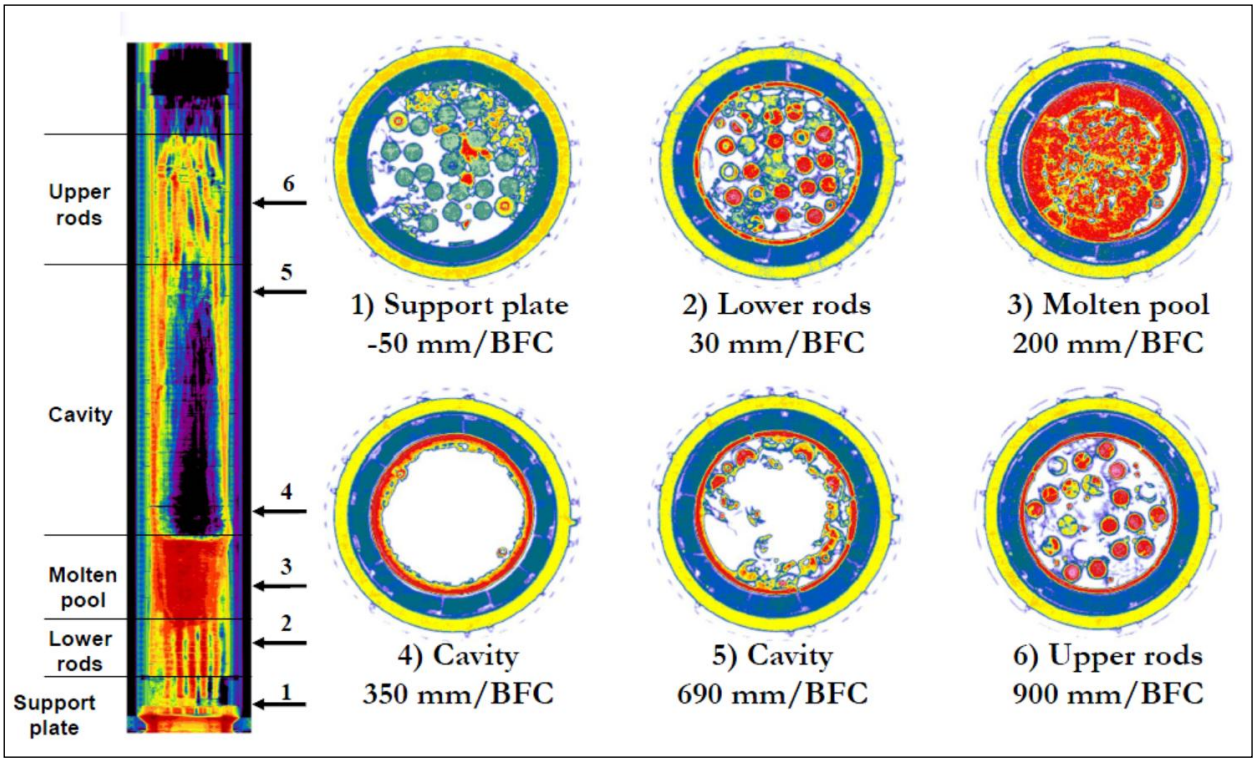

Figure 5.5 FPT2 Bundle degradation thermographs

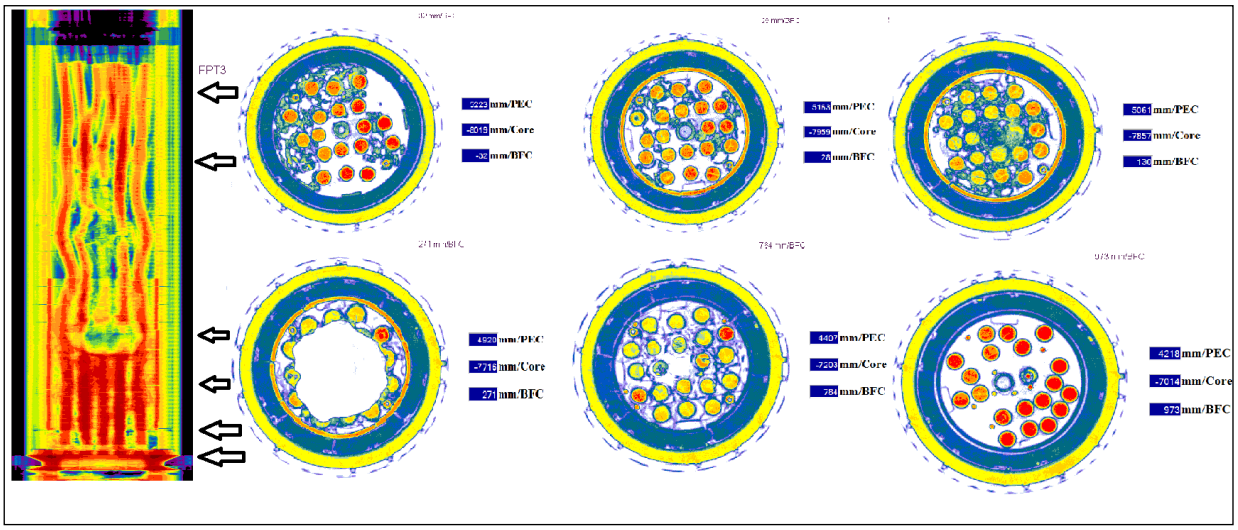

Figure 5.6 FPT3 Bundle degradation thermographs

5.3 Main Results from FPT2 and FPT3 Simulations

This paragraph summarizes the results obtained by ASTEC 2.0r2 and MELCOR 1.8.5 codes on FPT2 and FPT3 simulations. Another important aspect is the comparison between FPT2 and FPT3 on the basis of reference data obtained from the post processing of the tests.

FPT2 and FPT3 were prepared in order to have a complete picture of the iodine chemistry, considering in particular the effect of silver. The iodine is very important in order to estimate the source term and the presence of the SIC control rods could be able to block the iodine as Silver Iodide, removing it from the containment atmosphere during the washing phase. The FPT1 is the test with the largest amount of silver due to the SIC control rods and fuel rods inventory;in this test, the presence of silver in the CV sump is maximum. In FPT2, no silver has been observed inthe sump, because it contains boric acid. The less amount of silver is in FPT3 (silver is only generated as FP - Ag^{110m}) and the iodine concentration in containment atmosphere is maximum.

5.3.1 *FPT2 Source Term and Results*

As said in the previous paragraphs, FPT2 test (as FPT3) is characterized from a constant flow rate of steam with a value of 0.5 g/s. The bundle power profile, which simulates the decay heat power is rather high in this particular test, arriving to a maximum value of 52.1 KW. Only the external fuel rods conserve their shape; the internal fuel practically relocates near the support plate,

generating a cavity and a large pool of material relocated, as shown in Figure 5.7. The sketch of Figure 5.7 is very interesting; it gives a qualitative idea of the final state of the bundle. The bundle, as described before, is practically divided in 4 zones. The control rods are lost and a cavity is open in the central part of the rods in the simulation, similar to the thermograph. Other common point is the upper part of the rods, which conserves the integrity of the geometry. However, Figure 5.7 shows that the bundle is less damaged in the ASTEC simulation with respect to the thermograph view.

Due to the high temperature (Figure 5.8 and Figure 5.9) and the quasi-complete loss of geometry, the FP gas and aerosols are released in large amounts as gas and aerosols (Table 5.2). The volatile and semi volatile materials are released when the gases generated during the reactions are free to escape to the circuit and in CV. This is the first transport mechanism to take into account in the source term evaluation. The second is the temperature of the medium which can block the diffusion of FP. In this case the pool temperature of the molten material is favorable to the progression of the aerosol release.

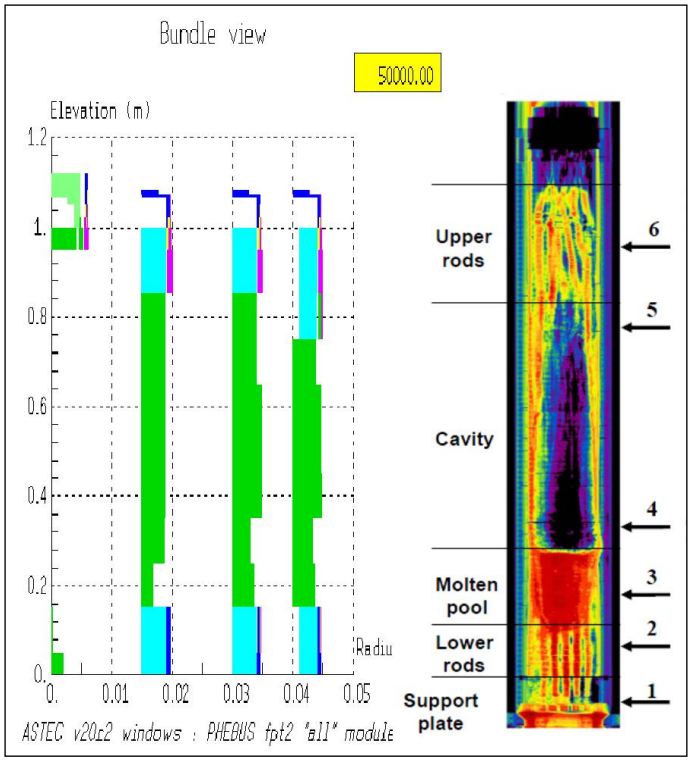

Figure 5.7 FPT2 ASTECv2r2 sketch vs. thermograph picture

FP Element	Reference (%)	ASTEC V2.0 R2
Zr_{95}	5	21.6
Ba_{140}	86	9.6
I_{131}	83	91.4
Te_{132}	81	88.7
La_{140}	86	0.03
Cs_{137}	68	91.4
Mo_{99}	14	75.30
Ru_{103}	11	31.3
Ag_{110m}	86	91

Table 5.2 Release Factors in FPT2

ASTEC typically overestimates the mass release (Table 5.2), with release fractions near 100% for almost all gas, volatile and semi-volatile materials; only Lanthanum and Barium releases are less than the reference release factors. In particular it has to be noticed the large release of iodine and silver.

However, the silver combines with iodine and the salt is wash-out by steam condensation, blocking this dangerous fission product in the containment pool. The hydrogen produced is practically the same for all FPT tests with PWR bundle (Figure 5.10 and Figure 5.11). The amount is estimated to 120 g and it is generated mainly during the early phase of the degradation, when the geometry is practically intact (around near 10000 s). The geometry gives the reaction surface able to generate hydrogen from Zyrcaloy and steam reaction. It is very interesting to evidence the plateau in Figure 5.10 due to the steam starvation phenomenon; when the molten pool is generated in the lower part of the bundle, the hydrogen production decreases.

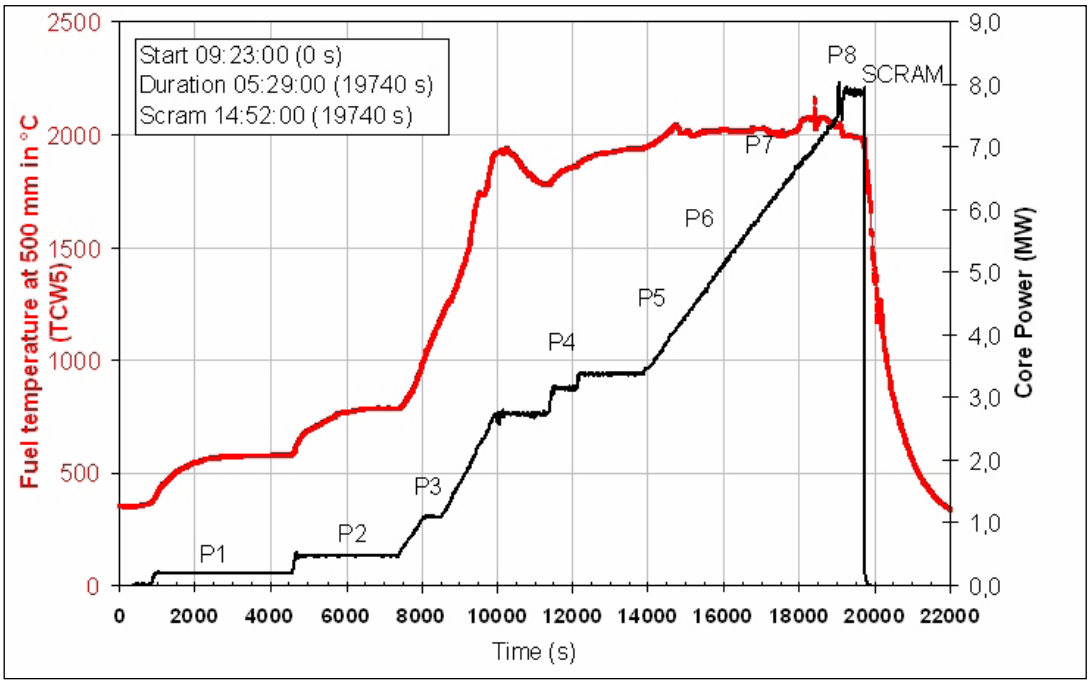

Figure 5.8 Fuel temperature and core power trends from FPT2 final report

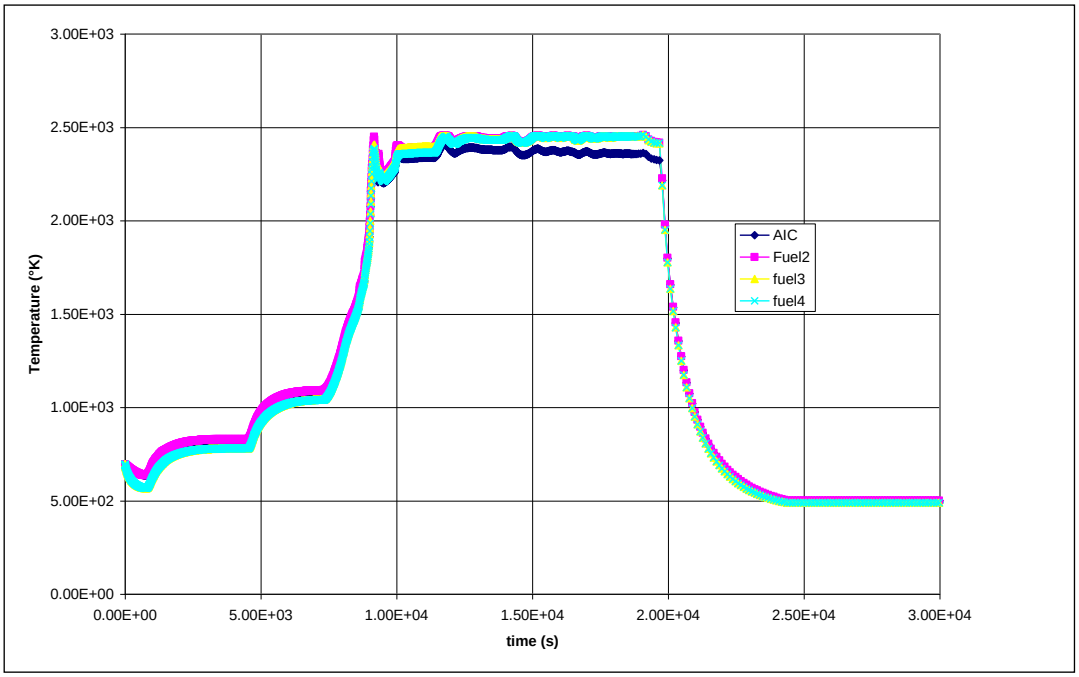

Figure 5.9 Fuel temperature between 0.30 m and 0.40 m of active length in ASTEC simulation

The ASTEC code is able to follow the progression of the severe accident, in particular the hydrogen production and the temperature trends.

The hydrogen production rate (Figure 5.11) is a little less and it is anticipated in comparison with the reference data, but substantially it is clear the steam starvation progression with the relocation of the materials and loss of geometry.

As for FPT1, the general good agreement of the temperature is due to the highly detailed modelling of the bundle power profile as a function of time, both for the axial and radial profiles (In particular the axial profile has the same detail of the meshes used for both codes). Also sophisticated models are used in order to simulate the dynamics of the cladding failure and fuel degradation as function of the linear power.

The containment pressure trend (Figure 5.13 and Figure 5.14) follows the shape of the bundle power as function of time except around 10000 s, when practically all steam reacts with the Zyrcaloy. This is evidenced in particular by CV steam partial pressure (Figure 5.13) and humidity (Figure 5.14): the phenomenon of Zr-steam reaction produces a considerable decrease of these quantities around 10000 s, until the phenomenon is reducing at 11000 s.

As for the FPT1, the last observation concerns the code overestimation of the mass inside the containment, consequence of the high aerosol mass released from the bundle,.

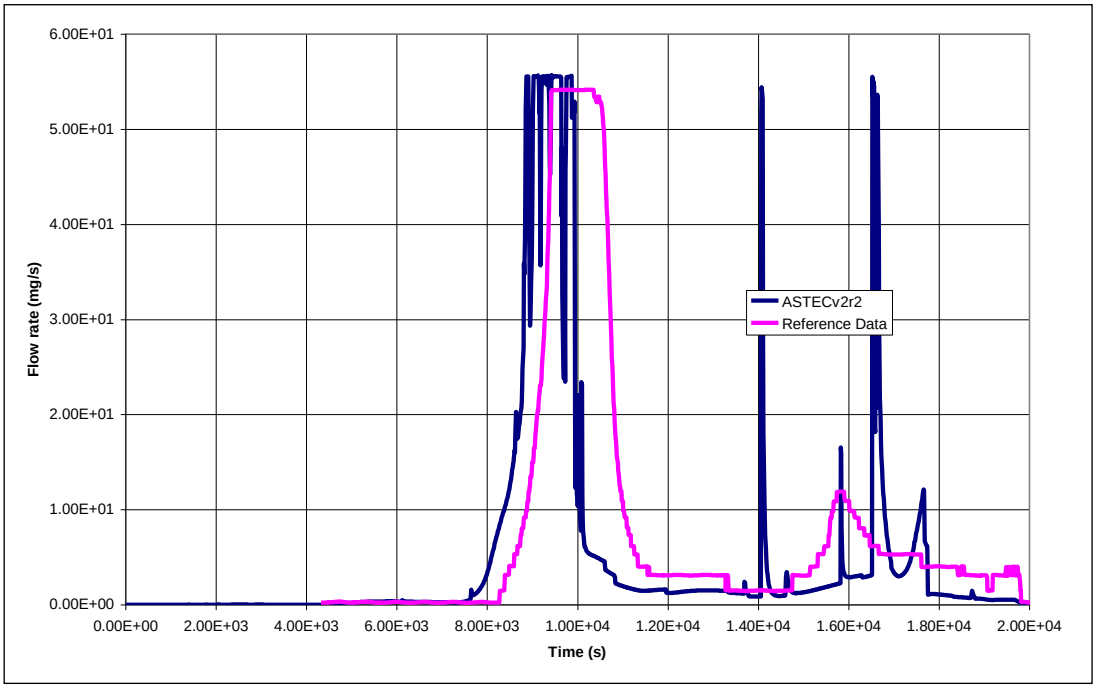

Figure 5.10 Hydrogen production rate

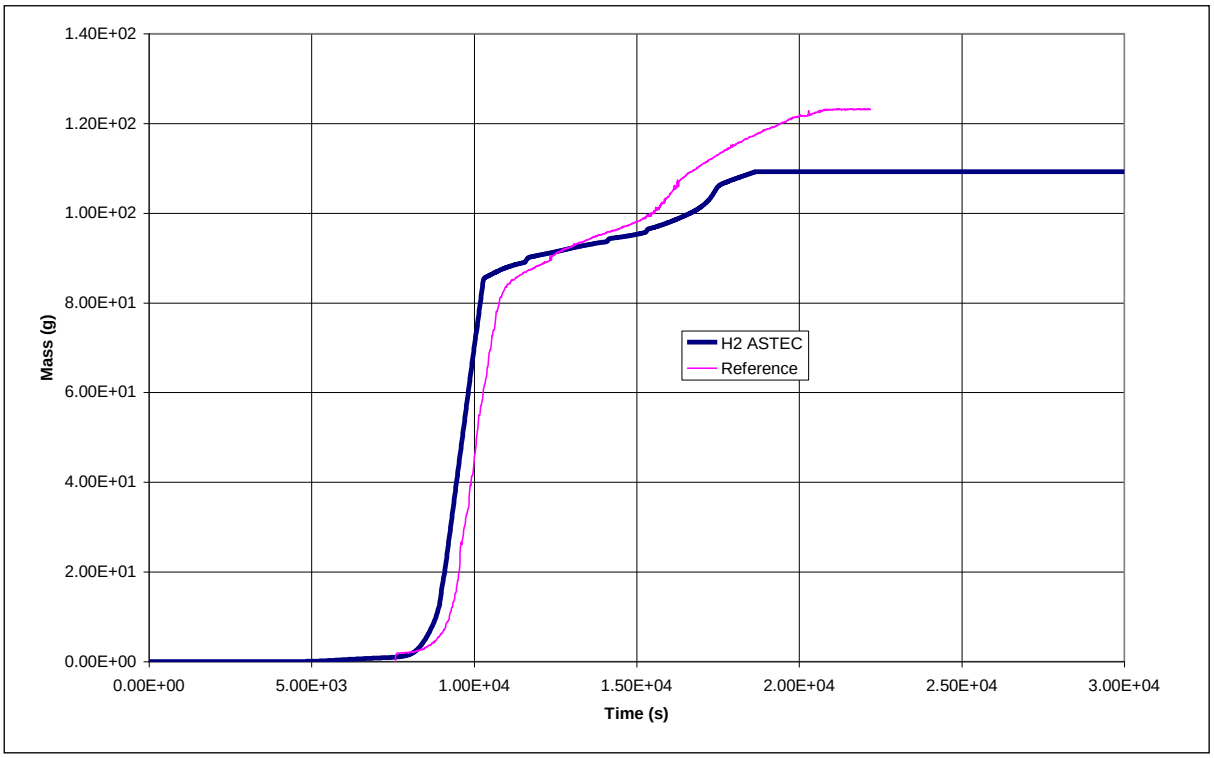

Figure 5.11 Hydrogen total release mass

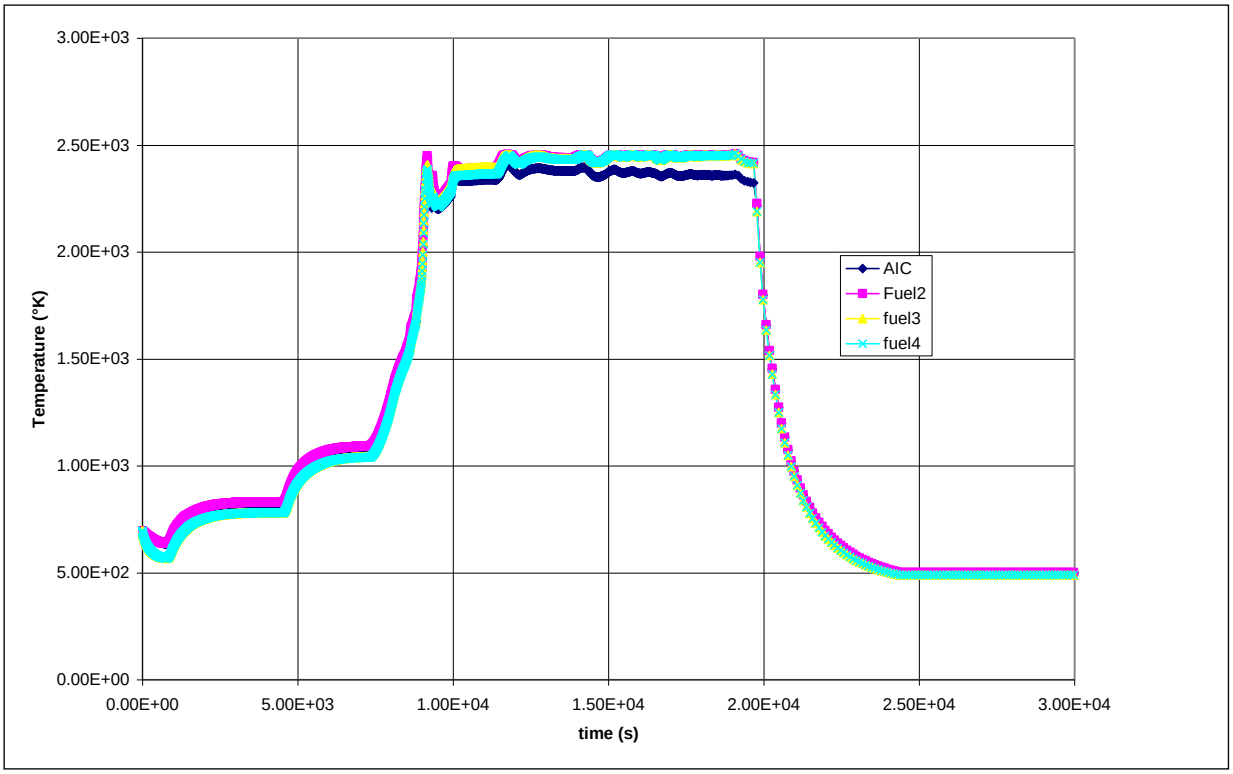

Figure 5.12 Fuel temperature between 0.30 m and 0.40 m of active length for ASTEC

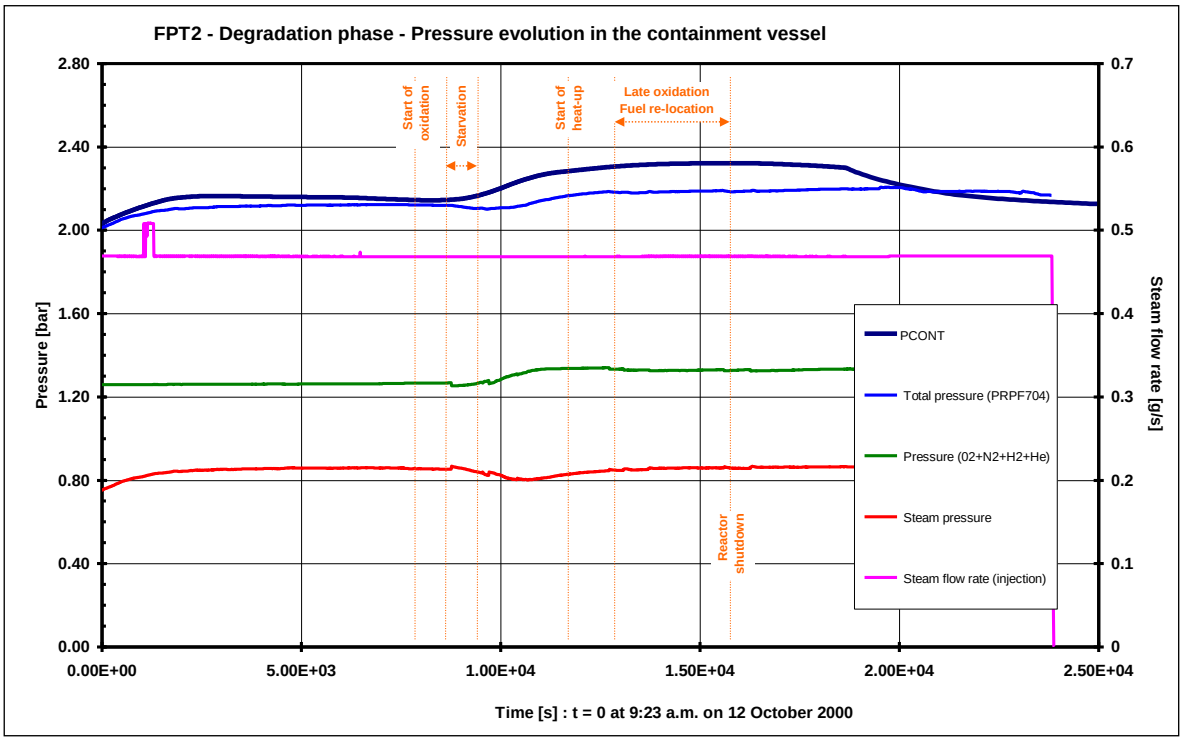

Figure 5.13 FPT2 CV pressure trend in comparison with the ASTEC results

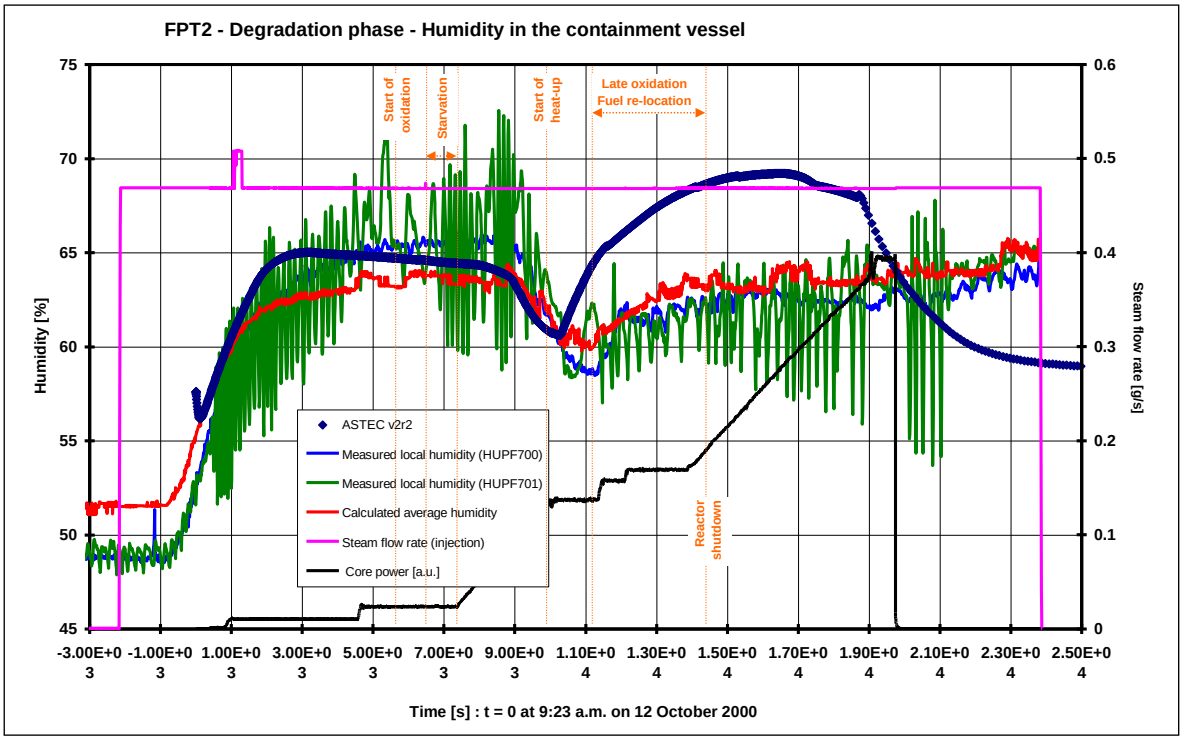

Figure 5.14 FPT2 CV humidity trends in comparison with the ASTEC results

5.3.2 *FPT3 Source Term and Results*

It is impressing how much a difference in the control rods materials can change the Source Term. This was well known from the theoretical point of view at the end of last century, but only with FPT3 we obtained good reference data sets for quantifying the phenomenon. In the future we could have a lot of data directly to the post analyses of the Fukushima accident. At the moment, FPT3 is however the most important "test-bed" for all codes, which are able to simulate the SA progression and to estimate the Source Term.

As for FPT2, the little sketch of Figure 5.14 shows the final image predicted by ASTEC and obtained from the thermograph. The first important difference is the saved part of B_4C control rod. In the FPT2 (Figure 5.7), the SIC material was relocated and mixed with the other materials inside the core (the color for this "alloy" is green). In FPT3, the saved part of boron carbide is red. The boron carbide is a refractory material; it can react with steam and other materials but it does not melt until the temperature is around 2800 K, similarly to the uranium dioxide.

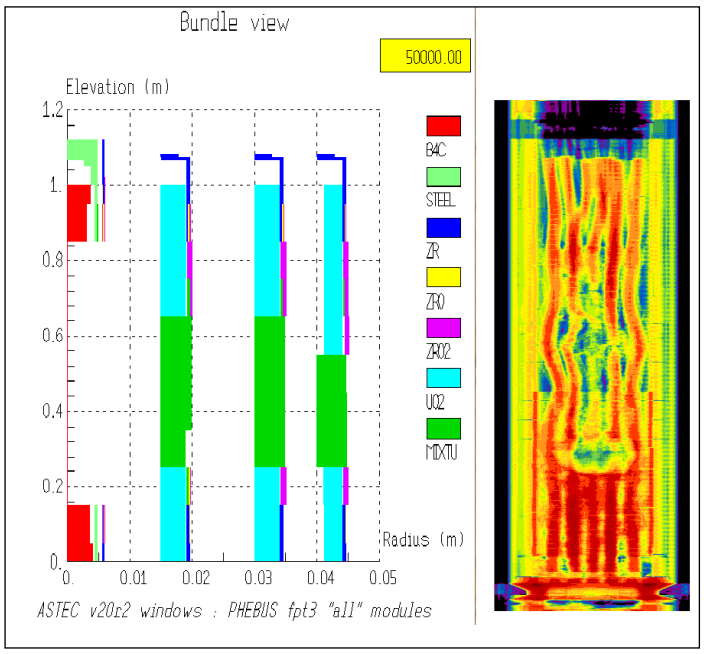

Figure 5.15 FPT3 ASTECv2r2 sketch vs. thermograph picture

The second important difference of FPT3 in comparison with FPT2 is the dimensions of the cavity and "the pool". Really the relocation material looks like a large candling around the control rods and the geometry is substantially saved; this is due to the minor bundle power.

As for the other tests, also in FPT3 the releases are rather important, even though the geometry is much more intact than in the other cases. This depends also from the boric acid and its chemical attack to Zyrcaloy. The early source term during a SA is due to gases and vopours in the gap and in UO_2 matrix, which escape when the clad breaks. This source term is estimated to be 20-30% of the total inventoryof vapors and gases as iodine ad xenon. As shown in Figure 5.16, Figure 5.17 and Figure 5.18, after the clad break (around 10000 s) iodine, cesium and other volatile materials escape from the bundle and go through the primary circuit in the containment (Table 5.3). In FPT3 the iodine arriving in the containment is 80% of the total iodine released from the bundle, due to the absence of silver. The releases in FPT3 are however less than the FPT2 source term due to the larger integrity of the bundle. This shape of the bundle is justified from the temperature trends (Figure 5.19 and Figure 5.20) of the fuel during the test: the fuel temperature is lower than in FPT2 and it is clear that it is directly proportional to the power of the bundle.

The hydrogen production rate (Figure 5.21) and mass are similar to FPT2: the lower production of the Zr-steam reaction is compensated by the chemical reactions involving steam and boron carbide. Infact, the hydrogen production arrives to 120g as in FPT2, with 20g of contribution from the B_4C reactions. At 10000 s, when the hydrogen production rate raises to the limit of steam starvation, the cladding of boron carbide starts to degrade and prepares the control rod to react with the steam, generating hydrogen, CO, methane, CO_2 and boric acid. The reaction of steam with B_4C, as with Zyrcaloy, produces some power (Figure 5.22), which increases further the bundle temperature.

As shown in Figure 5.23, Figure 5.24 and Figure 5.25, the FPT3 containment behavior is quite close to FPT2 one: practically, the pressure and the humidity have the same trends, with the decreases around 10000 s due to steam consumption by the bundle reactions.

Both ASTECr2v2 and MELCOR 1.8.5 codes are capable to follow the progression of relocation of bundle materials during the evolution of the degradation phase (up to 18000 s). The bundle temperatures (Figure 5.19 and Figure 5.20) in shape and in magnitude are similar to the reference data, as the hydrogen production (Figure 5.21). ASTEC overestimates slightly the hydrogen production (129 g), while MELCOR practically obtains the same mass value (119 g of hydrogen produced). This difference is due to the model of the B_4C reaction (Figure 5.21 and Figure 5.22), even thiugh with compensating errors. The MELCOR model is very simple, with few sensitivity

coefficients. Practically the timing of MELCOR simulation is wrong and there is a large initial reaction of boron carbide. This allows an initial start timing of hydrogen production at 9000 s, with subsequent decline. ASTEC is able to follow the timing of the reaction and the steam consumption phenomena better than MELCOR, but at the end it overestimates the reference data.

A limitation of ASTEC is due to the impossibility of simulating CO, CO_2 and CH_4, transport in the primary circuit,while follows the hydrogen and power generation from the B_4C reaction as well as the boron and carbon releases as aerosol materials. . on the contrary MELCOR is able to predict the mass of these gasses generated from the reaction and to describe their behavior in the primary circuit and in the CV, as any incondensable gas.

Both codes overestimate the aerosol releases (Table 5.4 and Figure 5.25), but ASTEC much more than MELCOR. The CV thermo-hydraulic behavior is the same than in FPT2. The two codes overestimate the pressure (Figure 5.23) and humidity (Figure 5.24) trends, but with the same shape of reference data. In particular, MELCOR has a lower condensation in the first part of the transient and after the closure of the injection from the circuit. The general over–estimation of aerosol releases and pressure trends can be due to keep a safety point of view and maximize the sequence.

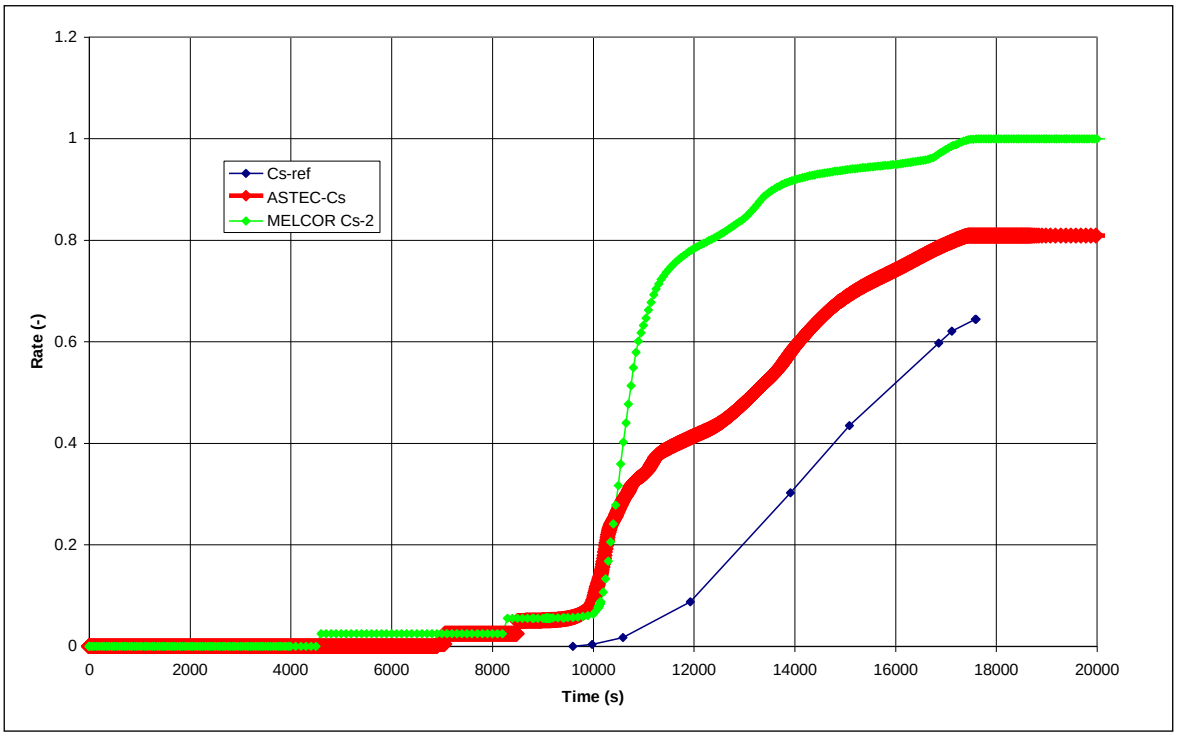

Figure 5.16 Cesium release factor

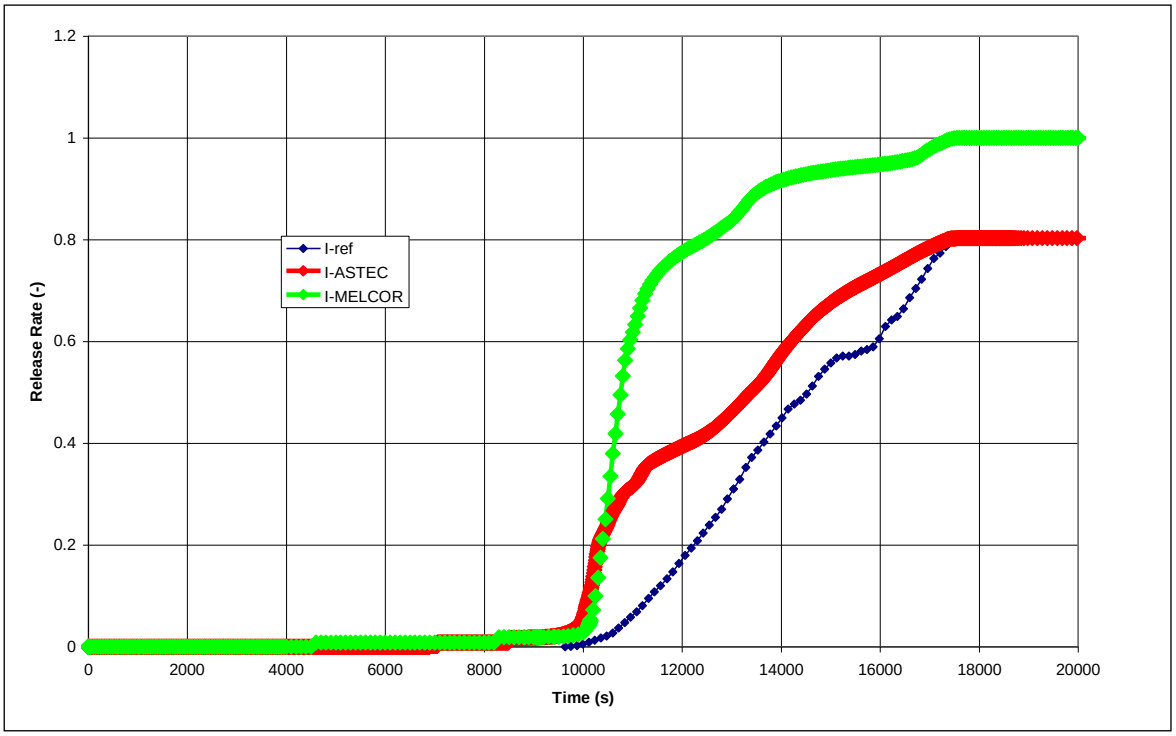

Figure 5.17 Iodine release factor

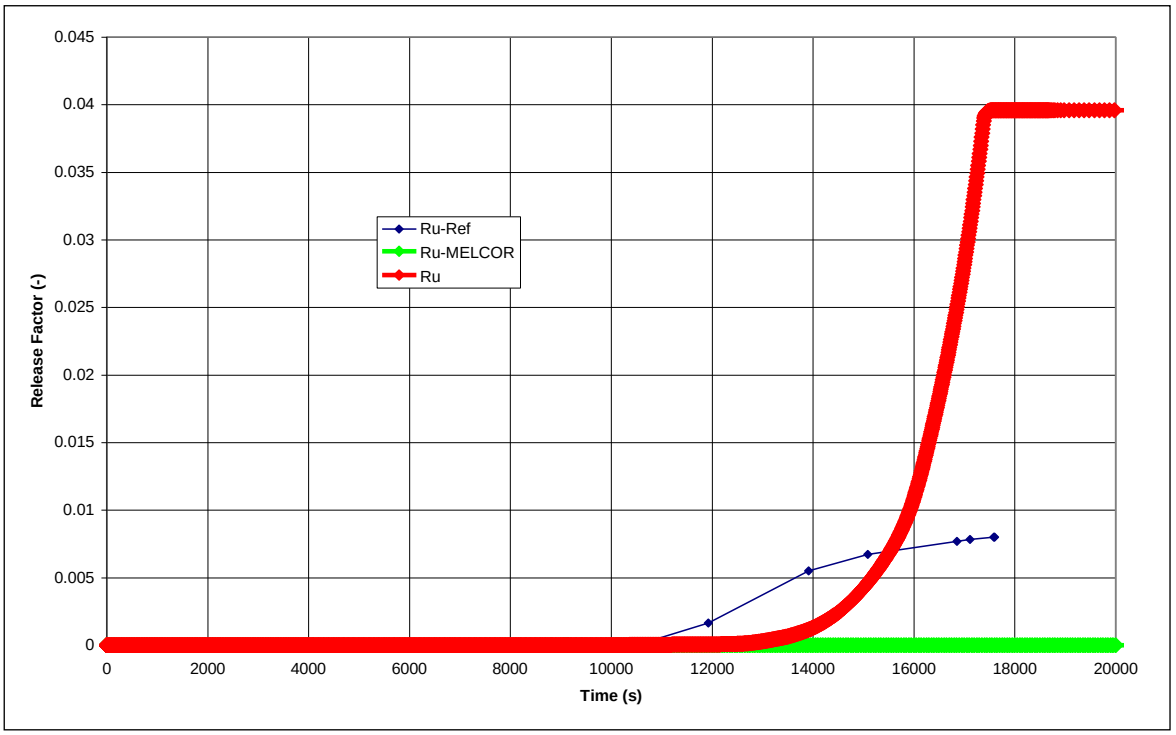

Figure 5.18 Ruthenium release factor

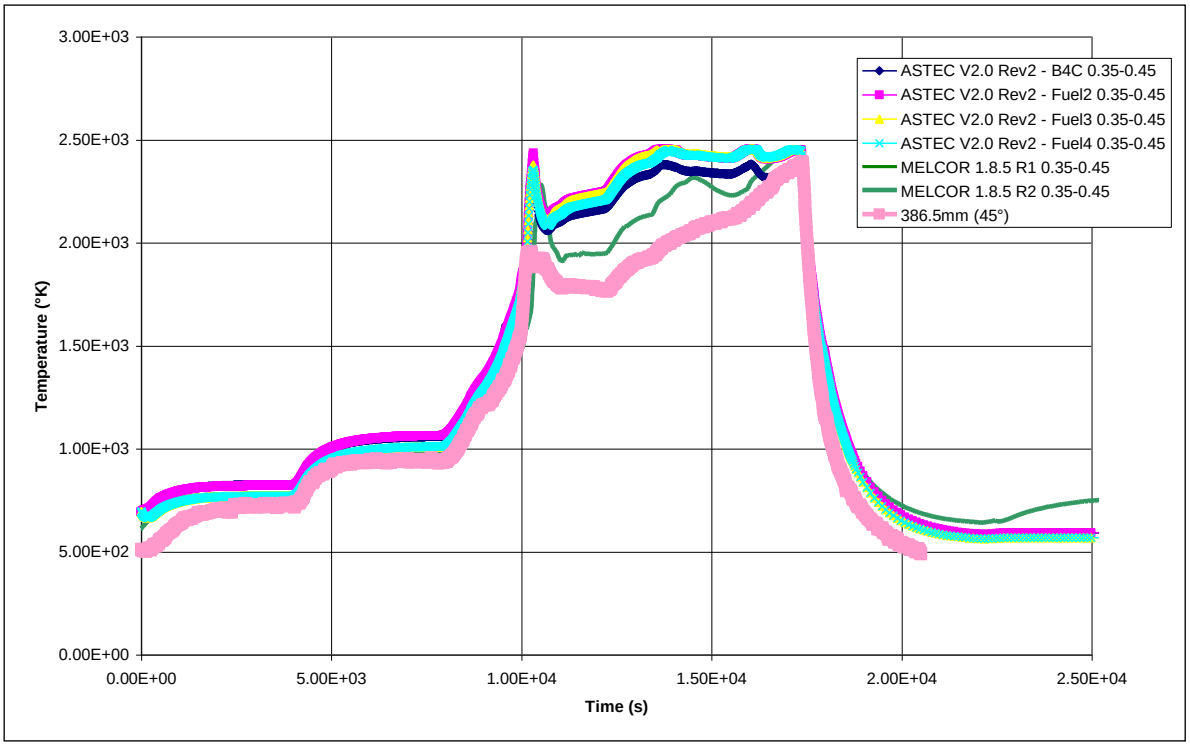

Figure 5.19 Fuel temperature between 0.30 m and 0.40 m of active length

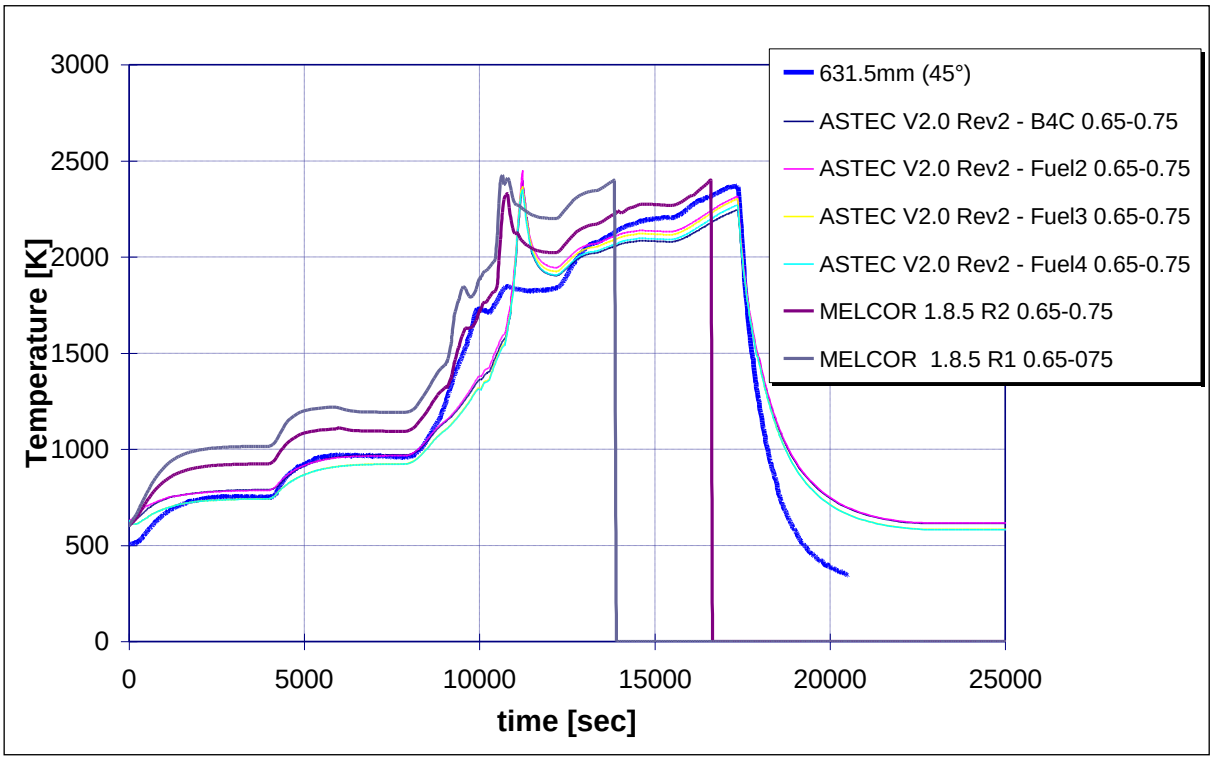

Figure 5.20 Fuel temperature between 0.60 m and 0.70 m of active length

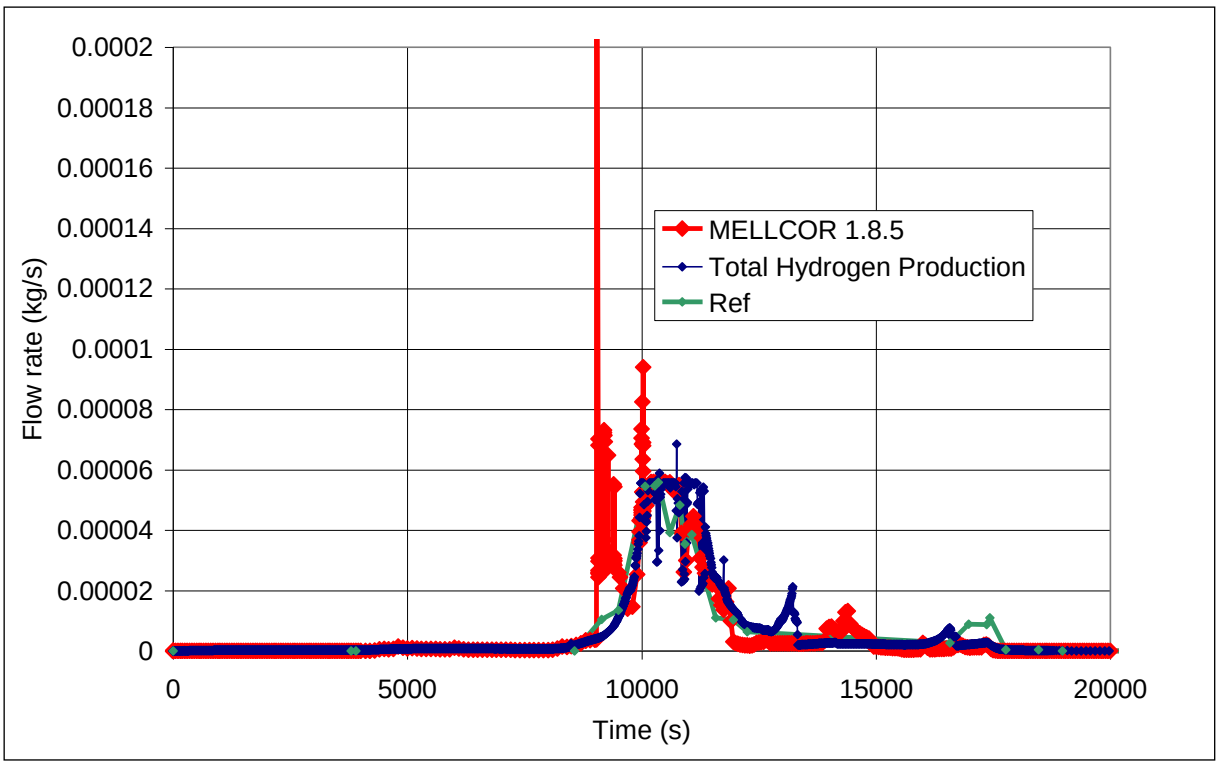

Figure 5.21 Hydrogen production rate

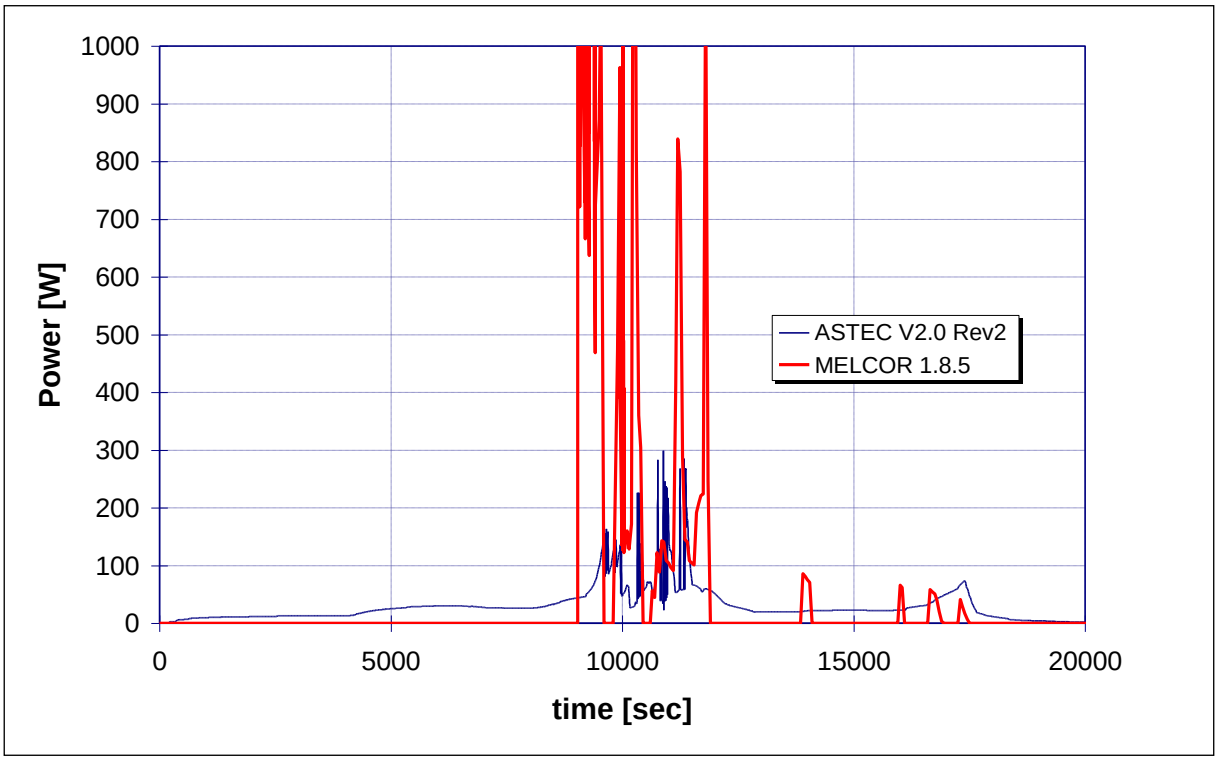

Figure 5.22 Power produced from boron carbide reactions

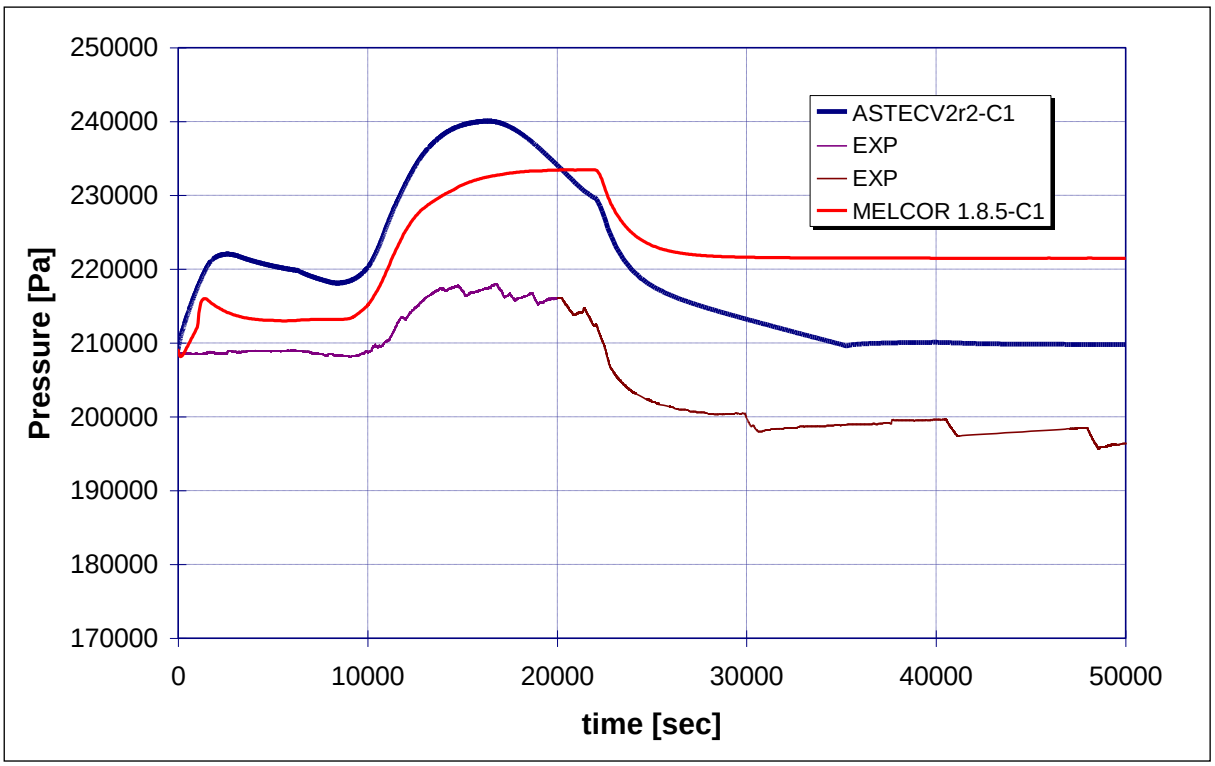

Figure 5.23 FPT3 CV Pressure

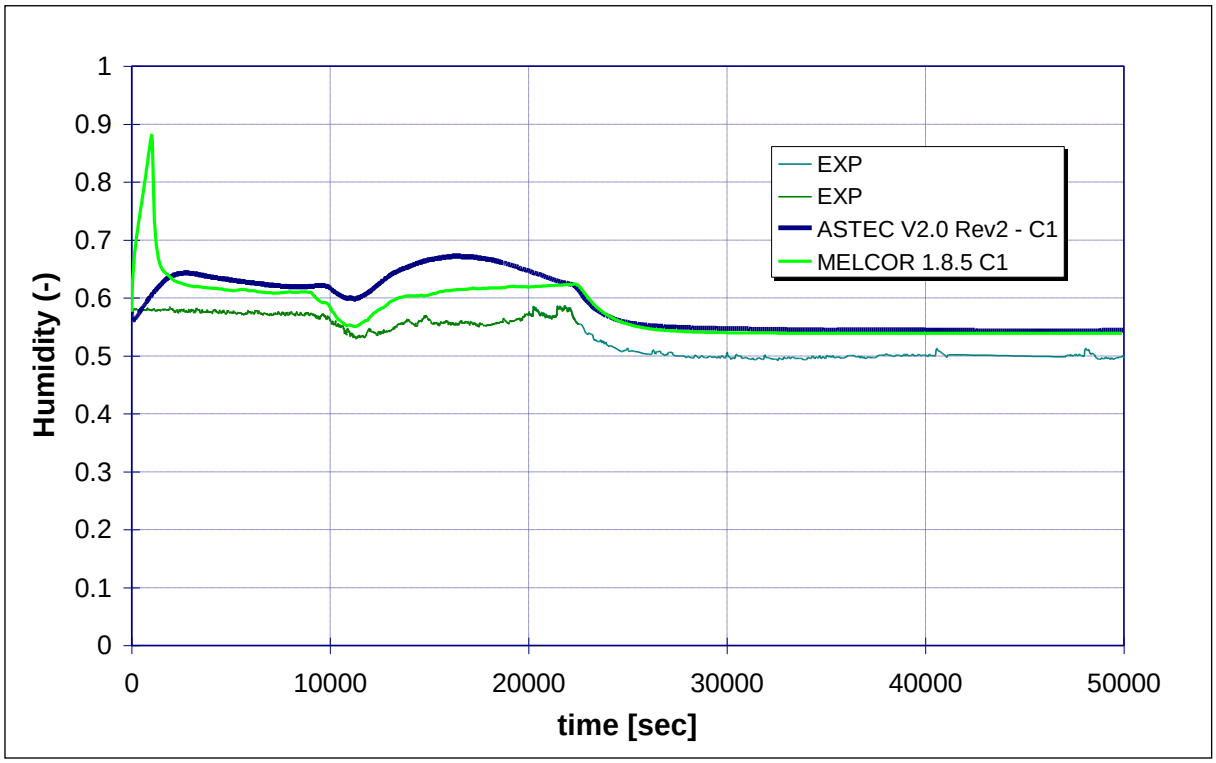

Figure 5.24 FPT3 CV Humidity

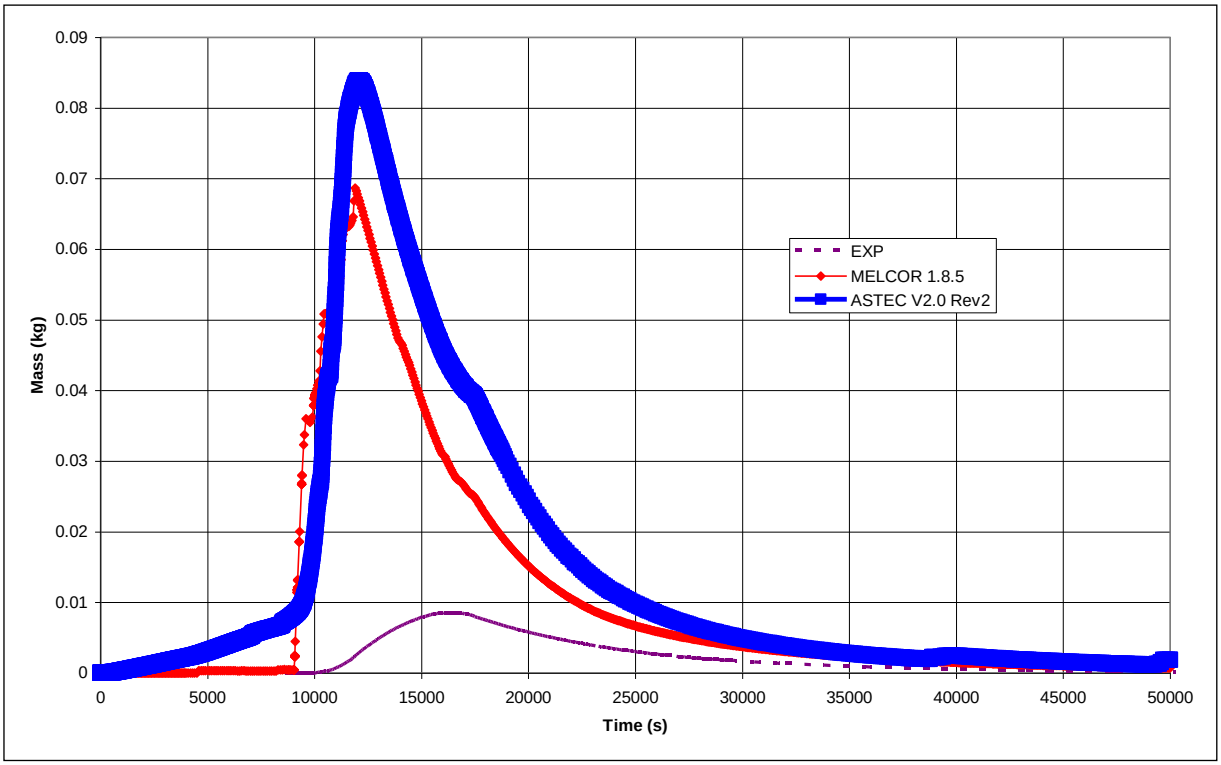

Figure 5.25 CV FPT3 Aerosol Suspended Mass

FP Element	Reference	ASTEC V2.0 R2	MELCOR 1.8.5
Sn	28.4	43.1	22.3
Ba_{140}	6	6.11	4.1
I_{131}	79	78	100
Te_{129}	79.9	74.8	100
B	76	78	99.8
Cs_{137}	64	80	100
Mo_{99}	23	73.1	22.82
Ru_{103}	0.7	3.4	0.0008
Ag_{110m}	70	78	22.3
Xe_{135}	82	79	95.2
U	0.08	0.026	0.038

Table 5.3 Release Factors in FPT3

Release (g)	Reference	ASTEC V2.0rev2	MELCOR 1.8.5
FP in the Containment	46	113	57
H_2 Release	120	127.2	119

Table 5.4 Containment in FPT3 Mass

5.4 General Remarks

The experience earned at DIMNP during several years of analyses on the SA phenomenology of has been precious for developing an adequate nodalization of the PHEBUS plant. In particular, the ISP46 experience has been the first step of the nodalization development, starting with the analysis of the containment behavior. To this aim, we initially assumed as boundary conditions the releases

of steam, hydrogen and FP from the pipe, which simulates the cold leg; The following steps were the progressive implementation of the complete nodalization, with the addition of the Circuit, and the Test Section (ISP46 complete analysis).

The investigation of the bundle degradation phenomena in the PHEBUS program has been performed for the evaluation of the models that simulate the release of FP aerosols and gases, the hydrogen production from the chemical reactions of Zyrcaloy and other materials and the relocation phenomena. The bundle degradation, hydrogen production, aerosol release and transport, atmosphere thermal-hydraulics and aerosol deposition mechanisms are the most important points of discussion in the nuclear technology. In particular the release of FP from the bundle, the transport and retention of FPs in the containment system of a nuclear power plant under conditions representative of severe accidents are in fact among the most important safety issues. Scaled integral experimental tests simulating the release of FPs and aerosol dynamics are of basic importance for the understanding of the interaction of complex phenomena taking place during a postulated accident. Moreover they provide a very useful set of data for the validation and assessment of the models developed for the computer programs used for the analysis of the source term. The availability of the experimental results from FPT0 and FPT1 has been very useful to better understand heat and mass transfer phenomena that take place in the containment system, a necessary condition for the correct simulation of aerosol dynamics.

The results of the analyses evidence the capability of ASTEC and MELCOR codes to simulate the FPT1, FPT2 and FPT3 experiments, and particularly a good behaviour for the prediction of the principal phenomena connected with the degradation of the bundle, material relocation and creation of the molten pool. This results also from the simulation of the FPT1, even though some discrepancies were detected, particularly with respect to the release of FP product and SM material, as well as for condensation heat and mass transfer. In particular MELRCOR 1.8.5 code evidences problems in simulating the release of SM or of FP from the melt pool.

FPT2 and FPT3 analyses evidence the necessity to improve the chemistry models for the material releases in order to estimate better the source term. In particular the boron carbide reactions area problem in relation with the following important factors:

- Increase of the hydrogen production,

- Generation of boric acid able to damage fuel and internal structures and to deposit on the primary circuit reducing the flow section; this can also aggravate the problem of criticality control during the reflooding phase

- Increase of iodine concentration in the containment (Table 5.6) in particular during the washing phase of the containment atmosphere.

Boron carbide reactions and silver iodide production are two important topics for outlined by PHEBUS program. As show in Table 5.5, the iodine released in the containment vessel is not so much in case of FPT3 due to the inertial deposition in the deposit of boric acid, but in form able to re-suspend at temperatures higher than 422 K or with hydrogen combustion. In the cases of FPT1 and FPT2 iodineis found mainly in the CV pool as silver iodide, due to the presence of large silver amounts coming from the control rods.

MELCOR and ASTEC codes are enough able to calculate the release and the transport of iodine from the bundle, through the circuit and inside the containment vessel, as evidenced in Table 5.6. In particular ASTEC v2.0r2 gives better results due a more detailed chemistry.

	FPT1	FPT2	FPT3
Iodine Release [mg]	974.4	1245	940.1
Silver Release [g]	89.6	466.6	0.123
Iodine Point G/Release [%]	64.10	56.70	47.02
Iodine in CV pool [mg]	635	224	38.95
Silver in CV pool [g]	30	7.1	0.0019

Table 5.5 Iodine and silver releases in CV and in the ontainment pool

Iodine Point G (mg)	FPT1	FPT2	FPT3
Reference data	625	705.9	442
ASTEC v2.0 r1/r2	363.7	716	600
MELCOR 1.8.5	595	-	748

Table 5.6 Iodine releases at CV inlet

The last observation concerns the validation of the lump parameter codes as MELCOR and ASTEC by the analyses of PHEBUS experiments. To this aim, similar nodalizations have been set-up for the analyses of FPT2 and FPT3, which have a lot of common points and are particularly suited for testing of models. The results are very interesting and evidence a general agreement of ASTEC and MELCOR simulations, with respect to the hydrogen production, the steam starvation phenomena and the behaviour of the containment. Some divergences are however evidenced as the timing of the sequences, the release magnitude and the steam condensation. In particular the models implemented in ELSA of ASTEC are improved with respect to CORSOR Both of MELCOR, due to the integration of a simplified chemistry and a detailed mechanical approach.

As final remarks, the limitations of MELCOR 1.8.5 to simulate the phenomena with simplified models are compensated by the larger flexibility of the code. ASTEC remains less flexible of MELCOR, in particular for the simulation of the behaviour of other gases, like CO and CO_2, in the primary circuit.

References

[1] P. von der Hardt, A. V. Jones, C. Lecomte and A. Tattegrain, Nuclear Safety Research: The Phebus FP Severe Accident Experimental Programme, *Nuclear Safety*, vol 35(2), July-December 1994, pp 187-205.

[2] M. Schwarz, G. Hache and P. von der Hardt, A Severe Accident Research Programme for Current and Advanced Light Water Reactors, *Nucl. Eng. and Design*, vol 187 (1999), pp 47-69.

[3] D. Jacquemain, S. Bourdon, A. de Braemaeker and M. Barrachin, FPT1 Final Report (Final version) IPSN/DRS/SEA/PEPF report SEA1/00, IP/00/479, December 2000.

[4] T. Haste, Specification of International Standard Problem ISP-46 (Phebus FPT1), Revision 0, IPSN Note Technique SEMAR 01/91, November 2001. A. C. Greogoire, et ali., ”FPT2 Final Report (Final version)”, IRSN. N° PH-PF: DOCUMENT Phébus PF, IP/08/579, Febbrary 2008.

[5] A. Bieliauskas, T. Haste, “SPECIFICATIONS OF SARNET2 PHEBUS FPT3 BENCHMARK”, IRSN, DPAM-SEMIC-2011-057, 5/07/2011

[6] R. Gauntt et al. MELCOR Computer Code Manuals Vol. 2: Reference manual, Version 1.8.6, September 2005 - NUREG/CR-6119, Vol. 2, Rev.3 SAND2005-5713 - Sandia National Laboratories.

[7] J. P. Van Dorsselaere et al. The ASTEC integral code for severe accident simulation, *Nucl. Technology* – NT-3-0846, vol.165, March, 2010.

[8] A. Kontautas, E. Urbonavicious. Analysis of aerosol deposition in PHEBUS containment during FPT-1 experiment, *Nucl. Engineering and Design* – vol 239 (2009), pp 1267-1274.

[9] L. Z. Waldmann, On the motion of spherical particles in non-homogeneous gases, *Rarefied Gas Dynamics*, Academic Press, New York (1961).

[10] G. Mazzini, A. Manfredini, Analysis of the Thermal-hydraulic and Aerosol Behaviour in the Phebus Containment Vessel During the FPT1 Test Using MELCOR and ASTEC Codes, *XXVIII Congresso UIT sulla Trasmissione del Calore*, Brescia (2010).

[11] T. Haste, F. Payot, C. Dominguez, Ph. March, B. Simondi-Teisseire, M. Steinbrück**,** **"**Study of boron behavior in the primary circuit of water reactors under severe accident conditions: A comparison of Phebus FPT3 results with other recent integral and separate-effects data", Nuclear Engineering and Design, 2011

[12] Luis E. Herranz, Mònica Vela-Garcìa, Joan Fontanet, Claudia Lòpez del Prà, "Experimental interpretation and code validation based on the PHEBUS-FP programme: Lessons learnt from the analysis of the containment scenario of FPT1 and FPT2 tests", Nuclear Engineering and Design 237 (2007) 2210–2218, 22 March 2007

[13] A. Manfredini, F. Oriolo, S. Paci," VALIDATION OF THE MELCOR V.1.8.5 CODE AGAINST THE FPT0 AND FPT1 PHEBUS EXPERIMENTAL TESTS", DIMNP, RL 932 (01), 2001

[14] A. Manfredini, F. Oriolo, S. Paci," DIMNP PRE TEST CALCULATIONS OF THE OECD/CSNI ISP-46 ON PHEBUS TEST FPT1 USING THE MELCOR V.1.8.5 COMPUTER CODE", DIMNP, DIMNP 006 (02), 2001, Paper presented at the Intermediate Comparison Workshop on "International Standard Problem 46" Aix-en Provence (F), 21 – 23 October 2002

PART III: SENSITIVITY ANALYSES ON ALWR REACTOR (AP1000)

6 AP1000 SPECIAL ADVANCED DESIGN FEATURES

6.1 Overview

The AP1000 standard design (Figure 6.1) [1], as the AP600 standard design [2] (Figure 6.2 and Figure 6.3), evolved from current PWR technology through incorporation of several passive design features and other design changes intended to make the plant safer, more available, and easier to operate. For example, in the primary circuit, the pumps are integrated in the Steam Generators in order to eliminate the Loop Seal pipes (Figure 6.4). Insights from the Probabilistic Safety Assessments (PSAs) [1] of operating reactors helped in designing such features, as well as in identifying other design changes. Therefore, the AP1000 design incorporates features intended to improve plant safety, thus reducing risk when compared to current generation nuclear power plants. Some of these special advanced design features are preventive in nature, while others are designed for accident mitigation. Preventive features aim to accomplish the following objectives [3]:

- minimize the probability of initiation of plant transients
- arrest the progression of plant transients once they start
- prevent severe accidents (core damage)

Figure 6.1 AP1000 prospective example [2]

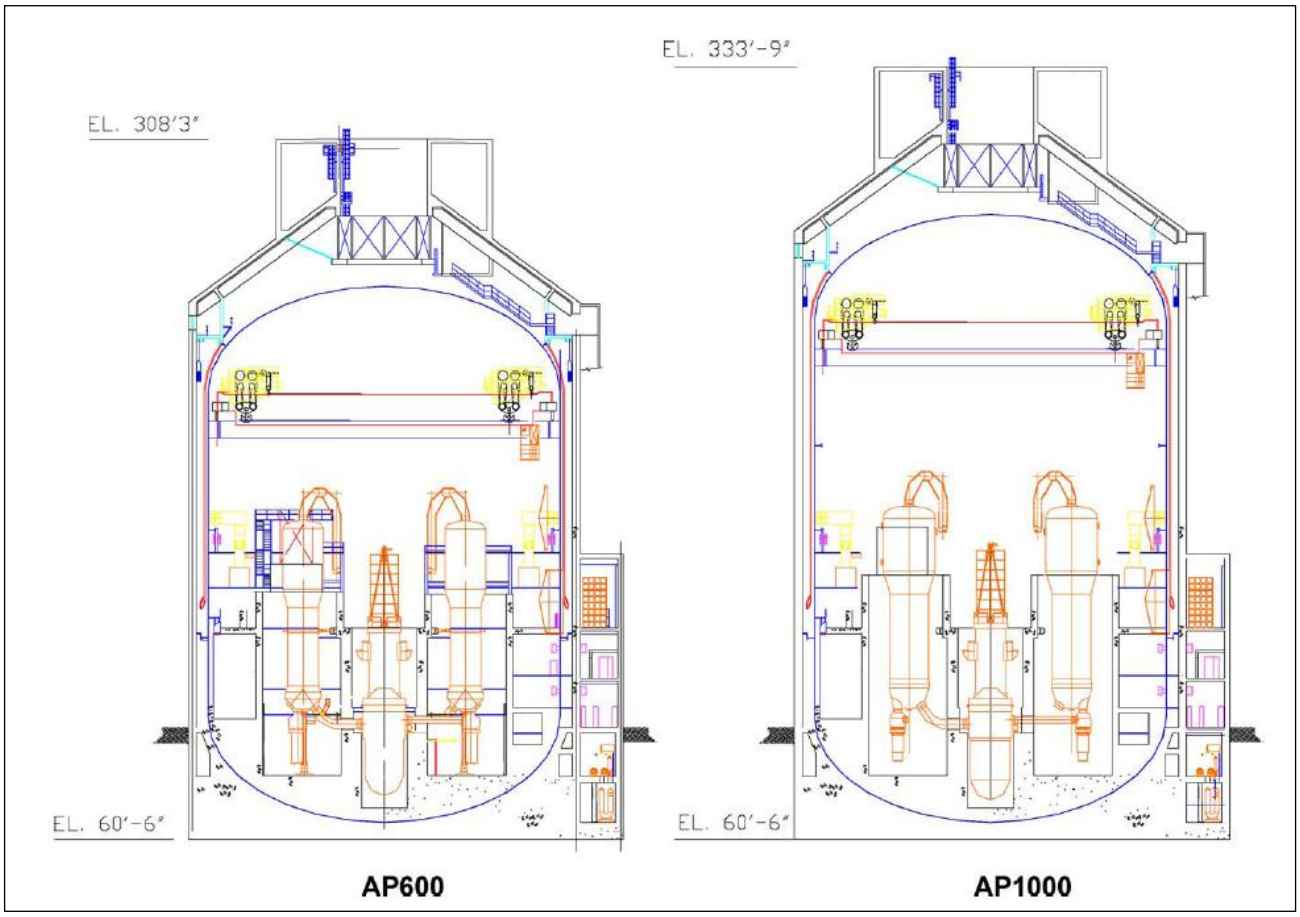

Figure 6.2 Westinghouse AP600 and AP1000 plants (section) [3]

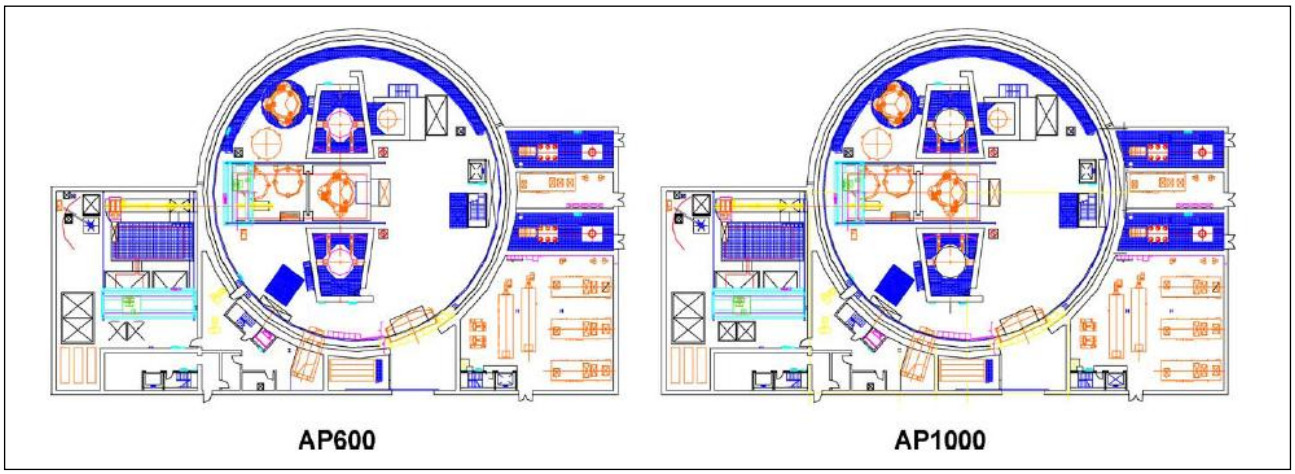

Figure 6.3 Westinghouse AP600 and AP1000 plants (plan)

Mitigative features aim to arrest the progression of core damage and prevent a breach of the reactor vessel and containment pressure boundary. The sections 6.2 and 6.3 describe the major preventive and mitigative special advanced design features of the AP1000, respectively. In these

descriptions, a brief qualitative discussion highlights the effect that each of these features has on various elements involved in severe accident prevention and mitigation [4].

This chapter describes briefly the principal systems involved in the analyses of the SA scenarios. The technical data are reported in the Appendix 2 [2].

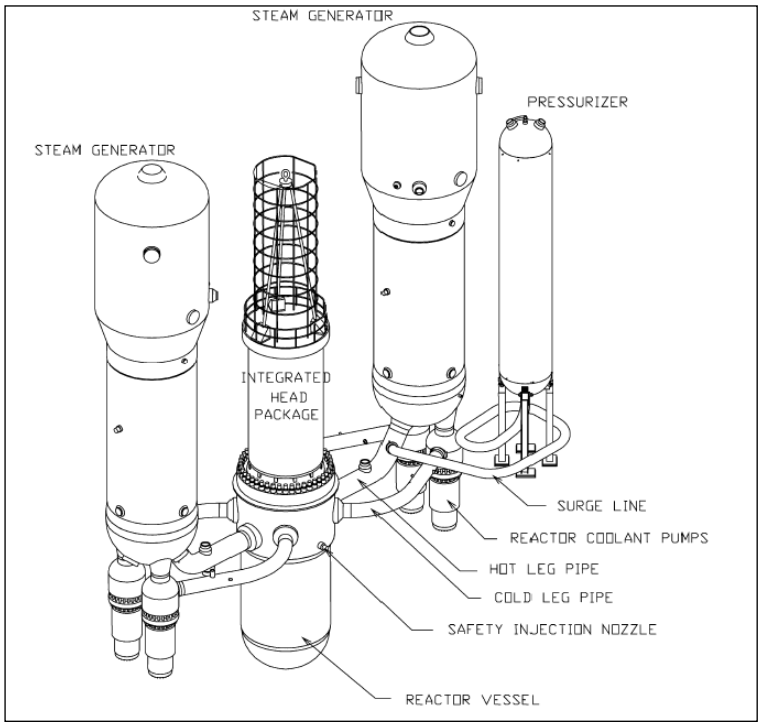

Figure 6.4 AP1000 Primary Circuit [4]

6.2 Special Advanced Design Features for Preventing Core Damage

The major features incorporated into the AP1000 design [1] for the purpose of limiting plant transients and preventing severe accidents are discussed in the following paragraphs.

6.2.1 *Passive Safety-Related Systems*

The AP1000 design relies on passive safety-related systems for accident prevention and mitigation. The passive systems rely on natural forces, such as gravity and stored energy, to perform their safety functions (once actuated and started). For actuating and starting such systems, certain active components, such as check valves, must operate. Such components do not require ac power for operation (to open) or for control, and no support systems are needed after actuation. This

reduces significantly the risk contribution from Loss of Outside Power (LOOP) and Station Blacout (SBO) events, as compared to operating nuclear power plants. In addition, because of the passive nature of these systems, the AP1000 design eliminates several important contributions to risk for operating nuclear power plants. These risks are associated with failure of support systems (e.g., ac power and component cooling) and failure of active components (e.g., pumps and diesel generators) to start and to run. Finally, the passive nature of the safety systems reduces the reliance on operator actions to mitigate accidents, as compared to operating nuclear reactor.

6.2.2 Defense-In-Depth Active Non-Safety-Related Systems

The AP1000 design [4] incorporates several active systems that are capable of performing some of the functions performed by the safety-related passive systems. The availability of such redundant systems minimizes the challenge to the safety-related passive systems by providing core cooling during normal plant shutdowns and a first line of defense during accidents. Operation of the non-safety-related system prevents a challenge to the Passive Residual Heat Removal (PRHR) heat exchanger during anticipated transients (see Figure 6.2). For accidents occurring during power operation, the non-safety-related normal residual heat removal system provides additional defense-in-depth to the feed portion of the feed-and-bleed core cooling function; it provides an alternate "pumped" mean of low-pressure injection from the In Refueling Water Storage Tank (IRWST), as shown in Figure 6.2, and long-term recirculation from the containment sump. The Diverse Actuation System (DAS) provides an alternate mean for initiating automatic and manual reactor trip and actuation of selected Engineering Safety Features (ESFs) which is diverse from the safety-related Protection and safety Monitoring System (PMS).

6.2.3 In-Containment Refueling Water Storage Tank

The important characteristics and functions of the IRWST [1] include the following (Figure 6.5):

- possess a large capacity
- acts as a heat sink for the PRHR system
- provides water for low-pressure emergency core cooling (IRWST injection and Normal Residual Heat Removal System **(**RNS) injection) after Reactor Core System (RCS) depressurization

- serves as the heat sink for the first three stages of the Advanced Depressurization System (ADS)
- provides debris cooling following a severe accident

The IRWST is a central feature in the AP1000 design that contributes to the simplicity and reliability of the passive safety systems. As heat sink for the PRHR heat exchanger, it allows reliable core cooling at high RCS pressures when cooling through the steam generators (Steam Generators) fails during anticipated transients or Steam Generator Tube Rupture (SGTR) events (i.e., the IRWST reduces the need for RCS depressurization and use of feed-and-bleed cooling). It is a reliable source of borated water for low-pressure emergency core cooling and eliminates the need for switching over from the injection mode to the recirculation mode during emergency core cooling operations (a risk-important failure at operating Pressurized Water Reactors (PWRs)).

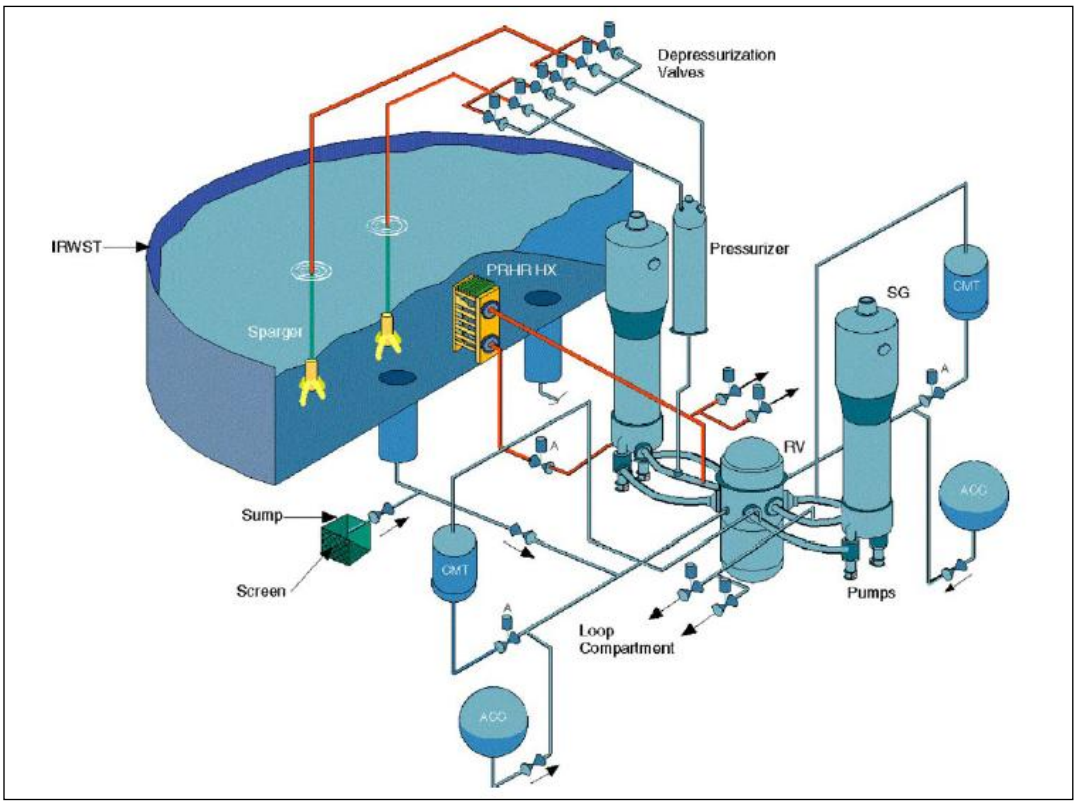

Figure 6.5 AP1000 RCS and passive core cooling system [5]

6.2.4 Redundant Decay Heat Removal Systems

Redundant DHR systems provide defense-in-depth during all possible scenarios of an accident. The following represent alternate means of core cooling:

- main feed water and condensate
- start-up feed water
- automatically actuated PRHR (with manual actuation backup capability)
- automatic, with manual backup, feed-and-bleed capability using systems with adequate redundancy and defense against common-cause failures (CCFs) throughout the RCS depressurization range for both the feed function (two core makeup tanks (CMTs), two accumulators, the two RNS pumps, and the two IRWST gravity injection lines) and the bleed function (four ADS stages with two paths in each of the first three stages and four paths in the fourth stage).

6.2.5 Automatic Depressurization System

The function of the ADS [1] is to provide a safety-related mean of reducing RCS pressure in a controlled fashion during accidents to allow safety injection. This constitutes the bleed portion of the feed-and-bleed means of core cooling. The ADS is actuated automatically, with manual backup actuation capability, and has incorporated redundancy (four ADS stages with two paths in each of the first three stages and four paths in the fourth stage) and defense against CCFs (motor operated valves (MOVs) in the first three stages and explosive valves in the fourth stage).

6.2.6 Redundant Safety Injection Systems

The AP1000 design includes redundant and diverse means of providing safety injection (i.e., the feed portion of the feed-and-bleed core cooling function) throughout the RCS depressurization range [1]. Safety injection is provided by safety-related systems (two CMTs, two accumulators, and two IRWST gravity injection lines), as well as by non-safety-related defense-depth systems (the two chemical and volume control pumps and the two RNS pumps).

6.2.7 Redundant Long-Term Recirculation Systems

RCS recirculation (Figure 1.2) is required for long-term core cooling during loss-of-coolant accidents (LOCAs) and whenever feed-and-bleed is used to cool the core during an accident [1]. In the AP1000, recirculation can be achieved either by gravity (through the safety-related IRWST injection lines) or by pumps (the non-safety-related RNS) with suction from the containment sump. There are two redundant recirculation lines (one for each of the two redundant IRWST injection lines). Furthermore, each recirculation line has two redundant paths.

6.2.8 Redundant Passive Containment Cooling Systems

Containment cooling, as the ultimate heat sink function for all accidents involving loss of feed water (main and startup) to both Steam Generators, is very important in the AP1000 design [2]. The containment cooling function is performed by two highly reliable and redundant means that remove thermal energy from the containment atmosphere to the environment via the steel containment vessel by natural external air circulation, and evaporation of water drained by gravity from an elevated tank (Figure 6.6).

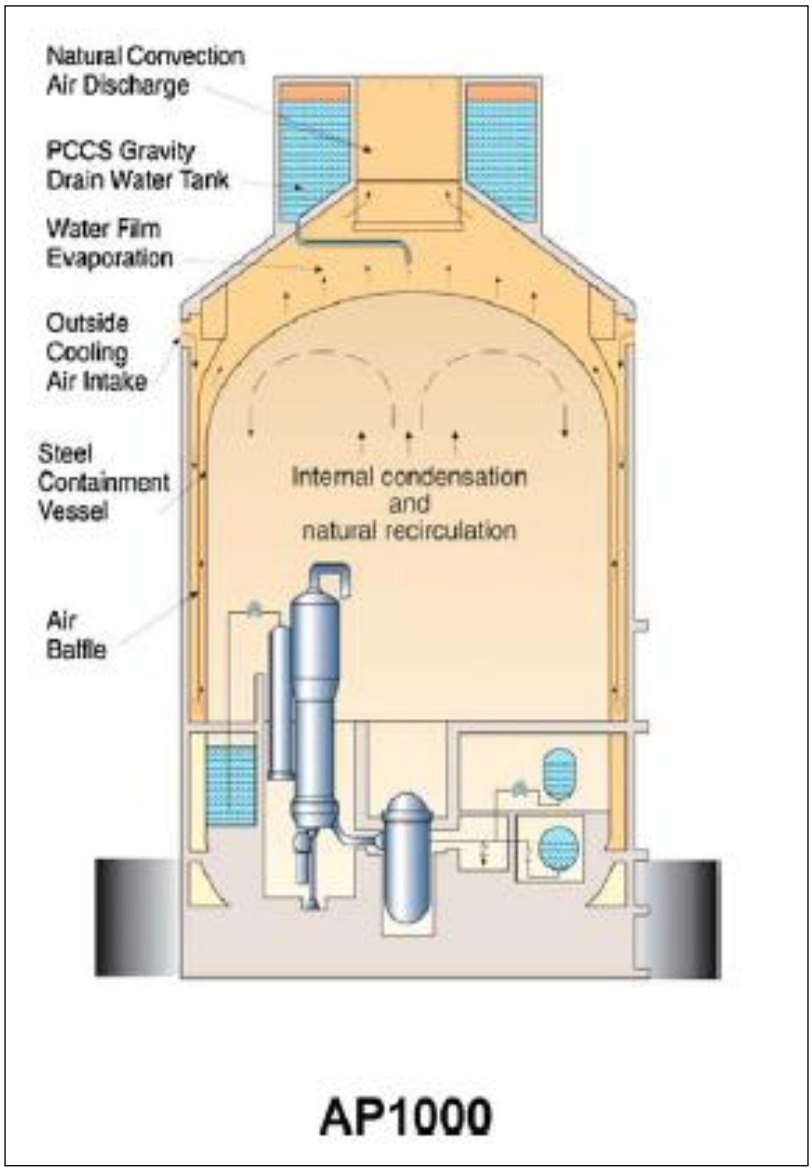

Figure 6.6 AP1000 Containment Building [2]

6.2.9 Canned Reactor Coolant Pumps

The AP1000 uses canned reactor coolant pumps (RCPs), as shown in Figure 1.3. A canned-motor pump contains the motor and all rotating components inside a pressure vessel. The pressure vessel consists of the pump casing, thermal barrier, stator shell, and stator cap, which are designed for full RCS pressure. Because the shaft for the impeller and rotor is contained within the pressure boundary, seals are not required to restrict leakage out of the pump into containment. The use of canned-motor RCPs in the AP1000 design eliminates the RCP seal LOCA (an important contributor to risk for operating nuclear power plants).

6.2.10 Improved Control Room Design and Digital Instrumentation and Control Systems

The AP1000 control room is an advanced design that is expected to provide more useful information to the operator than currently operating reactor designs. The AP1000 control room is still being designed. For this reason, the PSA took no credit for the impact of the advanced control room on normal operations (e.g., initiating event frequency) and emergency response.

6.2.11 Large-Pressurizer and Low-Power Density

The larger pressurizer, as compared to operating plants, reduces the frequency of reactor scrams by increasing transient operation margins. This feature also moderates the pressure rise during certain transient events, such as loss of Main Feed Water (MFW), thus reducing the likelihood of a challenge to the primary safety valves. A larger pressurizer volume also helps in lowering the peak pressure that can be reached after a postulated Anticipated Transient Without Scram (ATWS) event.

6.2.12 Physical Separation of Safety System Redundant Trains

The AP1000 design provides physical separation of safety systems or trains of systems that perform redundant safety-related functions. This increases the availability of these systems because of their protection from failures associated with internal fires, internal floods, and similar CCFs. Except for support systems, such as Class 1E dc power and instrumentation and control (I&C) systems and the passive containment cooling system (PCS), all passive safety-related systems are located inside the containment where external events, such as fires, floods, and tornadoes, are less likely to occur. This design feature contributes to the reduction of risk as compared to current plant designs.

6.2.13 Highly Reliable DC Power Supply With 72-Hour Station Blackout Coping Capability

Each of the four independent and physically separated divisions of 125-V dc Class 1E vital I&C power is provided with a separate and independent Class 1E 24-hour battery bank. In addition, two of the four divisions are provided with a Class 1E 72-hour battery bank. This permits operating I&C loads, which are associated with safety systems that may be required following the loss of ac power concurrent with a DBA, for 72 hours. This feature contributes to the large reduction of risk associated with SBO accidents as compared to current plant designs.

6.3 Special Advanced Design Features for Core Damage Consequence Mitigation

The following design features improve the ability of the containment to accommodate the challenges associated with severe core damage accidents. The AP1000 PSA and/or supporting deterministic analyses model the impact of these features on severe accident mitigation and containment performance.

6.3.1 *Automatic Depressurization System*

In addition to providing a core damage prevention function, the ADS also serve a mitigative function. Specifically, for core damage events in which early depressurization is not successful, late actuation of the ADS (i.e., before significant core damage and debris relocation into the lower plenum of the reactor vessel) can reduce or eliminate the potential for creep rupture of the Steam Generator tubes and the reactor vessel. Prevention of reactor vessel breach precludes severe accident phenomena associated with vessel failure (i.e., direct containment heating (DCH), large hydrogen combustion events at vessel breach, ex-vessel steam explosions, and core/concrete interactions (CCIs)), thereby reducing the probability of early containment failure. The ADS also reduces the amount of fission products released to the containment atmosphere by routing a portion of the discharge flow (from ADS Stages 1 through 3) through a sparger network in the IRWST. However, in many sequences, the RCS is vented to the containment airspace (via the fourth stage of the ADS) at the time when most fission products are released, and the potential for fission product scrubbing is not fully realized. Finally, RCS depressurization can reduce or terminate fission product releases to the environment during SGTR events.

6.3.2 *Large, Passively Cooled Steel Containment*

The AP1000 design includes a large, passively cooled steel containment [4]. The ratio of the containment building volume to reactor power for the AP1000 is similar to that for typical operating PWRs with large, dry containments. The large volume to power ratio reduces the potential for developing detonable concentrations of hydrogen under severe accident conditions and the potential for containment overpressure from no-condensable gas build-up. The containment pressure capacity is sufficiently large that the pressure loads associated with early challenges (e.g., hydrogen combustion and DCH) are at or below the applicant's Service Level C estimate (728.8 kPa (91 psig)) and pose an insignificant threat to containment integrity (i.e., a containment failure probability of less than 1 percent). The Passive Containment System (PCS) provides water to the external surface of the containment shell from the PCS water storage tanks or the post-72-hour water tank (Figure 1.2). Alternative water sources can be provided via separate connections outside containment, in accordance with accident management guidelines to be developed by the COL applicant. Without operation of the PCS, air cooling alone is not sufficient to maintain containment pressure below the applicant's Service Level C estimate in the long term, and the containment will need to be vented after 24 hours to prevent overpressure failure of containment.

6.3.3 In-Containment Refueling Water Storage Tank

The AP1000 design incorporates an IRWST [1] (Figure 6.5). In addition to serving the typical function of the refueling water storage tank at operating plants, this system performs water collection, delivery, and heat sink functions inside the containment during accident conditions. The IRWST is important to the progression of a severe accident because of its ability to condense steam and scrub fission products for releases into the IRWST via Stages 1 through 3 of the ADS, as well as its ability to reduce the likelihood of reactor vessel failure and Molten Core Concrete Interaction (MCCI or CCI) by enabling reactor cavity flooding via gravity draining (Figure 6.7).

The potential for hydrogen-rich mixtures to form in the vicinity of the IRWST (e.g., as a result of steam condensation as the hydrogen-steam blowdown passes through the IRWST) represents a unique containment challenge for the AP1000, but is minimized by locating the IRWST pipe vents in areas where diffusion flames will not impinge on the containment shell, and by equipping the

IRWST vents along the containment wall with louvers that will reclose following an initial release into the IRWST.

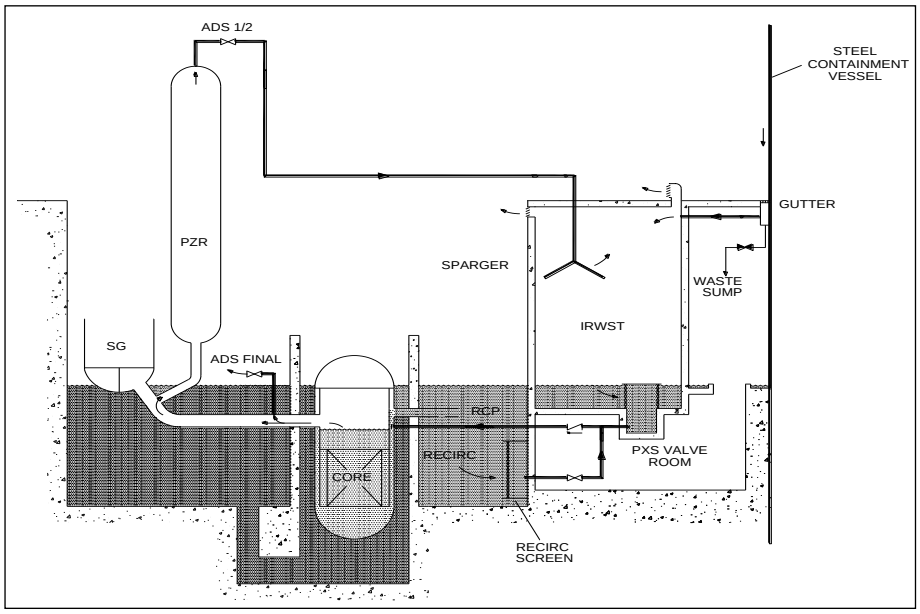

Figure 6.7 Enabling reactor cavity flooding via gravity draining (By ANSALDO) [5]

6.3.4 External Reactor Vessel Cooling

The capability to fully flood the AP1000 reactor cavity and depressurize the RCS in the majority of core melt sequences minimizes the potential for a reactor vessel breach by molten core debris [4]. By maintaining reactor vessel integrity, the potential for large releases caused by ex-vessel severe accident phenomena is substantially reduced; however, a residual threat from hydrogen combustion remains. The ability to flood the reactor cavity is enhanced in the AP1000 design by the following attributes:

- A containment and reactor cavity arrangement which permits break flow from the RCS to drain to the cavity without significant holdup in containment.
- The inclusion of manually actuated, safety-grade valves which allow additional water from the IRWST to be drained to the cavity.

The AP1000 emergency response guideline specifies the operator action to flood the cavity. It instructs the operator to flood the reactor cavity only if injection to the RCS cannot be recovered or containment radiation reaches levels that indicate fission product releases, as determined by a core damage assessment guideline. The operator instructions to flood the cavity have been moved from

the end of the procedure (as in the AP600) to the beginning of the procedure to achieve the higher water depths and earlier flooding times required to successfully cool the external reactor vessel of the AP1000. The following design features contribute to the effectiveness of Emergency Reactor Vessel Cavity in the AP1000:

- a reactor vessel lower head that contains no in-core instrument or other penetrations
- a reactor vessel insulation system that limits thermal losses during normal operations, but provides an engineered pathway for supplying water cooling to the vessel and venting steam from the reactor cavity during severe accidents
- refinements in the reactor vessel insulation system design (relative to the AP600) to increase the heat transfer capability (critical heat flux) from the reactor pressure vessel (RPV) to the surrounding water and to accommodate the higher decay heat level in the AP1000

6.3.5 Reactor Cavity Design

The AP1000 design relies primarily on safety-grade RCS depressurization and reactor cavity flooding capabilities to prevent high-pressure core melt events and reactor vessel breach [4]. In the event that vessel breach occurs, the AP1000 reactor cavity design can accommodate the loads associated with ex-vessel severe accident phenomena without early loss of containment integrity. These challenges include DCH, fuel-coolant interactions (FCIs), and CCI. The specific reactor cavity features that deal with each challenge are summarized below.

1. DCH: The paths from the reactor cavity to the upper containment volume in the AP1000 include the following:
    - the area around the reactor vessel flange
    - the area where the coolant loops penetrate through the biological shield
    - a ventilation shaft from the roof of the reactor coolant drain tank room leading to the Steam Generator compartments

These paths are convoluted; hence a portion of the corium will be de-entrained and removed from the atmosphere before reaching the upper containment region, thereby reducing the pressure rise associated with DCH. The peak containment pressure for a postulated DCH event is expected to be sufficiently low that the corresponding probability of containment failure is negligible (less than 0.1 percent).

2. FCI: The deterministic evaluation of ex-vessel FCIs indicates that the impulse loads from ex-vessel steam explosions may fail the reactor cavity floor and wall structures, but the integrity of the embedded steel liner will be maintained. The evaluation also indicates that containment vessel integrity will not be compromised by the displacement of the RPV as a result of the impulse loading.
3. CCI: The AP1000 reactor cavity design incorporates features generally consistent with the Electric Power Research Institute's (EPRI) Utility Requirements Document (URD) guidance, including the following (Figure 6.8):
    - a cavity floor area and sump curb that provide for debris spreading without debris ingression into the reactor cavity sump
    - a manually actuated reactor cavity flood system that would cover the core debris with water and maintain long-term debris coolability
    - a minimum 0.85-m (2.8 ft) layer of concrete to protect the embedded containment shell, with an additional 1.8 m (6 ft) of concrete below the liner elevation

The enhanced capability to retain a molten core in-vessel results in a low expected frequency of basemat melt-through in the AP1000 PSA in conjunction with these design features. Compared to other advanced light-water reactors (ALWRs), the AP1000 ex-vessel debris bed is deeper and the concrete basemat is thinner. The AP1000 design does not impose any restrictions on the type of concrete that can be used for the containment basemat and the reactor cavity walls. Although these factors tend to increase the severity of basemat erosion, analyses using the Melt spread and Modular Accident Analysis Program (MAAP) codes indicate that in the event of unabated CCI, containment basemat penetration or containment over pressurization will not occur until after 2 days, regardless of concrete composition. For a limestone basemat, which maximizes no-condensable gas generation and minimizes concrete ablation, basemat penetration would occur after about 3 days following the onset of core damage. Containment pressure will not reach the applicant's Service Level C estimate (728.8 kPa (91 psig)) until even later. Use of basaltic concrete, which maximizes concrete ablation and minimizes no-condensable gas generation, would reduce the time of basemat melt-through to about 2 days, but containment pressure would not reach Service Level C until much later. Thus, in the event that core debris is not retained in vessel, the AP1000 design provides adequate protection against early containment failure and large releases resulting from CCIs.

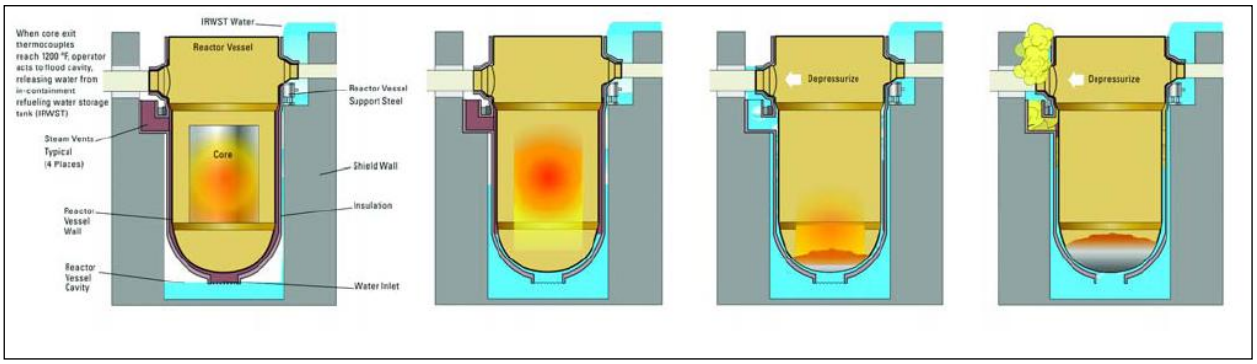

Figure 6.8 Reactor Cavity during a Severe Accident [4]

6.3.6 Hydrogen Igniter System

The AP1000 design incorporates a distributed ignition system to promote combustion at lean hydrogen concentrations and to minimize the potential for large deflagrations or detonations [1]. The igniter system is non-safety-related, but is subject to investment protection, short-term availability controls. The system uses 64 glow plug igniters powered from the non-safety-related onsite ac power system and is manually actuated from the control room when the core exit temperature exceeds 648.9 °C (1200 °F). The hydrogen igniters system is capable of being powered by either offsite ac power or onsite nonessential diesel generators. In the event of an SBO, which represents less than 1 percent of the Core Damage Frequency (CDF), the system can be powered from the non-Class 1E batteries using dc-to-ac inverters. However, the PSA did not credit this feature. The AP1000 design also includes two non-safety-related Passive Autocatalytic Recombiners (PARs) located within the containment. The PARs are provided for defense-in-depth protection against the build-up of hydrogen following a design-basis LOCA. Although the PARs are expected to function and reduce combustible gas concentrations during severe accidents, they are not credited in the PSA. The proven design of the glow plug igniters and the diverse means of powering the system, in conjunction with the small fraction of core melt sequences involving loss of onsite power in the AP1000 design, significantly reduce the threat of containment failure due to hydrogen deflagrations or detonations. The use of PARs further reduces the threat from hydrogen burns in those events in which the igniters are unavailable.

6.3.7 Non-Safety Containment Spray System

The AP1000 includes a non-safety containment spray system for severe accident management. The system consists of two spray rings located above the containment polar crane, with flow supplied from the normal fire main header [1]. The source of water is provided by either the primary or secondary fire protection system water tank (depending on tank and inventory availability) using either the motor-driven or diesel-driven fire protection system pumps. The Level 2 and Level 3 PSA do not credit the impact of the non-safety-grade containment spray system on containment response and fission product releases. Containment sprays could significantly reduce the estimated risk in the baseline PSA because the sprays would be effective in reducing the source terms in the risk-dominant release categories.

6.3.8 Containment Vent

The AP1000 design configuration will include a containment vent path that can be used to control containment pressure in the unlikely event of long-term over pressurization of the containment. The Containment Vent applicant, as part of Containment Vent Action Item regarding the severe accident management program, will identify the specific penetration(s) to be used for containment venting and develop and implement severe accident management guidance for venting containment using the framework provided in [6]. The PSA does not credit the impact of the containment vent on containment response.

References

[1] US-NRC, "Final Safety Evaluation Report Related to Certification of the AP1000 Standard Design", *NUREG-1793,* 2006

[2] Westinghouse Electric Co., “The Westinghouse AP1000 Advanced Nuclear Plant – Plant Description”, Copyright © 2003.

[3] T.L. Schulz. “Westinghouse AP1000 advanced passive plant”, Nuclear Engineering and Design 236 1547–1557, 2006

[4] US-NRC, “AP1000 Design Control Document – Supplement 2 to the Final Safety Evaluation Report to the AP1000 Standard Design Certification," NUREG-1793-Supplement 2 , Rev. 19, 2011

[5] ANSALDO Nucleare and Westinghouse private communications

[6] US-NRC, Volume 1, "Individual Plant Examination Program: Perspectives on Reactor Safety and Plant Performance," Part 1., NUREG-1560, 2001

7 SUMMARY OF RISK ANALYSIS OF AP1000 AT POWER OPERATION

7.1 Summary of Level 1 Internal Events PSA

The results of PSA of level 1 [1] [2] are discussed below, focusing on the few sequences (and related risks) which foresee severe accident scenarios. The methodology of PSA is reported in Appendix 1 [3]. These initial events are the first step to study the Severe Accidents' Phenomena.

The applicant estimated the mean CDF [3] for the AP1000 design from internal events during operation at power to be about $2.4*10^{-7}$/yr. In Table 7.1 the most relevant sequences responsible of 90% CDF are shown, together with their contribution to CDF risk. Ranges of mean CDFs, by initiating event category, for currently operating PWR reactor designs are also shown for comparison. The applicant estimated the total CDF of the AP1000 design, from internal events at power operation, to be roughly two orders of magnitude smaller than the corresponding total CDF of an average operating PWR reactor.

For the AP1000 design [4] [5], the various LOCA categories of initiating events essentially dominate the CDF profile, representing about 85% contribution to risk, followed by reactor vessel rupture (about 4 percent) and transient events (about 4 percent). Contributions from SGTR events (about 3 percent), ATWS sequences (about 2 percent), and LOOP/SBO events (less than 1 percent) are relatively small.

7.2 The Dominant Accident Sequences Leading to Core Damage

The applicant's PSA [1] [2] results identify 100 sequences initiated by internal events that contribute almost 100 percent of the estimated CDF from internal events. The top 10 sequences, contributing about 80 percent of the total CDF from internal events, are summarized below. In order to give a complete view, all sequences are described in Appendix 3 [2].

7.2.1 Sequence N°1

The 1st Sequence [1], with a CDF of about $9.5*10^{-8}$/yr and about 28.5 percent contribution, is initiated by a break in one of the two safety injection lines (a LOCA event) followed by failure of

the IRWST injection line not affected by the break to remove the decay heat from the core (CMT injection and RCS depressurization via the ADS system are successful).

Initial Event	AP1000 (CDF /yr)	Operating PWRs from NUREG-1560 (CDF range/yr)
LOCAs (Total)	**$2.1*10^{-7}$**	**$8*10^{-5}$ to 10^{-6}**
Large	$4.3*10^{-8}$	
Spurios ADS activation	$3*10^{-8}$	
Safety Injection Line Break	$9.5*10^{-8}$	
Medium	$1.6*10^{-8}$	
Small	$1.8*10^{-8}$	
CMT Line Break	$4*10^{-9}$	
RCS Leak	$3*10^{-9}$	
Steam Generator Tube Rupture	$7*10^{-9}$	**$3*10^{-5}$ to $9*10^{-9}$**
Transients	$8*10^{-9}$	**$3*10^{-4}$ to $5*10^{-7}$**
LOOP/SBO	10^{-9}	**$7*10^{-5}$ to 10^{-8}**
ATWS	$5*10^{-9}$	**$4*10^{-5}$ to 10^{-8}**
Interfacing System LOCA	$5*10^{-11}$	**$8*10^{-6}$ to 10^{-9}**
Vessel Rupture	$1.8*10^{-8}$	**10^{-7}**
Total	**$2.4*10^{-7}$**	**$3*10^{-4}$ to $4*10^{-6}$**

Table 7.1 Summarized Event Table [1]

In addition to the initiating event, the following risk-important failures appear in this sequence:

- plugging of the IRWST discharge line strainer in the intact line
- CCF of the two CVs in the intact IRWST discharge line
- CCF of the two explosive (squib) valves in the intact IRWST discharge line

7.2.2 Sequence N°2

The 2nd Sequence [1], with a CDF of about $4.3*10^{-8}$/yr and about 18 percent contribution, is initiated by a large LOCA event which is not caused by spurious ADS actuation (equivalent break diameter greater than 9 inches, but smaller than a vessel rupture) followed by failure of any one of the two accumulators to inject. In addition to the initiating event, the following risk-important failures appear in this sequence:

- failure of any Check Valve in the accumulator injection lines to open
- plugging of any flow-tuning orifice in the accumulator injection lines

7.2.3 Sequence N°3

The 3rd Sequence [1], with a CDF of about $2.1*10^{-8}$/yr and about 9 percent contribution, is initiated by a spurious ADS actuation event that results in a large LOCA. The RCS rapidly depressurizes and at least one of the accumulators injects, making up the RCS water loss in the short timeframe. However, because of the failure of either CMT injection or ADS actuation, the automatic IRWST injection is not actuated. In addition to the initiating event, risk-important failures appearing in this sequence are listed below:

- CCF of hardware in the PMS ESF input logic groups (causes CMT injection actuation failure which results in failure of automatic IRWST injection actuation with inadequate time for manual actuation)
- CCF of CMT-level sensors which prevents IRWST injection actuation
- CCF of CMT injection AOVs to open
- CCF of CMT injection CVs to open
- CCF of two or more fourth stage ADS explosive (squib) valves to operate

7.2.4 Sequence N°4

The 4th Sequence [1], with a CDF of about $2*10^{-8}$/yr and about 8 percent contribution, is initiated by a break in one of the two safety injection lines (a LOCA event) followed by successful CMT injection, but failure of full RCS depressurization (to allow low-pressure IRWST injection). The failure that dominates the risk associated with this sequence is the CCF of ADS Stage 4 explosive (squib) valves.

7.2.5 Sequence N°5

The 5th Sequence [1], with a CDF of 10^{-8}/yr and over 4 percent contribution, is a reactor vessel rupture event which leads directly to core damage.

7.2.6 *Sequence N°6*

The 6th Sequence [1], with a CDF of about $8.5*10^{-9}$/yr and over 3 percent contribution, is initiated by a small LOCA event (0.952 cm to 5.08 cm (0.375 in. to 2 in.) equivalent break diameter) followed by failure to establish recirculation from the containment sump when the IRWST inventory is depleted (high-pressure injection by the CMTs, heat removal by the PRHR, containment isolation, depressurization, and low-pressure injection by either the RNS or the IRWST are successful). The following risk-important failures, in addition to the initiating event, appear in this sequence:

- CCF of both sump recirculation lines due to sump screen plugging
- CCF of all IRWST level transmitters (causes failure of automatic actuation of sump recirculation)
- operator failure to manually actuate sump recirculation (when automatic actuation fails)

7.2.7 Sequence N°7

The 7th Sequence [1], with a CDF of about $7.5*10^{-9}$/yr and about 3 percent contribution, is initiated by a medium LOCA event (5.08 cm to 22.9 cm (2 in. to 9 in.) equivalent break diameter) followed by failure to establish recirculation from the containment sump when the IRWST inventory is depleted (high-pressure injection by the CMTs, containment isolation, depressurization, and low-pressure injection are successful). With the exception of the initiating event, the risk important failures appearing in this sequence are the same as those for Sequence 6th.

7.2.8 Sequence N°8

The 8th Sequence [1], with a CDF of about $5*10^{-9}$/yr and over 2 percent contribution, is initiated by a small LOCA event (0.952 cm to 5.08 cm (0.375 in. to 2 in.) equivalent break diameter) followed by failure of full depressurization (required for low-pressure injection from the IRWST), by success of partial depressurization (below the point at which injection by the RNS is possible), and by failure of the RNS. High-pressure injection by the CMTs, RCP trip, and heat removal by the

PRHR are successful. The following risk-important failures, in addition to the initiating event, appear in this sequence:

- CCF of two or more fourth stage ADS explosive (squib) valves to operate
- failure of any of four RNS isolation valves (V055, V011, V022, V023) to open
- unavailability of the cask-loading pit due to fueling unloading operations

7.2.9 Sequence N°9

The 9th Sequence [1], with a CDF of about $4.5*10^{-9}$/yr and about 2 percent contribution, is initiated by a medium LOCA event (5.08 cm to 22.9 cm (2 in. to 9 in.) equivalent break diameter) followed by failure of full depressurization (required for low-pressure injection from the IRWST), by success of partial depressurization (below the point at which injection by the RNS is possible), and by failure of the RNS to inject. High-pressure injection by the CMTs, RCP trip, and heat removal by the PRHR are successful. With the exception of the initiating event, the risk-important failures appearing in this sequence are the same as those for Sequence 8th.

7.2.10 Sequence N°10

The 10th Sequence [1], with a CDF of about $3.7*10^{-9}$/yr and about 1.5 percent contribution, is initiated by a spurious ADS actuation event that results in a large LOCA followed by failure of any one of the two accumulators to inject. In addition to the initiating event, the failure that dominates the risk associated with this sequence is the CCF of two accumulator CVs, one in each of the two accumulator injection lines.

7.3 Risk-Important Design Features

Listed below are the major features that contribute to the reduced CDF of the AP1000 design [1], as compared to operating PWR, for each of the initiating event categories contributing the most to this reduction.

7.3.1 *Loss of Offsite Power and Station Blackout Sequences*

The following are the most important features of the AP1000 design that contribute to the reduction in the estimated CDF associated with LOOP, including SBO, sequences (CDF reduced to 10^{-9}/yr from the $7*10^{-5}$/yr to 10^{-8}/yr range at operating PWR) [2]:

- Safety-related passive systems that do not rely on ac power for operation, and instead rely on natural forces, such as gravity and stored energy, to perform their accident mitigation functions once actuated and started. When power is needed to actuate and start such passive systems, dc power provided by Class 1E batteries is used.
- The PRHR is automatically actuated, without the need for any electrical power, to provide core cooling upon LOOP (AOVs are fail-safe in the open position).
- Class 1E dc batteries with capability to support all front line passive safety-related systems for 72 hours.
- Defense-in-depth, which provide alternative means for removing decay heat from the RCS during a LOOP/SBO accident. Most current PWR plants rely on two alternative means for core cooling:
    - an auxiliary feed water system, with at least one turbine-driven pump for SBO events, in addition to motor-driven pump(s)
    - A manual feed and bleed capability when onsite ac power is available.

      In contrast, the AP1000 design provides better and more reliable defense-in-depth by-relying on the following alternative means for core cooling:

        - the automatically actuated non-safety-related SFW system when onsite ac power is available
        - the automatically actuated safety-related PRHR system
        - an automatic, with manual backup, feed-and-bleed capability using systems with adequate redundancy and defense against CCFs throughout the RCS depressurization range for both the feed function (two CMTs, two accumulators, the two RNS pumps, and the two IRWST gravity injection lines) and the bleed function (four ADS stages with two paths in each of the first three stages and four paths in the fourth stage)
- The improved reliability of the PRHR system (as compared to the auxiliary feed water system used in most current PWR plants) contributes significantly to the reduced risk associated with LOOP/SBO sequences (the function of the PRHR following a LOOP/SBO event is similar to the auxiliary feed water system function in operating PWRs).

- Canned RCPs eliminate seal LOCAs, which are likely in operating PWRs during an SBO accident.

7.3.2 Transient Sequences

The following are the most important features of the AP1000 design which contribute to the reduction in the estimated CDF associated with transient sequences (CDF reduced to $8*10^{-9}$/yr from the $3*10^{-4}$/yr to $5*10^{-7}$/yr range at operating PWR) [2]:

- Defense-in-depth, which provides several alternative means for core cooling during all possible scenarios of the accident. Most current PWR plants rely on three alternative means for core cooling following a transient initiator (MFW and condensate, AFW and manual feed-and-bleed).
- The AP1000 design provides better and more reliable defense-in-depth by relying on the following alternative means for core cooling:
    - MFW and condensate
    - SFW
    - automatically actuated (with manual actuation backup capability) PRHR
    - automatic, with manual backup, feed and bleed capability using systems with adequate redundancy and defense against CCFs throughout the RC depressurization range for both the feed function (two CMTs, two accumulators, the two RNS pumps, and the two IRWST gravity injection lines) and the bleed function (four ADS stages with two paths in each of the first three stages and four paths in the fourth stage).

A reliable PRHR system (which is needed only when the non-safety-related SFW system is unavailable) significantly reduces the need for RCS depressurization and reliance on feed-and-bleed cooling, as compared to operating PWRs, and contributes to the reduced risk associated with transient sequences. (The functions of the SFW and PRHR following a transient event are redundant and similar to the function performed by the auxiliary feed water system in operating PWRs.)

The use of two redundant and diverse ESF actuation systems with automatic and manual actuation capability (one is safety-related) minimizes the likelihood of actuation failures, including common-cause actuation failures.

The use of passive safety-related systems, which do not need traditional support systems, such as component cooling water and ac power, to operate, eliminates all failures associated with such support systems in operating PWRs and contributes significantly to the increased reliability of most AP1000 safety-related systems, as compared to systems for operating plants performing similar functions.

The use of a larger pressurizer than those at comparable operating PWR plants reduces the frequency of transient initiating events by increasing transient operation margins.

7.3.3 Steam Generator Tube Rupture Sequences

The following are the most important features of the AP1000 design which contribute to the reduction in the estimated CDF associated with SGTR sequences (CDF reduced to about $7*10^{-9}$/yr from the $3*10^{-5}$/yr to $9*10^{-9}$/yr range at operating PWR) [2]:

- Three lines of defense against core damage following an SGTR event:
    - use of non-safety-related systems (the chemical and volume control system (CVS) and the SFW system) and manual Steam Generator isolation
    - use of passive safety-related systems (PRHR, CMT, and PCS) and automatic Steam Generator isolation
    - use of feed-and-bleed if the leak cannot be isolated (ADS, CMT, accumulators, RNS, IRWST injection, and PCS)

  For comparison, operating PWRs have two lines of defense. One is similar to the AP1000 design's first line of defense, but uses safety-related systems (high-pressure safety injection, and auxiliary feed water) and the other is manual feed-and-bleed using the pressurizer power-operated relief valves (PORVs).

- Redundant means for reactor coolant inventory control:
    - automatic CVS injection at the upper end of the RCS pressure range
    - automatic CMT injection once an "S" signal is generated
    - manual ADS actuation to allow accumulator injection if CMT injection fails
- The improved reliability of the PRHR, as compared to the auxiliary feed water system used in operating PWR plants, reduces the reliance on feed-and-bleed cooling as the last defense against core damage.

- The ADS provides an alternative DHR path through primary feed-and-bleed which is much more reliable and faster than the high-pressure manual feed-and-bleed cooling of currently operating PWRs.
- Good capability for long-term recovery from no-isolable Steam Generator leaks, which bypass the containment, exists by venting the RCS into the containment through the large ADS Stage 4 valves to allow low-pressure core cooling by IRWST gravity injection and containment sump recirculation. The large IRWST capacity, combined with the capability to refill either the IRWST or the containment sump, prevents depletion of borated water through the open path that bypasses the containment, and ensures that the water level in the sump is adequate to establish recirculation by gravity.
- Steam Generators have a secondary-side water inventory which is larger than comparable operating plants. This feature extends the time available to recover feed water or other means of core heat removal.

7.3.4 Loss-of-Coolant Accident Sequences

The following are the most important features of the AP1000 design that contribute to the reduction in the estimated CDF associated with LOCA sequences (CDF reduced to about $2.1*10^{-7}$/yr from the $8*10^{-5}$/yr to 10^{-6}/yr range at operating PWR reactors) [2]:

- Defense-in-depth, which provides several alternative means for coolant makeup at both high- and low-pressures using both safety and non-safety-related systems (CVS pumps, CMTs, accumulators, RNS, and IRWST injection), increases the reliability of the coolant makeup function. For comparison, most operating PWRs use their chemical and volume control system (CVCS) pumps and HPSI pumps for high-pressure injection, while providing accumulators and low-pressure safety injection (LPSI) pumps for LPSI.
- Defense-in-depth, which provides several alternative means for core cooling during all possible scenarios and sizes of a LOCA accident using both safety and non-safety-related systems, increases the reliability of the core cooling function (both in the short and long-term). Operating PWRs rely on fewer and less reliable alternative means for core cooling during LOCAs (e.g., manual feed-and-bleed as compared to the automatic, with manual backup, feed-and-bleed capability of the AP1000 design).

- The ADS provides an alternate DHR path through primary feed-and-bleed which is much more reliable and faster than the high-pressure manual feed-and-bleed cooling of currently operating PWRs.
- The AP1000 design is expected to have a reduced frequency of LOCA initiators (breaks) as compared to operating PWR plants because the number of welds in the AP1000 RCS pressure boundary is significantly reduced and leak-before-break (LBB) objective is applied in the design of all piping larger than 7.62 cm (3 in.).

7.3.5 Anticipated Transient without Scram Sequences

The following are the most important features of the AP1000 design that contributes to the reduction in the estimated CDF associated with ATWS sequences (CDF reduced to $5*10^{-9}$/yr from the $4*10^{-5}$/yr to 10^{-8}/yr range at operating PWR) [2]:

- The AP1000 design has two redundant and diverse reactor trip systems. The non-safety-related mechanical failure is a reliable system capable of initiating automatic and manual reactor trip using the motor-generator sets when the reactor fails to trip via the PMS. At operating reactors, the mechanical failure is less reliable and cannot automatically initiate a reactor trip.
- The ADS allows the use of the low-pressure injection systems (accumulators, RNS pumps, and IRWST injection) for long-term reactivity control and core cooling when the charging pumps are unavailable. At operating reactors, the less reliable PORVs must be used to allow low-pressure injection.
- The AP1000 design employs a low-boron core that contributes to a more negative moderator temperature coefficient of reactivity than in conventional cores. This feature also contributes to a significant reduction in the peak pressure established in the RCS during an ATWS event.
- Because the AP1000 reactor uses a larger pressurizer than those at comparable operating plants, the frequency of ATWS precursors is reduced by increasing transient operation margins.

7.4 Insights from the Uncertainty Analysis (from the References)

The applicant performed an uncertainty analysis to determine the magnitude of uncertainties that characterize the Level 1 PRA results (CDF from internal events), as well as the major contributors to these uncertainties [1] [2] [5]. The AP1000 CDF estimates, for internal events, are defined in terms of a mean value and an associated error factor. The error factor (EF) is a measure of uncertainty that expresses the spread of a fitted log-normal distribution. The total CDF from internal events, as estimated by the applicant, has a mean value of about $2.4*10^{-7}$/yr and an EF of approximately 6. Thus, the 95^{th} and 5^{th} percentiles are about $1.4*10^{-6}$/yr and $4*10^{-8}$/yr, respectively. It should be emphasized that only uncertainties associated with reliability and availability data were considered. Uncertainties associated with modeling (or lack of modeling) of accident sequences, system failure modes, and human errors were not included. The uncertainty analysis resulted in the following conclusions:

- The majority of the major contributors to the dominant accident sequences and total CDF have relatively small uncertainties associated with them.
- The following are major contributors to the uncertainty associated with the plant CDF estimate:
    - LOCA initiating event frequencies (e.g., safety injection line break), LOCA breaks of all sizes (large, medium and small), and CMT line break
    - reactor vessel failure probability
    - containment sump screen plugging probability (both single and CCFs)
    - IRWST discharge line strainer plugging probability (both single and CCFs)
    - CCF probability of hardware in the PMS ESF input logic groups
    - CCF probabilities of several sensor groups, such as the CMT-level heat sensor resistance temperature detectors, tank-level transmitters, pressurizer level sensors, and sensors in high-pressure environment
    - failure probability of the turbine impulse pressure transmitter (DAS trip permissive)
    - CCF probability of the reactor trip breakers to open (mechanical failure)
    - CCF of the reactor trip portion of PMS hardware or software (no signal to open the PMS reactor trip breakers)
- Failure probability of a Motor Generator set circuit breaker to open by mechanical failure.

7.5 Hypothesis for the evolution of the different scenarios

In order to have a better view, the following figures Figure 7.1 and Figure 7.2 synthesize the results obtained from the Level 1 PSA. It is interesting to note that, as already said, the major risk in terms of CDF is due to large break LOCA. Other events, i.e. transient and ATWS are quite low risk. The integral of the PSA Level 1 risk is around $2.4*10^{-7}$ CDF/year and it is three orders of magnitude less than US-NRC and 2 for EUR requirements [3] (these figures reduce of an order of magnitude with the evaluation of the Uncertainties).

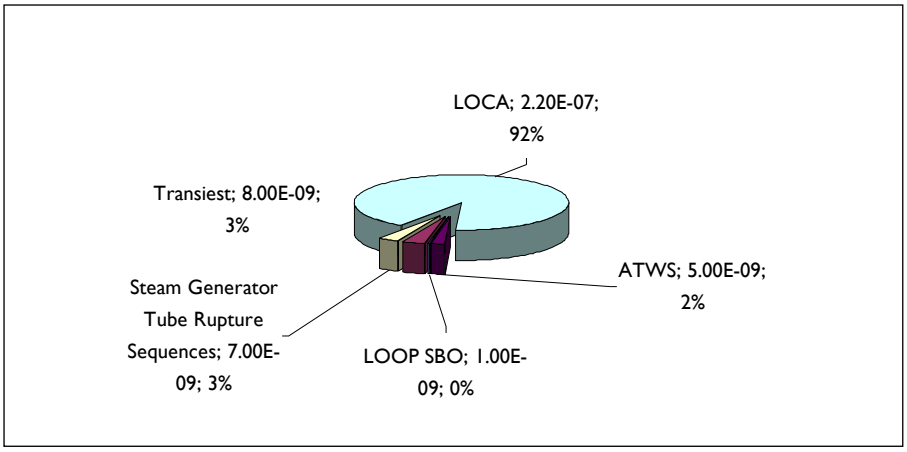

Figure 7.1 magnitude of risks associated to different types of initial events

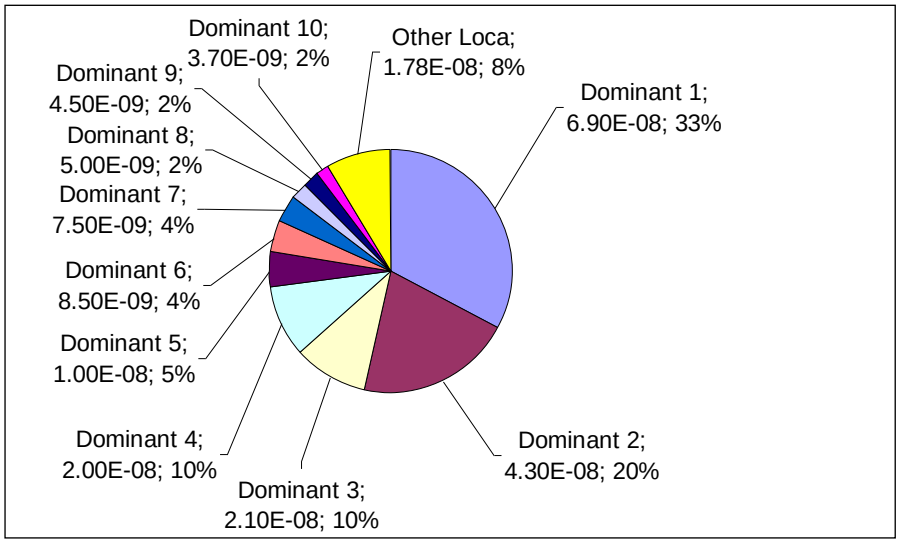

Figure 7.2 Contributions to CFD of the 10 Dominant Sequences

Table 7.2 shows the hypotheses of the considered cases. The risk related to the occurrence of the selected severe accident transients is some order of magnitude lower than the dominant sequence from in PSA level 1 [1]. The assumptions of the study are set in order to analyze the phenomenology involved in the passive systems concept implemented in the AP1000.

The study starts with a simple SBO analyzed in 3 different cases. After that we introduce the analyses of DVI break (Case2A and 2B), arriving to describe the two most relevant SA accident analyzed during this research (Case 3A and Case 3B).

Hypothesis	Case 1A	Case 1B	Case 1C	Case 2A	Case 2B	Case 3A	Case 3B
Complete SBO	Yes	Yes	Yes	Yes	Yes	Yes	Yes
PCS tank Activation	Yes	No	No	Yes	Yes	Yes	Yes
Stratification of the atmosphere	No	No	Yes	No	No	No	No
LOCA - Direct Vessel Injection Line Break in Side A	No	No	No	Yes	Yes	Yes	Yes
Double Side Break LOCA	No	No	No	Yes	No	Yes	Yes
Failure of the valve in IRWST Line in Side B	No	No	No	No	Yes	Yes	Yes
Cavity Flooding (SA Management)	No	No	No	No	No	No	Yes

Table 7.2 Calculation Cases' Hypotheses

In the case of SBO in the AP1000, the results are not very significant from severe accident point of view, because it is almost impossible to reach the melting of the core: the aim was to evidence as the passive approach reduces the risk to a negligible level. The calculations have been performed taking into account the consequence of Fukushima accident, where some BWRs experienced severe accident conditions. The aim of these analyses is to investigate the transport of the decay heat power from the core to the PRHR in the IRWST. The evaporation of the water in the IRWST activates the internal circulation. The atmosphere of the containment exchanges the decay power directly with the external air. In particular three cases are prepared in order to evaluate the capability of heat transfer from the containment to environment activating the forced convection with a water film evaporation (Case1A), forced convection with air (Case1B) or natural convection (Case 1C). The containment conditions are assumed from the EUR requirements [3] in order to

bound the worst condition of the environment in winter and in summer (stratification of the atmosphere, temperature around 37 °C and humidity to 60% for 1 day).

Besides, in order to highlight possible phenomena occurring in a severe accident, we choose the 1st Dominant Sequence (DVI Break side A with failure of the IRWST line injection side B), without any auxiliary system operation (without Chemical and Volume Control System (CVCS) for example) as for the SBO. The case 2A is a simple DVI break double sides. Also the case 2B is a simple DBA medium break LOCA, but with the fault of the valve connecting the IRWST to the DVI.

The cases 3A and 3B are both severe due to the DVI break double sides and the fault of the valve connecting the IRWST to the DVI. The difference is that in the case 2B an accident management procedure is actuated by the operator with the flooding of the vessel cavity (really the flooding is in Accumulators cavity, but for computational simplification we supposed to occur in the vessel cavity); this actuation starts when the fuel temperature grows up the 923 °K [4].

References

[1] US-NRC, "Final Safety Evaluation Report Related to Certification of the AP1000 Standard Design", *NUREG-1793*, 2006

[2] UKEA, “AP1000 Pre-Construction Safety Report”, UKP-GW-GL-732, Revision 1, 2009

[3] EUR, “European Utility Requirements for LWR Nuclear Power Plants”, April 2001

[4] ANSALDO Nucleare and Westinghouse private communications

[5] US-NRC, “AP1000 Design Control Document – Supplement 2 to the Final Safety Evaluation Report to the AP1000 Standard Design Certification," NUREG-1793-Supplement 2 , Rev. 19, 2011

8 NODALIZATION OF AP1000 PLANT

8.1 AP1000 MELCOR First Nodalization

The AP1000 MELCOR Nodalization is based on the experience of the severe accident team of DIMNP on TMI [1], but with the redistribution of the Control Volumes, Heat Structures and the Junctions of the AP1000 RELAP 5 Nodalization [2] [3]. Indeed the main differences between the two codes are due to the models and the physical interpretation of phenomena. The Nodalization has been set-up, firstly with a database description according with the references and after modifying the Nodalization in order to perform the comparison with the results of SGTR [4] obtained by the RELAP 5 Code [5]. The validation process, steady state and SGTR one tube break sequence, is reported in Appendix 4. In particular the steady state is closed to the design data and the comparison with the RELAP analyses: the uncertainty is less than 1% for all most main parameters as primary and feed water flow rates, primary and secondary pressure, pressure drops and etc.

8.1.1 AP1000 RELAP Nodalization

The AP1000 model developed by ANSALDO for Relap5/Mod3.2 code [2] [4] [5] represents the primary, secondary and passive safety components of the plant. The correspondence between the zones of the plant and the nodes of the model is given in Figure 8.1. The plant is divided in general zones, each in turn composed by single components:

- vessel;
- pressurizer and surge line;
- piping and pumps;
- steam generator and steam line;
- PXS (including Accumulators, CMT, IRWST and PRHR systems)

The two loops of the plant are separately modelled, each including the hot leg, the steam generator, the two cold legs and the associated canned pumps. The pressurizer is located in the loop‘1’ and the CMT pressure balance lines are connected to the cold legs of loops‘2’. The accumulators, CMTs discharge lines and the IRWST are connected to the DVI lines.

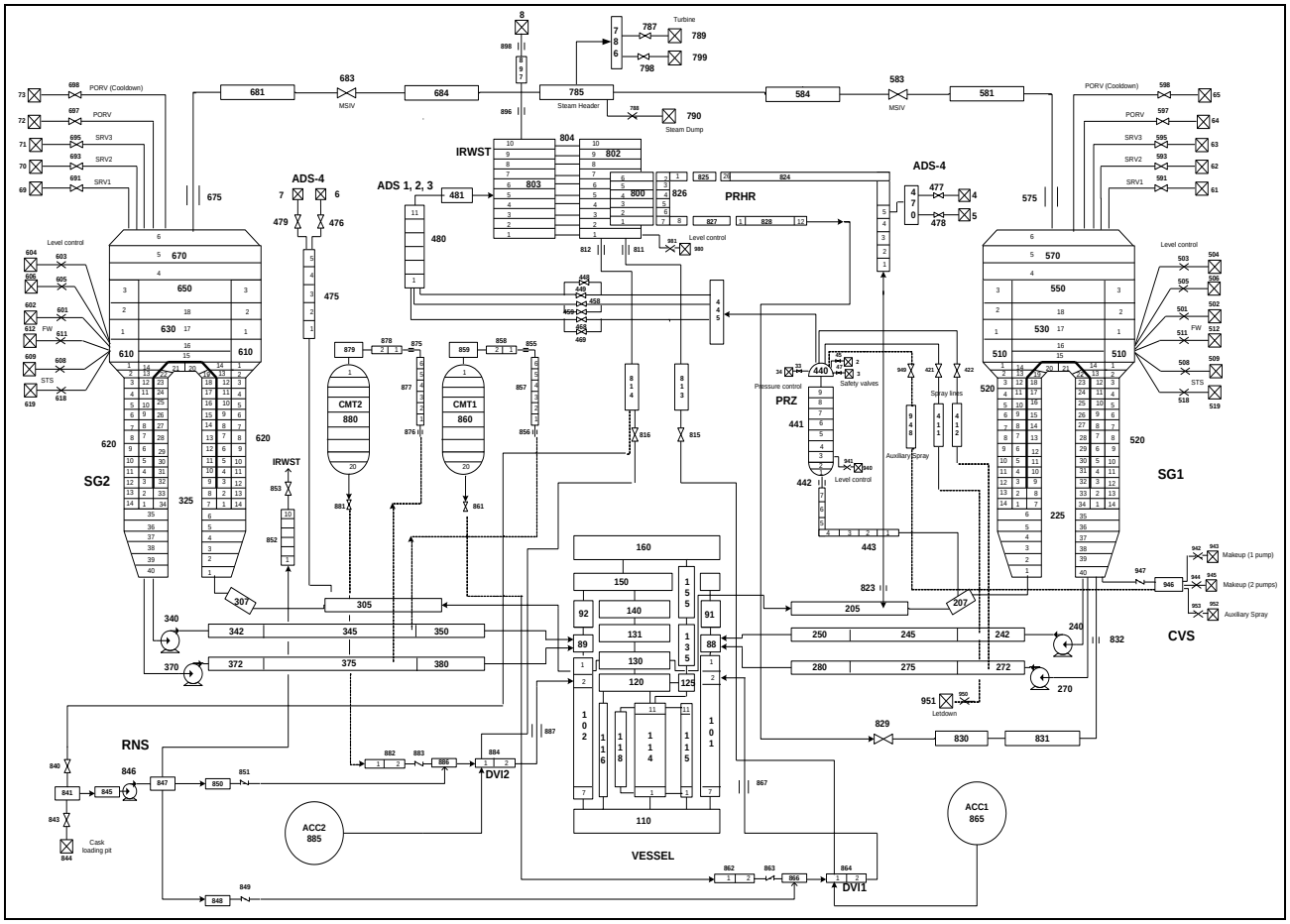

Figure 8.1 ANSALDO RELAP Nodalization [2]

8.1.2 TMI Phase 1 and 2 MELCOR Nodalization

The Nodalization of the TMI-2 [1] primary system for the MELCOR 1.8.5 [6] code is presented in Figure 8.2. Both primary loops have been modelled simulating each Steam Generator and considering a single equivalent main pump and cold leg. The secondary system is modelled only up to the main feed and isolation valves, while the Steam Generators were modelled with a high level of detail. The secondary side is connected to an imposed pressure control volume and to a "spill&feed" level control, which assure the desired imposed boundary conditions.

Particular care has also been devoted to core simulation (Figure 8.3). The core schematization is constituted by five radial rings and twelve axial levels; four thermal-hydraulic levels are used in each ring of the core region, with three core axial cells in each thermal-hydraulic control volume. Radial and axial flow paths in the core region allow for the prediction of 2-D flow patterns. Heat

structures representative of the control rod guide tubes and upper tie plate in the upper plenum have been added to the MELCOR model to permit condensation heat transfer and coolant recirculation inside the vessel. The input deck was developed using standard default MELCOR modeling parameters as long as possible, and allows for a complete description of severe progression of an accidental transient.

The VENT valves are also explicitly modelled between the cold and hot collectors. The plant geometry, the boundary conditions and the accident scenario have been strictly defined according to the TMI-2 scenario benchmark specifications provided by IRSN, as well as to recommended values of code physical parameters for the sensitivity study.

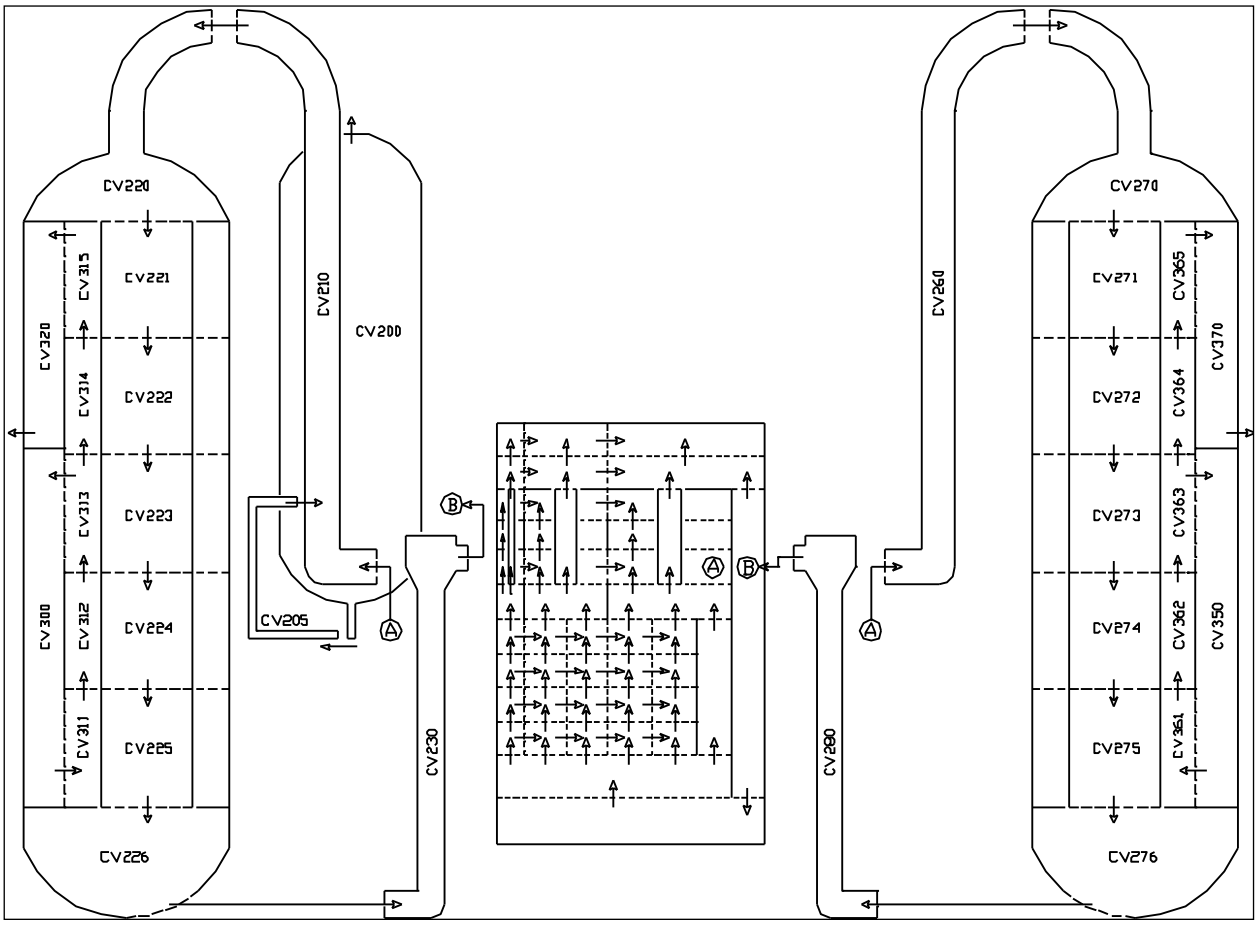

Figure 8.2 TMI Phase 1 and 2 MELCOR Nodalization (By DIMNP) [1]

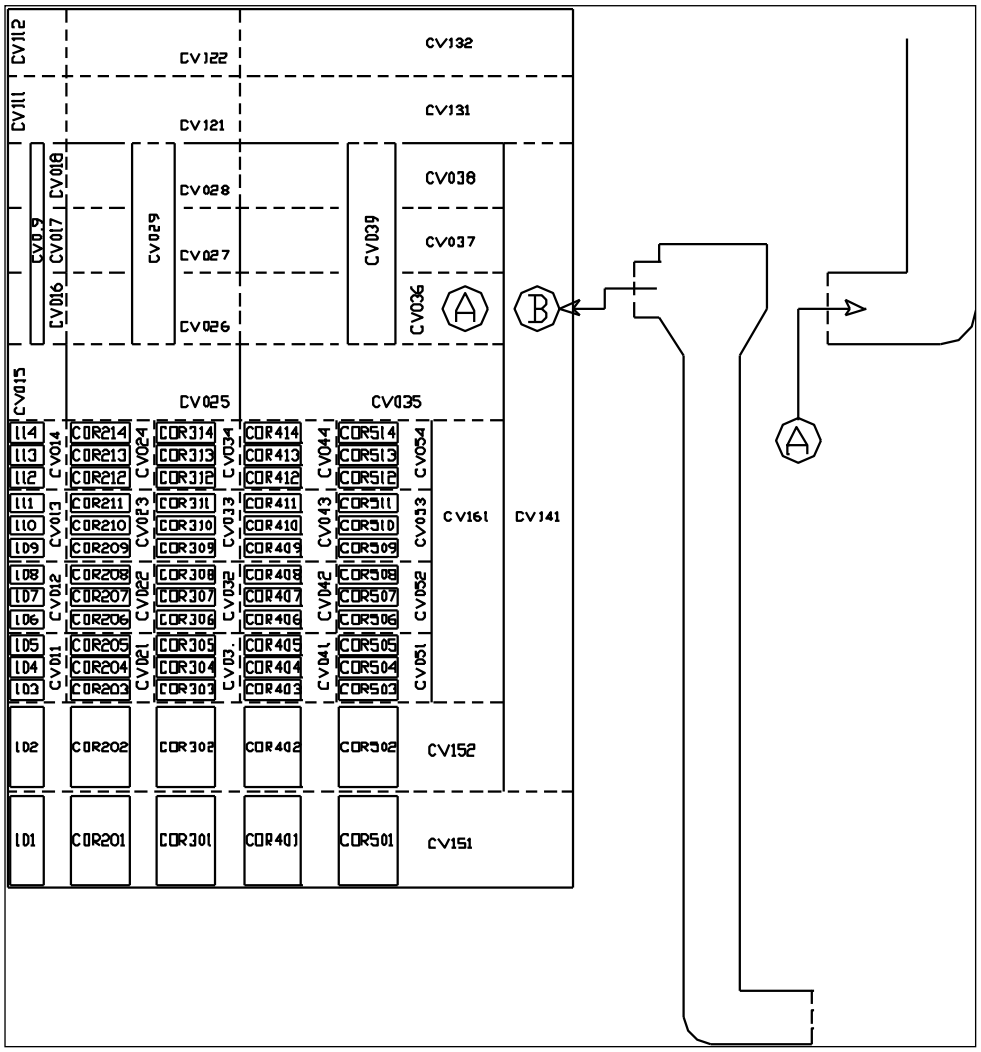

Figure 8.3 TMI-2 core simulation with MELCOR [1]

8.2 AP1000 MELCOR Final Nodalization

As said before, the Nodalization for MELCOR 1.8.5 code [6] is based on the TMI DIMNP experience and on the database of the AP1000 ANSALDO RELAP Nodalization. Other information derives from unclassified materials from US-NRC [7] including DCD [4] and Probabilistic Risk Assessment. In particular TMI-2 [1] is very important for 2 important aspects:

1. The core of the AP1000 is prepared with the same detail of the core of TMI in order to take in count the relocation phenomena. The TMI Nodalization is qualified with several years of benchmarks and analyses.

2. The TMI is practically the only one reference data of a SA in a PWR. The Aim of AP1000 is to not exceed this scenario and it is very important aspect to take in count during the analyses in order to well understand the code simulation.

We used the older MELCOR 1.8.5 code version [6], because it allows a simpler but more realistic modeling of the location of the lower core support plate within the lower plenum of the vessel, so allowing for a better simulation of the elevation of the core. The latest version of the code could give problems for the simulation of the core, due to the upgraded model of the lower plenum molten material relocation.

One of the most significant works in setting-up the nodalization has been to rebuild some of control volumes that are similar to the original for principal denominations (total primary and secondary volumes, lengths of pipes, flow areas, heat transfer areas of the heat transfer structures, etc.). This is necessary due the differences of phenomena's models in the two codes: MELCOR doesn't need a very detailed nodalization as RELAP, but it is important to know the physical behaviour of the plant in order to use the models as well as possible.

Practically, the results of this first phase are shown in Figure 8.4. This Nodalization is used for the SBO sequence and for the validation process, because it is much detailed in PRHR structures and takes into account a simplified down-comer.

Subsequently, the Nodalization has been improved in the geometry of down-comer and adding a direct injection in the Lower Head, due to the computational instability of the code (this implies a very small time step with increase of the computational errors) in order to simulate the DVI break sequences. For the same reason a simplification of PRHR has been applied, due to the modest effects of this system in the DVI Break sequence. The changes of the Nodalization are evidenced in yllow in the Figure 8.5.

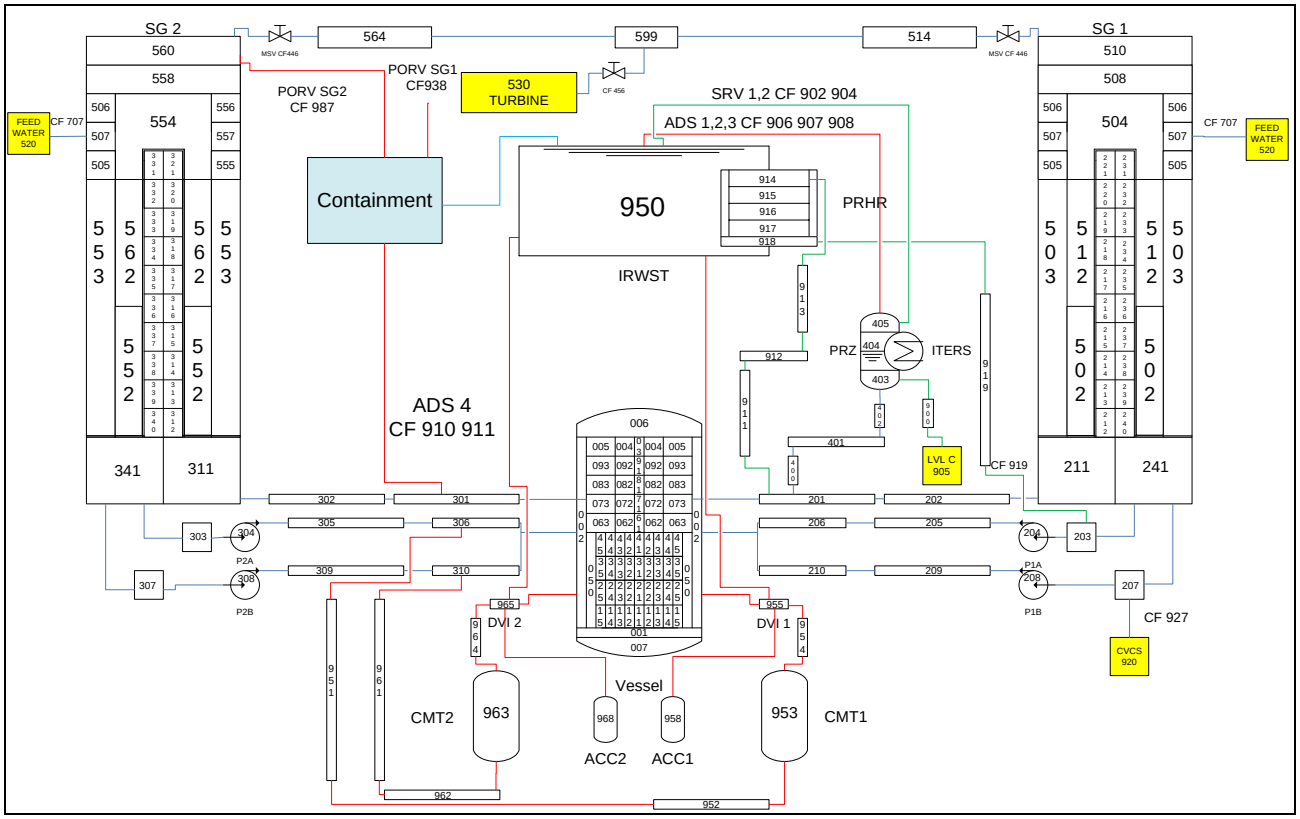

Figure 8.4 AP1000 MELCOR Nodalization for SBO sequences

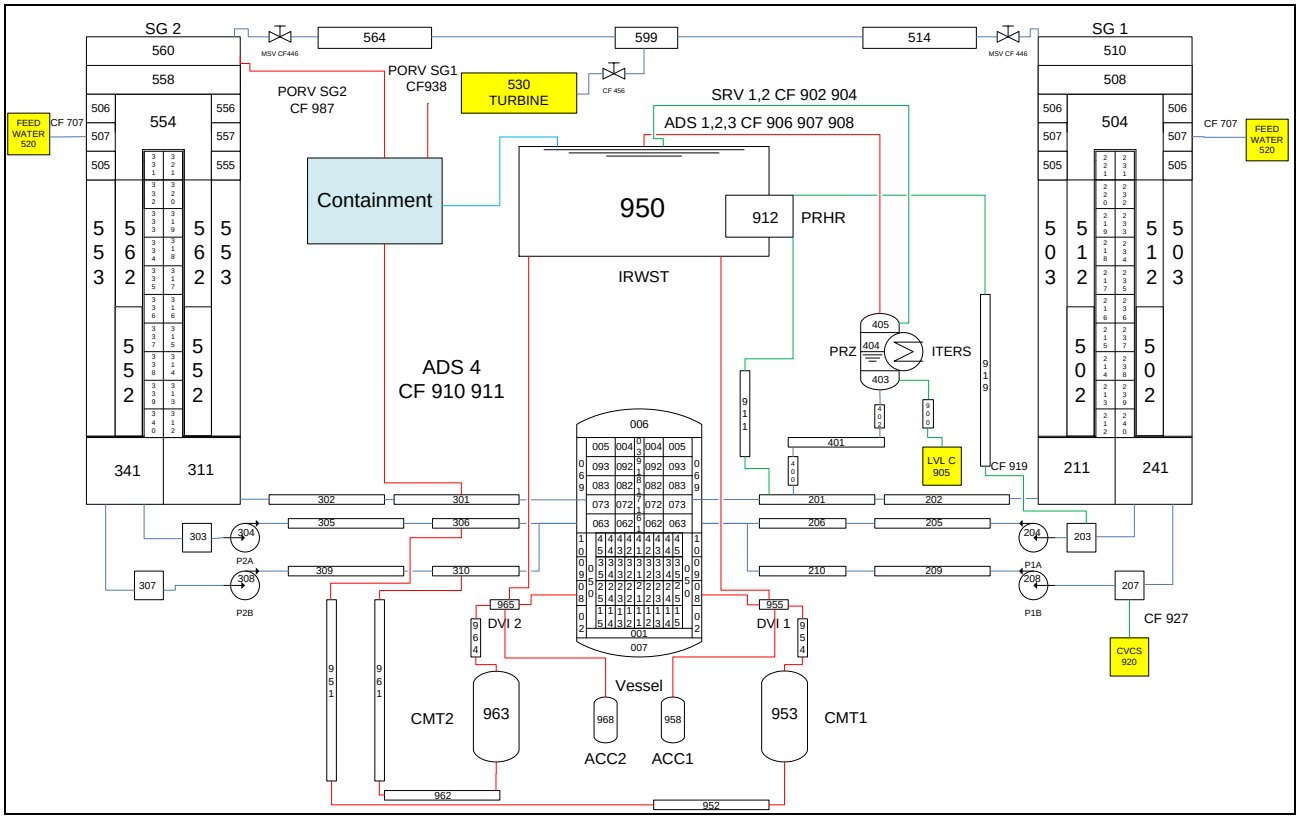

Figure 8.5 AP1000 MELCOR Nodalization v2 (modifications for DVI break sequences)

8.3 AP1000 Containment Nodalization

Finally, the MELCOR Nodalization has been completed with the Containment Nodalization. The Containment is very important in the evolution of a accident sequence (in particular during a SA with gas and aerosol release) in AP1000, because it is practically integrated with the primary. The CV assures the main thermal inertia of the Primary due to the presence of IRWST and the reintegration of the water from the condensation of the steam on the metallic layer of CV. It is important to add this system on the Nodalization in order to have a correct simulation of the evolution of the transient, in particular for the long simulation (as SBO sequence).

Initially the Containment was described with a single volume, without the external spray and the external circulation of air-water on the steel layer. Subsequently it has been changed with a better volume distribution, more similar to the reality. In fact, taking into account that the AP600 has practically the same distribution of the internal buildings and cavities of AP1000 [3], it was possible

to replace the unknown AP1000 containment volumes with those of the FUMO AP600 [20]. Nodalization. However it was taken into account that AP1000 containment has the same transversal surface of AP600, but with different volumes for Steam Generator Cavities, Reactor Cavity and the Dome. The IRWST is the same of AP100.0 as the Accumulators and CVCS Cavities. Finally, also the external natural and forced circulation was introduced, with the simulation of the external spray;,it assures the containment atmosphere cooling for 72 hours, with a significant reduction of the internal pressure, an improvement of heat transfer and aerosol deposition in the severe accident sequences.

The Figure 8.6 describes the structure of the Containment Nodalization connected with the AP1000 Nodalization. Really the first termohydraulic analyses of the containment were done considering the containment as independent from the plant. The inputs used during the analyses of only SBO sequences are prepared with simplified boundary conditions obtained from SBO PRHR heat transfer analyses. The aim is to obtain simplified results of external natural circulation with the PCS tank system activated, with only air in EUR summer heavy condition and, finally, natural convection in stratified atmosphere in EUR summer heavy condition. The final calculations are performed with the complete AP1000 Nodalization

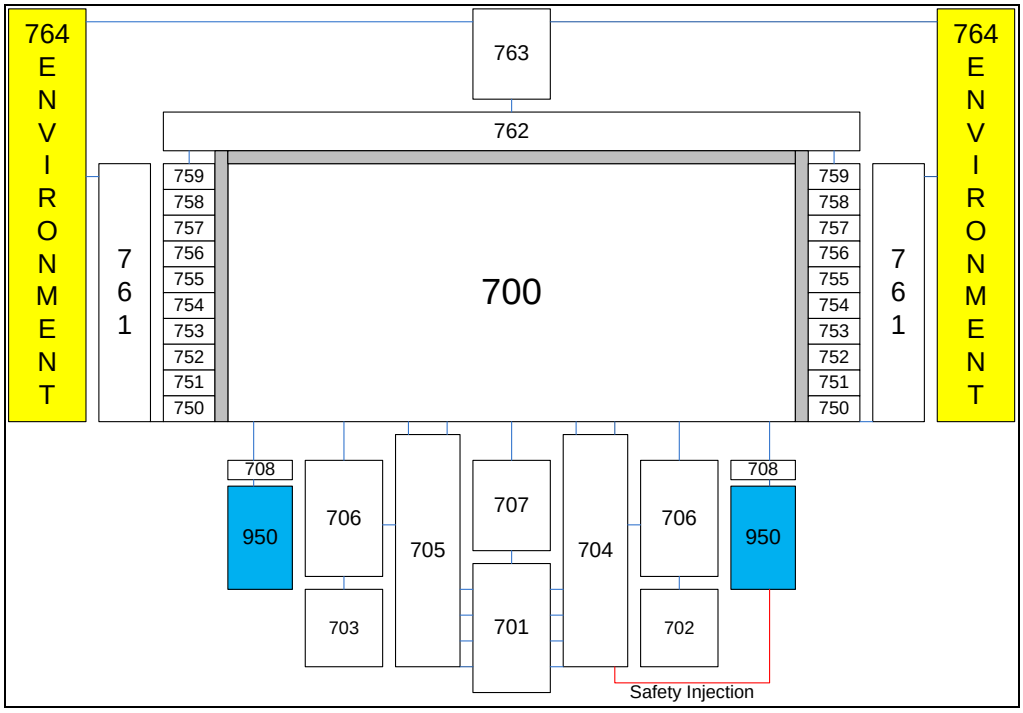

Figure 8.6 AP1000 Containment Nodalization

References

[1] A. Manfredini, “OECD/CSNI – Alternative TMI-2 Scenario Benchmark”, DINMP – University of Pisa, Pisa. 2001

[2] ANSALDO Nucleare and Westinghouse private communications

[3] Westinghouse Electric Co., “The Westinghouse AP1000 Advanced Nuclear Plant – Plant Description”, Copyright © 2003.

[4] US-NRC, “AP1000 Design Control Document – Supplement 2 to the Final Safety Evaluation Report to the AP1000 Standard Design Certification," NUREG-1793-Supplement 2 , Rev. 19, 2011

[5] Nuclear Safety Analysis Division, “RELAP5/MOD3.3 CODE MANUAL”, Information Systems Laboratories, Inc. , Rockville, Maryland, December 2001

[6] R. O. Gauntt et al. “MELCOR Computer Code Manuals – Version 1.8.6”, NUREG/CR-6119, Vol. 2, Rev. 3, September 2005

[7] US-NRC, "Final Safety Evaluation Report Related to Certification of the AP1000 Standard Design", *NUREG-1793,* 2006

[8] A.Manfredini, G. Mazzini “Analysis of the Physics of Severe Accidents in Advanced Light Water Reactors”, 29th UIT National Heat Transfer Conference 2010, Torino, Giugno, 2011

9 SENSITIVITY ANALYSES OF SBO AND DVI BREAK

9.1 Overview

The following paragraphs report the main results and the relevant phenomena of the analyses done by MELCOR code [1]. This is a summary of the sensitivity analyses, which involved many hours of calculations and some other cases. We start from SBO sequence without any long term human interaction, as happened in the Fukushima [2] accident for several hours or days, on the basis of EUR requirements [3] (also the stratification of the external air in one case) with and without the actuation of the Passive Containment Cooling System (PCCS) tank (conservative hypothesis) [4]. After that, we introduce the SA analyses of the reference DBA sequence (the DVI 1 break without any failure in the second ECCS train) during a SBO and without the PCCS tank. Finally the investigation is focused on a qualitative analysis of the 1st Dominant sequence in order to evidence some interesting aspects and phenomena, which could be present in a reactor with passive safety philosophy approach as AP1000.

9.2 Sensitivity Analyses of Station Blackout

Ii is important to evidence the large inertia of the AP1000 due to the presence of a lot of water storages. Practically the long resistance of AP1000 during a SBO sequence, assured also with totally loss of the feed water and the emergency feed water of the Steam Generators, is due to the 2 CMTs from 70 m^3 of water connected directly in the primary, and the heat capacity of the IRWST, which contains a proximately 2300 m^3 of fresh water. The follow analysis gives an idea of the evolution of a SBO sequence with a parametric analysis of the capacity of the heat transfer of CV in normal and extreme conditions. The primary behaviour is practically the same for all 3 Case1 and it is important for the transfer of decay heat and water mass.

9.2.1 *Station Blackout with the support of PCCS tank – Case 1A*

The SBO sequence starts with the grids interruption, the failure of Diesel Generators and the complete fault of the internal batteries, that causes in few seconds the reactor and pump trip. The first part of the transient is characterized by a continuous loss of water from the Steam Generators

through the secondary safety valves. Practically the mass contained in the 2 Steam Generators is sufficient to remove the decay heat power for approximately 2000 s. Once a low level in the Steam Generator water is reached (at about 1700 s since the beginning of the transient), the PRHR is actuated; the PRHR is a heat exchanger connected from the hot leg to the DVI 1 able to bring the decay heat from the core to the IRWST tank, without any loss of primary mass. The PRHR systems transfer the decay heat (approximately 30-20 MW), with a flow rate of 50 kg/s, to the IRWST (Figure 9.1 and Figure 9.2); as a consequence the IRWST starts evaporating with an increase of the containment pressure.

The first peak of the pressure is due to the release of steam in Containment atmosphere due to the opening of the Steam Generators PORV. All calculations practically have this first peak. The PORV actuation is due to the Steam Generator high pressure signal in the first 200 s until the level and the pressure of the Steam Generator became low and the PRHR natural circulation is activated. In this case the heat transfer from the Containment Vessel atmosphere to the environment is able to remove this first energy release until the IRWST starts to evaporate. The other cases, as shown in the next subparagraphs, are characterized a very low increase of containment pressure.

Moreover, after the PRHR actuation, the 2 CMTs (Figure 9.3) start after 3190 s since the initial event, due to the "S signal" activation caused by Low Cold Leg Temperature signal (Figure 9.4). The large thermal inertia of the CMTs and the IRWST tanks assures the cooling of the fuel (Figure 9.5) and the cladding (Figure 9.6); the decay heat power is transferred from the primary system to the containment through the PRHR heat exchangers.

The analysis is focused on the containment behaviour; after the initial increase of pressure due to the PORV activation (Figure 9.7), the external circulation of air with the film of water due to the PCCS tank reduces the Containment Vessel atmosphere pressure and temperature (Figure 9.7 and Figure 9.8) until the IRWST starts boiling. The IRWST water temperature slowly increases with a temperature gradient of about 10-17 °C/h, arriving to boil and to generate steam at 398 °K and near $2.2*10^5$ Pa (Figure 9.9). The pressure peak of about $2.21*10^5$ Pa is achieved at near 2000 s, very below the design pressure of $5.5*10^5$ Pa, is consequence of the balance between the PRHR heat transfer to the IRWST and the power removed through the steel containment liner to the external environment. The steam creates a condensation film inside the containment, that reintegrates the

water inside the IRWST. Eventually, the large inertia of IRWST is sufficient to assure a cold condition for the fuel in case of a simple SBO.

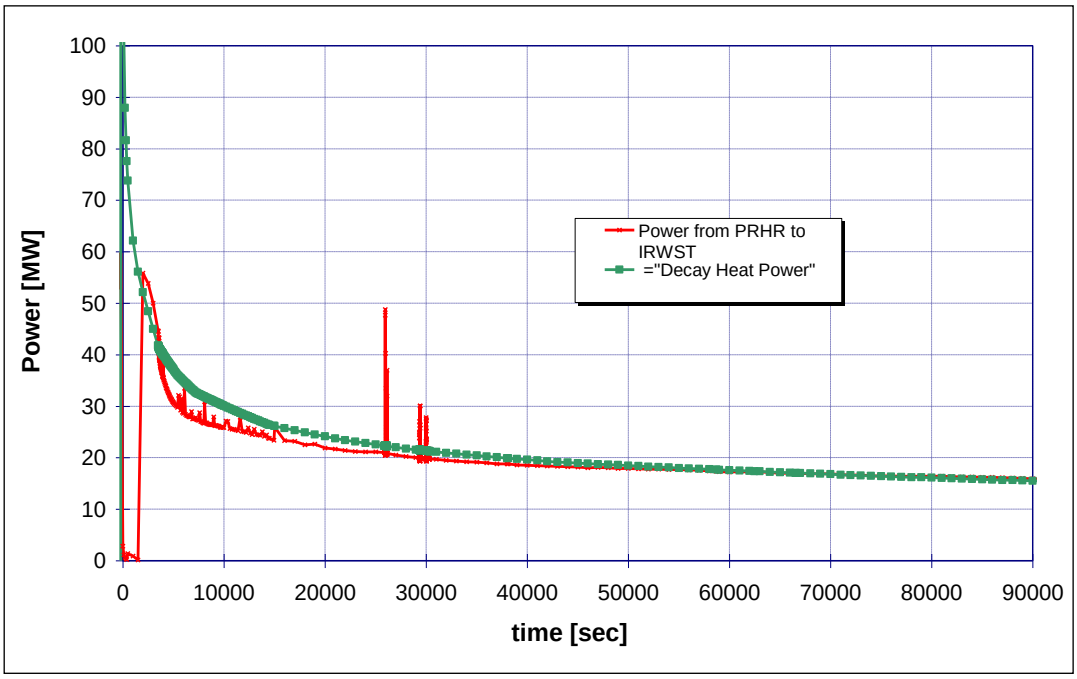

Figure 9.1 Case1A: Power balance from Decay Heat and PRHR

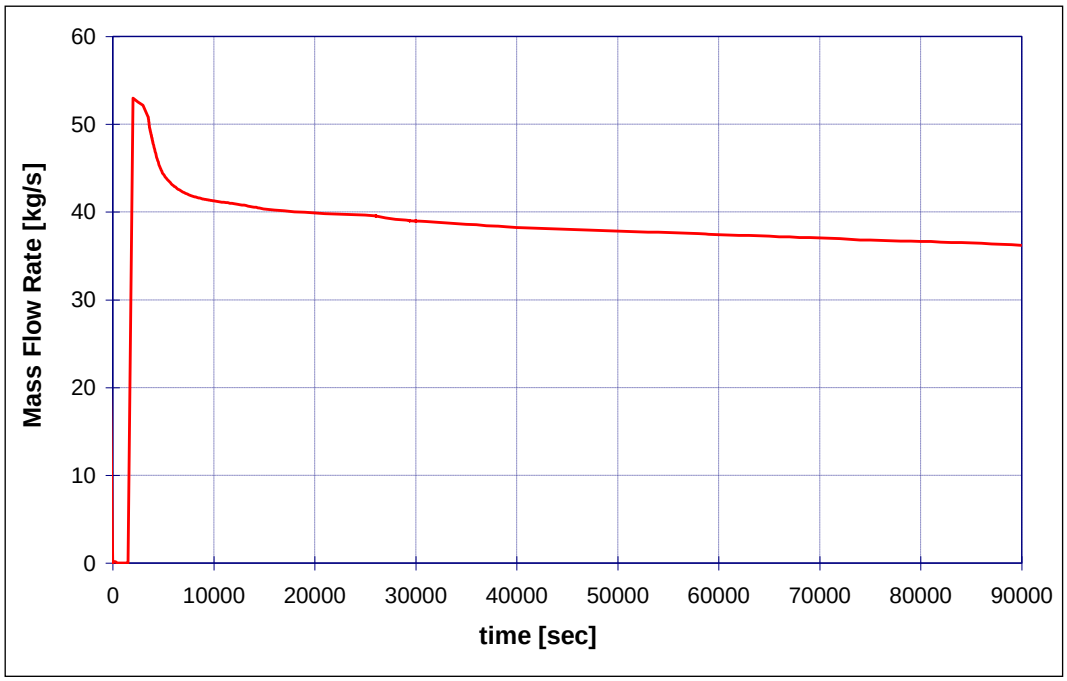

Figure 9.2 Case 1A: PRHR Flow-rate profile

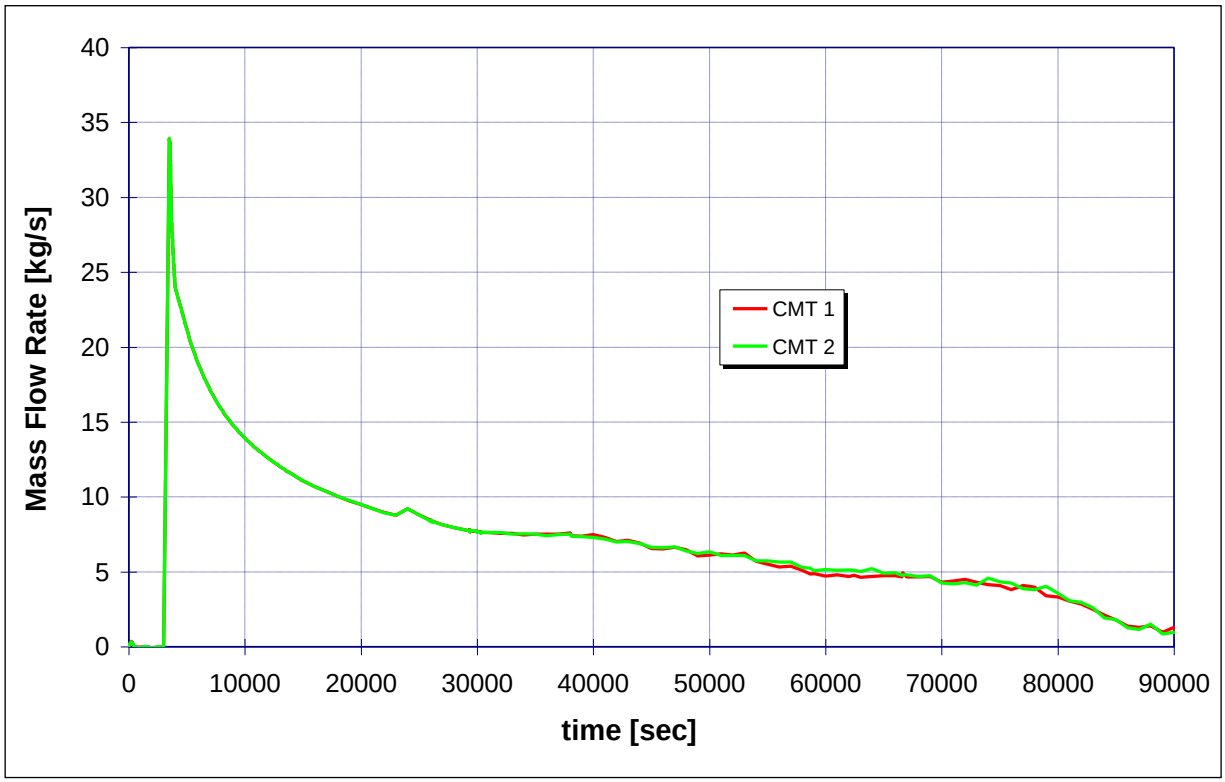

Figure 9.3 Case 1A: CMTs Flow-rate profiles

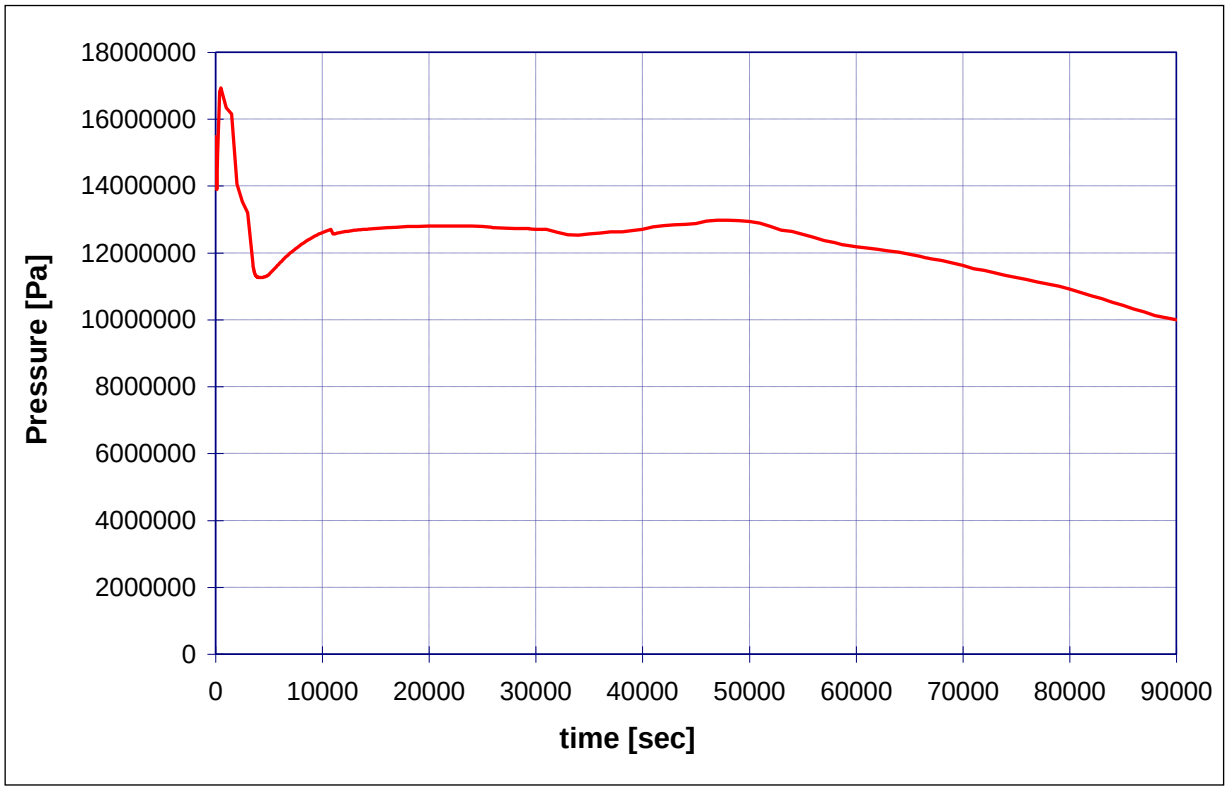

Figure 9.4 Case1A: Primary Pressure

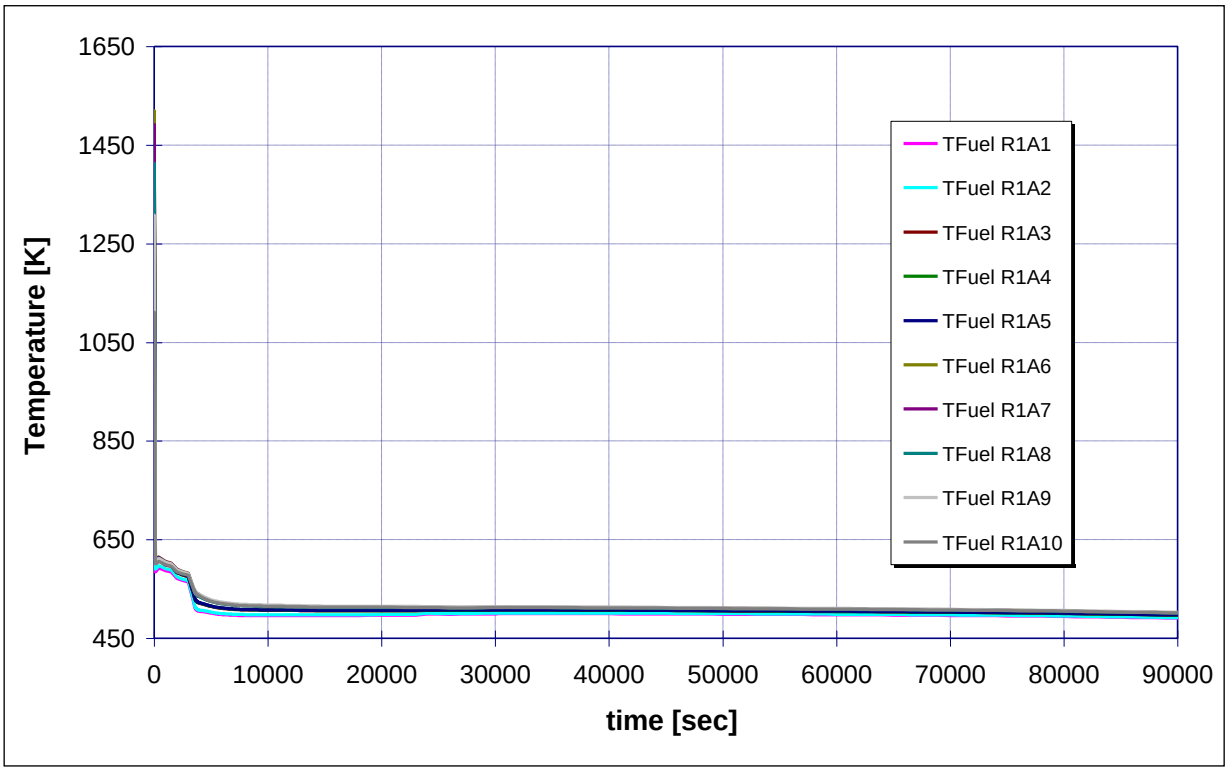

Figure 9.5 Case1A: Axial temperature evolutions of the fuel elements in the 1st ring

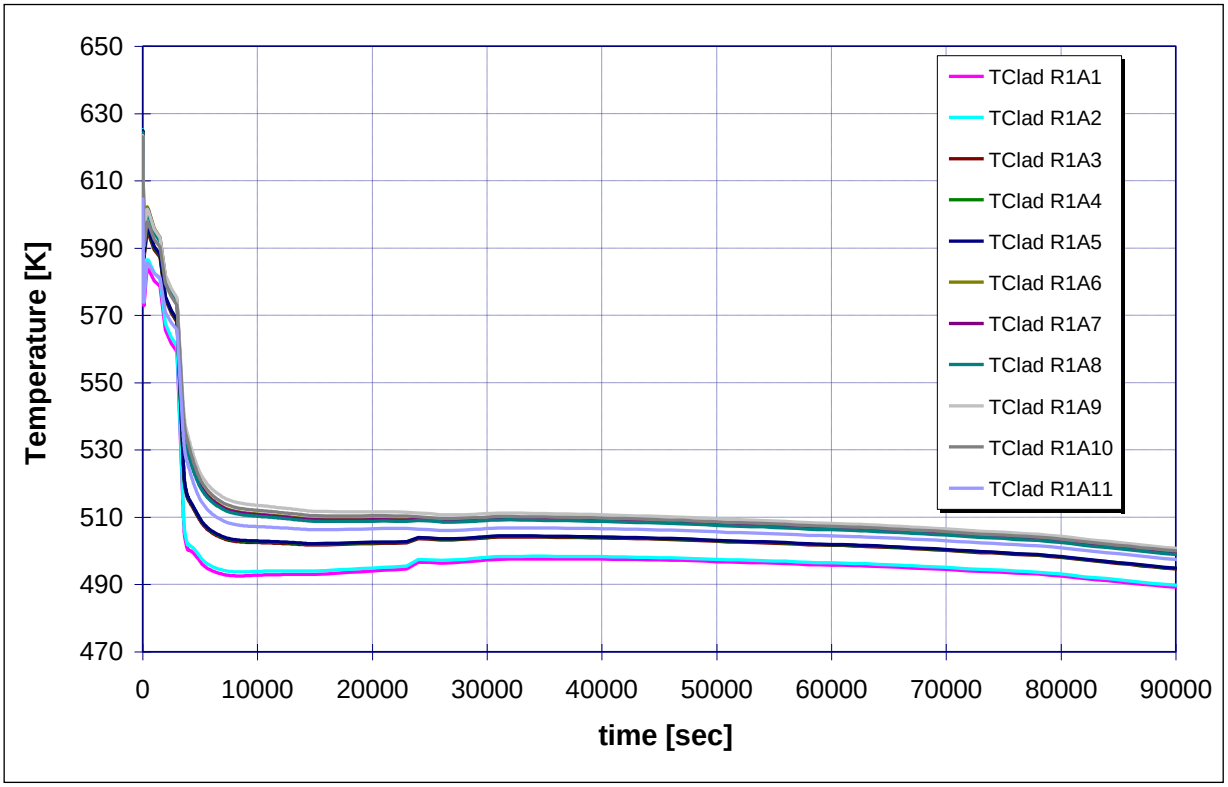

Figure 9.6 Case 1A: Axial temperature evolutions of the clads in the 1st ring

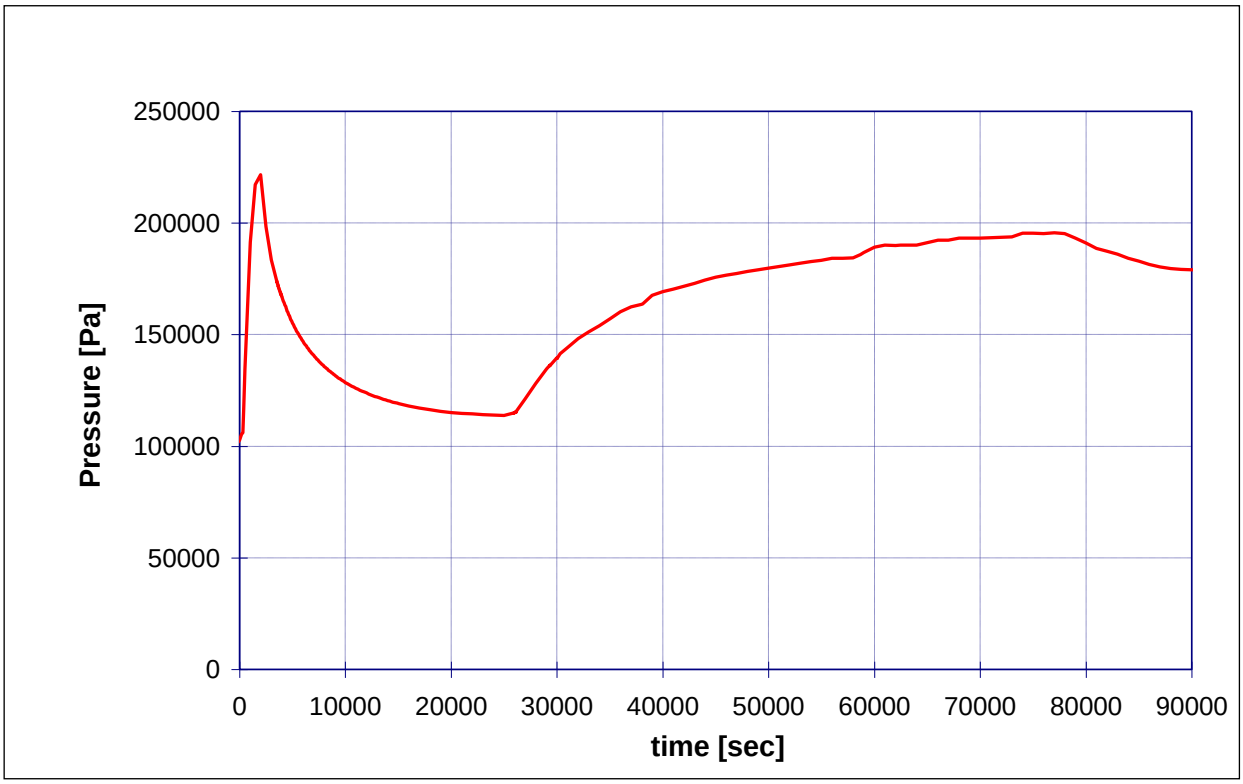

Figure 9.7 Case 1A: Containment Pressure

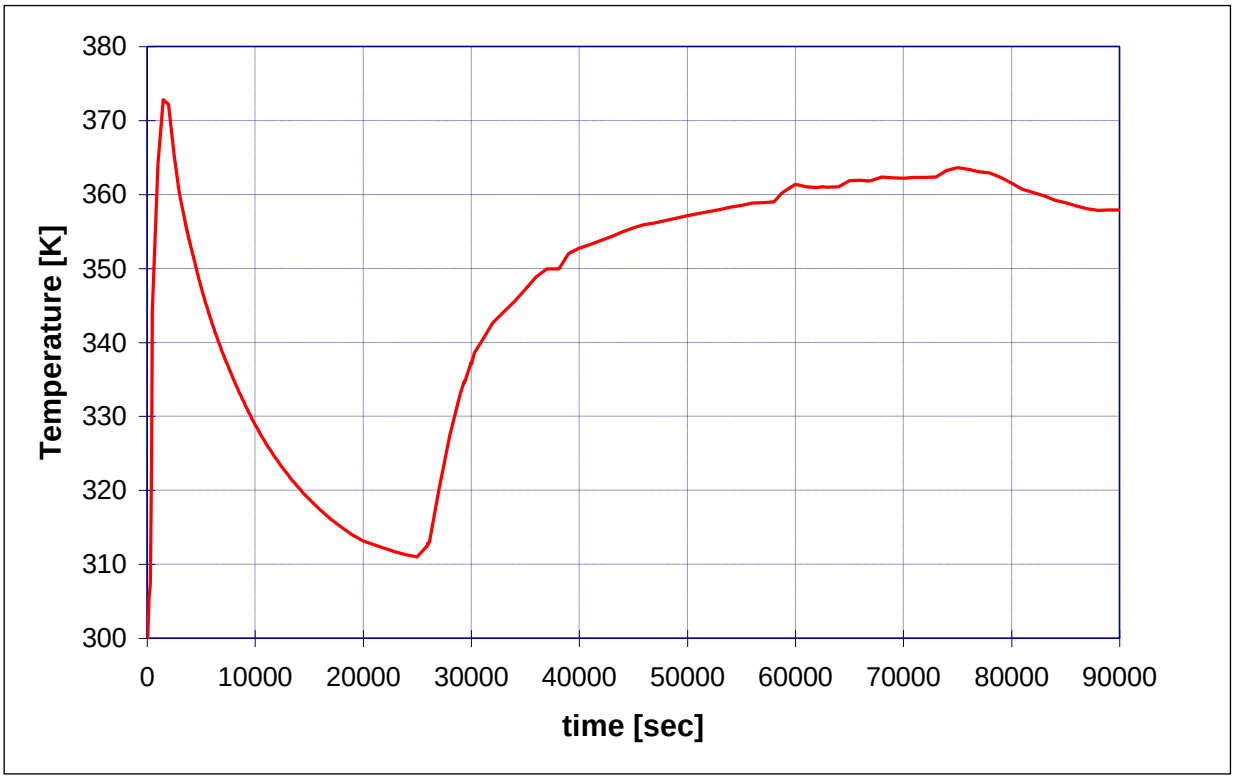

Figure 9.8 Case 1A: Containment atmosphere temperature

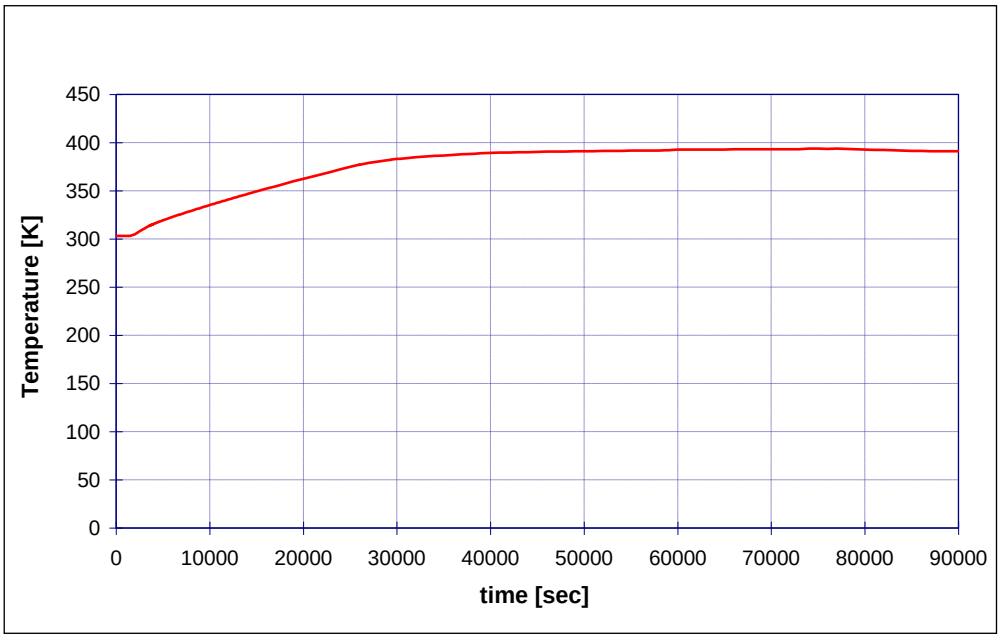

Figure 9.9 Case 1A: IRWST Liquid Temperature

9.2.2 *Station Blackout without the Support of PCCS tank – Case 1B*

As for the Case 1A, the Case 1B sequence starts with the grids interruption, loss of the active systems and start of external/internal natural circulation. The differences in the primary system are minimal, as show in the Figure 9.10, Figure 9.11, Figure 9.13, Figure 9.14 and Figure 9.15. Indeed some little differences are evident as perhaps the temperature of flow-rate of the CMTs.

The shown calculations are performed without the intervention of the tank of the PCCS on top of the containment and very heavy concentrated friction losses in order to maximize the SBO consequences. As shown in Figure 9.16, the pressure continually grows, arriving to a peak of about $2.5*10^5$ Pa at near 2000 s; this peak is due to the Steam Generator PORV release in the containment atmosphere, balanced by the PRHR heat transfer to the IRWST and by the power removed through the steel containment to the external environment. The temperature of the Containment Vessel follows the shape of the Pressure (Figure 9.17). The IRWST water temperature increases with a temperature gradient of about 15-20 °C/h, arriving to boil and to generate steam at 420 °K at 36000 s (Figure 9.18). The steam creates a condensation film, which reintegrates the water inside the IRWST (other little flow-rates enter in containment cavities). The heat transfer coefficient from the Containment Vessel wall and the external air in forced convection is near 5-10 W/m^2K Eventually,

the large inertia of IRWST is sufficient to assure a cold condition for the fuel also in this case of SBO.

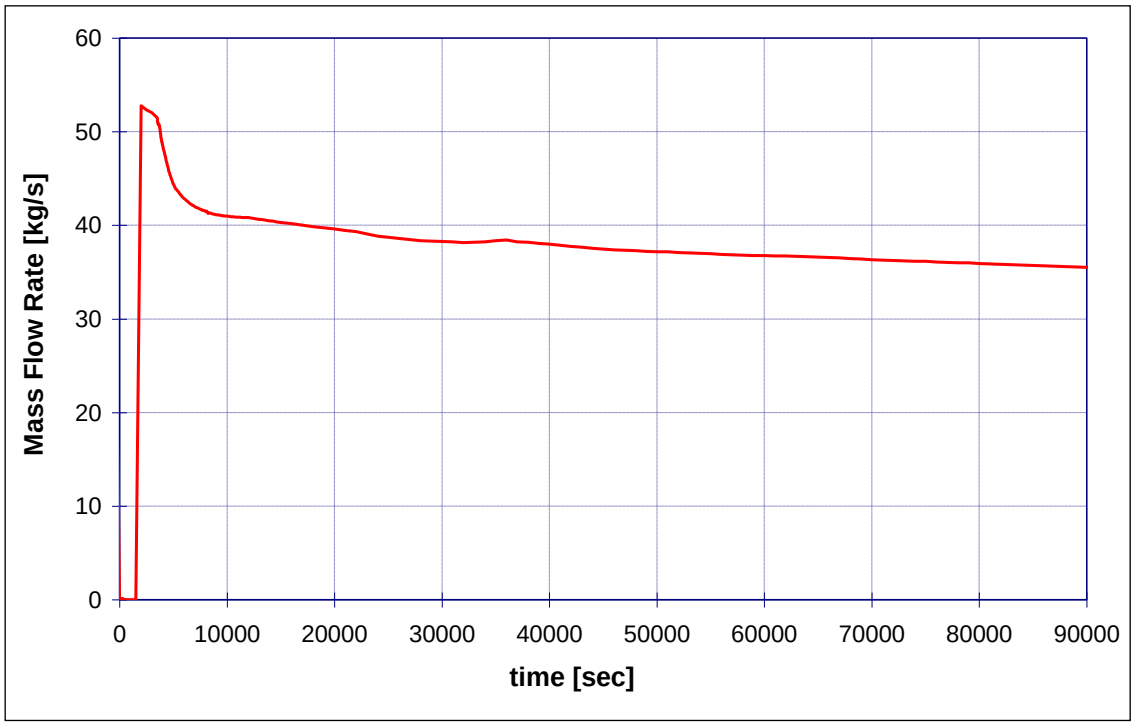

Figure 9.10 Case 1B: PRHR Flowrate profile

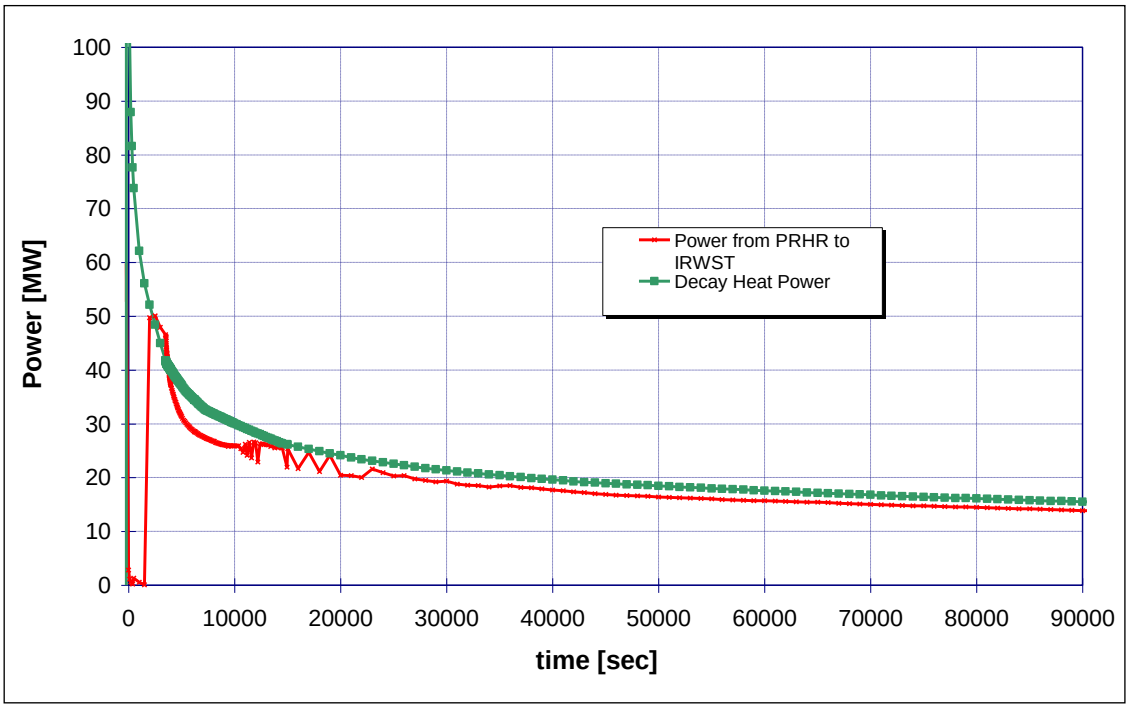

Figure 9.11 Case1B: Power balance from Decay Heat and PRHR

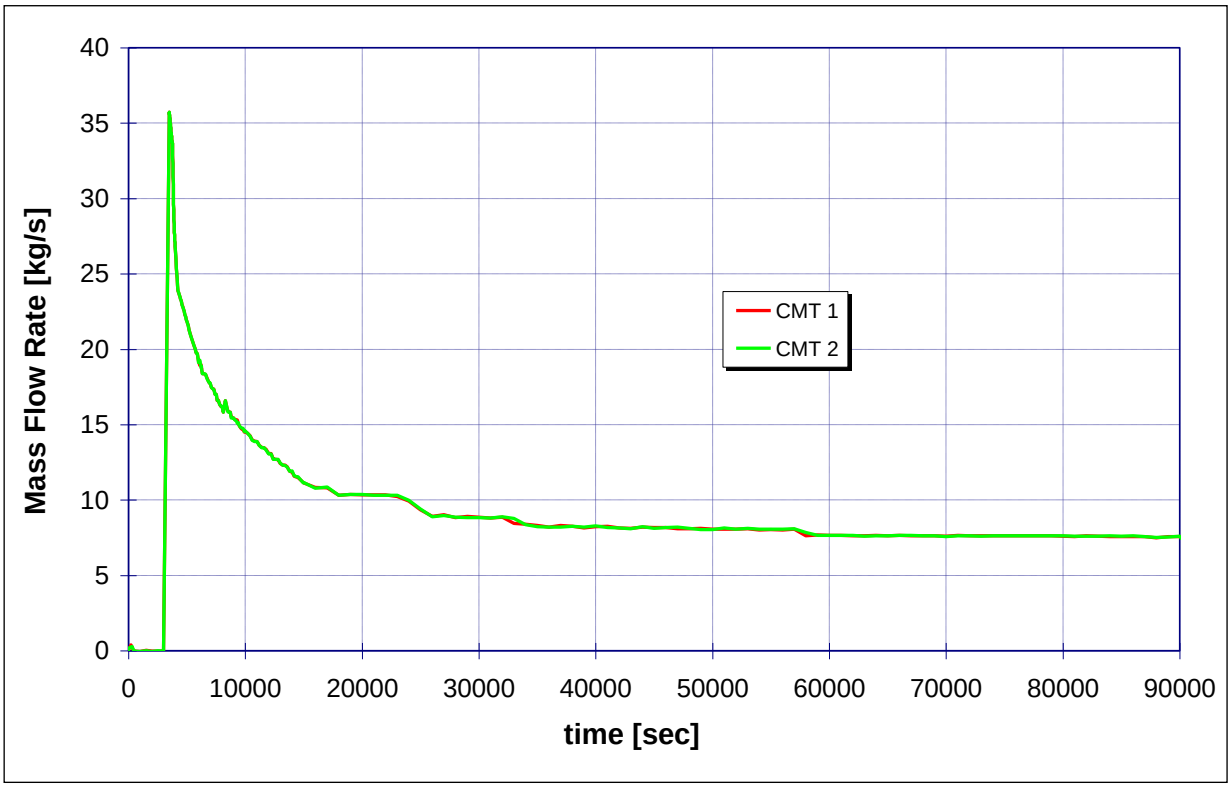

Figure 9.12 Case 1B: CMTs Flowrate profiles

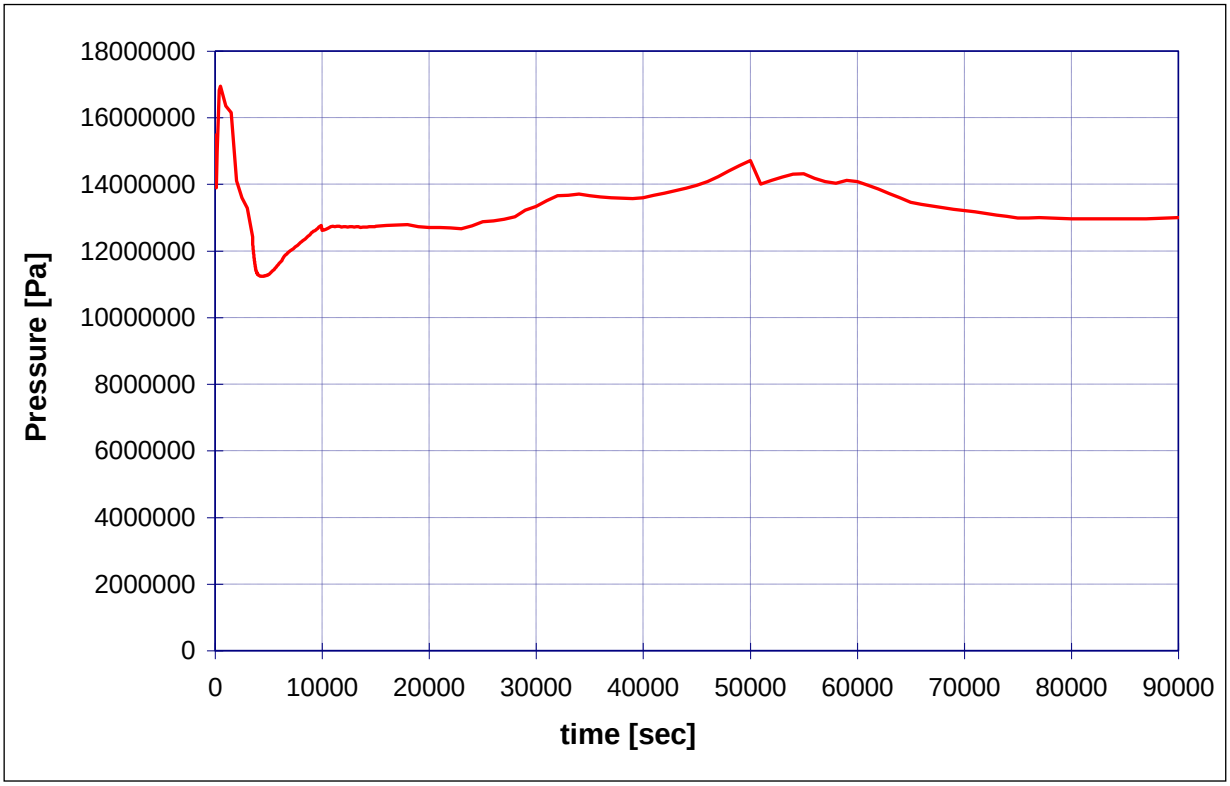

Figure 9.13 Case1B: Primary Pressure

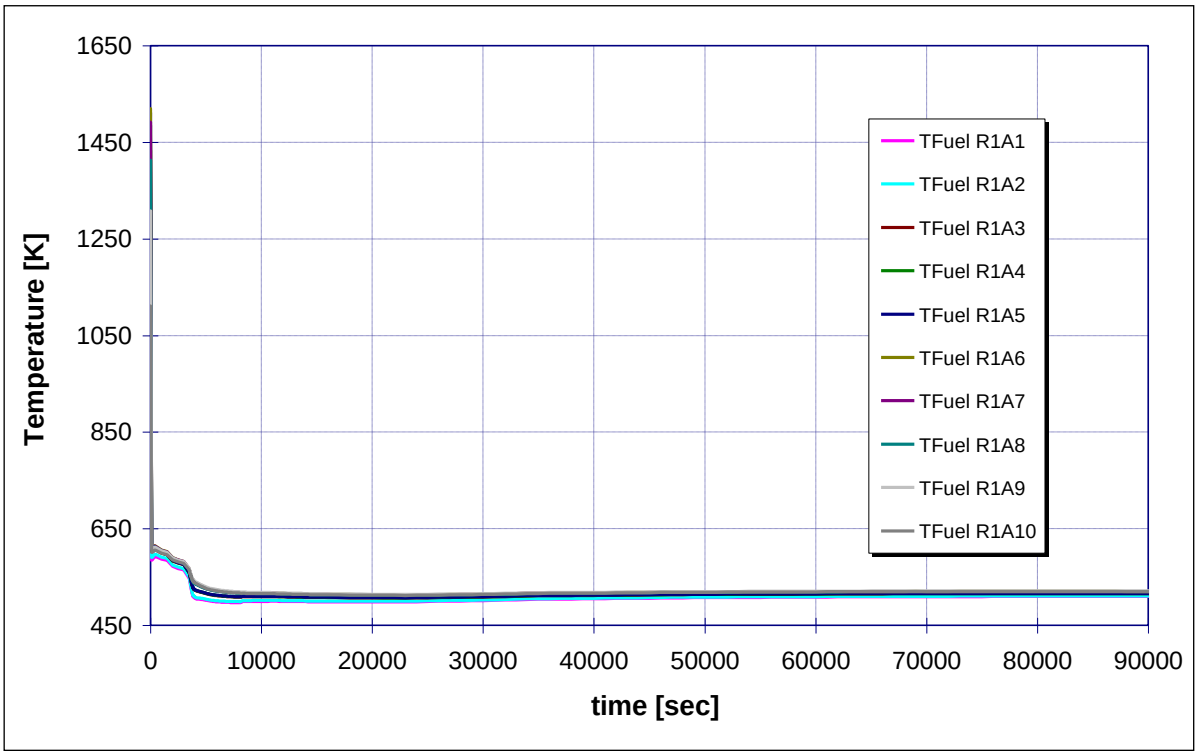

Figure 9.14 Case1B: Axial temperature evolutions of the fuel elements in the 1st ring

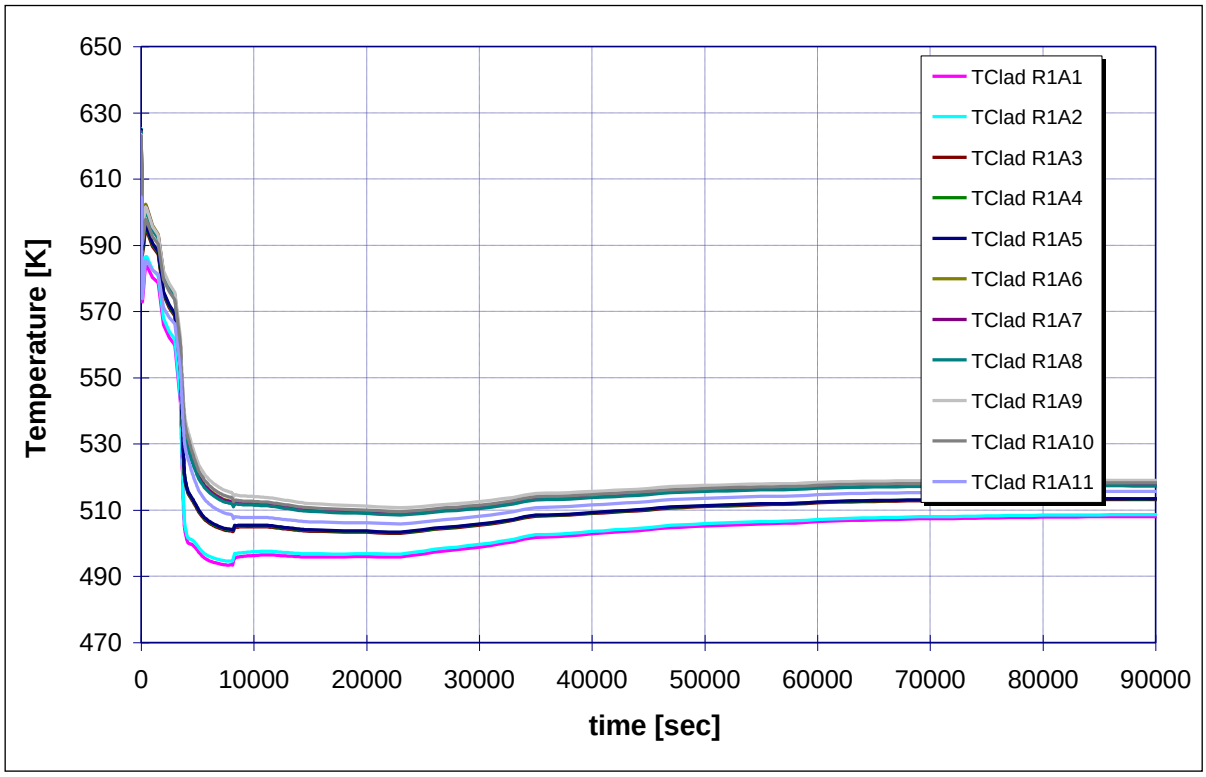

Figure 9.15 Case 1B: Axial temperature evolutions of the clads in the 1st ring

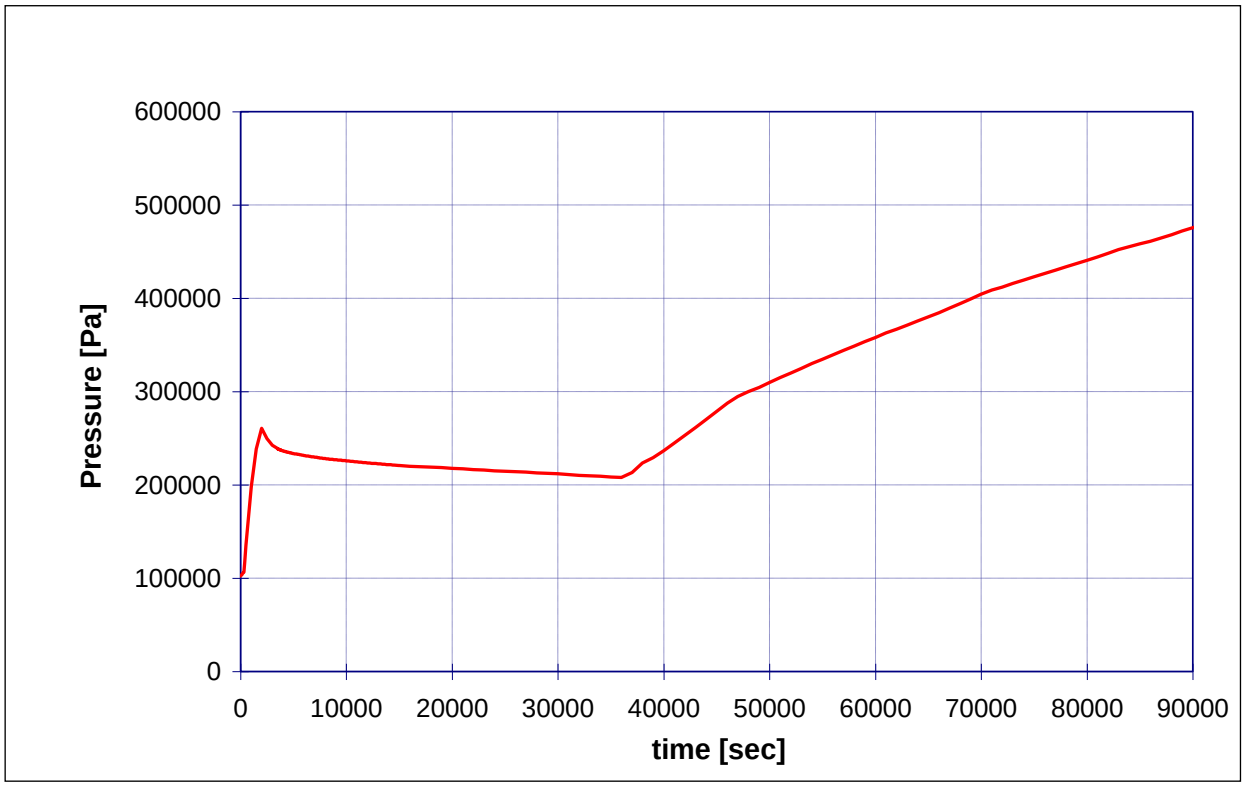

Figure 9.16 Case 1B: Containment Pressure

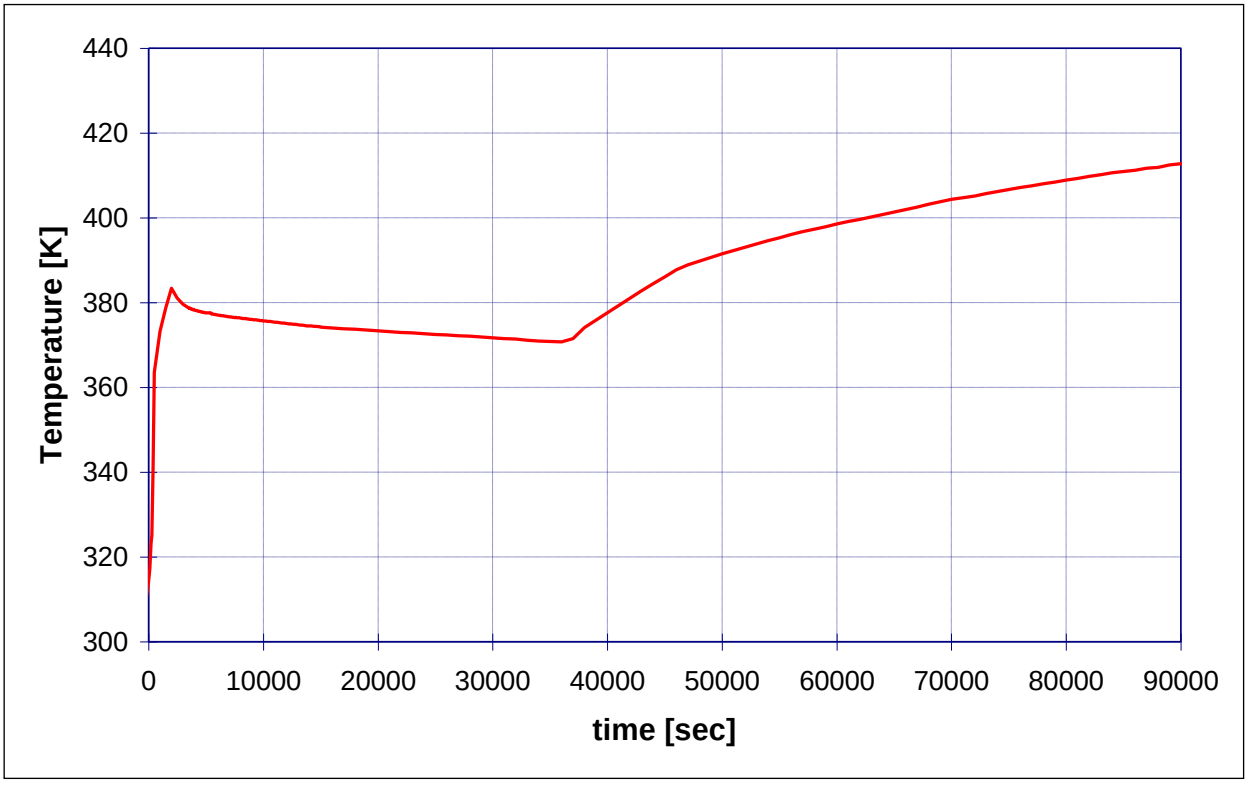

Figure 9.17 Case 1B: Containment atmosphere temperature

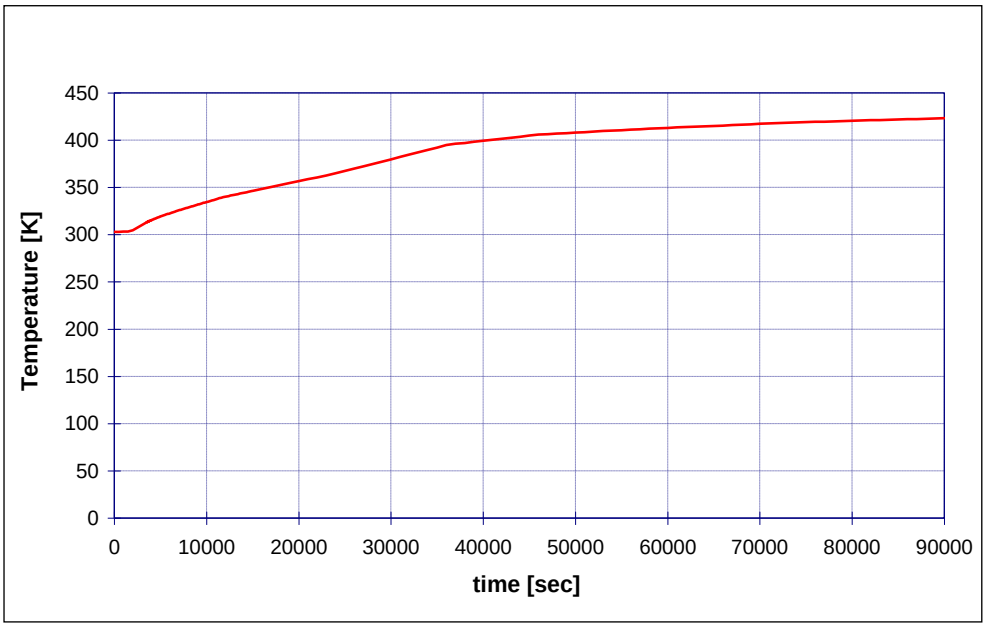

Figure 9.18 Case 1B: IRWST Liquid Temperature

9.2.3 *Station Blackout without the Support of PCCS Tank, in External Atmosphere Stratification – Case 1C*

This sequence is similar to the previous Cases 1A and 1B. The main difference with the case 1B is in the heat transfer from the containment. The case 1C is very extreme, because the external control volumes are removed, except for the environment which is directly connected to the Containment Vessel wall and dome, in order to introduce the external stratification of the air and reducing the Containment Vessel heat transfer. It causes an increase of the pressure and temperature of the containment with respect to Case 1A, but less than in the Case 1B where the friction losses are maximised and the convection heat transfer is reduced. As for Case 1B the primary system quantities are practically identical (Figure 9.19, Figure 9.20, Figure 9.21, Figure 9.22, Figure 9.23 and Figure 9.24).

The Containment Vessel temperature and pressure stay below respectively 400 °K and $3.7*10^5$ Pa (Figure 9.25 and Figure 9.26). The IRWST water temperature slowly increases with a temperature gradient of about 15-20 °C/h, arriving to boil and to generate steam at 410 °K at near $3.57*10^5$ Pa (Figure 9.25 and Figure 9.27). After the initial pressure peak of about $2.5*10^5$ Pa at near 2000 s, the steam inside containment creates a condensation film, which reintegrates the water

inside the IRWST (and enters in other containment cavities). Eventually, the large inertia of IRWST is sufficient to assure a cold safe condition for the fuel also in this case of SBO.

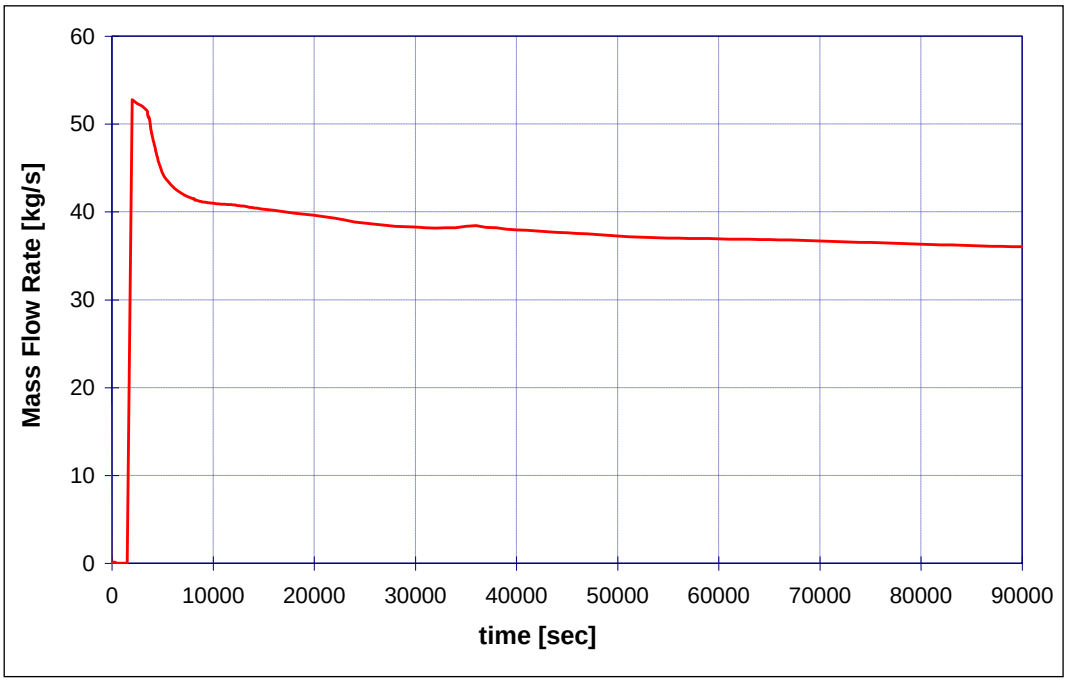

Figure 9.19 Case 1C: PRHR Flowrate profile

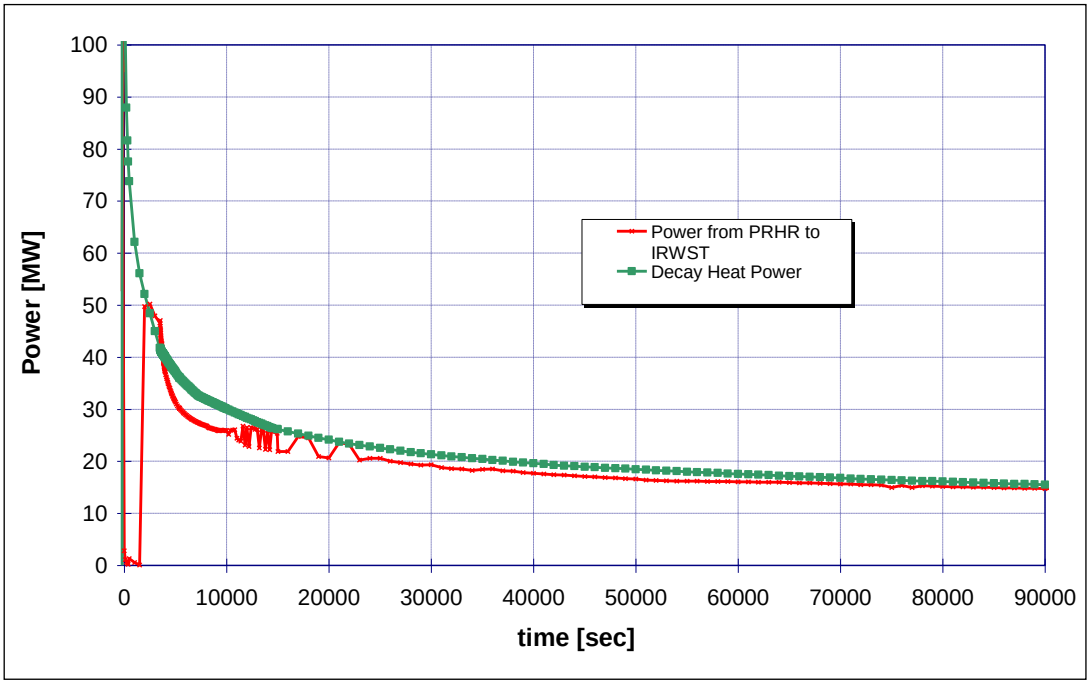

Figure 9.20 Case1C: Power balance from Decay Heat and PRHR

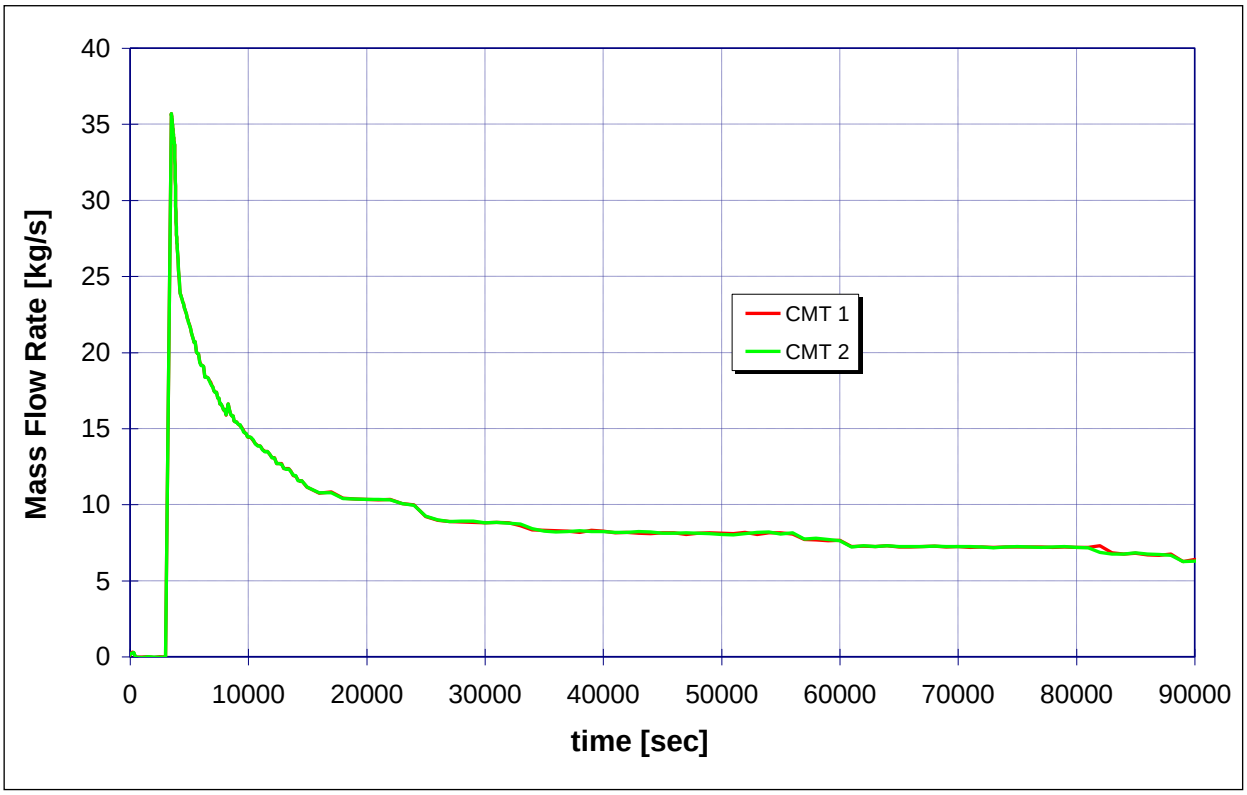

Figure 9.21 Case 1C: CMTs Flowrate profiles

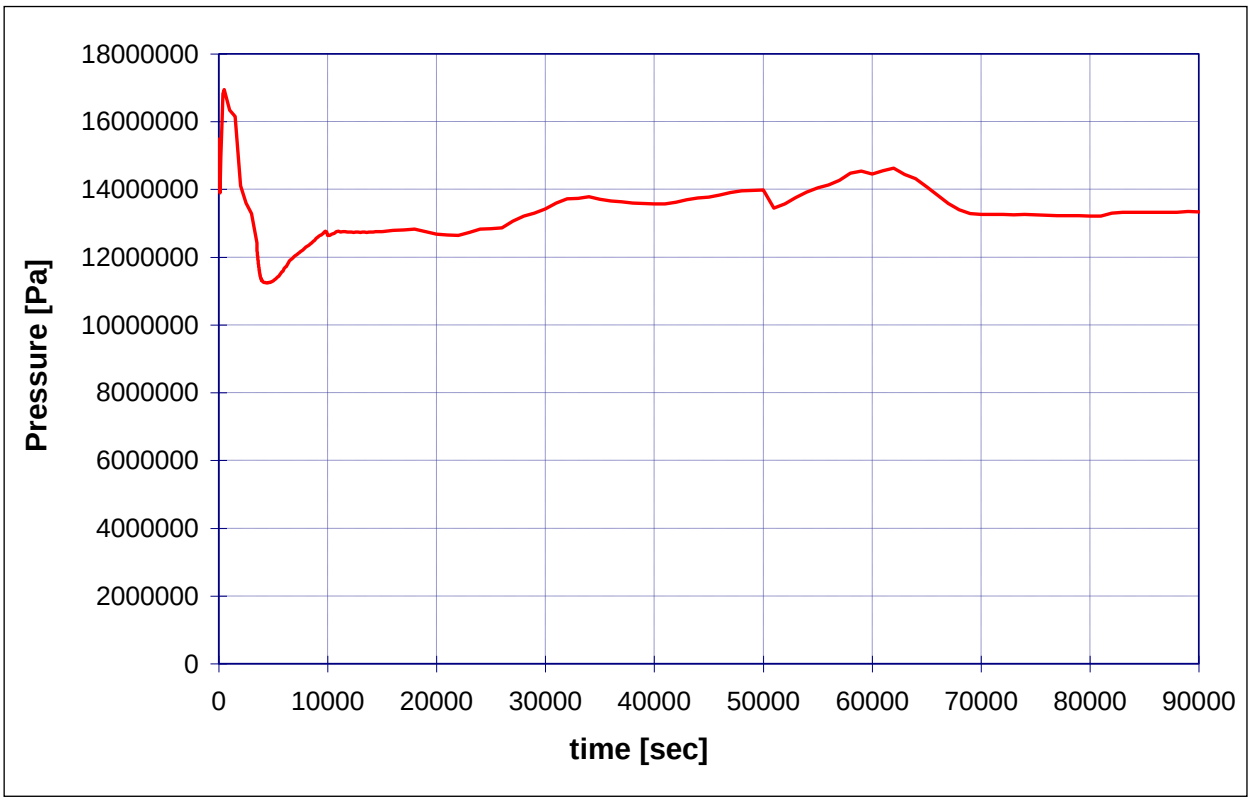

Figure 9.22 Case1C: Primary Pressure

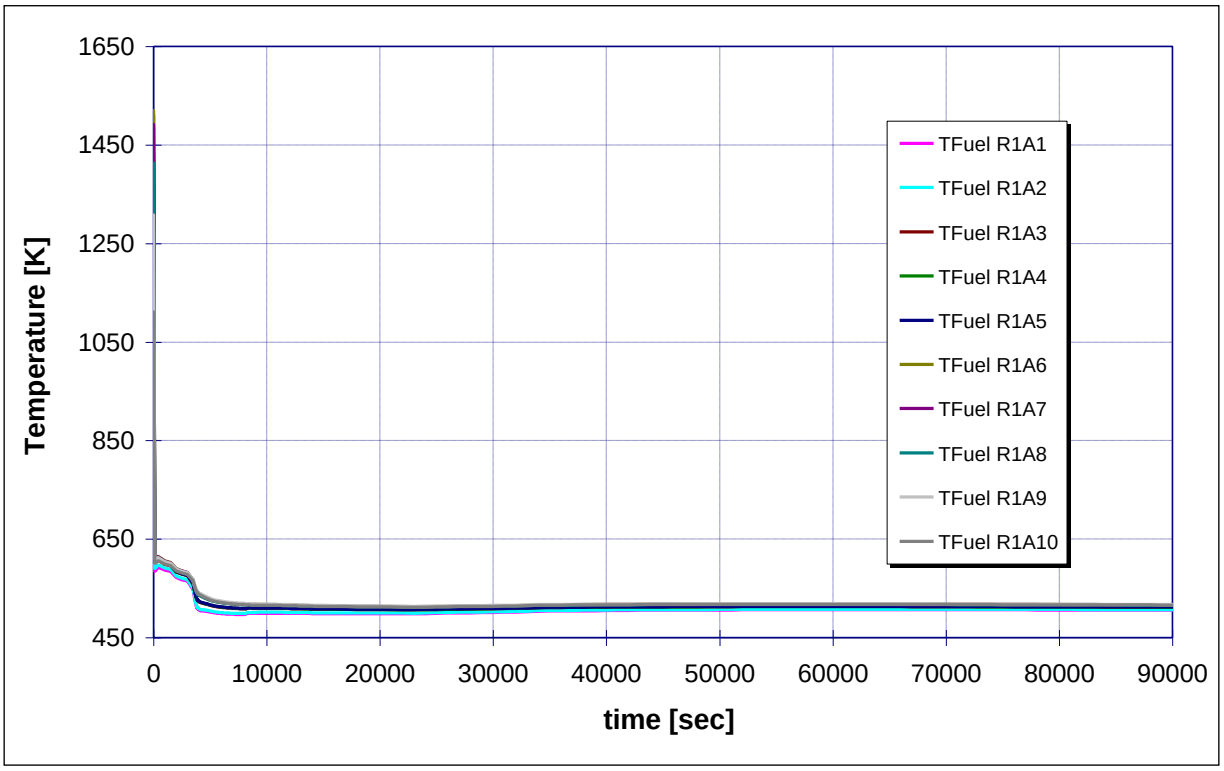

Figure 9.23 Case1C: Axial temperature evolutions of the fuel elements in the 1st ring

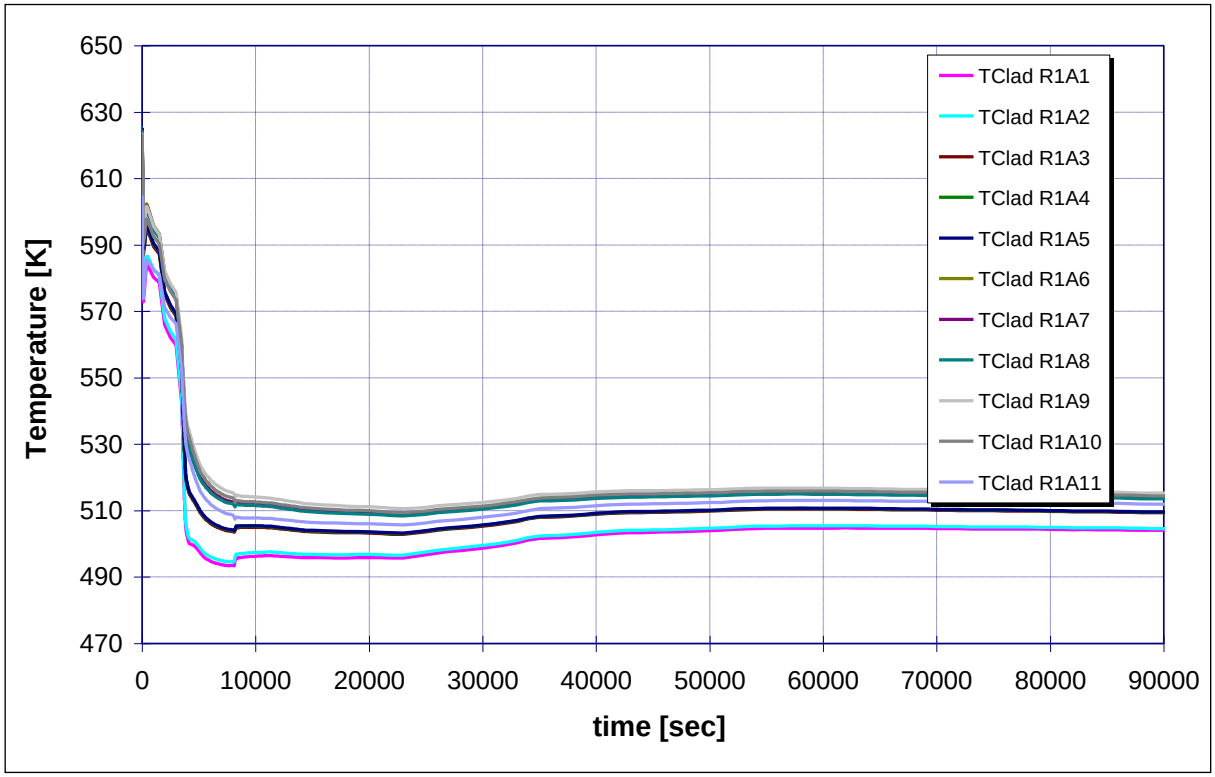

Figure 9.24 Case 1C: Axial temperature evolutions of the clads in the 1st ring

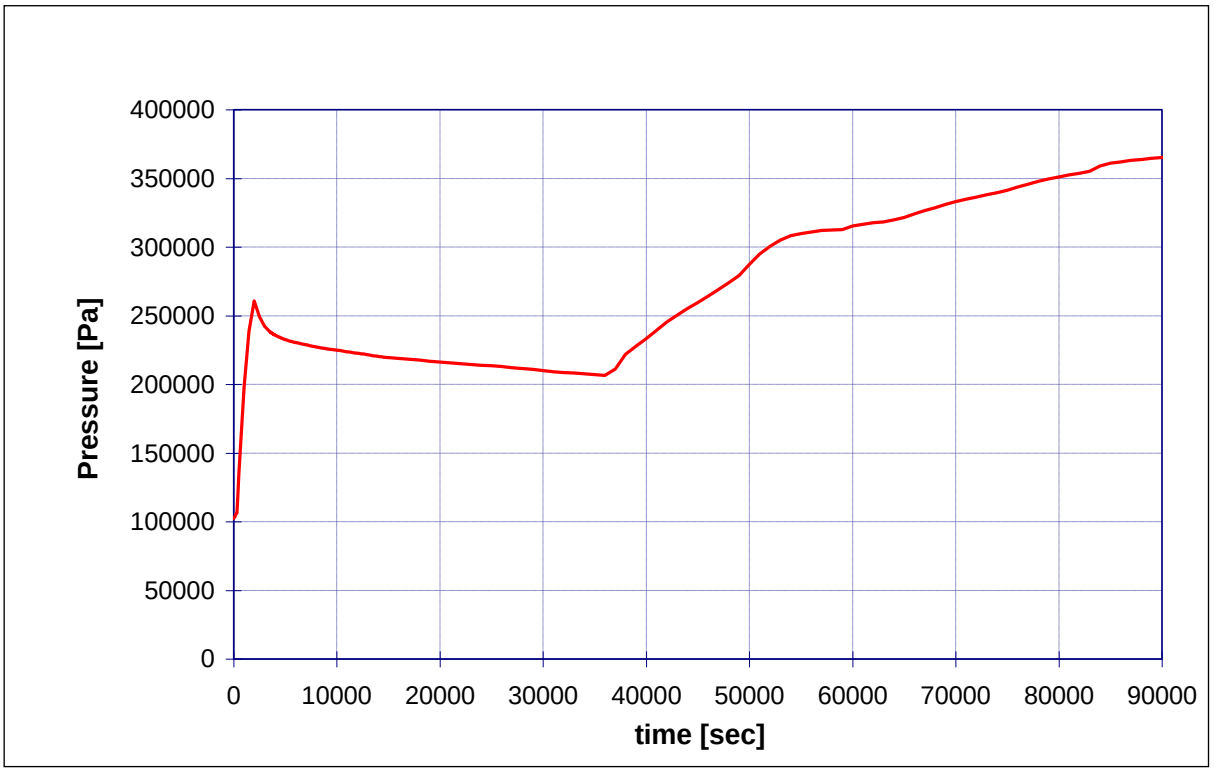

Figure 9.25 Case 1C: Containment Pressure

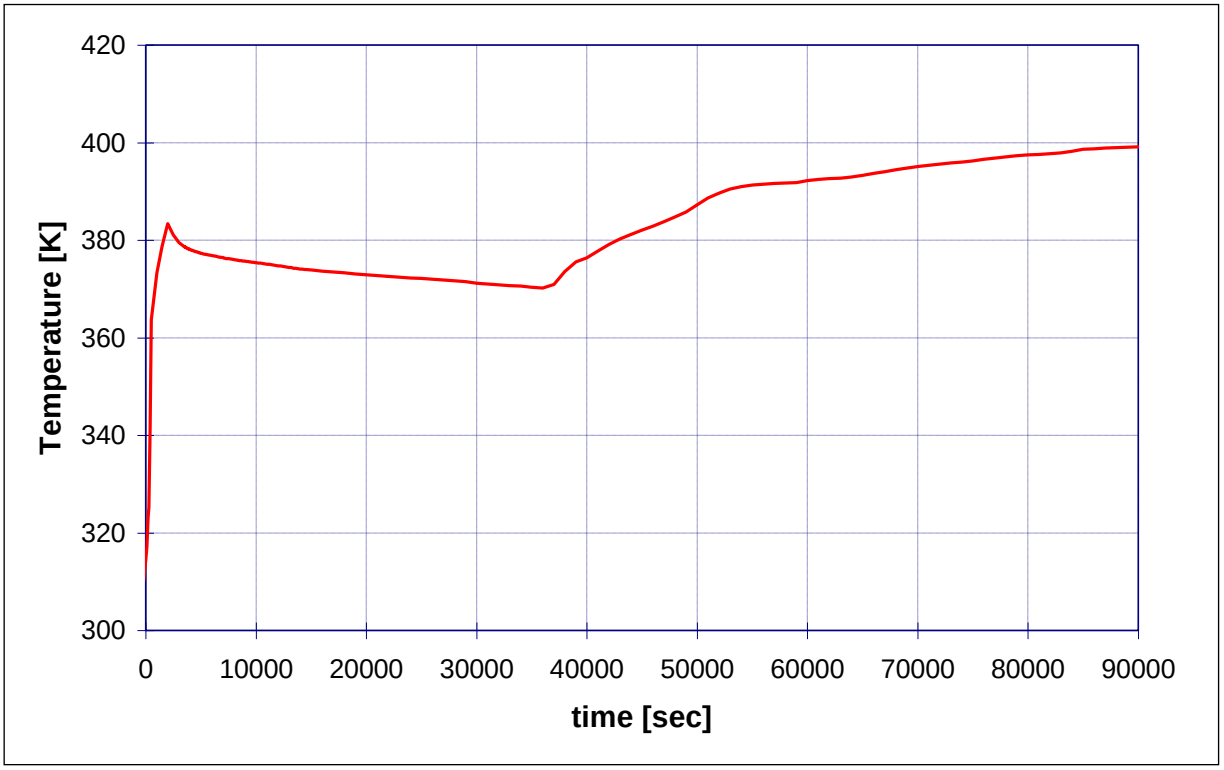

Figure 9.26 Case 1C: Atmosphere Temperature

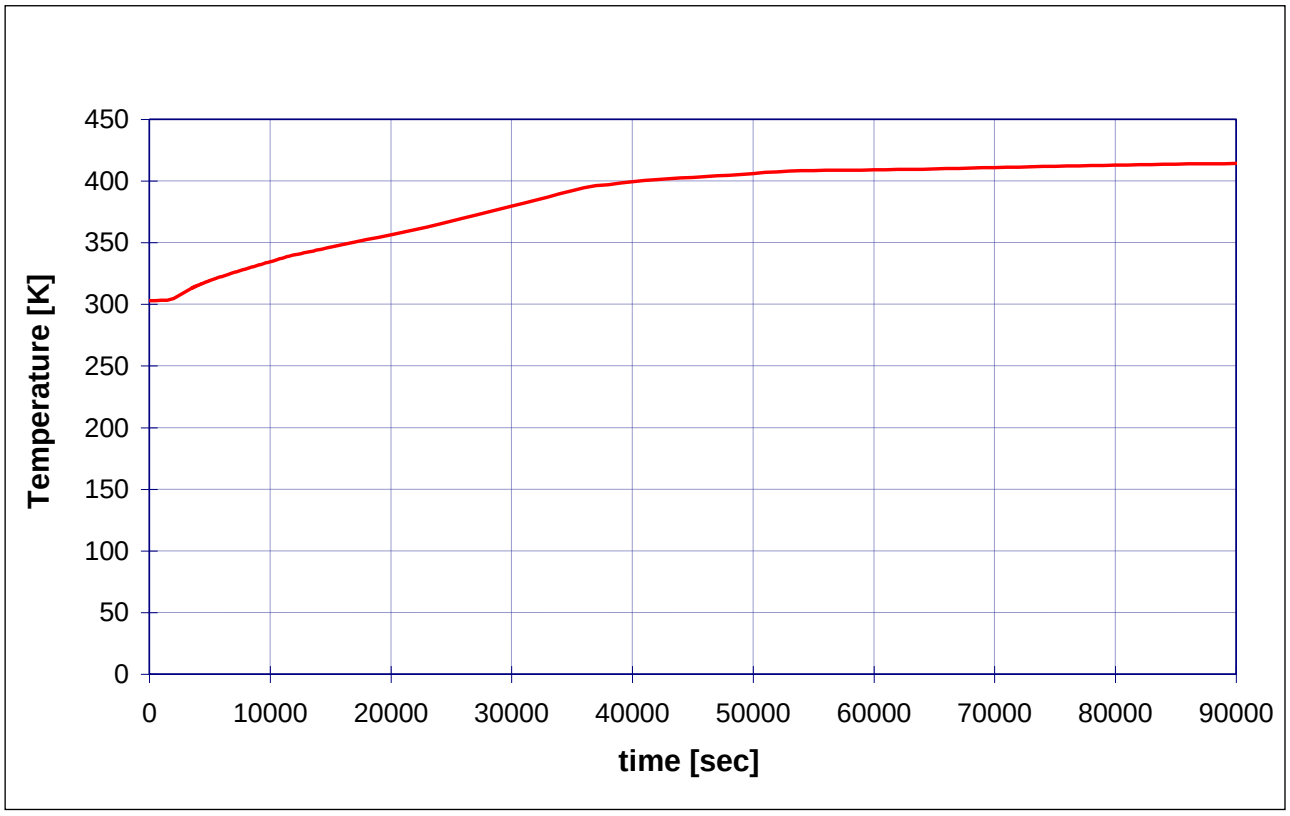

Figure 9.27 Case 1C: IRWST Liquid Temperature

9.3 Parametric Analyses of DVI Break

Due to the importance of the Sequence, the DVI Break analysis (with the complication of the second IRWST line injection valve failure) is the main part of the performed analyses. The large depressurization due to the LOCA implies critical blow down at the rupture and on the ADS systems. Another important characteristic of the sequence is the pool generated from the blow down in the Reactor Cavity that after a short time can produce a reintegration of the water in the primary circuit. We start with the analysis of the Base Case and the related sensitivity analysis. After that, we will verify the effect of the dimension of the rupture in order to check if all types could bring to severe conditions.

Continuously the sensitivity analyses are subdivided in two groups that take into account the velocity of the transient.

The first group concerns the sequences that are very fast due to the break of the large pipe that connects the IRWST at the Steam Generator Cavity. The flooding of the cavity is too fast in order to observe the lost of the core geometry, except for local melting. In these sequences we observe the prompt release of fission products, including the halogens, the candling phenomenon, local melt with foul of debris when the water enter in the core and a substantially good geometry. Also the SB-DVI-LOCA is inside this group, but this sequence does not arrive at severe accident conditions.

The second group is characterized by a slow evolution of the phenomena, with large melting of the core due to the delay of water inlet. In these sequences there is the partial or total loss of the geometry, with large melting of fuels' assemblies that fall down as molten material or debris on the lower support plate. With the reflooding of the core, this material generates a crust. In some cases this molten material can bring to the break of the support plate, due to local high temperatures, and fall down in the lower head. Unfortunately, MELCOR code uses only Temperature Criteria to decide the break of the plate. One of the open questions of this work is to analyse the behaviour of the support plate when it arrives at this critical point. It is very important to evidence that these sequences are less realistic than the previous group, with an occurrence frequency 2 o 3 orders of magnitude lower with respect to the 1st dominant sequence [4].

The Case 3A and 3B are the reference analyses for each group. NOTE: these analyses are limited only to follow the melting phenomena and chemical interactions of the material inside the Vessel.

9.3.1 *DVI Break as DBA Accident – Case 2A*

The sequence has been studied on a different timing with respect to previous ones, up to the time when the transient can be considered under control. The accident starts with the double-ended break of the DVI-1 line with simultaneous SBO in order to set a maximized scenario. In this case, the reactor, turbine and pumps trips take place almost at the same time (12 s after the initial event), while the CVCs and heaters systems are assumed as set off. The sequence is characterized by a fast depressurization of the primary circuit due to the blow-down (Figure 9.28) and ADS stages activation, leading to a quick equilibration between the pressure of the Primary and the Containment systems ((Figure 9.29) and Figure 9.30).

Practically the two CMTs operate instantly, discharging their water inside the vessel (in the loop 2) and in the containment system through the break. The second accumulator actuates after the progressive emptying of the PRHR and of the 2 CMTs (≈200 s), while the first accumulator practically enters in function in few seconds due to the broken line depressurization.

The DVIs are designed to let the water from IRWST to enter directly the reactor vessel. In this sequence the water goes from DVI-1 directly into the containment cavity, which is then flooded until the level arrive up to the break. The flow-rates in the DVI-2 are between 10 kg/s and 50 kg/s between 0 and 470 s. After this, the flow-rate stays between 20 kg/s and 80 kg/s until the end of the sequence due to the progressive emptying of the IRWST tank. Only near ≈4600 s, when the water enters in the reactor from the DVI break, the two flow-rates are practically the same. Fuels and clad temperatures are practically under control (Figure 9.31 and Figure 9.32) without any production of hydrogen (Figure 9.43). For this reason the sequence is considered as safely closed.

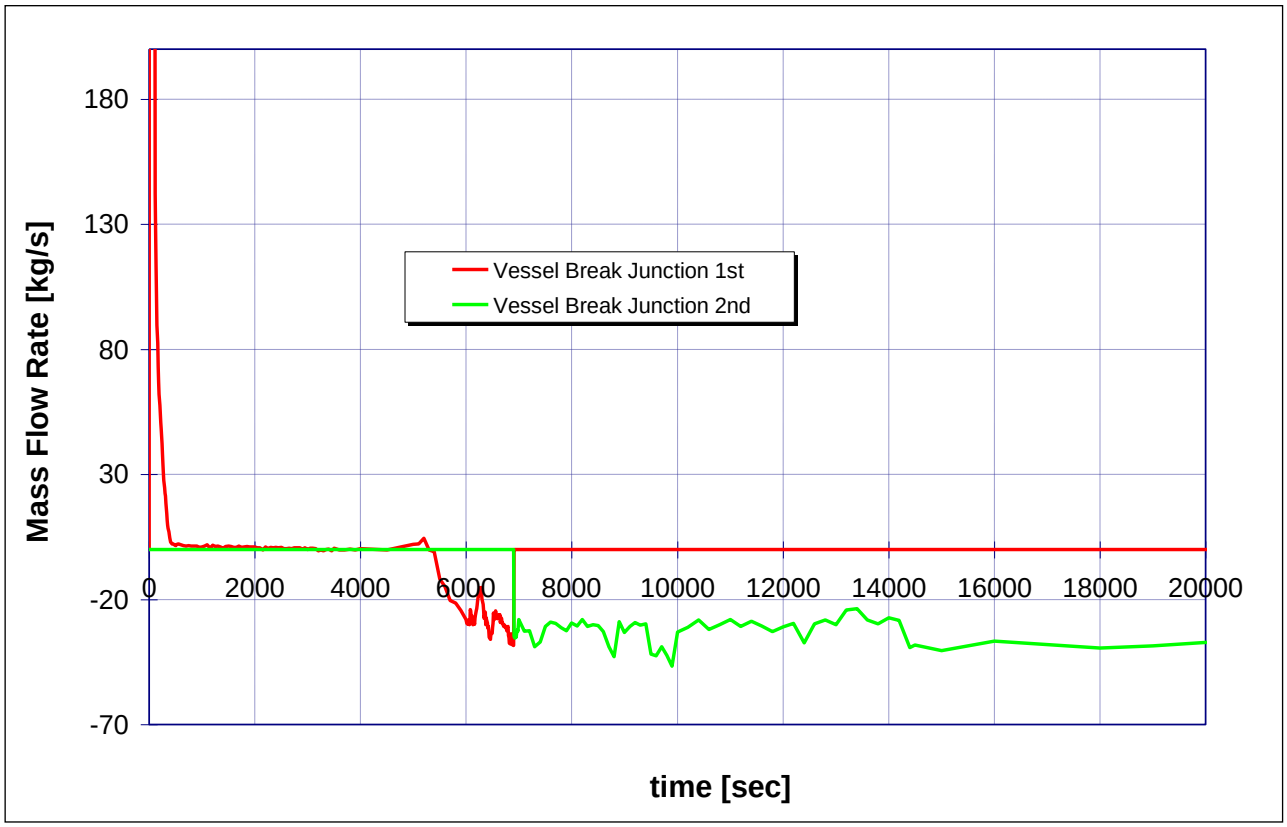

Figure 9.28 Case 2A: Break-line flow rate from Vessel side

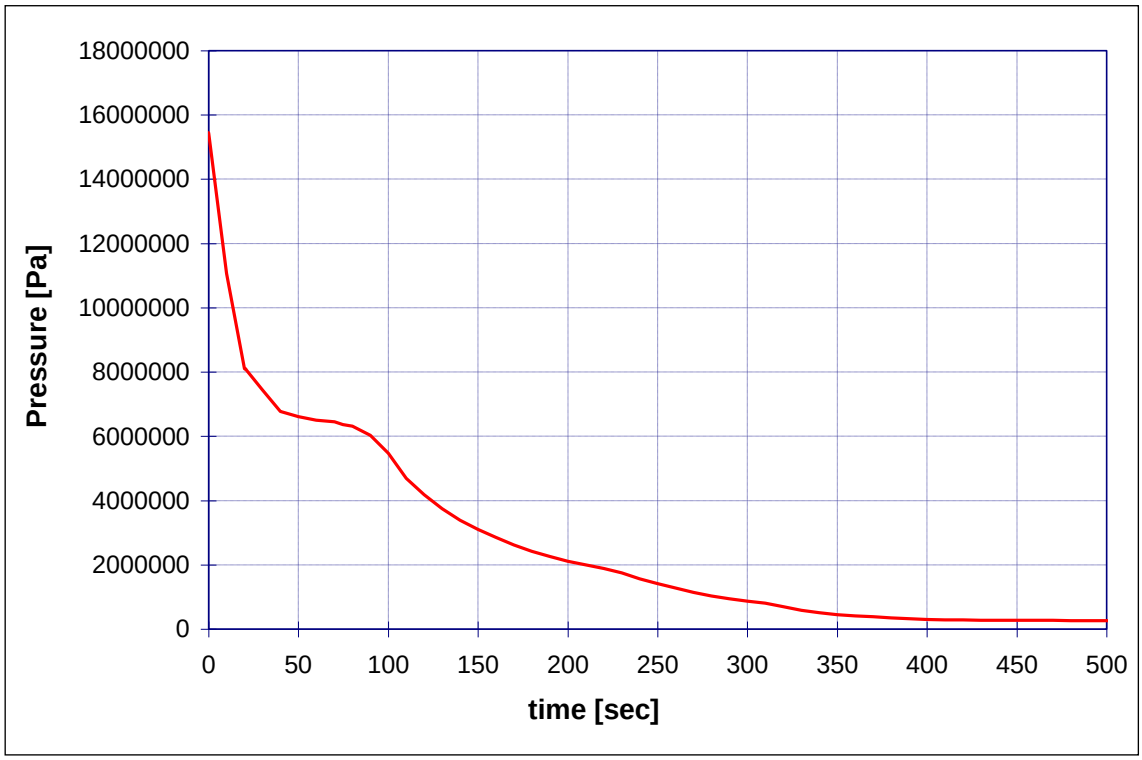

Figure 9.29 Case 2A:Primary Pressure [500 sec]

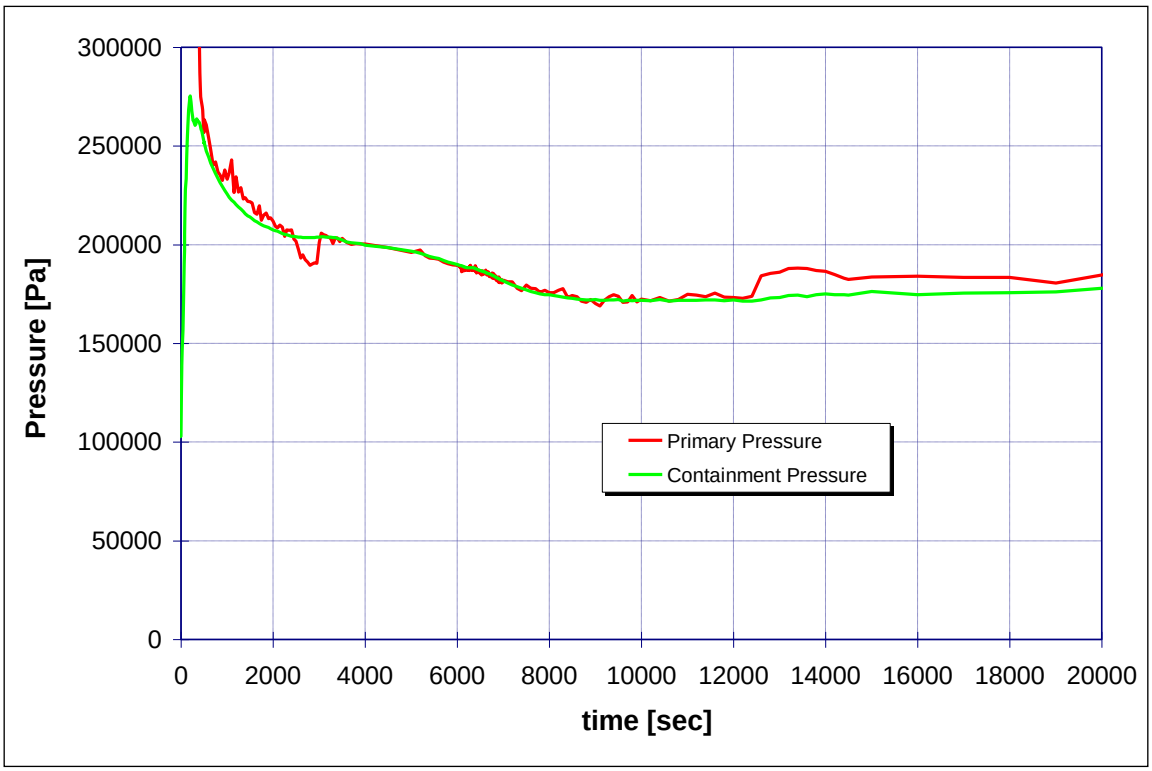

Figure 9.30 Case 2A: Primary and Containment System Pressure

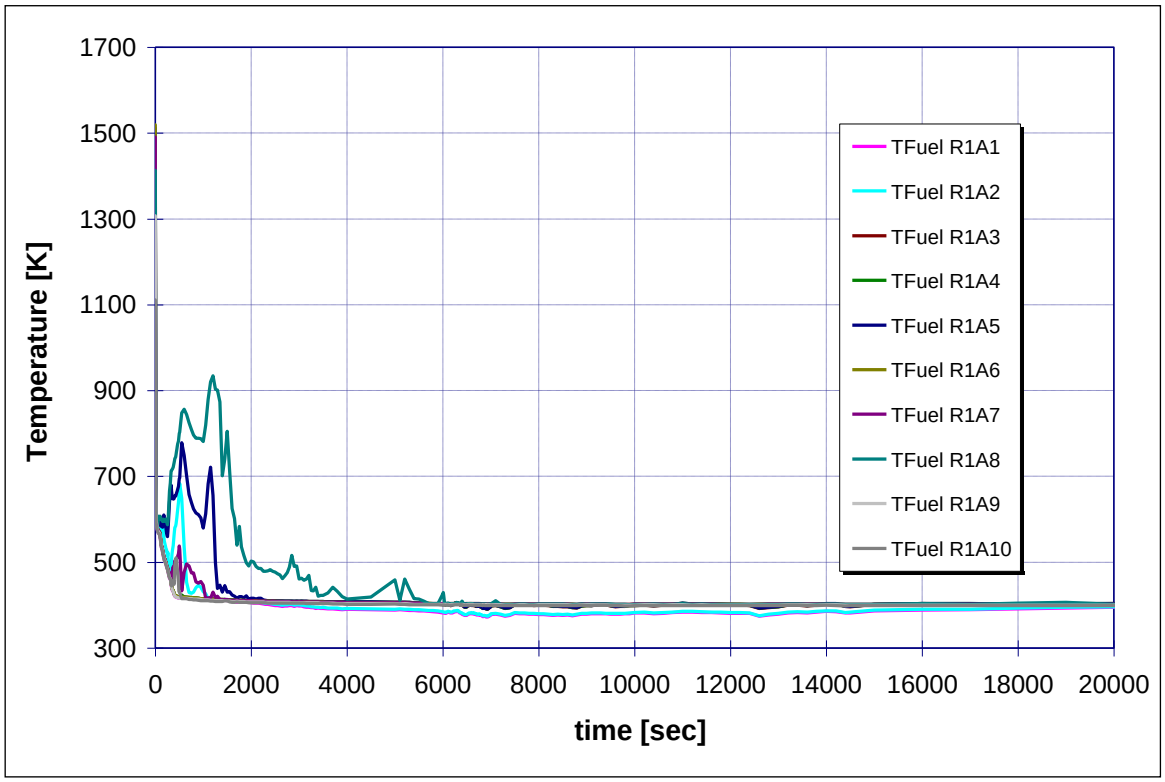

Figure 9.31 Case 2A: Axial temperature evolutions of the Fuels in the 1st ring

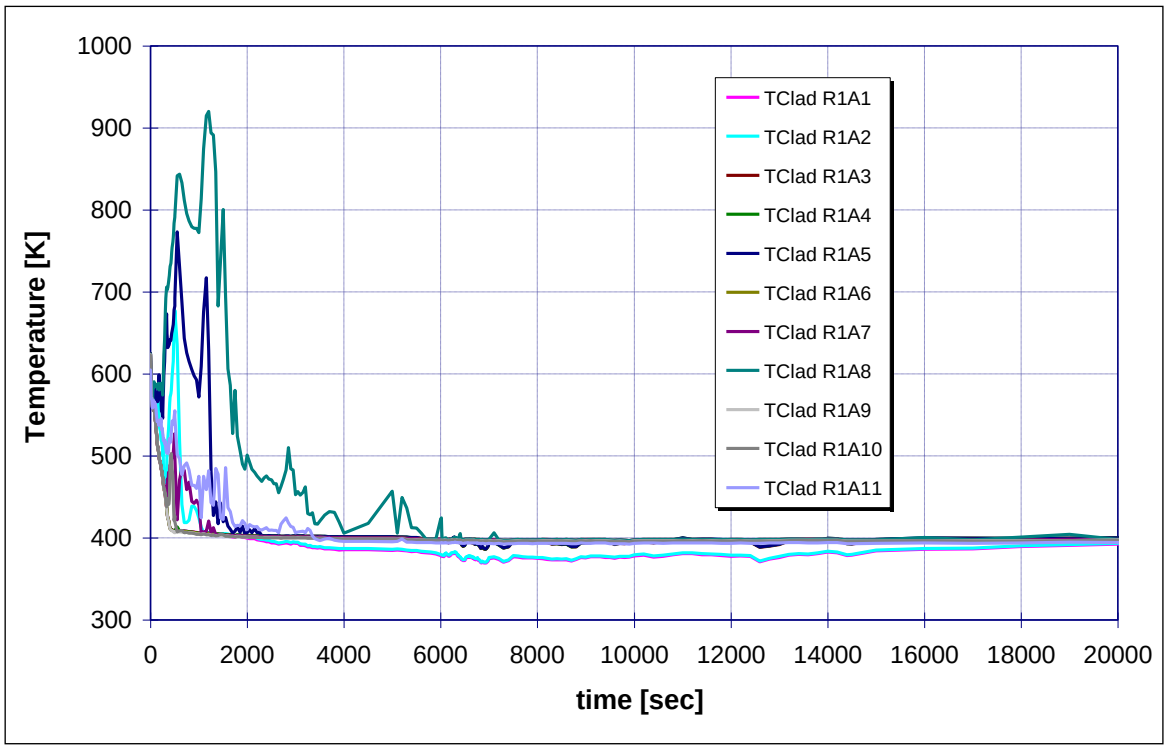

Figure 9.32 Case 2A: Axial temperature evolutions of the clads in the 1st ring

9.3.2 *DVI Break as SB-LOCA – Case 2B*

The first question that we must answer is: how much large should be the rupture? As first assumption, we take into account a rupture with a break area similar to max corrosion and radioactive damages in the Vessel, in order to maximise the water loss (Figure 9.33).

The transient is practically the same of the previous sequence, with the fast depressurization of the system (Figure 9.34); the ECCS enters in the same order: CMTs, Accumulator 1, Accumulator 2, IRWST line 1. But, when the IRWST line 2 should operate in order to reflood the reactor core, the Squib Valves fail to open (Figure 9.35). Without the contribution of the DVI B line, the reactor could be in a severe sequence except for the contribution of the DVI A line that, with its partial flow-rate can reflood the core in some minutes, prevents the core degradation (Figure 9.36), without any core damage (Figure 9.37). After 11500 s the water enters in the reactor vessel from the break and the sequence could be considered closed. The hydrogen production of the sequences is practically null due to the water mass entered from the partial pipe of the ECCS train 1.

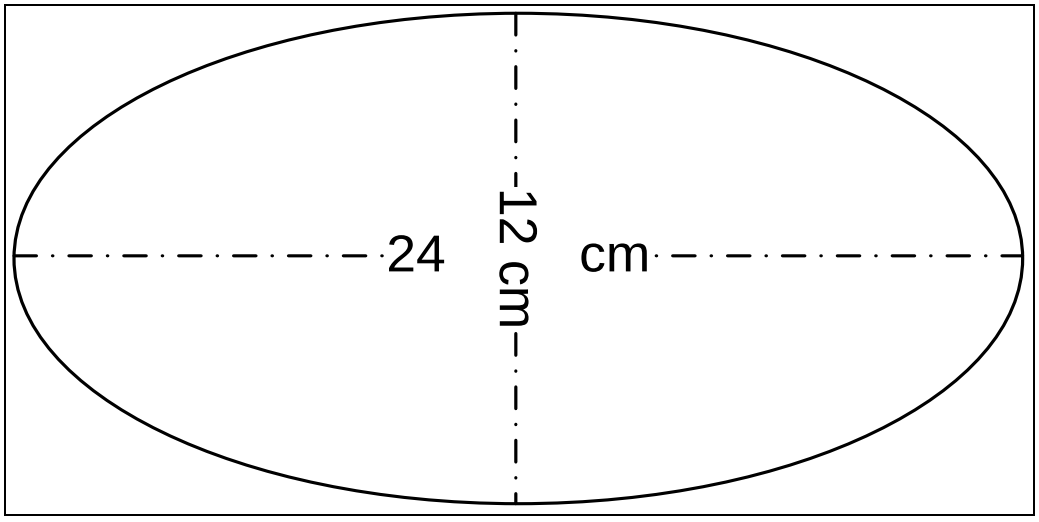

Figure 9.33 Case 2B: Sizes of the rupture

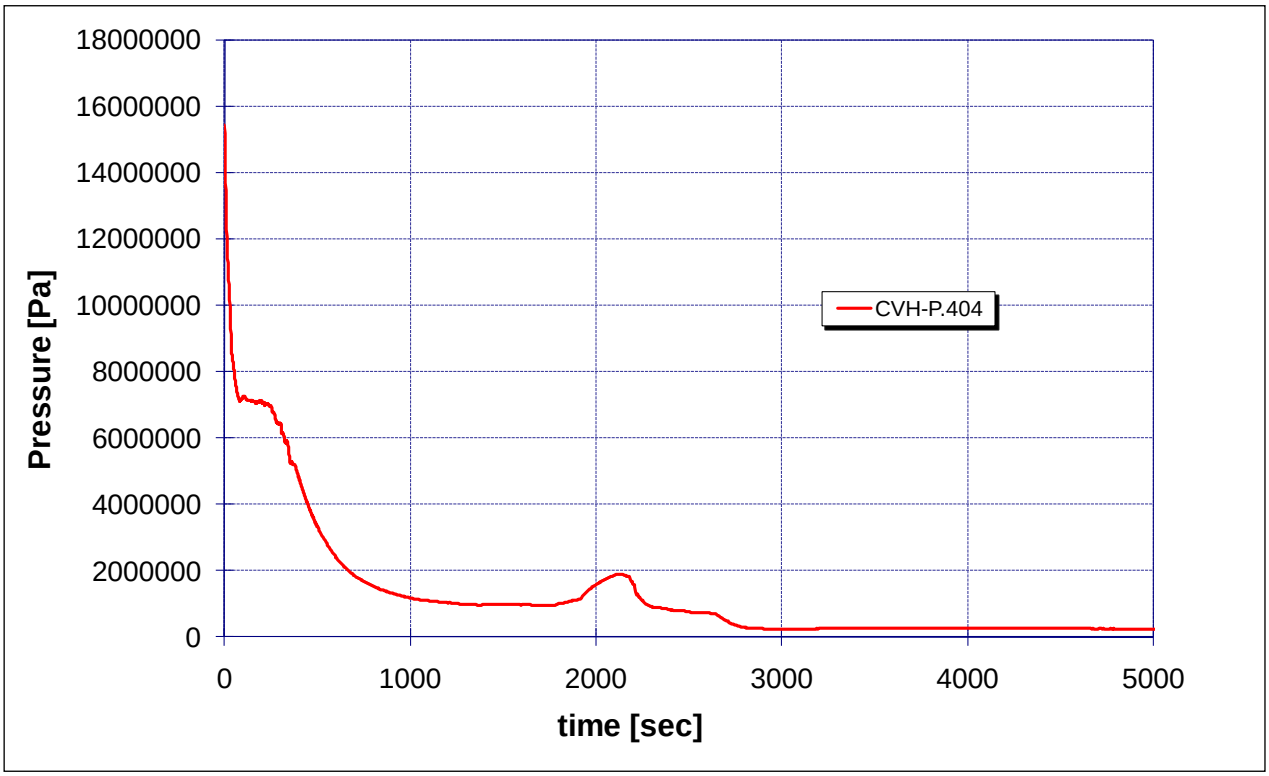

Figure 9.34 Case 2B: Primary pressure

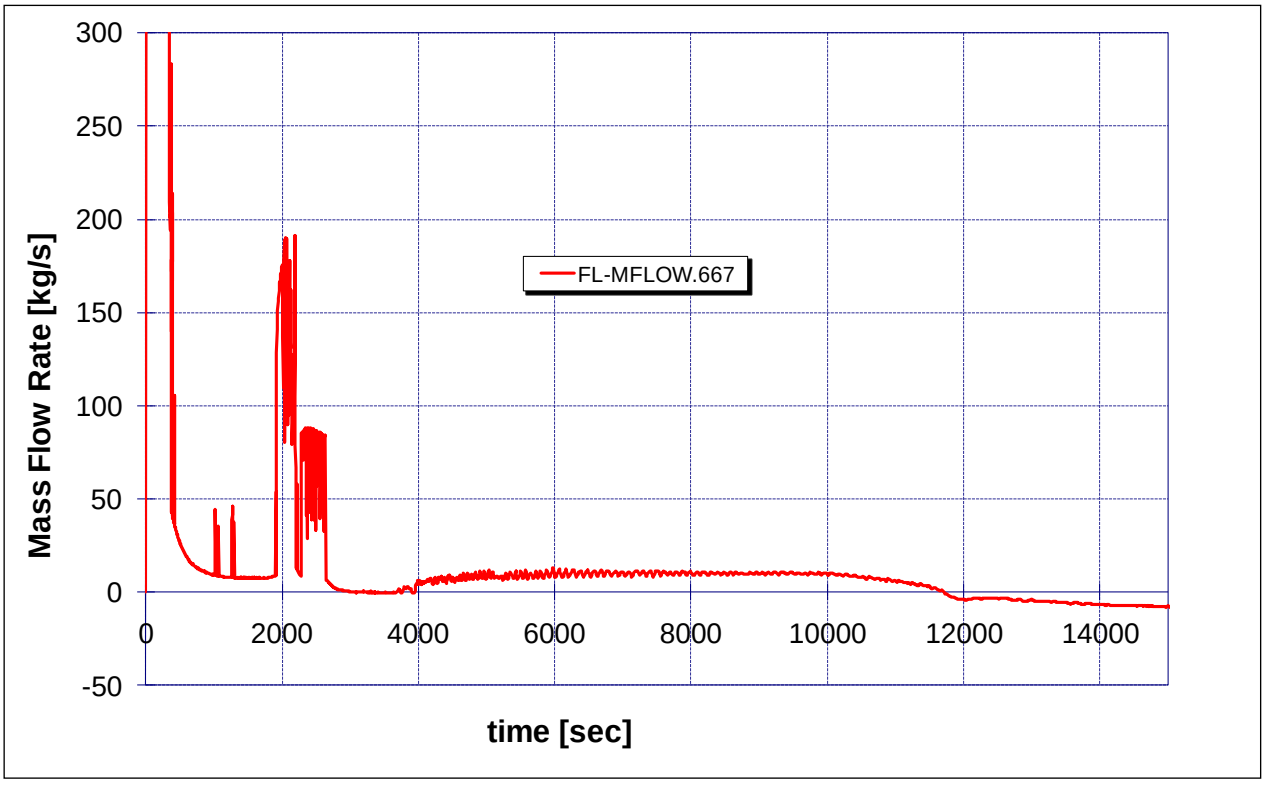

Figure 9.35 Case 2B: Breakline flow rate from Vessel side

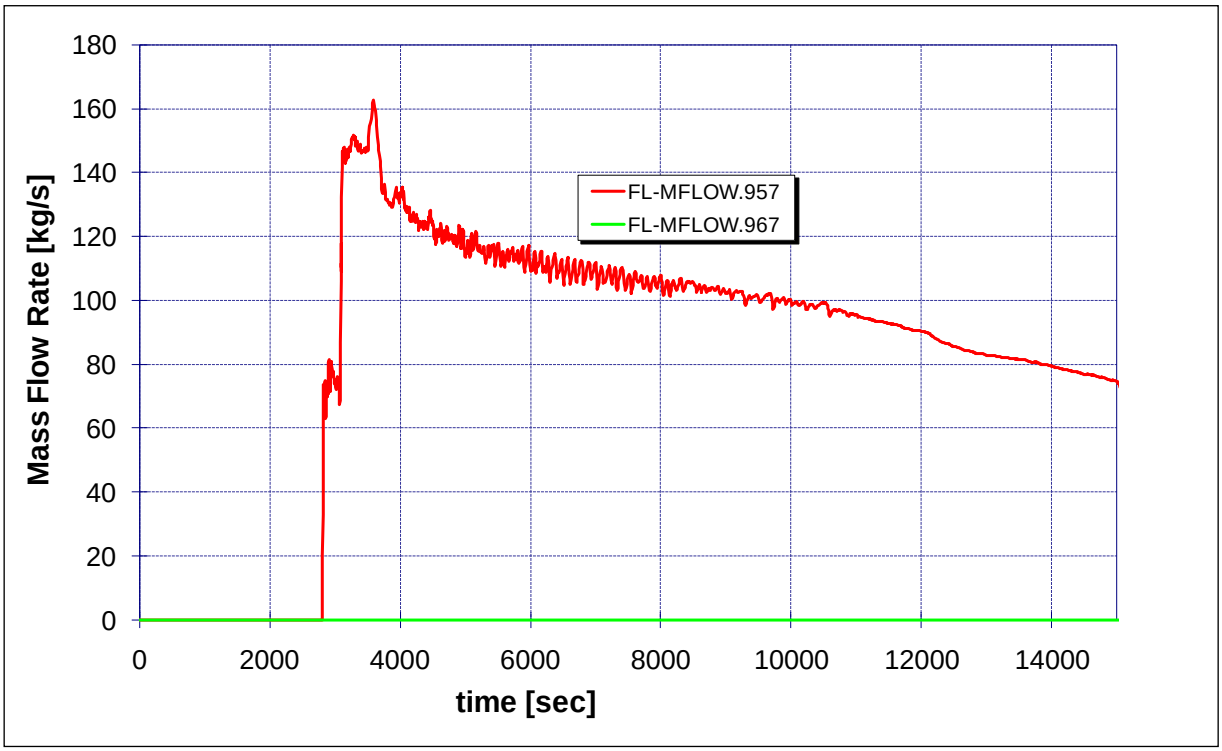

Figure 9.36 Case 2B: IRWST injection lines flow rates

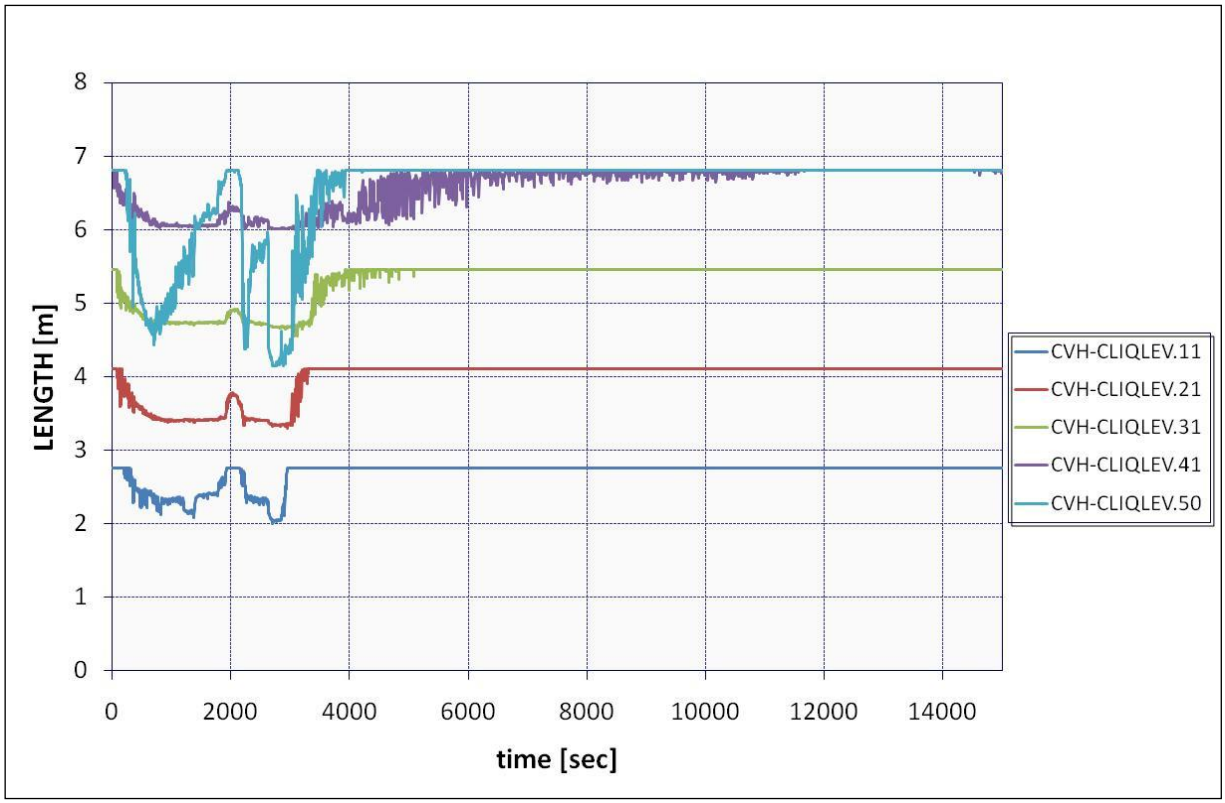

Figure 9.37 Case 2B: Core water level

9.3.3 *DVI Break in SA Condition – Case 3A and 3B*

The Case 3A and 3B simulate the double side break of the DVI line 1 pipe that connects the IRWST to the reactor vessel, the same initial event as for the Case 2A, but with the difference that the DVI line 2 do not open due to a postulated multiple failure of the injection squib valves. The valves open in the broken DVI line and drain the IRWST water into the containment.

Unfortunately the Case 3A is incomplete because the reflooding process in a large degraded core is difficult to be carried-out by MELCOR [1]: the time step of the calculation falls down around 10^{-8} s/cycle. However it is clear that the melt progression is blocking as for the hydrogen production and the sequence could be considered sufficiently closed.

The difference between Case 3A and Case 3B is the vessel cavity flooding due to the accident management set up in case of SA. A manual action is required when the temperature grows up to 923°K in order to accelerate the flooding of the cavity to assure the retention of the molten corium inside the vessel. During the Case 3B it is assumed this operator action, which is able to accelerate the reflooding of the core reducing the possibility of losing the core coolability. The inlet of the water inside the core in case 3B is estimated to take place after 6900 s since the beginning of the transient (Figure 9.38b). The case 3A is characterized by the absence of the foregoing accident management and for this reason, the entry of the water into the vessel, is estimated to take place after 7400 s (Figure 9.38a).

As in Case 2, the primary pressure (Figure 9.39) falls in both cases (due to the blow down and ADS stages activation) leading to the equilibrium with the containment pressure (Figure 9.40), so allowing for the injection of the IRWST through the broken DVI line. The containment pressure reaches a peak of about 3 bar after 400 s, with a subsequent constantly decrease of the pressure due to heat removal through the external circulation.

As a consequence of these very unlikely accidental scenarios, with the failure of the IRWST line B injection valve, the sequences become severe due to the loss of water and steam through the break, without any reintegration; the fuel and the claddings suffer and start to melt (Figure 9.41 and Figure 9.42), arriving at a peak temperature of ≈2500 °K for the Case 3A and to a peak temperature of ≈2300 °K for the Case 3B. As a consequence of the strong core degradation and oxidation reactions, the relocated core material falls down on the centre of the support plate (in the Case 3A

much more than in the Case 3B), with a large increase of the temperature of the support structures. When the water finally is able to go back into the vessel through the break (because the IRWST water is draining into the containment through broken DVI line 1.), the interaction between the cold water and the hot internals structures produces some pressure oscillations due to the sudden formation of steam. These phenomena (especially in the Case 3A) generate some computation instabilities due to the fast transient oscillations, until the natural circulation trough the break is established. Eventually, the injection of the water in the down-comer and in the reactor core is able to cool the internals and the core. The evaporation of the water removes the heat in the molten core and the hot internals and the temperatures of the fuel decrease under safety levels (Figure 9.41b and Figure 9.42b).

As shown in the Figure 9.43, the hydrogen produced by the oxidation of Zircalloy arrives to 188 kg during the Case 3A, while the Case 3B evidences a more intact core arriving to an amount of 126 kg. Anyway, the production of hydrogen is a major threat for the integrity of the containment system; for this reason the flooding of the cavity (Case 3B) could be useful in order to obtain faster cooling of the core, so reducing the amount of hydrogen in the containment.

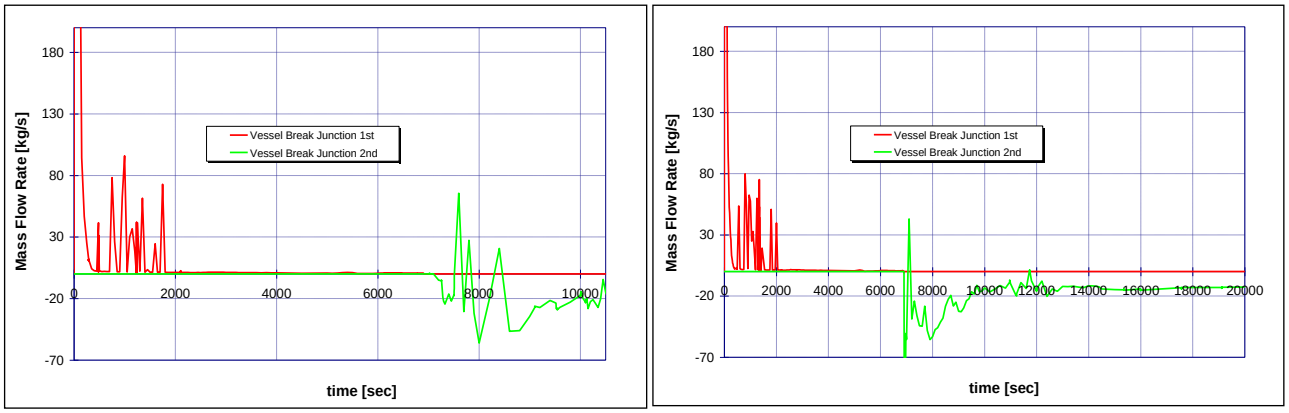

Figure 9.38 Break line flow-rate at Vessel side for Case 3A (left) and Case 3B (right)

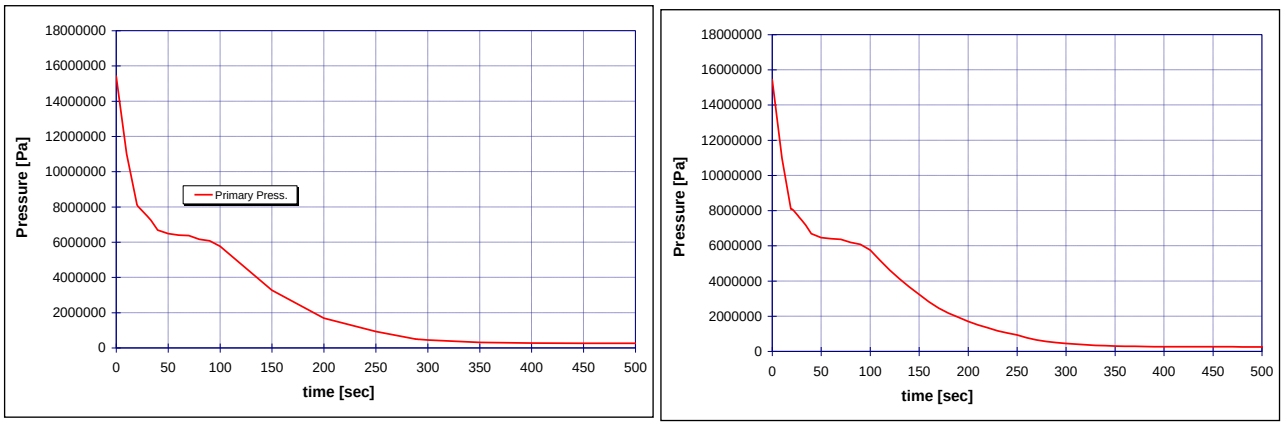

Figure 9.39 Primary Pressure for Case 3A (left) and Case 3B (right)

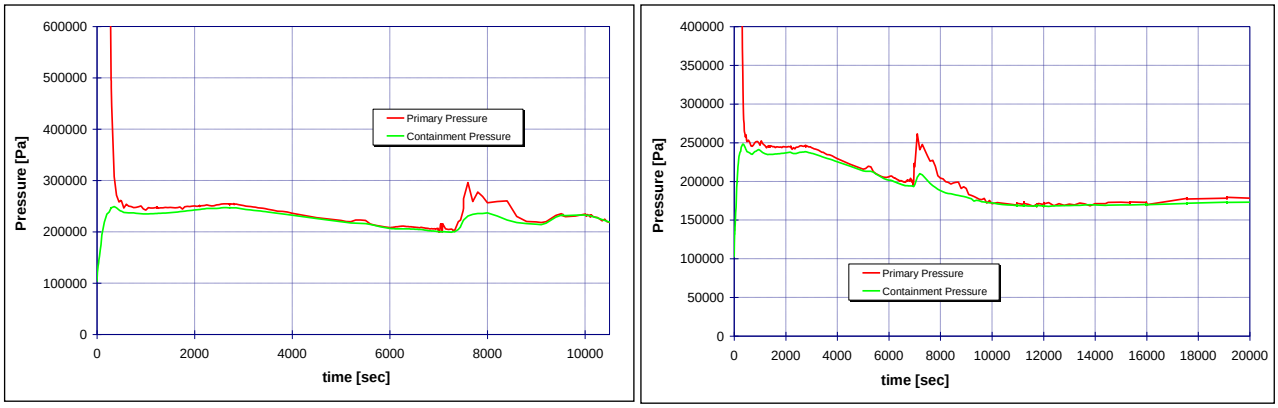

Figure 9.40 Containment and Primary System Pressure for Case 3A (left) and Case 3B (right)

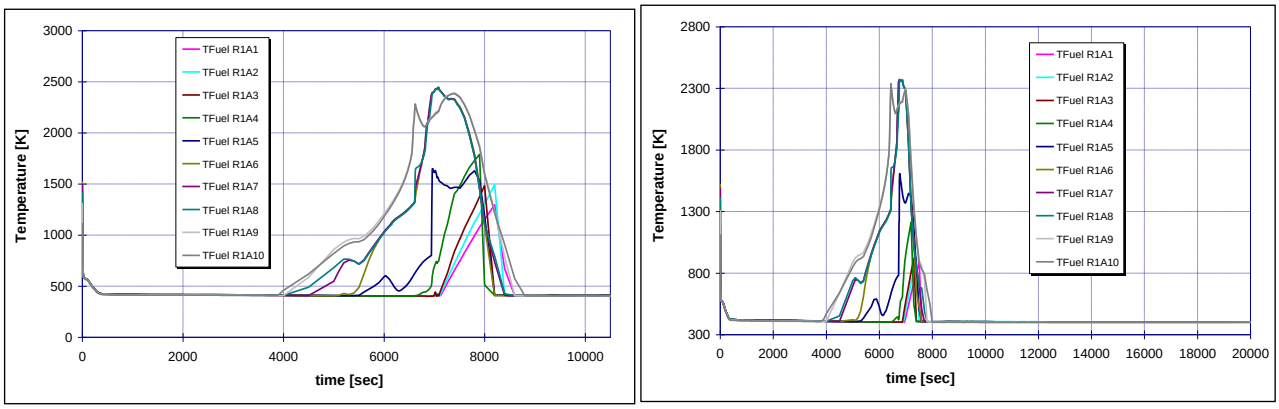

Figure 9.41 Axial temperature evolutions of the fuel elements in the 1st ring for Case 3A (left) and Case 3B (right)

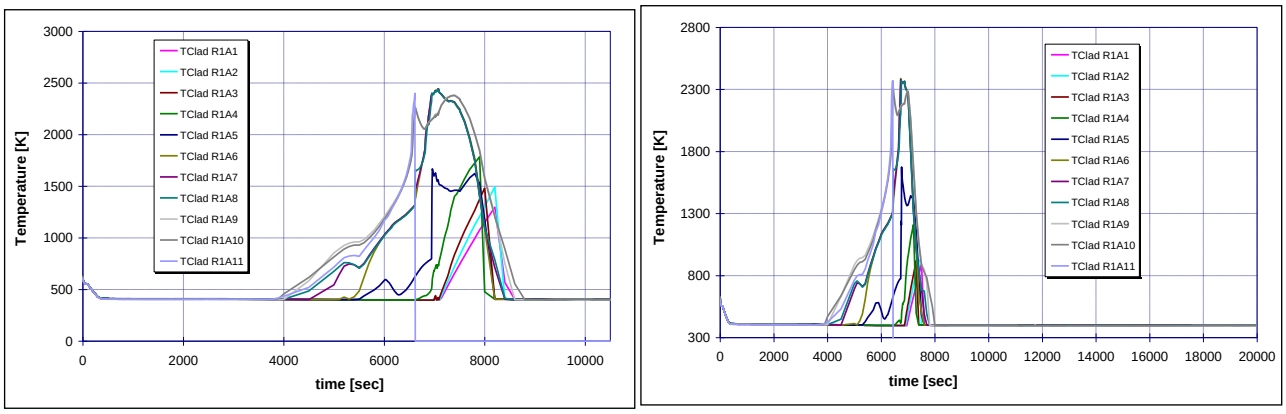

Figure 9.42 Axial temperature evolutions of the claddings in the 1st ring for Case 3A (left) and Case 3B (right)

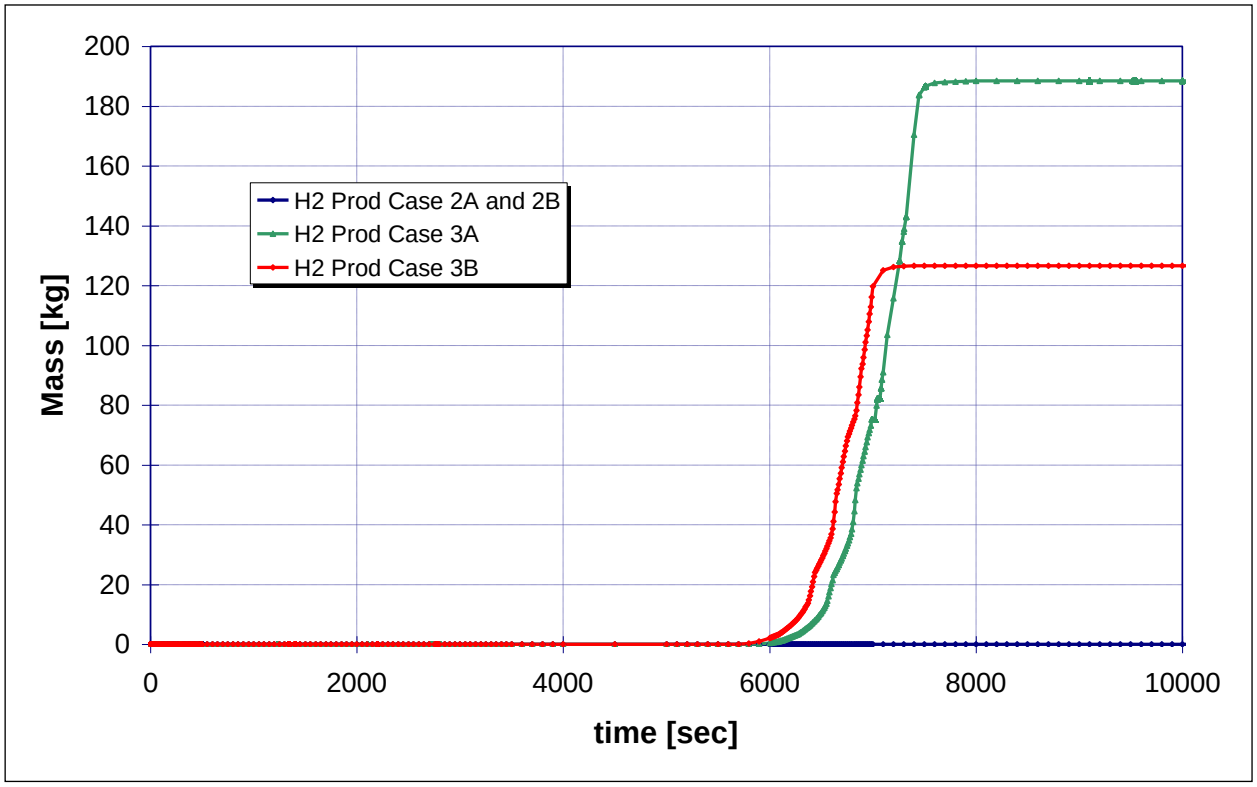

Figure 9.43 Hydrogen production for Case 2, Case 3A and 3B

9.4 General Remarks

From the above analyses it is clear that the IRWST is the most important safety feature for the accident management from a normal DBA to SA. The large thermal inertia given from the water storage in this tank reduces practically near to 10^{-9} CDF/y the risk to incur in a SA for SBO sequences [5] [5]. The risk is so low, that practically it is more correct to think to SBO sequence as

an aggravating circumstance of other sequences, for example the 1st dominant sequence. Successive Containment Vessel heat transfer to the atmosphere assures the removal of the decay heat power from the core to IRWST through the PRHR and from IRWST to the containment atmosphere, thanks to the boiling of the water; the condensation film on the steel layer of the Containment Vessel produces the restoration of the amount of the water inside the IRWST. The PCCS tank could be useful in order to assure the Containment Vessel integrity with the removal of the decay power from the containment during a SBO for more than 1 day.

The sequence characterized by the LB-LOCA and the failure of the direct IRWST injection water in the vessel is accommodated by the configuration of the primary system, with the reflowing of the core directly from the vessel side break. This work evidences few interesting points and also a qualitative idea of few phenomena (core damage and melting, hydrogen production, upper support plate thermal stresses, etc.) to evaluate in other in deep analyses. Due to the fast transient, the calculation with MELCOR code results sometimes very difficult with problems of computational instability. Further investigations are needed in order to check the results obtained in these preliminary analyses. However, it demonstrates that the AP1000 nodalization is an original and interesting tool in order to study the phenomena that other codes cannot. Especially, the behaviour of the containment and in vessel core melt retention are successfully taken into account by a lumped parameter code, as MELCOR. Practically, it evidences various important areas that could be very interesting to study: the hydrogen production occurring in a passive containment versus a full pressure containment, the thermal stresses and resistance of the lower support plate with the mitigation of the internal temperature due to the heat transfer with the external cavity, thermal stresses and evaporation phenomena connected with the re-inlet of the water from the rupture, thermal stresses of the vessel during the core melt retention and the behaviour of FP aerosol in a passive containment.

References

[1] R. O. Gauntt et al. “MELCOR Computer Code Manuals – Version 1.8.6”, NUREG/CR-6119, Vol. 2, Rev. 3, September 2005

[2] INPO, “Special Report on the Nuclear Accident at the Fukushima Daiichi Nuclear Power Station”, November 2011, special report

[3] EUR, “European Utility Requirements for LWR Nuclear Power Plants”, April 2001

[4] ANSALDO Nucleare and Westinghouse private communications

[5] US-NRC, "Final Safety Evaluation Report Related to Certification of the AP1000 Standard Design", *NUREG-1793,* 2006

[6] UKEA, “AP1000 Pre-Construction Safety Report”, UKP-GW-GL-732, Revision 1, 2009

CONCLUSIONS

The SA phenomenology is characterized by a large number of phenomena very complex depending from the time and the phase of the SA progression. These phenomena have to be modelled and the related modules implemented in Lump Parameter Codes. In order to qualify the models as implemented in the codes analyses investigating the phenomenology and the mechanisms involved in SA sequences are carried out in comparison with the data obtained from SA accidents and in ad hoc test facilities. In particular the models must reproduce the complex combination of:

- Relocation and Degradation Mechanisms
- Thermodynamic behaviour of the system
- Chemistry of the reactions taking place in the sequence.

The combination of these main phenomenological "families" could increase the accuracy of the prediction of the release from the core of FP gas, aerosols and vapour and their interactions in the primary circuit and in the containment.

Only once acquired enough experience in the use of the main SA simulation codes (user qualification) and having validated the models by the analysis of various SA experiments carried out inside the PHEBUS program, the application of these codes to real plants can be performed with results sufficiently adequate.

What mentioned above has been the objective and also the road-map of the research work discussed in present thesis.

The experience earned at DIMNP during several years of analyses on the SA phenomenology has been precious for developing an adequate nodalization of the PHEBUS plant. In particular, the ISP46 experience has been the first step of the nodalization development, starting with the analysis of the containment behavior. To this aim, we initially assumed as boundary conditions the releases of steam, hydrogen and FP from the pipe, which simulates the cold leg; the following steps were the progressive implementation of the complete nodalization, with the addition of the Circuit, and the Test Section (ISP46 complete analysis).

The investigation of the bundle degradation phenomena in the PHEBUS program has been performed for the evaluation of the models that simulate the release of FP aerosols and gases, the hydrogen production from the chemical reactions of Zyrcaloy and other materials, and the relocation phenomena. These scaled integral experimental tests simulating the release of FPs and aerosol dynamics are of basic importance for the understanding of the interaction of complex phenomena taking place during a postulated accident. Moreover they provide a very useful set of data for the validation and assessment of the models developed for the computer programs used for the analysis of the source term.

The availability of the experimental results from FPT0, FPT1, FPT2 and FPT3 has been very useful to better understand heat and mass transfer phenomena that take place in the containment system, a necessary condition for the correct simulation of aerosol dynamics.

The results of the analyses carried out evidence the capability of ASTEC and MELCOR codes to simulate the FPT1, FPT2 and FPT3 experiments, and particularly a good behaviour for the prediction of the principal phenomena connected with the degradation of the bundle, material relocation and creation of the molten pool. This results also from the simulation of the FPT1, even though some discrepancies were detected, particularly with respect to the release of FP product and SM material, as well as for condensation heat and mass transfer. In particular MELRCOR 1.8.5 code evidences problems in simulating the release of SM and of FP from the melt pool.

FPT2 and FPT3 analyses evidence the necessity to improve the chemistry models for the material releases in order to estimate better the source term. In particular boron carbide reactions and silver iodide production are two important topics for outlined by PHEBUS program. In fact, the boron carbide reactions arise problems in relation with the following important factors:

- Increase of the hydrogen production,
- Generation of boric acid able to damage fuel and internal structures and to deposit on the primary circuit reducing the flow section; this can also aggravate the problem of criticality control during the reflooding phase
- Increase of iodine concentration in the containment, in particular during the washing phase of the containment atmosphere.

The iodine released in the containment vessel is not so much in case of FPT3 (the test with B_4C control rods) due to the inertial deposition in the deposit of boric acid; hoever it is in a form able to re-suspend at temperatures higher than 422 K or with hydrogen combustion. In the cases of FPT1 and FPT2 iodine is found mainly in the CV pool as silver iodide, due to the presence of large silver amounts coming from the control rods.

MELCOR and ASTEC codes are enough able to calculate the release and the transport of iodine from the bundle, through the circuit and inside the containment vessel. In particular ASTEC v2.0r2 gives better results due a more detailed chemistry.

The last observation concerns the validation of the lump parameter codes as MELCOR and ASTEC by the analyses of PHEBUS experiments. To this aim, similar nodalizations have been set-up for the analyses of FPT2 and FPT3, which have a lot of common points and are particularly suited for testing of models. The results are very interesting and evidence a general agreement of ASTEC and MELCOR simulations, with respect to the hydrogen production, the steam starvation phenomena and the behaviour of the containment. Some divergences are however evidenced as the timing of the sequences, the release magnitude and the steam condensation. In particular the models implemented in ELSA of ASTEC are improved with respect to CORSOR Booth of MELCOR, due to the integration of a simplified chemistry and a detailed mechanical approach.

As final remarks, it has to be noticed that the limitations of MELCOR 1.8.5 to simulate the phenomena with simplified models are compensated by the larger flexibility of the code. ASTEC remains less flexible of MELCOR, in particular for the simulation of the behaviour of other gases, like CO and CO_2, in the primary circuit.

Finally we prepared a AP1000 nodalization in order to estimate the hydrogen production and the progression of SA in this ALWR. From the analyses it is clear that, the IRWST is the most important feature for the accident management from normal DBAs to SAs. The large thermal inertia given from the water storage in this tank reduces practically near 10^{-9} CDF/y the risk for SBO sequences. Successively, the CV with its passive heat transfer to the external atmosphere, assures the removal of the decay heat power: from the core to IRWST through the PRHR, from IRWST to the internal CV atmosphere thanks to the boiling of the IRWST water and the condensation film on the CV steel layer which restores the amount of the water inside the IRWST, and finally with the

heat transfer from the CV internal atmosphere to the external atmosphere due to the natural circulation of the air in the annulus between CV wall and external concrete structure.. The PCS tank is useful in order to assure the CV integrity during the first day and becomes necessary for assuring the removal of decay power from the containment during a SBO lasting more than 1 day.

The risk from SBO sequences is so low that practically this type of sequences can be seen as an aggravating circumstance of other sequences, for example the 1st dominant sequence. This sequence is characterized by a LB-LOCA and the failure of the IRWST injection water into the vessel. The configuration of the AP1000 primary circuit allows the reflowing of the core directly from the vessel. The work done allows to outline the following points:

- the AP1000 nodalization is an original tool able to study some phenomena that other codes cannot. Especially, the behaviour of the containment and in vessel core melt retention are successfully taken into account, even though with the level of detail of a lumped parameter code, as MELCOR.
- the performed analysis evidences various important areas that could be very interesting to study:
  - ❖ the hydrogen production and its behaviour in a passive containment,
  - ❖ the thermal stresses and resistance of the lower support plate during the phase of mitigation of the internal temperatures due to the heat transfer to the external cavity,
  - ❖ the thermal stresses and evaporation phenomena connected with the re-inlet of water from the rupture,
  - ❖ the thermal stresses of the vessel during the core melt retention,
  - ❖ the behaviour of FP aerosols in a passive containment.

With respect to the MELCOR code and its use with the nodalization set-up, it has to be noticed that:

- The calculation results sometimes very difficult with problems of computational instability. In case of very fast changes of some parameters (like melt temperature during the reflooding):

- The AP1000 nodalization could be improved with a larger number of nodes than the actual for the simulation of heat transfer inside and from the containment. Moreover the nodalization model could be improved with RN package for better investigating the release and the transport of FP inside the containment coupled with gases release.

The newest versions as MELCOR 1.8.6, MELCOR 2.1 should allow a better simulation of relocation, reflooding and oxidation phenomena of core materials in the lower head. In particular, the reflooding of a damaged and melted core is one of the most important challenges of the models for the future.

APEENDIX 1: PROBABILISTIC SAFETY ASSESSMENT

Objective of PSA Method

Probabilistic Safety Assessment (PSA) has been used essentially to assess in a consistent and integrated model the safety level and balance of safety provisions of operating Nuclear Power Plants (NPPs). This is essential to gain insights about the robustness of the design and its tolerance of severe accidents, and in providing risk-informed input to pre- and post-certification activities.

As part of the AP1000 advanced design certification application, the applicant submitted a PSA in accordance with the requirements of 10 CFR 52.47[1] and the Commission's policy statement entitled "Severe Reactor Accidents Regarding Future Designs and Existing Plants". An analogous description is in the EUR's requirement document of PSA (Probabilistic Safety Assessment) analyses. The assessment of the AP1000 PSA consisted of the traditional evaluation of events that could lead to core damage and offsite consequences, as well as of an evaluation of what the PSA revealed about the AP1000 design.

As a support to design, PSA should cover all initiating events for both power and shutdown modes. When verifying the design against probabilistic safety goals, internal and external hazards should be included.

Given the aim of the verification that the plant design complies with the probabilistic safety goals, the scope of PSA covers the assessment of the CDF, the evaluation of containment response and the estimation of frequency for exceeding the Criteria for Limiting Impact [6]. Therefore, the PSA shall include a Level-2 type of analysis. This may be simplified during the basic design phase to give a preliminary assessment of Plant Damage State Frequency. The reference [9] provides guidance on this simplified approach. The intent is to use the accident sequence information provided in the Level-1 PSA to estimate the frequency of large early release being associated with early containment failure or bypass. However a complete level 2 PSA needs to be developed during the detailed design phase to provide a basis for the demonstration of coherence with safety Criteria for Limiting Impact (frequency and magnitude).

Specific guidance on PSA for low power and shutdown modes can be found in [8].

Definition of Core Damage Frequency

The Core Damage Frequency (CDF) requests a precise definition of Core Damage.

The following criteria were used by the designer in order to discriminate between sequences that lead to success and sequences that would lead to Core Damage:

- If the active part of reactor core remains covered during the whole accident phase, it may be assured that no core damage occurs.
- If the fuel cladding peak temperature does not exceed 1204°C, it may be assumed that there aren't fuel damages.
- If peak enthalpy deposited in the fuel pellets does not exceed 837 KJ/Kg, it may be assumed that there aren't core damages.

Although more realistic criteria could have been selected to characterize the Core Damage, these were chosen to remain compatible with IAEA definition of safety targets.

It is stated that Core Damage is prevented if the core remain covered. In practice, severe Core Damage is not expected to occur until water level decreases significantly lower than top of active core level for a sustained period of time.

For cladding temperatures higher that 1500°C, the Zircaloy oxidation rate increases rapidly, leading to a drastic acceleration of core degradation. With a rather large margin, a critical temperature of 1204°C (2200°F) allows excessive clad oxidation to be avoided according to the actual Emergency Core Cooling System (ECCS) design criteria.

For reactivity accidents, the two previous criteria are not adequate in order to identify whether or not a sequence leads to Core Damage. Therefore, the third criteria shall be used in addition to either of the two former ones.

Methodology

All reactor operational modes are studied in the PSA, from full power operation to refuelling shutdown with at least one fuel element in the reactor vessel. The durations of the various reactor operational modes are evaluated by considering outages. Typically in the case of equivalent data from different sources, the most conservative data are used.

The Methodology implies to evaluate the initial event sequences with tools as Event Trees or Failure Trees, taking into accountthe various protective systems and engineering safeguards, as well as Common Cause Failures (CCF) and Human Factor. The following pointsintroduce briefly some of these tools according with PSA Methodology from and with the US-NRC and EUR requirements.

As said before, for the AP1000 PSA the similarity between AP1000 and AP600 designs has been taken into count in order to reduce the review effort. This similarity (e.g., in system design and overall plant layout) allowed the use of the AP600 PSA as the starting point in the development of the AP1000 PSA. A team of experts reviewed the quality of the AP1000 PSA by evaluating the applicant's use of models, techniques, methodologies, assumptions, data, and calculation tools. In addition, the staff checked the AP1000 PSA for completeness by engaging in the following activities:

- comparing the AP1000 PSA with PSAs performed for current generation and advanced pressurized-water reactor (PWR) designs to ensure that known safety-significant PWR issues either do not apply to the AP1000 design or are appropriately modeled in the PSA
- ensuring that the final resolution of various deterministic issues, raised by the staff during the certification process, are appropriately incorporated into the PSA models.

As with the certification of previous advanced reactor designs (e.g., the AP600 design), the review of the quality and completeness of the AP1000 PSA included the issuance of requests for additional information (RAIs) to the applicant, followed by the evaluation of the applicant's responses to the RAIs.

The team of experts placed a special emphasis on PSA modeling of novel and passive features in the design, as well as addressing issues related to these features, such as thermal-hydraulic (T-H) uncertainties. The issue of T-H uncertainties arises from the "passive" nature of the safety-related systems used for accident mitigation. Passive safety systems rely on natural forces, such as gravity,

to perform their functions. Such driving forces are small compared to those of pumped systems, and the uncertainty in their values, as predicted by a "best-estimate" T-H analysis, can be of comparable magnitude to the predicted values themselves. Therefore, some accident sequences with a frequency high enough to impact results, but which are not predicted to lead to core damage by a "best-estimate" T-H analysis, may actually lead to core damage when T-H uncertainties are considered in the PSA models.

The initiating events considered are limited to internal events, except for external hazards which can affect the safety of the reactor (i.e. loss of the ultimate heat sink (water intake)). The initiating events studied in the AP1000 probabilistic evaluation are grouped as follows:

- Loss of primary cooling accident [LOCA],
- Containment bypass,
- Secondary system break (SSB):
- Breaks on secondary side (steam or feed water) (SLB, FLB),
- Steam line break and Steam generator tubes rupture (SGTR),
- Secondary system transients
- Loss of off-site power (LOOP):
    - total loss of off-site power (2h),
    - total loss of off-site power (24h),
    - total loss of long-term off-site power,
- Primary system transients:
    - homogeneous boron dilutions,
    - total loss of SIS/RHR in shutdown states,
    - uncontrolled drop of primary coolant level,

  - loss of pumping.

- Loss of cooling water systems:
  - partial or total loss of cooling chain,
  - loss of ultimate heat sink.
- Transient without automatic reactor shutdown (ATWS),
- Heterogeneous boron dilution.

The design PSA, developed as part of the design certification process, should be revised to account for site-specific information, as-built (plant-specific) information refinements in the level of design detail, plant-specific emergency operating procedures, and design changes.

Methods for IE Frequency Quantification

The quantification method depends essentially on the initiating event group. For initiating events already observed the mean frequency is evaluated as:

- F = n/T : where n is the number of occurrences of the event in the sample studied and T is the observation period of the sample (in reactor-years);

For initiating events not observed in the international framework, the frequency may be evaluated in two ways:

- **The 2χ method at 50% at two degrees of freedom:** The estimator of the frequency is calculated as the upper bound of the unilateral confidence interval at the 50% confidence level. In fact, the estimator value is such that the actual frequency at the same probability could be lower or higher than 0.5.
- By ‘expert judgement’ based on design studies or other special studies.

Generally, the systematic use of the 2χ method at 50% is to be avoided because it leads to a homogenisation of the frequencies of all hypothetical initiating events around two values. This homogenisation conflicts with the PSA objective, which is to give priority to sequences leading to core damage. As far as possible, expert judgement is preferred for initiating events not observed in nuclear applications.

For the initiating events due to equipment failure: the frequency is calculated from reliability data on the equipment considered.

The reliability data is generally available either in the form of an hourly rate of operational failure (λ, occurrences/hour) or in the form of a probability of failure on demand (γ).

The frequency of the initiating event is thus:

$$f = \lambda \cdot Tm$$

or

$$f = n \cdot \gamma$$

where:

Tm: duration of equipment mission considered in hours/year,

n: number of demands on equipment, per year

For constructing the accident scenarios, the missions of the required protection systems, identified by functional analysis, are firstly modelled. The modelling of the system mission uses a Boolean method based on fault trees.

A fault tree is developed for each system mission. This allows a qualitative identification of the minimum cut sets leading to failure of the system mission, the calculation of the probability of failure and the contributions to the corresponding minimum cut sets:

- A cut set represents a combination of equipment failures or human errors leading to an event (such as a top event), or to a sequence or consequence,

- The expression “minimum cut sets” refers to any cut set corresponding to the smallest possible combination of independent equipment failures or human errors leading to the occurrence of an event, sequence or consequence.

As a Boolean method is used, the reliability of systems may be uniquely quantified for a single mission time with no possibility of repair, independently from the actual duration of the various missions required.

Event Trees

An event tree is a decision tree made up of an initiating event and successive events (headings) for success or failure of safety functions, characterising the accident sequences.

An accident sequence in an event tree represents an accident scenario. The structure of an event tree comprises all possible accident sequences, i.e. all accident scenarios following a given initiating event. Detailed functional analysis, previously carried out to identify the system missions, is used in the construction of the event trees. For each initiating event, accident sequences are drawn up, indicating success or failure of the required missions to restore safety functions, in the form of a tree structure. A consequence is then linked to each accident sequence. In summary, the following elements are necessary to build an event tree:

- initiating event data,
- identification of the required safeguard missions (functional analysis) and their modelling,
- the construction of a tree structure constituting a graphic representation of the accident sequences**.**

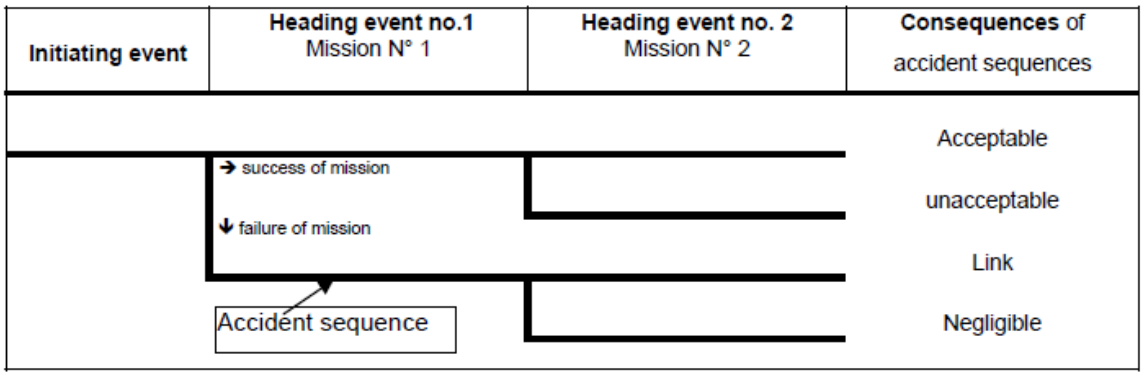

Figure 0.1 Example of an event tree

Consequences

A consequence represents the endpoint of an event sequence within a given time interval (sequence monitoring time). The consequences could be grouped in four types:

1. "acceptable consequences" indicate that all the system missions and human actions carried out in response to the occurrence of an initiating event have ensured that the core damage criteria were not exceeded,
2. "unacceptable consequences" characterise event sequences leading to core damage,
3. "negligible consequences" indicate that the frequency of occurrence of the consequences due to the considered accident sequences is less than 10^{-12}/ry. This type of consequence is introduced in the PSA for exemplification purposes.
4. "link" is referred to the case when the consequences of an accident sequence are reintroduced into another event tree in the form of an initiating event.

Common Cause Failure

Common Cause Failures (CCF) are those failures on demand or during operation or during the mission period that could simultaneously affect several components, when the failures are due to the same cause. Common cause failures include failures of the equipment itself due to errors of design, manufacture, installation or utilisation. CCF concerns groups of identical redundant equipment, operating in comparable conditions. An identical model is used for various types of component: pumps, valves, diesels, high and medium voltage circuit breakers, sensors, etc.

No account is taken of CCF on a group of identical pieces of equipment in the following cases:

- When certain pieces of equipment do not change state during the sequence (e.g.: switchboards). In this case, failures may be detected as disturbances to normal operation. These failures may thus increase the failure rate and an analysis is carried out regarding repair and prevention of effects on the other redundant equipment;
- When several identical components, such as contactors and emergency switchgear, operate under similar conditions. In this case most of the failures will be detected by observation, allowing corrective measures to be carried out.

Human Reliability Analysis

In normal operation, human errors may contribute to an accident. In accident situations, both safeguard systems and human actions are necessary to bring the facility back into a state of 'control'. In normal or accident situations, the study of pre-accident and post-accident human errors is performed by the Human Reliability Analysis (HRA). Incorporation of human factors in the PSA consists of:

1. listing all the potential and significant human errors capable of causing an accident or causing the failure of a safeguard mission after the occurrence of an initiating event,
2. assigning a probability to these human errors;
3. in case of "pre-accident errors", reintroducing them as basic events in the fault trees that model the safeguard system missions (e.g. valve left in closed position),
4. in case of "post-accident errors", reintroducing them in point-value form as leading (top) events in the accident sequences (e.g. failure of implementation of feed and bleed).

The method for deriving Human Error Probabilities (HEPs) is based on the work of Swain and, essentially, on the simplified model for quantification of post-accident errors (the 'screening model') termed 'ASEP HRA Procedure' method [ASEP: Accident Sequence Evaluation Programme]. As human errors before or during an accident can be recovered in certain circumstances, the simplified model has been adapted to allow for error recovery factors.

Pre-accident errors

Pre-accident errors are those made during normal operation. As they affect safeguard systems, they may contribute to an accident or hinder its recovery.

These errors may occur in any case where an actuator is manually adjusted or operated. In safety systems, such manual adjustments are performed, in particular, during periodic testing and maintenance. For this reason, errors prior to an initiating event are often assimilated with errors made during testing or maintenance, although there is no complete equivalence (e.g. manually operated EFWS gate valve left in the closed position).

The probability of such an error is quantified by:

$$P = P_b \cdot P_{NR}$$

where

P_b: Basic probability of human error for the considered pre-accident tasks,

P_{NR}: Probability of non-recovery on the basis of favourable recovery factors (e. G., supervisor action).

Post-accident human errors

These errors fall within the scope of accident management. Post-accident errors include diagnosis errors (e.g. selection of incorrect accident procedure or non-compliance with the correct procedure) and operator errors due to incorrect or late implementation of safeguard actions specified in accident operating procedures.

The probability of such an error is calculated from:

$$P = P_d + (1 - P_d) \cdot P_a \cdot P_{NRa}$$

where:

P_d : Probability of incorrect diagnosis,

P_a : Probability of incorrect action following a correct diagnosis,

P_{NRa}: Probability of non-recovery from an incorrect a

APENDIX 2: AP1000 TECHNICAL DATA

General plant data

Power plant output, gross 1200 MWe

Power plant output, net 1115 MWe

Reactor thermal output [core power 3400 MWt] 3415 MWt

Power plant efficiency, net 33 %

Cooling water temperature 30.5 °C

Nuclear steam supply system

Number of coolant loops 2 hot legs/4 cold legs

Steam flow rate at nominal conditions 1886 kg/s

Feed-water flow rate at nominal conditions 1887 kg/s

Steam temperature/pressure 272.9/5.76 °C/MPa

Feed-water temperature 226.7 °C

Reactor coolant system

Primary coolant flow rate, per loop 9.94 m^3/s

Reactor operating pressure 15.5 MPa

Coolant inlet temperature, at RPV inlet 280.7 °C

Coolant outlet temperature, at RPV outlet 321.1 °C

Mean temperature rise across core 40.4 °C

Reactor core

Active core height 4.267 m

Equivalent core diameter 3.04 m

Heat transfer surface in the core 5268 m^2

Fuel inventory 84.5 t U

Average linear heat rate 18.7 kW/m

Average fuel power density 40.2 kW/kg U

Average core power density (volumetric) 109.7 kW/l

Thermal heat flux, Fq 2.60 kW/m^2

Enthalpy rise, FH 1.65

Fuel material Sintered UO2

Fuel assembly total length 4 795 mm

Rod array square, 17´17 (XL)

Number of fuel assemblies 157

Number of fuel rods/assembly 264

Number of control rod guide tubes 24

Number of structural spacer grids 10

Number of intermediate flow mixing grids 4

Enrichment (range) of first core 2.35-4.45Wt% U-235

Enrichment of reload fuel at equilibrium core 4.8 Wt% U-235

Operating cycle length (fuel cycle length) 18 months

Average discharge burnup of fuel (nominal) 60 000 MWd/t

Cladding tube material ZIRLO TM

Cladding tube wall thickness 0.57 mm

Outer diameter of fuel rods 9.5 mm

Overall weight of assembly 799.7 kg

Burnable absorber, strategy/material discrete burnable absorber, integral fuel burnable,

Absorber

Number of control rods 69 (53 black, 16 gray)

Absorber rods per control assembly 24

Absorber material Ag-In-Cd (black),

Ag-In-Cd/304SS (gray)

Drive mechanism Magnetic jack

Positioning rate [in steps/min or mm/s] 45 steps/min

Soluble neutron absorber Boric acid

Reactor pressure vessel

Cylindrical shell inner diameter 3 988 mm

Wall thickness of cylindrical shell 203 mm

Total height 12056 mm

Base material: cylindrical shell Carbon steel /

RPV head Carbon steel

Liner Stainless steel

Design pressure/temperature 17.1/ 343.3 MPa/°C

Steam generators

Type Delta 125, vertical, U-tube

Number of SG 2

Heat transfer surface 11477 m^2

Number of heat exchanger tubes 10025

Tube dimensions 17.5/15.4 mm

Maximum outer diameter 5575.3 mm

Total height 22460 mm

Transport weight 663.7 t

Shell and tube sheet material Carbon steel

Tube material Inconel 690-TT

Reactor coolant pump

Type canned motor

Number of pump 4

Design pressure/temperature 17.1/343.3 MPa/°C

Rated flow rate 4.97 m^3/s

Rated head 111.3 m

Pump speed (nominal) 1750 rpm

Pressurizer

Total volume 59.47 m^3

Steam volume: nominal full load 31.14 m^3

Design pressure/temperature 17.1/360 MPa/°C

Heating power of the heater rods 1600 kW

Inner diameter 2.28 m

Total height (surge nozzle safe end to 16.27 m spray nozzle safe end)

Pressurizer relief tank Not applicable

Primary containment

Type Dry, free standing, steel

Overall form (spherical/cyl.) Cylindrical

Dimensions (diameter/height) 39.6/65.63 m

Design pressure/temperature (DBEs) 406.7/148.9 kPa-g/°C

(severe accident situations) 889.4 /204.4kPa-g/°C

Design leakage rate 0.10 vol%/day

Secondary Concrete Containment: Shell around CV with penetration area

Material SA 738, Grade B

Safety injection

Passive residual heat removal

Number heat exchangers 1

Type Vertical C-tube

Heat transfer, design 2.01x108 Btu/hr

Design pressure/temperature 17.2/343.3 MPa/ °C

Core Makeup Tanks

Number 2

Volume 70.8 m^3

Design pressure/temperature 17.2/343.3 MPa/ °C

Accumulators

Number 2

Volume 56.6 m3

Design pressure/temperature 5.6/148.9 MPa/ °C

Incontainment Refueling Water Storage Tank (IRWST)

Number 1

Volume (minimum) 2092.6 m3

Design pressure/temperature 0.14/65.6 MPa/ °C

Reactor auxiliary systems

Reactor water cleanup, capacity 6.3 kg/s

(chemical volume & control) filter type Cartridge

Residual heat removal, shutdown cooling 89.3 kg/s

(normal RHR) low pressure makeup 68.9 kg/s

Power supply systems

Main transformer, rated voltage 24 kV/site specific

rated capacity 1250 MVA

Unit auxiliary transformers, rated voltage 24/6.9 kV

rated capacity 70 MVA

Start-up transformer, rated voltage Site specific/6.9 kV

rated capacity 70 MVA

Medium voltage bus-bars 6

Number of low voltage bus-bar systems 10

Standby diesel generating units: number 2

rated power 4 MW

Number of diesel-backed bus-bar systems 2

Voltage level of these 6900 V ac

Number of DC distributions 10

Voltage level of these 125 V dc

Number of battery-backed bus-bar systems 11

Voltage level of these 125 V ac

Turbine plant

Number of turbines per reactor 1

Type of turbine(s) Tandem-compound, 6-flow, 54 in.

(1372 mm) last-stage blade

Number of turbine sections per unit 1HP/ 3LP

Turbine speed 1800 rpm

1500 rpm (for 50 Hz)

HP inlet pressure/temperature 5.5/271 MPa/°C

Generator

Type 3-phase, synchronous

Rated power 1250 MVA

Active power 1200 MWe

Voltage 24 kV

Frequency 50 / 60 Hz

Condenser

Type Multi-pressure, single pass

Cooling water flow rate 37.85 m3 /s

Cooling water temperature 30.5 °C

Condenser pressure 9.1 kPa

Condensate clean-up system

Full flow/part flow part flow, 33%

Filter type Deep bed

Feed-water pumps

Main Feed-water Pumps

Number 3

Start-up Feed-water Pumps

Number 2

Design flow rate 0.033 m^3/s

Pump head 990.6 m

Feed-water temperature 267 °C

Pump Speed 3600 rpm

Condensate and feed-water heaters

Number of heating stages 6

APPENDIX 3: SEQUENCES CUTSETS DATA

In the following tables, extracted from UK Safety Report, the 10 most relevant sequences, bringing to severe accidents, are described. The tables show step by step, the sequences.

(Sheet 1 of 3)

SEQUENCE 1 – SAFETY INJECTION LINE BREAK DOMINANT CUTSETS (SI-LB-07)

NUMBER	CUTSET PROB.	PERCENTAGE	BASIC EVENT NAME		
1	5.09E-08	74.04	SAFETY INJECTION LINE BREAK INITIATING EVENT OCCURS	2.12E-04	IEV-SI-LB
			IRWST DISCHARGE LINE "A" STRAINER PLUGGED	2.40E-04	IWA-PLUG
2	6.36E-09	9.25	SAFETY INJECTION LINE BREAK INITIATING EVENT OCCURS	2.12E-04	IEV-SI-LB
			CCF OF 4 GRAVITY INJECTION CVs	3.00E-05	IWX-CV-AO
3	5.51E-09	8.01	SAFETY INJECTION LINE BREAK INITIATING EVENT OCCURS	2.12E-04	IEV-SI-LB
			CCF OF 4 GRAVITY INJECTION & 2 RECIRCULATION SQUIB VALVES	2.60E-05	IWX-EV-SA
4	1.23E-09	1.79	SAFETY INJECTION LINE BREAK INITIATING EVENT OCCURS	2.12E-04	IEV-SI-LB
			CCF OF 2 GRAVITY INJECTION SQUIB VALVES IN 1/1 LINES TO OPEN	5.80E-06	IWX-EV1-SA
5	6.49E-10	.94	SAFETY INJECTION LINE BREAK INITIATING EVENT OCCURS	2.12E-04	IEV-SI-LB
			CHECK VALVE 122A FAILS TO OPEN	1.75E-03	IWACV122AO
			CHECK VALVE 124A FAILS TO OPEN	1.75E-03	IWACV124AO
6	5.42E-10	.79	SAFETY INJECTION LINE BREAK INITIATING EVENT OCCURS	2.12E-04	IEV-SI-LB
			CHECK VALVE 122A FAILS TO OPEN	1.75E-03	IWACV122AO
			HARDWARE FAILURE OF VALVE 125A	1.46E-03	IRWMOD06
7	5.42E-10	.79	SAFETY INJECTION LINE BREAK INITIATING EVENT OCCURS	2.12E-04	IEV-SI-LB
			HARDWARE FAILURE OF VALVE 123A	1.46E-03	IRWMOD05
			CHECK VALVE 124A FAILS TO OPEN	1.75E-03	IWACV124AO
8	4.52E-10	.66	SAFETY INJECTION LINE BREAK INITIATING EVENT OCCURS	2.12E-04	IEV-SI-LB
			HARDWARE FAILURE OF VALVE 123A	1.46E-03	IRWMOD05
			HARDWARE FAILURE OF VALVE 125A	1.46E-03	IRWMOD06
9	3.25E-10	.47	SAFETY INJECTION LINE BREAK INITIATING EVENT OCCURS	2.12E-04	IEV-SI-LB
			CHECK VALVE 122A FAILS TO OPEN	1.75E-03	IWACV122AO
			RELAY FAILS TO OPERATE	8.76E-04	IWDRS125AFA
10	3.25E-10	.47	SAFETY INJECTION LINE BREAK INITIATING EVENT OCCURS	2.12E-04	IEV-SI-LB
			CHECK VALVE 124A FAILS TO OPEN	1.75E-03	IWACV124AO
			RELAY FAILS TO OPERATE	8.76E-04	IWBRS123AFA
11	2.71E-10	.39	SAFETY INJECTION LINE BREAK INITIATING EVENT OCCURS	2.12E-04	IEV-SI-LB
			HARDWARE FAILURE OF VALVE 123A	1.46E-03	IRWMOD05
			RELAY FAILS TO OPERATE	8.76E-04	IWDRS125AFA

(Sheet 2 of 3)

SEQUENCE 1 – SAFETY INJECTION LINE BREAK DOMINANT CUTSETS (SI-LB-07)

NUMBER	CUTSET PROB.	PERCENTAGE	BASIC EVENT NAME		
12	2.71E-10	.39	SAFETY INJECTION LINE BREAK INITIATING EVENT OCCURS	2.12E-04	IEV-SI-LB
			HARDWARE FAILURE OF VALVE 125A	1.46E-03	IRWMOD06
			RELAY FAILS TO OPERATE	8.76E-04	IWBRS123AFA
13	1.63E-10	.24	SAFETY INJECTION LINE BREAK INITIATING EVENT OCCURS	2.12E-04	IEV-SI-LB
			RELAY FAILS TO OPERATE	8.76E-04	IWBRS123AFA
			RELAY FAILS TO OPERATE	8.76E-04	IWDRS125AFA
14	1.14E-10	.17	SAFETY INJECTION LINE BREAK INITIATING EVENT OCCURS	2.12E-04	IEV-SI-LB
			CCF OF GRAVITY INJECTION CVs IN 1/1 LINES TO OPEN	5.40E-07	IWX-CV1-AO
15	1.11E-10	.16	SAFETY INJECTION LINE BREAK INITIATING EVENT OCCURS	2.12E-04	IEV-SI-LB
			CHECK VALVE 122A FAILS TO OPEN	1.75E-03	IWACV122AO
			BUS UNAVAILABLE DUE TO TEST OR CORRECTIVE MAINTENANCE	3.00E-04	IDDBSDS1TM
16	1.11E-10	.16	SAFETY INJECTION LINE BREAK INITIATING EVENT OCCURS	2.12E-04	IEV-SI-LB
			CHECK VALVE 122A FAILS TO OPEN	1.75E-03	IWACV122AO
			BUS UNAVAILABLE DUE TO TEST OR CORRECTIVE MAINTENANCE	3.00E-04	IDDBSDD1TM
17	1.11E-10	.16	SAFETY INJECTION LINE BREAK INITIATING EVENT OCCURS	2.12E-04	IEV-SI-LB
			CHECK VALVE 124A FAILS TO OPEN	1.75E-03	IWACV124AO
			BUS UNAVAILABLE DUE TO TEST OR CORRECTIVE MAINTENANCE	3.00E-04	IDBBSDS1TM
18	1.11E-10	.16	SAFETY INJECTION LINE BREAK INITIATING EVENT OCCURS	2.12E-04	IEV-SI-LB
			CHECK VALVE 124A FAILS TO OPEN	1.75E-03	IWACV124AO
			BUS UNAVAILABLE DUE TO TEST OR CORRECTIVE MAINTENANCE	3.00E-04	IDBBSDD1TM
19	9.29E-11	.14	SAFETY INJECTION LINE BREAK INITIATING EVENT OCCURS	2.12E-04	IEV-SI-LB
			HARDWARE FAILURE OF VALVE 123A	1.46E-03	IRWMOD05
			BUS UNAVAILABLE DUE TO TEST OR CORRECTIVE MAINTENANCE	3.00E-04	IDDBSDS1TM
20	9.29E-11	.14	SAFETY INJECTION LINE BREAK INITIATING EVENT OCCURS	2.12E-04	IEV-SI-LB
			HARDWARE FAILURE OF VALVE 123A	1.46E-03	IRWMOD05
			BUS UNAVAILABLE DUE TO TEST OR CORRECTIVE MAINTENANCE	3.00E-04	IDDBSDD1TM
21	9.29E-11	.14	SAFETY INJECTION LINE BREAK INITIATING EVENT OCCURS	2.12E-04	IEV-SI-LB
			HARDWARE FAILURE OF VALVE 125A	1.46E-03	IRWMOD06
			BUS UNAVAILABLE DUE TO TEST OR CORRECTIVE MAINTENANCE	3.00E-04	IDBBSDS1TM

(Sheet 3 of 3)

SEQUENCE 1 – SAFETY INJECTION LINE BREAK DOMINANT CUTSETS (SI-LB-07)

NUMBER	CUTSET PROB.	PERCENTAGE	BASIC EVENT NAME		
22	9.29E-11	.14	SAFETY INJECTION LINE BREAK INITIATING EVENT OCCURS	2.12E-04	IEV-SI-LB
			HARDWARE FAILURE OF VALVE 125A	1.46E-03	IRWMOD06
			BUS UNAVAILABLE DUE TO TEST OR CORRECTIVE MAINTENANCE	3.00E-04	IDBBSDD1TM
23	5.57E-11	.08	SAFETY INJECTION LINE BREAK INITIATING EVENT OCCURS	2.12E-04	IEV-SI-LB
			RELAY FAILS TO OPERATE	8.76E-04	IWDRS125AFA
			BUS UNAVAILABLE DUE TO TEST OR CORRECTIVE MAINTENANCE	3.00E-04	IDBBSDS1TM
24	5.57E-11	.08	SAFETY INJECTION LINE BREAK INITIATING EVENT OCCURS	2.12E-04	IEV-SI-LB
			RELAY FAILS TO OPERATE	8.76E-04	IWDRS125AFA
			BUS UNAVAILABLE DUE TO TEST OR CORRECTIVE MAINTENANCE	3.00E-04	IDBBSDD1TM
25	5.57E-11	.08	SAFETY INJECTION LINE BREAK INITIATING EVENT OCCURS	2.12E-04	IEV-SI-LB
			RELAY FAILS TO OPERATE	8.76E-04	IWBRS123AFA
			BUS UNAVAILABLE DUE TO TEST OR CORRECTIVE MAINTENANCE	3.00E-04	IDDBSDS1TM

SEQUENCE 2 – LARGE LOCA DOMINANT CUTSETS (LLOCA-09)

NUMBER	CUTSET PROB.	PERCENTAGE	BASIC EVENT NAME		
1	8.75E-09	20.55	LARGE LOCA INITIATING EVENT OCCURS	5.00E-06	IEV-LLOCA
			CHECK VALVE 029A FAILS TO OPEN	1.75E-03	ACACV029GO
2	8.75E-09	20.55	LARGE LOCA INITIATING EVENT OCCURS	5.00E-06	IEV-LLOCA
			CHECK VALVE 028A FAILS TO OPEN	1.75E-03	ACACV028GO
3	8.75E-09	20.55	LARGE LOCA INITIATING EVENT OCCURS	5.00E-06	IEV-LLOCA
			CHECK VALVE 029B FAILS TO OPEN	1.75E-03	ACBCV029GO
4	8.75E-09	20.55	LARGE LOCA INITIATING EVENT OCCURS	5.00E-06	IEV-LLOCA
			CHECK VALVE 028B FAILS TO OPEN	1.75E-03	ACBCV028GO
5	3.64E-09	8.55	LARGE LOCA INITIATING EVENT OCCURS	5.00E-06	IEV-LLOCA
			FLOW TUNING ORIFICE PLUGS	7.27E-04	ACAOR001SP
6	3.64E-09	8.55	LARGE LOCA INITIATING EVENT OCCURS	5.00E-06	IEV-LLOCA
			FLOW TUNING ORIFICE PLUGS	7.27E-04	ACBOR001SP
7	2.55E-10	.60	LARGE LOCA INITIATING EVENT OCCURS	5.00E-06	IEV-LLOCA
			COMMON CAUSE FAILURE OF 2 ACCUMULATOR CHECK VALVES	5.10E-05	ACX-CV-GO
8	1.20E-11	.03	LARGE LOCA INITIATING EVENT OCCURS	5.00E-06	IEV-LLOCA
			ACCUMULATOR TANK A (T001A) RUPTURES	2.40E-06	ACATK001AF
9	1.20E-11	.03	LARGE LOCA INITIATING EVENT OCCURS	5.00E-06	IEV-LLOCA
			ACCUMULATOR TANK B (T001B) RUPTURES	2.40E-06	ACBTK001AF
10	3.60E-12	.01	LARGE LOCA INITIATING EVENT OCCURS	5.00E-06	IEV-LLOCA
			FLOW TUNING ORIFICE RUPTURE	7.20E-07	ACAOR001EB
11	3.60E-12	.01	LARGE LOCA INITIATING EVENT OCCURS	5.00E-06	IEV-LLOCA
			FLOW TUNING ORIFICE RUPTURE	7.20E-07	ACBOR001EB
12	6.00E-13	.00	LARGE LOCA INITIATING EVENT OCCURS	5.00E-06	IEV-LLOCA
			COMMON CAUSE FAILURE OF ACCUMULATOR TANKS	1.20E-07	ACX-TK-AF

(Sheet 1 of 3)

SEQUENCE 3 – SPURIOUS ADS ACTUATION DOMINANT CUTSETS (SPADS-08)

NUMBER	CUTSET PROB.	PERCENTAGE	BASIC EVENT NAME		
1	5.56E-09	26.14	SPURIOUS ADS INITIATING EVENT OCCURS	5.40E-05	IEV-SPADS
			CCF OF ESF INPUT LOGIC (HARDWARE)	1.03E-04	CCX-INPUT-LOGIC
2	3.35E-09	15.75	SPURIOUS ADS INITIATING EVENT OCCURS	5.40E-05	IEV-SPADS
			COMMON CAUSE FAILURE OF 4 AOVS TO OPEN	6.20E-05	CCX-AV-LA
3	3.19E-09	15.00	SPURIOUS ADS INITIATING EVENT OCCURS	5.40E-05	IEV-SPADS
			CCF OF 2 SQUIB VALVES TO OPERATE	5.90E-05	ADX-EV-SA2
4	2.75E-09	12.93	SPURIOUS ADS INITIATING EVENT OCCURS	5.40E-05	IEV-SPADS
			COMMON CAUSE FAILURE OF 4 CHECK VALVES TO OPEN	5.10E-05	CMX-CV-GO
5	2.07E-09	9.73	SPURIOUS ADS INITIATING EVENT OCCURS	5.40E-05	IEV-SPADS
			CCF OF RTD LEVEL TRANSMITTERS	3.84E-05	CMX-VS-FA
6	1.62E-09	7.62	SPURIOUS ADS INITIATING EVENT OCCURS	5.40E-05	IEV-SPADS
			DUE TO CCF OF 4TH STAGE ADS SQUIB VALVES TO OPERATE	3.00E-05	ADX-EV-SA
7	5.94E-10	2.79	SPURIOUS ADS INITIATING EVENT OCCURS	5.40E-05	IEV-SPADS
			CCF OF ESF INPUT LOGIC SOFTWARE	1.10E-05	CCX-IN-LOGIC-SW
8	5.94E-10	2.79	SPURIOUS ADS INITIATING EVENT OCCURS	5.40E-05	IEV-SPADS
			CCF OF PMS ESF ACTUATION LOGIC SOFTWARE	1.10E-05	CCX-PMSMOD2-SW
9	5.94E-10	2.79	SPURIOUS ADS INITIATING EVENT OCCURS	5.40E-05	IEV-SPADS
			CCF OF PMS ESF OUTPUT LOGIC SOFTWARE	1.10E-05	CCX-PMSMOD1-SW
10	4.65E-10	2.19	SPURIOUS ADS INITIATING EVENT OCCURS	5.40E-05	IEV-SPADS
			CCF OF EPO BOARDS IN PMS	8.62E-06	CCX-EP-SAM
11	6.48E-11	.30	SPURIOUS ADS INITIATING EVENT OCCURS	5.40E-05	IEV-SPADS
			SOFTWARE CCF OF ALL CARDS	1.20E-06	CCX-SFTW
12	2.85E-11	.13	SPURIOUS ADS INITIATING EVENT OCCURS	5.40E-05	IEV-SPADS
			FLOW TUNING ORIFICE PLUGS	7.27E-04	CMA-PLUG
			FLOW TUNING ORIFICE PLUGS	7.27E-04	CMB-PLUG
13	1.82E-11	.09	SPURIOUS ADS INITIATING EVENT OCCURS	5.40E-05	IEV-SPADS
			HARDWARE FAILURE OF ST. #4 LINE 3	5.80E-04	AD4MOD09
			HARDWARE FAILURE OF ST. #4 LINE 4	5.80E-04	AD4MOD10

Table 19.59-6 (Sheet 2 of 3)

SEQUENCE 3 – SPURIOUS ADS ACTUATION DOMINANT CUTSETS (SPADS-08)

NUMBER	CUTSET PROB.	PERCENTAGE	BASIC EVENT NAME		
14	1.82E-11	.09	SPURIOUS ADS INITIATING EVENT OCCURS	5.40E-05	IEV-SPADS
			HARDWARE FAILURE OF ST. #4 LINE 2	5.80E-04	AD4MOD08
			HARDWARE FAILURE OF ST. #4 LINE 4	5.80E-04	AD4MOD10
15	1.82E-11	.09	SPURIOUS ADS INITIATING EVENT OCCURS	5.40E-05	IEV-SPADS
			HARDWARE FAILURE OF ST. #4 LINE 2	5.80E-04	AD4MOD08
			HARDWARE FAILURE OF ST. #4 LINE 3	5.80E-04	AD4MOD09
16	1.82E-11	.09	SPURIOUS ADS INITIATING EVENT OCCURS	5.40E-05	IEV-SPADS
			HARDWARE FAILURE OF ST. #4 LINE 1	5.80E-04	AD4MOD07
			HARDWARE FAILURE OF ST. #4 LINE 4	5.80E-04	AD4MOD10
17	1.82E-11	.09	SPURIOUS ADS INITIATING EVENT OCCURS	5.40E-05	IEV-SPADS
			HARDWARE FAILURE OF ST. #4 LINE 1	5.80E-04	AD4MOD07
			HARDWARE FAILURE OF ST. #4 LINE 3	5.80E-04	AD4MOD09
18	1.82E-11	.09	SPURIOUS ADS INITIATING EVENT OCCURS	5.40E-05	IEV-SPADS
			HARDWARE FAILURE OF ST. #4 LINE 1	5.80E-04	AD4MOD07
			HARDWARE FAILURE OF ST. #4 LINE 2	5.80E-04	AD4MOD08
19	6.85E-12	.03	SPURIOUS ADS INITIATING EVENT OCCURS	5.40E-05	IEV-SPADS
			COMMON CAUSE FAILURE OF THE BATTERIES IDSA-DB-1A/1B	4.70E-05	CCX-BY-PN
			UNAVAILABILITY OF BUS ECS ES 2 DUE TO UNSCHEDULED MAINTENANCE	2.70E-03	EC2BS002TM
20	6.85E-12	.03	SPURIOUS ADS INITIATING EVENT OCCURS	5.40E-05	IEV-SPADS
			COMMON CAUSE FAILURE OF THE BATTERIES IDSA-DB-1A/1B	4.70E-05	CCX-BY-PN
			BUS UNAVAILABLE DUE TO UNSCHEDULED MAINTENANCE	2.70E-03	EC2BS022TM
21	6.85E-12	.03	SPURIOUS ADS INITIATING EVENT OCCURS	5.40E-05	IEV-SPADS
			COMMON CAUSE FAILURE OF THE BATTERIES IDSA-DB-1A/1B	4.70E-05	CCX-BY-PN
			BUS UNAVAILABLE DUE TO UNSCHEDULED MAINTENANCE	2.70E-03	EC2BS221TM
22	6.85E-12	.03	SPURIOUS ADS INITIATING EVENT OCCURS	5.40E-05	IEV-SPADS
			COMMON CAUSE FAILURE OF THE BATTERIES IDSA-DB-1A/1B	4.70E-05	CCX-BY-PN
			UNAVAILABILITY OF BUS ECS ES 1 DUE TO UNSCHEDULED MAINTENANCE	2.70E-03	EC1BS001TM

(Sheet 3 of 3)

SEQUENCE 3 – SPURIOUS ADS ACTUATION DOMINANT CUTSETS (SPADS-08)

NUMBER	CUTSET PROB.	PERCENTAGE	BASIC EVENT NAME		
23	6.85E-12	.03	SPURIOUS ADS INITIATING EVENT OCCURS	5.40E-05	IEV-SPADS
			COMMON CAUSE FAILURE OF THE BATTERIES IDSA-DB-1A/1B	4.70E-05	CCX-BY-PN
			BUS UNAVAILABLE DUE TO UNSCHEDULED MAINTENANCE	2.70E-03	EC1BS012TM
24	6.85E-12	.03	SPURIOUS ADS INITIATING EVENT OCCURS	5.40E-05	IEV-SPADS
			COMMON CAUSE FAILURE OF THE BATTERIES IDSA-DB-1A/1B	4.70E-05	CCX-BY-PN
			BUS UNAVAILABLE DUE TO UNSCHEDULED MAINTENANCE	2.70E-03	EC1BS121TM
25	6.83E-12	.03	SPURIOUS ADS INITIATING EVENT OCCURS	5.40E-05	IEV-SPADS
			PMBMOD32	5.02E-03	PMBMOD32
			PMCMOD33	5.02E-03	PMCMOD33
			PMDMOD34	5.02E-03	PMDMOD34

(Sheet 1 of 3)

SEQUENCE 4 – SAFETY INJECTION LINE BREAK DOMINANT CUTSETS (SI-LB-08)

NUMBER	CUTSET PROB.	PERCENTAGE	BASIC EVENT NAME		
1	1.25E-08	63.00	SAFETY INJECTION LINE BREAK INITIATING EVENT OCCURS	2.12E-04	IEV-SI-LB
			CCF OF 2 SQUIB VALVES TO OPERATE	5.90E-05	ADX-EV-SA2
2	6.36E-09	32.06	SAFETY INJECTION LINE BREAK INITIATING EVENT OCCURS	2.12E-04	IEV-SI-LB
			DUE TO CCF OF 4TH STAGE ADS SQUIB VALVES TO OPERATE	3.00E-05	ADX-EV-SA
3	7.13E-11	.36	SAFETY INJECTION LINE BREAK INITIATING EVENT OCCURS	2.12E-04	IEV-SI-LB
			HARDWARE FAILURE OF ST. #4 LINE 3	5.80E-04	AD4MOD09
			HARDWARE FAILURE OF ST. #4 LINE 4	5.80E-04	AD4MOD10
4	7.13E-11	.36	SAFETY INJECTION LINE BREAK INITIATING EVENT OCCURS	2.12E-04	IEV-SI-LB
			HARDWARE FAILURE OF ST. #4 LINE 2	5.80E-04	AD4MOD08
			HARDWARE FAILURE OF ST. #4 LINE 4	5.80E-04	AD4MOD10
5	7.13E-11	.36	SAFETY INJECTION LINE BREAK INITIATING EVENT OCCURS	2.12E-04	IEV-SI-LB
			HARDWARE FAILURE OF ST. #4 LINE 2	5.80E-04	AD4MOD08
			HARDWARE FAILURE OF ST. #4 LINE 3	5.80E-04	AD4MOD09
6	7.13E-11	.36	SAFETY INJECTION LINE BREAK INITIATING EVENT OCCURS	2.12E-04	IEV-SI-LB
			HARDWARE FAILURE OF ST. #4 LINE 1	5.80E-04	AD4MOD07
			HARDWARE FAILURE OF ST. #4 LINE 4	5.80E-04	AD4MOD10
7	7.13E-11	.36	SAFETY INJECTION LINE BREAK INITIATING EVENT OCCURS	2.12E-04	IEV-SI-LB
			HARDWARE FAILURE OF ST. #4 LINE 1	5.80E-04	AD4MOD07
			HARDWARE FAILURE OF ST. #4 LINE 3	5.80E-04	AD4MOD09
8	7.13E-11	.36	SAFETY INJECTION LINE BREAK INITIATING EVENT OCCURS	2.12E-04	IEV-SI-LB
			HARDWARE FAILURE OF ST. #4 LINE 1	5.80E-04	AD4MOD07
			HARDWARE FAILURE OF ST. #4 LINE 2	5.80E-04	AD4MOD08
9	3.65E-11	.18	SAFETY INJECTION LINE BREAK INITIATING EVENT OCCURS	2.12E-04	IEV-SI-LB
			COND. PROB. OF REC-MANDAS (FAILURE OF MANUAL DAS AC	5.06E-01	REC-MANDASC
			OPER. FAILS TO RECOG. THE NEED FOR RCS DEPRESS. DURING MLOCA	3.30E-03	LPM-MAN02
			CCF OF ESF INPUT LOGIC (HARDWARE)	1.03E-04	CCX-INPUT-LOGIC
10	3.34E-11	.17	SAFETY INJECTION LINE BREAK INITIATING EVENT OCCURS	2.12E-04	IEV-SI-LB
			COND. PROB. OF REC-MANDAS (FAILURE OF MANUAL DAS AC	5.06E-01	REC-MANDASC
			OPER. FAILS TO FULFIL MANUAL ACTUATION OF ADS	3.02E-03	ADN-MAN01
			CCF OF ESF INPUT LOGIC (HARDWARE)	1.03E-04	CCX-INPUT-LOGIC

(Sheet 2 of 3)

SEQUENCE 4 – SAFETY INJECTION LINE BREAK DOMINANT CUTSETS (SI-LB-08)

NUMBER	CUTSET PROB.	PERCENTAGE	BASIC EVENT NAME		
11	2.71E-11	.14	SAFETY INJECTION LINE BREAK INITIATING EVENT OCCURS	2.12E-04	IEV-SI-LB
			FAILURE OF MANUAL DAS ACT.	1.16E-02	REC-MANDAS
			CCF OF PMS ESF OUTPUT LOGIC SOFTWARE	1.10E-05	CCX-PMXMOD1-SW
12	2.69E-11	.14	SAFETY INJECTION LINE BREAK INITIATING EVENT OCCURS	2.12E-04	IEV-SI-LB
			COMMON CAUSE FAILURE OF THE BATTERIES IDSA-DB-1A/1B	4.70E-05	CCX-BY-PN
			UNAVAILABILITY OF BUS ECS ES 2 DUE TO UNSCHEDUL MAINTENANCE	2.70E-03	EC2BS002TM
13	2.69E-11	.14	SAFETY INJECTION LINE BREAK INITIATING EVENT OCCURS	2.12E-04	IEV-SI-LB
			COMMON CAUSE FAILURE OF THE BATTERIES IDSA-DB-1A/1B	4.70E-05	CCX-BY-PN
			BUS UNAVAILABLE DUE TO UNSCHEDULED MAINTENANCE	2.70E-03	EC2BS022TM
14	2.69E-11	.14	SAFETY INJECTION LINE BREAK INITIATING EVENT OCCURS	2.12E-04	IEV-SI-LB
			COMMON CAUSE FAILURE OF THE BATTERIES IDSA-DB-1A/1B	4.70E-05	CCX-BY-PN
			BUS UNAVAILABLE DUE TO UNSCHEDULED MAINTENANCE	2.70E-03	EC2BS221TM
15	2.69E-11	.14	SAFETY INJECTION LINE BREAK INITIATING EVENT OCCURS	2.12E-04	IEV-SI-LB
			COMMON CAUSE FAILURE OF THE BATTERIES IDSA-DB-1A/1B	4.70E-05	CCX-BY-PN
			UNAVAILABILITY OF BUS ECS ES 1 DUE TO UNSCHEDULED MAINTENANCE	2.70E-03	EC1BS001TM
16	2.69E-11	.14	SAFETY INJECTION LINE BREAK INITIATING EVENT OCCURS	2.12E-04	IEV-SI-LB
			COMMON CAUSE FAILURE OF THE BATTERIES IDSA-DB-1A/1B	4.70E-05	CCX-BY-PN
			BUS UNAVAILABLE DUE TO UNSCHEDULED MAINTENANCE	2.70E-03	EC1BS012TM
17	2.69E-11	.14	SAFETY INJECTION LINE BREAK INITIATING EVENT OCCURS	2.12E-04	IEV-SI-LB
			COMMON CAUSE FAILURE OF THE BATTERIES IDSA-DB-1A/1B	4.70E-05	CCX-BY-PN
			BUS UNAVAILABLE DUE TO UNSCHEDULED MAINTENANCE	2.70E-03	EC1BS121TM
18	2.33E-11	.12	SAFETY INJECTION LINE BREAK INITIATING EVENT OCCURS	2.12E-04	IEV-SI-LB
			FAILURE OF MANUAL DAS REACTOR TRIP HARDWARE	1.00E-02	MDAS
			CCF OF PMS ESF OUTPUT LOGIC SOFTWARE	1.10E-05	CCX-PMXMOD1-SW
19	2.12E-11	.11	SAFETY INJECTION LINE BREAK INITIATING EVENT OCCURS	2.12E-04	IEV-SI-LB
			FAILURE OF MANUAL DAS ACT.	1.16E-02	REC-MANDAS
			CCF OF EPO BOARDS IN PMS	8.62E-06	CCX-EP-SAM

(Sheet 3 of 3)

SEQUENCE 4 – SAFETY INJECTION LINE BREAK DOMINANT CUTSETS (SI-LB-08)

NUMBER	CUTSET PROB.	PERCENTAGE	BASIC EVENT NAME		
20	1.91E-11	.10	SAFETY INJECTION LINE BREAK INITIATING EVENT OCCURS	2.12E-04	IEV-SI-LB
			BUS UNAVAILABLE DUE TO TEST OR CORRECTIVE MAINTENANCE	3.00E-04	IDDBSDS1TM
			BUS UNAVAILABLE DUE TO TEST OR CORRECTIVE MAINTENANCE	3.00E-04	IDBBSDS1TM
21	1.91E-11	.10	SAFETY INJECTION LINE BREAK INITIATING EVENT OCCURS	2.12E-04	IEV-SI-LB
			BUS UNAVAILABLE DUE TO TEST OR CORRECTIVE MAINTENANCE	3.00E-04	IDDBSDS1TM
			BUS UNAVAILABLE DUE TO TEST OR CORRECTIVE MAINTENANCE	3.00E-04	IDBBSDD1TM
22	1.91E-11	.10	SAFETY INJECTION LINE BREAK INITIATING EVENT OCCURS	2.12E-04	IEV-SI-LB
			BUS UNAVAILABLE DUE TO TEST OR CORRECTIVE MAINTENANCE	3.00E-04	IDDBSDD1TM
			BUS UNAVAILABLE DUE TO TEST OR CORRECTIVE MAINTENANCE	3.00E-04	IDBBSDS1TM
23	1.91E-11	.10	SAFETY INJECTION LINE BREAK INITIATING EVENT OCCURS	2.12E-04	IEV-SI-LB
			BUS UNAVAILABLE DUE TO TEST OR CORRECTIVE MAINTENANCE	3.00E-04	IDDBSDD1TM
			BUS UNAVAILABLE DUE TO TEST OR CORRECTIVE MAINTENANCE	3.00E-04	IDBBSDD1TM
24	1.91E-11	.10	SAFETY INJECTION LINE BREAK INITIATING EVENT OCCURS	2.12E-04	IEV-SI-LB
			BUS UNAVAILABLE DUE TO TEST OR CORRECTIVE MAINTENANCE	3.00E-04	IDCBSDS1TM
			BUS UNAVAILABLE DUE TO TEST OR CORRECTIVE MAINTENANCE	3.00E-04	IDABSDS1TM
25	1.91E-11	.10	SAFETY INJECTION LINE BREAK INITIATING EVENT OCCURS	2.12E-04	IEV-SI-LB
			BUS UNAVAILABLE DUE TO TEST OR CORRECTIVE MAINTENANCE	3.00E-04	IDCBSDS1TM
			BUS UNAVAILABLE DUE TO TEST OR CORRECTIVE MAINTENANCE	3.00E-04	IDABSDD1TM

SEQUENCE 5 – REACTOR VESSEL RUPTURE CUTSET (RV-RP-02)

NUMBER	CUTSET PROB.	PERCENTAGE	BASIC EVENT NAME		
1	1.00E-08	100.00	REACTOR VESSEL RUPTURE INITIATING EVENT OCCURS	1.00E-08	IEV-RV-RP

(Sheet 1 of 3)

SEQUENCE 6 – SMALL LOCA DOMINANT CUTSETS (SLOCA-05)

NUMBER	CUTSET PROB.	PERCENTAGE	BASIC EVENT NAME		
1	6.00E-09	71.10	SMALL LOCA INITIATING EVENT OCCURS	5.00E-04	IEV-SLOCA
			PLUGGING OF BOTH RECIRC LINES DUE TO CCF OF SUMP SCREENS	1.20E-05	REX-FL-GP
2	2.39E-09	28.32	SMALL LOCA INITIATING EVENT OCCURS	5.00E-04	IEV-SLOCA
			CCF OF TANK LEVEL TRANSMITTERS	4.78E-04	IWX-XMTR
			OPER. FAILS TO ACT. SUMP RECIRC GIVEN IRW LEVEL SIGNAL FAILUR	1.00E-02	REN-MAN04
3	2.88E-11	.34	SMALL LOCA INITIATING EVENT OCCURS	5.00E-04	IEV-SLOCA
			SUMP SCREEN A PLUGS AND PREVENTS FLOW	2.40E-04	REA-PLUG
			SUMP SCREEN B PLUGS AND PREVENTS FLOW	2.40E-04	REB-PLUG
4	9.18E-12	.11	SMALL LOCA INITIATING EVENT OCCURS	5.00E-04	IEV-SLOCA
			CCF OF TANK LEVEL TRANSMITTERS	4.78E-04	IWX-XMTR
			CCF OF CMT LEVEL SWITCHES	3.84E-05	CCX-VS-FA
5	2.63E-12	.03	SMALL LOCA INITIATING EVENT OCCURS	5.00E-04	IEV-SLOCA
			CCF OF PMS ESF OUTPUT LOGIC SOFTWARE	1.10E-05	CCX-PMXMOD1-SW
			CCF OF TANK LEVEL TRANSMITTERS	4.78E-04	IWX-XMTR
6	2.63E-12	.03	SMALL LOCA INITIATING EVENT OCCURS	5.00E-04	IEV-SLOCA
			CCX-PMXMOD4-SW	1.10E-05	CCX-PMXMOD4-SW
			CCF OF TANK LEVEL TRANSMITTERS	4.78E-04	IWX-XMTR
7	2.06E-12	.02	SMALL LOCA INITIATING EVENT OCCURS	5.00E-04	IEV-SLOCA
			CCF OF EPO BOARDS IN PMS	8.62E-06	CCX-EP-SAM
			CCF OF TANK LEVEL TRANSMITTERS	4.78E-04	IWX-XMTR
8	3.07E-13	.00	SMALL LOCA INITIATING EVENT OCCURS	5.00E-04	IEV-SLOCA
			HARDWARE FAILURE CAUSE RECIRC. CV 119A FAILS TO OPEN	1.75E-03	REACV119GO
			SUMP SCREEN B PLUGS AND PREVENTS FLOW	2.40E-04	REB-PLUG
			HARDWARE FAILURE OF SQUIB VALVE 118A	1.46E-03	IRWMOD09
9	3.07E-13	.00	SMALL LOCA INITIATING EVENT OCCURS	5.00E-04	IEV-SLOCA
			HARDWARE FAILURE CAUSE RECIRC. CV 119B FAILS TO OPEN	1.75E-03	REBCV119GO
			SUMP SCREEN A PLUGS AND PREVENTS FLOW	2.40E-04	REA-PLUG
			HARDWARE FAILURE OF SQUIB VALVE 118B	1.46E-03	IRWMOD11
10	2.87E-13	.00	SMALL LOCA INITIATING EVENT OCCURS	5.00E-04	IEV-SLOCA
			SOFTWARE CCF OF ALL CARDS	1.20E-06	CCX-SFTW
			CCF OF TANK LEVEL TRANSMITTERS	4.78E-04	IWX-XMTR

(Sheet 2 of 3)

SEQUENCE 6 – SMALL LOCA DOMINANT CUTSETS (SLOCA-05)

NUMBER	CUTSET PROB.	PERCENTAGE	BASIC EVENT NAME		
11	2.56E-13	.00	SMALL LOCA INITIATING EVENT OCCURS	5.00E-04	IEV-SLOCA
			HARDWARE FAILURE OF SQUIB VALVE 120A	1.46E-03	IRWMOD10
			SUMP SCREEN B PLUGS AND PREVENTS FLOW	2.40E-04	REB-PLUG
			HARDWARE FAILURE OF SQUIB VALVE 118A	1.46E-03	IRWMOD09
12	2.56E-13	.00	SMALL LOCA INITIATING EVENT OCCURS	5.00E-04	IEV-SLOCA
			HARDWARE FAILURE OF SQUIB VALVE 120B	1.46E-03	IRWMOD12
			SUMP SCREEN A PLUGS AND PREVENTS FLOW	2.40E-04	REA-PLUG
			HARDWARE FAILURE OF SQUIB VALVE 118B	1.46E-03	IRWMOD11
13	2.39E-13	.00	SMALL LOCA INITIATING EVENT OCCURS	5.00E-04	IEV-SLOCA
			INDICATION FAILURE	1.00E-06	ALL-IND-FAIL
			CCF OF TANK LEVEL TRANSMITTERS	4.78E-04	IWX-XMTR
14	1.84E-13	.00	SMALL LOCA INITIATING EVENT OCCURS	5.00E-04	IEV-SLOCA
			HARDWARE FAILURE CAUSE RECIRC. CV 119A FAILS TO OPEN	1.75E-03	REACV119GO
			SUMP SCREEN B PLUGS AND PREVENTS FLOW	2.40E-04	REB-PLUG
			RELAY FAILS TO OPERATE	8.76E-04	IWBRS118AFA
15	1.84E-13	.00	SMALL LOCA INITIATING EVENT OCCURS	5.00E-04	IEV-SLOCA
			HARDWARE FAILURE CAUSE RECIRC. CV 119B FAILS TO OPEN	1.75E-03	REBCV119GO
			SUMP SCREEN A PLUGS AND PREVENTS FLOW	2.40E-04	REA-PLUG
			RELAY FAILS TO OPERATE	8.76E-04	IWARS118BFA
16	1.68E-13	.00	SMALL LOCA INITIATING EVENT OCCURS	5.00E-04	IEV-SLOCA
			CCF OF 2 OUT 2 LOW PRESSURE RECIRCULATION SQUIB VALVES	5.80E-05	IWX-EV4-SA
			CCF OF MOV 120A AND 120B	5.80E-06	IWX-EV2-SA
17	1.53E-13	.00	SMALL LOCA INITIATING EVENT OCCURS	5.00E-04	IEV-SLOCA
			HARDWARE FAILURE OF SQUIB VALVE 120A	1.46E-03	IRWMOD10
			SUMP SCREEN B PLUGS AND PREVENTS FLOW	2.40E-04	REB-PLUG
			RELAY FAILS TO OPERATE	8.76E-04	IWBRS118AFA
18	1.53E-13	.00	SMALL LOCA INITIATING EVENT OCCURS	5.00E-04	IEV-SLOCA
			HARDWARE FAILURE OF SQUIB VALVE 118A	1.46E-03	IRWMOD09
			SUMP SCREEN B PLUGS AND PREVENTS FLOW	2.40E-04	REB-PLUG
			RELAY FAILS TO OPERATE	8.76E-04	IWDRS120AFA

(Sheet 3 of 3)

SEQUENCE 6 – SMALL LOCA DOMINANT CUTSETS (SLOCA-05)

NUMBER	CUTSET PROB.	PERCENTAGE	BASIC EVENT NAME		
19	1.53E-13	.00	SMALL LOCA INITIATING EVENT OCCURS	5.00E-04	IEV-SLOCA
			HARDWARE FAILURE OF SQUIB VALVE 120B	1.46E-03	IRWMOD12
			SUMP SCREEN A PLUGS AND PREVENTS FLOW	2.40E-04	REA-PLUG
			RELAY FAILS TO OPERATE	8.76E-04	IWARS118BFA
20	1.53E-13	.00	SMALL LOCA INITIATING EVENT OCCURS	5.00E-04	IEV-SLOCA
			HARDWARE FAILURE OF SQUIB VALVE 118B	1.46E-03	IRWMOD11
			SUMP SCREEN A PLUGS AND PREVENTS FLOW	2.40E-04	REA-PLUG
			RELAY FAILS TO OPERATE	8.76E-04	IWCRS120BFA
21	9.21E-14	.00	SMALL LOCA INITIATING EVENT OCCURS	5.00E-04	IEV-SLOCA
			RELAY FAILS TO OPERATE	8.76E-04	IWDRS120AFA
			SUMP SCREEN B PLUGS AND PREVENTS FLOW	2.40E-04	REB-PLUG
			RELAY FAILS TO OPERATE	8.76E-04	IWBRS118AFA
22	9.21E-14	.00	SMALL LOCA INITIATING EVENT OCCURS	5.00E-04	IEV-SLOCA
			RELAY FAILS TO OPERATE	8.76E-04	IWCRS120BFA
			SUMP SCREEN A PLUGS AND PREVENTS FLOW	2.40E-04	REA-PLUG
			RELAY FAILS TO OPERATE	8.76E-04	IWARS118BFA
23	8.88E-14	.00	SMALL LOCA INITIATING EVENT OCCURS	5.00E-04	IEV-SLOCA
			HARDWARE FAILURE CAUSE RECIRC. CV 119B FAILS TO OPEN	1.75E-03	REBCV119GO
			CCF OF 2 OUT 2 LOW PRESSURE RECIRCULATION SQUIB VALVES	5.80E-05	IWX-EV4-SA
			HARDWARE FAILURE CAUSE RECIRC. CV 119A FAILS TO OPEN	1.75E-03	REACV119GO
24	7.41E-14	.00	SMALL LOCA INITIATING EVENT OCCURS	5.00E-04	IEV-SLOCA
			HARDWARE FAILURE CAUSE RECIRC. CV 119B FAILS TO OPEN	1.75E-03	REBCV119GO
			CCF OF 2 OUT 2 LOW PRESSURE RECIRCULATION SQUIB VALVES	5.80E-05	IWX-EV4-SA
			HARDWARE FAILURE OF SQUIB VALVE 120A	1.46E-03	IRWMOD10
25	7.41E-14	.00	SMALL LOCA INITIATING EVENT OCCURS	5.00E-04	IEV-SLOCA
			HARDWARE FAILURE CAUSE RECIRC. CV 119A FAILS TO OPEN	1.75E-03	REACV119GO
			CCF OF 2 OUT 2 LOW PRESSURE RECIRCULATION SQUIB VALVES	5.80E-05	IWX-EV4-SA
			HARDWARE FAILURE OF SQUIB VALVE 120B	1.46E-03	IRWMOD12

(Sheet 1 of 3)

SEQUENCE 7 – MEDIUM LOCA DOMINANT CUTSETS (MLOCA-05)

NUMBER	CUTSET PROB.	PERCENTAGE	BASIC EVENT NAME		
1	5.23E-09	71.13	MEDIUM LOCA INITIATING EVENT OCCURS	4.36E-04	IEV-MLOCA
			PLUGGING OF BOTH RECIRC LINES DUE TO CCF OF SUMP SCREENS	1.20E-05	REX-FL-GP
2	2.08E-09	28.29	MEDIUM LOCA INITIATING EVENT OCCURS	4.36E-04	IEV-MLOCA
			CCF OF TANK LEVEL TRANSMITTERS	4.78E-04	IWX-XMTR
			OPER. FAILS TO ACT. SUMP RECIRC GIVEN IRW LEVEL SIGNAL FAILUR	1.00E-02	REN-MAN04
3	2.51E-11	.34	MEDIUM LOCA INITIATING EVENT OCCURS	4.36E-04	IEV-MLOCA
			SUMP SCREEN A PLUGS AND PREVENTS FLOW	2.40E-04	REA-PLUG
			SUMP SCREEN B PLUGS AND PREVENTS FLOW	2.40E-04	REB-PLUG
4	8.00E-12	.11	MEDIUM LOCA INITIATING EVENT OCCURS	4.36E-04	IEV-MLOCA
			CCF OF TANK LEVEL TRANSMITTERS	4.78E-04	IWX-XMTR
			CCX-VS-FA	3.84E-05	CCX-VS-FA
5	2.29E-12	.03	MEDIUM LOCA INITIATING EVENT OCCURS	4.36E-04	IEV-MLOCA
			CCF OF PMS ESF OUTPUT LOGIC SOFTWARE	1.10E-05	CCX-PMXMOD1-SW
			CCF OF TANK LEVEL TRANSMITTERS	4.78E-04	IWX-XMTR
6	2.29E-12	.03	MEDIUM LOCA INITIATING EVENT OCCURS	4.36E-04	IEV-MLOCA
			CCX-PMXMOD4-SW	1.10E-05	CCX-PMXMOD4-SW
			CCF OF TANK LEVEL TRANSMITTERS	4.78E-04	IWX-XMTR
7	1.80E-12	.02	MEDIUM LOCA INITIATING EVENT OCCURS	4.36E-04	IEV-MLOCA
			CCF OF EPO BOARDS IN PMS	8.62E-06	CCX-EP-SAM
			CCF OF TANK LEVEL TRANSMITTERS	4.78E-04	IWX-XMTR
8	2.67E-13	.00	MEDIUM LOCA INITIATING EVENT OCCURS	4.36E-04	IEV-MLOCA
			HARDWARE FAILURE CAUSE RECIRC. CV 119A FAILS TO OPEN	1.75E-03	REACV119GO
			SUMP SCREEN B PLUGS AND PREVENTS FLOW	2.40E-04	REB-PLUG
			HARDWARE FAILURE OF SQUIB VALVE 118A	1.46E-03	IRWMOD09
9	2.67E-13	.00	MEDIUM LOCA INITIATING EVENT OCCURS	4.36E-04	IEV-MLOCA
			HARDWARE FAILURE CAUSE RECIRC. CV 119B FAILS TO OPEN	1.75E-03	REBCV119GO
			SUMP SCREEN A PLUGS AND PREVENTS FLOW	2.40E-04	REA-PLUG
			HARDWARE FAILURE OF SQUIB VALVE 118B	1.46E-03	IRWMOD11
10	2.50E-13	.00	MEDIUM LOCA INITIATING EVENT OCCURS	4.36E-04	IEV-MLOCA
			SOFTWARE CCF OF ALL CARDS	1.20E-06	CCX-SFTW
			CCF OF TANK LEVEL TRANSMITTERS	4.78E-04	IWX-XMTR

(Sheet 2 of 3)

SEQUENCE 7 – MEDIUM LOCA DOMINANT CUTSETS (MLOCA-05)

NUMBER	CUTSET PROB.	PERCENTAGE	BASIC EVENT NAME		
11	2.23E-13	.00	MEDIUM LOCA INITIATING EVENT OCCURS	4.36E-04	IEV-MLOCA
			HARDWARE FAILURE OF SQUIB VALVE 120A	1.46E-03	IRWMOD10
			SUMP SCREEN B PLUGS AND PREVENTS FLOW	2.40E-04	REB-PLUG
			HARDWARE FAILURE OF SQUIB VALVE 118A	1.46E-03	IRWMOD09
12	2.23E-13	.00	MEDIUM LOCA INITIATING EVENT OCCURS	4.36E-04	IEV-MLOCA
			HARDWARE FAILURE OF SQUIB VALVE 120B	1.46E-03	IRWMOD12
			SUMP SCREEN A PLUGS AND PREVENTS FLOW	2.40E-04	REA-PLUG
			HARDWARE FAILURE OF SQUIB VALVE 118B	1.46E-03	IRWMOD11
13	2.08E-13	.00	MEDIUM LOCA INITIATING EVENT OCCURS	4.36E-04	IEV-MLOCA
			INDICATION FAILURE	1.00E-06	ALL-IND-FAIL
			CCF OF TANK LEVEL TRANSMITTERS	4.78E-04	IWX-XMTR
14	1.60E-13	.00	MEDIUM LOCA INITIATING EVENT OCCURS	4.36E-04	IEV-MLOCA
			HARDWARE FAILURE CAUSE RECIRC. CV 119A FAILS TO OPEN	1.75E-03	REACV119GO
			SUMP SCREEN B PLUGS AND PREVENTS FLOW	2.40E-04	REB-PLUG
			RELAY FAILS TO OPERATE	8.76E-04	IWBRS118AFA
15	1.60E-13	.00	MEDIUM LOCA INITIATING EVENT OCCURS	4.36E-04	IEV-MLOCA
			HARDWARE FAILURE CAUSE RECIRC. CV 119B FAILS TO OPEN	1.75E-03	REBCV119GO
			SUMP SCREEN A PLUGS AND PREVENTS FLOW	2.40E-04	REA-PLUG
			RELAY FAILS TO OPERATE	8.76E-04	IWARS118BFA
16	1.47E-13	.00	MEDIUM LOCA INITIATING EVENT OCCURS	4.36E-04	IEV-MLOCA
			CCF OF 2 OUT 2 LOW PRESSURE RECIRCULATION SQUIB VALVES	5.80E-05	IWX-EV4-SA
			CCF OF MOV 120A AND 120B	5.80E-06	IWX-EV2-SA
17	1.34E-13	.00	MEDIUM LOCA INITIATING EVENT OCCURS	4.36E-04	IEV-MLOCA
			HARDWARE FAILURE OF SQUIB VALVE 120A	1.46E-03	IRWMOD10
			SUMP SCREEN B PLUGS AND PREVENTS FLOW	2.40E-04	REB-PLUG
			RELAY FAILS TO OPERATE	8.76E-04	IWBRS118AFA
18	1.34E-13	.00	MEDIUM LOCA INITIATING EVENT OCCURS	4.36E-04	IEV-MLOCA
			HARDWARE FAILURE OF SQUIB VALVE 118A	1.46E-03	IRWMOD09
			SUMP SCREEN B PLUGS AND PREVENTS FLOW	2.40E-04	REB-PLUG
			RELAY FAILS TO OPERATE	8.76E-04	IWDRS120AFA

(Sheet 3 of 3)

SEQUENCE 7 – MEDIUM LOCA DOMINANT CUTSETS (MLOCA-05)

NUMBER	CUTSET PROB.	PERCENTAGE	BASIC EVENT NAME		
19	1.34E-13	.00	MEDIUM LOCA INITIATING EVENT OCCURS	4.36E-04	IEV-MLOCA
			HARDWARE FAILURE OF SQUIB VALVE 120B	1.46E-03	IRWMOD12
			SUMP SCREEN A PLUGS AND PREVENTS FLOW	2.40E-04	REA-PLUG
			RELAY FAILS TO OPERATE	8.76E-04	IWARS118BFA
20	1.34E-13	.00	MEDIUM LOCA INITIATING EVENT OCCURS	4.36E-04	IEV-MLOCA
			HARDWARE FAILURE OF SQUIB VALVE 118B	1.46E-03	IRWMOD11
			SUMP SCREEN A PLUGS AND PREVENTS FLOW	2.40E-04	REA-PLUG
			RELAY FAILS TO OPERATE	8.76E-04	IWCRS120BFA
21	8.03E-14	.00	MEDIUM LOCA INITIATING EVENT OCCURS	4.36E-04	IEV-MLOCA
			RELAY FAILS TO OPERATE	8.76E-04	IWDRS120AFA
			SUMP SCREEN B PLUGS AND PREVENTS FLOW	2.40E-04	REB-PLUG
			RELAY FAILS TO OPERATE	8.76E-04	IWBRS118AFA
22	8.03E-14	.00	MEDIUM LOCA INITIATING EVENT OCCURS	4.36E-04	IEV-MLOCA
			RELAY FAILS TO OPERATE	8.76E-04	IWCRS120BFA
			SUMP SCREEN A PLUGS AND PREVENTS FLOW	2.40E-04	REA-PLUG
			RELAY FAILS TO OPERATE	8.76E-04	IWARS118BFA
23	7.74E-14	.00	MEDIUM LOCA INITIATING EVENT OCCURS	4.36E-04	IEV-MLOCA
			HARDWARE FAILURE CAUSE RECIRC. CV 119B FAILS TO OPEN	1.75E-03	REBCV119GO
			CCF OF 2 OUT 2 LOW PRESSURE RECIRCULATION SQUIB VALVES	5.80E-05	IWX-EV4-SA
			HARDWARE FAILURE CAUSE RECIRC. CV 119A FAILS TO OPEN	1.75E-03	REACV119GO
24	6.46E-14	.00	MEDIUM LOCA INITIATING EVENT OCCURS	4.36E-04	IEV-MLOCA
			HARDWARE FAILURE CAUSE RECIRC. CV 119B FAILS TO OPEN	1.75E-03	REBCV119GO
			CCF OF 2 OUT 2 LOW PRESSURE RECIRCULATION SQUIB VALVES	5.80E-05	IWX-EV4-SA
			HARDWARE FAILURE OF SQUIB VALVE 120A	1.46E-03	IRWMOD10
25	6.46E-14	.00	MEDIUM LOCA INITIATING EVENT OCCURS	4.36E-04	IEV-MLOCA
			HARDWARE FAILURE CAUSE RECIRC. CV 119A FAILS TO OPEN	1.75E-03	REACV119GO
			CCF OF 2 OUT 2 LOW PRESSURE RECIRCULATION SQUIB VALVES	5.80E-05	IWX-EV4-SA
			HARDWARE FAILURE OF SQUIB VALVE 120B	1.46E-03	IRWMOD12

(Sheet 1 of 3)

SEQUENCE 8 – SMALL LOCA DOMINANT CUTSETS (SLOCA-12)

NUMBER	CUTSET PROB.	PERCENTAGE	BASIC EVENT NAME		
1	4.16E-10	8.14	SMALL LOCA INITIATING EVENT OCCURS	5.00E-04	IEV-SLOCA
			CCF OF 2 SQUIB VALVES TO OPERATE	5.90E-05	ADX-EV-SA2
			MECHANICAL FAILURE OF RNS MOV V055	1.41E-02	RN55MOD1
2	4.16E-10	8.14	SMALL LOCA INITIATING EVENT OCCURS	5.00E-04	IEV-SLOCA
			CCF OF 2 SQUIB VALVES TO OPERATE	5.90E-05	ADX-EV-SA2
			HARDWARE FAILURE OF ISOLATION MOV 011	1.41E-02	RN11MOD3
3	4.16E-10	8.14	SMALL LOCA INITIATING EVENT OCCURS	5.00E-04	IEV-SLOCA
			CCF OF 2 SQUIB VALVES TO OPERATE	5.90E-05	ADX-EV-SA2
			HARDWARE FAILS TO OPEN MOV V022/CB FTC/RELAY FTC	1.41E-02	RN22MOD4
4	4.16E-10	8.14	SMALL LOCA INITIATING EVENT OCCURS	5.00E-04	IEV-SLOCA
			CCF OF 2 SQUIB VALVES TO OPERATE	5.90E-05	ADX-EV-SA2
			HARDWARE FAILS TO OPEN MOV V023/CB FTC/RELAY FTC	1.41E-02	RN23MOD5
5	2.95E-10	5.77	SMALL LOCA INITIATING EVENT OCCURS	5.00E-04	IEV-SLOCA
			CCF OF 2 SQUIB VALVES TO OPERATE	5.90E-05	ADX-EV-SA2
			CASK LOADING PIT UNAVAILABLE DUE TO FUEL UNLOADING OPERATIONS	1.00E-02	CLP-UNAVAILABLE
6	2.11E-10	4.13	SMALL LOCA INITIATING EVENT OCCURS	5.00E-04	IEV-SLOCA
			DUE TO CCF OF 4TH STAGE ADS SQUIB VALVES TO OPERATE	3.00E-05	ADX-EV-SA
			MECHANICAL FAILURE OF RNS MOV V055	1.41E-02	RN55MOD1
7	2.11E-10	4.13	SMALL LOCA INITIATING EVENT OCCURS	5.00E-04	IEV-SLOCA
			DUE TO CCF OF 4TH STAGE ADS SQUIB VALVES TO OPERATE	3.00E-05	ADX-EV-SA
			HARDWARE FAILURE OF ISOLATION MOV 011	1.41E-02	RN11MOD3
8	2.11E-10	4.13	SMALL LOCA INITIATING EVENT OCCURS	5.00E-04	IEV-SLOCA
			DUE TO CCF OF 4TH STAGE ADS SQUIB VALVES TO OPERATE	3.00E-05	ADX-EV-SA
			HARDWARE FAILS TO OPEN MOV V022/CB FTC/RELAY FTC	1.41E-02	RN22MOD4
9	2.11E-10	4.13	SMALL LOCA INITIATING EVENT OCCURS	5.00E-04	IEV-SLOCA
			DUE TO CCF OF 4TH STAGE ADS SQUIB VALVES TO OPERATE	3.00E-05	ADX-EV-SA
			HARDWARE FAILS TO OPEN MOV V023/CB FTC/RELAY FTC	1.41E-02	RN23MOD5
10	1.50E-10	2.93	SMALL LOCA INITIATING EVENT OCCURS	5.00E-04	IEV-SLOCA
			DUE TO CCF OF 4TH STAGE ADS SQUIB VALVES TO OPERATE	3.00E-05	ADX-EV-SA
			CASK LOADING PIT UNAVAILABLE DUE TO FUEL UNLOADING OPERATIONS	1.00E-02	CLP-UNAVAILABLE

(Sheet 2 of 3)

SEQUENCE 8 – SMALL LOCA DOMINANT CUTSETS (SLOCA-12)

NUMBER	CUTSET PROB.	PERCENTAGE	BASIC EVENT NAME		
11	1.45E-10	2.84	SMALL LOCA INITIATING EVENT OCCURS	5.00E-04	IEV-SLOCA
			CCF OF 2 SQUIB VALVES TO OPERATE	5.90E-05	ADX-EV-SA2
			CCF OF STOP CHECK VALVES V015A/B TO OPEN	4.90E-03	RNX-KV1-GO
12	8.55E-11	1.67	SMALL LOCA INITIATING EVENT OCCURS	5.00E-04	IEV-SLOCA
			CCF OF 2 SQUIB VALVES TO OPERATE	5.90E-05	ADX-EV-SA2
			OPERATOR FAILS TO ALIGN AND ACTUATE THE RNS	2.90E-03	RHN-MAN01
13	7.97E-11	1.56	SMALL LOCA INITIATING EVENT OCCURS	5.00E-04	IEV-SLOCA
			CCF OF 2 SQUIB VALVES TO OPERATE	5.90E-05	ADX-EV-SA2
			UNAVAILABILITY OF BUS ECS ES 1 DUE TO UNSCHEDUL MAINTENANCE	2.70E-03	EC1BS001TM
14	7.97E-11	1.56	SMALL LOCA INITIATING EVENT OCCURS	5.00E-04	IEV-SLOCA
			CCF OF 2 SQUIB VALVES TO OPERATE	5.90E-05	ADX-EV-SA2
			BUS UNAVAILABLE DUE TO UNSCHEDULED MAINTENANCE	2.70E-03	EC1BS012TM
15	7.97E-11	1.56	SMALL LOCA INITIATING EVENT OCCURS	5.00E-04	IEV-SLOCA
			CCF OF 2 SQUIB VALVES TO OPERATE	5.90E-05	ADX-EV-SA2
			BUS UNAVAILABLE DUE TO UNSCHEDULED MAINTENANCE	2.70E-03	EC1BS122TM
16	7.58E-11	1.48	SMALL LOCA INITIATING EVENT OCCURS	5.00E-04	IEV-SLOCA
			CCF OF 2 SQUIB VALVES TO OPERATE	5.90E-05	ADX-EV-SA2
			HARDWARE FAILURE OF VALVES ON DVI LINE A (V015A & 017	5.07E-02	RNAMOD09
			HARDWARE FAILURE OF VALVES ON DVI LINE B (V015B & 017	5.07E-02	RNBMOD10
17	7.35E-11	1.44	SMALL LOCA INITIATING EVENT OCCURS	5.00E-04	IEV-SLOCA
			DUE TO CCF OF 4TH STAGE ADS SQUIB VALVES TO OPERATE	3.00E-05	ADX-EV-SA
			CCF OF STOP CHECK VALVES V015A/B TO OPEN	4.90E-03	RNX-KV1-GO
18	6.35E-11	1.24	SMALL LOCA INITIATING EVENT OCCURS	5.00E-04	IEV-SLOCA
			COMMON CAUSE FAILURE OF THE BATTERIES IDSA-DB-1A/1B	4.70E-05	CCX-BY-PN
			UNAVAILABILITY OF BUS ECS ES 2 DUE TO UNSCHEDULED MAINTENANCE	2.70E-03	EC2BS002TM
19	6.35E-11	1.24	SMALL LOCA INITIATING EVENT OCCURS	5.00E-04	IEV-SLOCA
			COMMON CAUSE FAILURE OF THE BATTERIES IDSA-DB-1A/1B	4.70E-05	CCX-BY-PN
			BUS UNAVAILABLE DUE TO UNSCHEDULED MAINTENANCE	2.70E-03	EC2BS022TM
20	6.35E-11	1.24	SMALL LOCA INITIATING EVENT OCCURS	5.00E-04	IEV-SLOCA
			COMMON CAUSE FAILURE OF THE BATTERIES IDSA-DB-1A/1B	4.70E-05	CCX-BY-PN
			BUS UNAVAILABLE DUE TO UNSCHEDULED MAINTENANCE	2.70E-03	EC2BS221TM

(Sheet 3 of 3)

SEQUENCE 8 – SMALL LOCA DOMINANT CUTSETS (SLOCA-12)

NUMBER	CUTSET PROB.	PERCENTAGE	BASIC EVENT NAME		
21	6.35E-11	1.24	SMALL LOCA INITIATING EVENT OCCURS	5.00E-04	IEV-SLOCA
			COMMON CAUSE FAILURE OF THE BATTERIES IDSA-DB-1A/1B	4.70E-05	CCX-BY-PN
			UNAVAILABILITY OF BUS ECS ES 1 DUE TO UNSCHEDULED MAINTENANCE	2.70E-03	EC1BS001TM
22	6.35E-11	1.24	SMALL LOCA INITIATING EVENT OCCURS	5.00E-04	IEV-SLOCA
			COMMON CAUSE FAILURE OF THE BATTERIES IDSA-DB-1A/1B	4.70E-05	CCX-BY-PN
			BUS UNAVAILABLE DUE TO UNSCHEDULED MAINTENANCE	2.70E-03	EC1BS012TM
23	6.35E-11	1.24	SMALL LOCA INITIATING EVENT OCCURS	5.00E-04	IEV-SLOCA
			COMMON CAUSE FAILURE OF THE BATTERIES IDSA-DB-1A/1B	4.70E-05	CCX-BY-PN
			BUS UNAVAILABLE DUE TO UNSCHEDULED MAINTENANCE	2.70E-03	EC1BS121TM
24	5.16E-11	1.01	SMALL LOCA INITIATING EVENT OCCURS	5.00E-04	IEV-SLOCA
			CCF OF 2 SQUIB VALVES TO OPERATE	5.90E-05	ADX-EV-SA2
			CHECK VALVE V013 FAILURE TO OPEN	1.75E-03	RNNCV013GO
25	4.50E-11	.88	SMALL LOCA INITIATING EVENT OCCURS	5.00E-04	IEV-SLOCA
			BUS UNAVAILABLE DUE TO TEST OR CORRECTIVE MAINTENANCE	3.00E-04	IDBBSDS1TM
			BUS UNAVAILABLE DUE TO TEST OR CORRECTIVE MAINTENANCE	3.00E-04	IDDBSDS1TM

(Sheet 1 of 3)

SEQUENCE 9 – MEDIUM LOCA DOMINANT CUTSETS (MLOCA-12)

NUMBER	CUTSET PROB.	PERCENTAGE	BASIC EVENT NAME		
1	3.63E-10	8.14	MEDIUM LOCA INITIATING EVENT OCCURS	4.36E-04	IEV-MLOCA
			CCF OF 2 SQUIB VALVES TO OPERATE	5.90E-05	ADX-EV-SA2
			MECHANICAL FAILURE OF RNS MOV V055	1.41E-02	RN55MOD1
2	3.63E-10	8.14	MEDIUM LOCA INITIATING EVENT OCCURS	4.36E-04	IEV-MLOCA
			CCF OF 2 SQUIB VALVES TO OPERATE	5.90E-05	ADX-EV-SA2
			HARDWARE FAILURE OF ISOLATION MOV 011	1.41E-02	RN11MOD3
3	3.63E-10	8.14	MEDIUM LOCA INITIATING EVENT OCCURS	4.36E-04	IEV-MLOCA
			CCF OF 2 SQUIB VALVES TO OPERATE	5.90E-05	ADX-EV-SA2
			HARDWARE FAILS TO OPEN MOV V022/CB FTC/RELAY FTC	1.41E-02	RN22MOD4
4	3.63E-10	8.14	MEDIUM LOCA INITIATING EVENT OCCURS	4.36E-04	IEV-MLOCA
			CCF OF 2 SQUIB VALVES TO OPERATE	5.90E-05	ADX-EV-SA2
			HARDWARE FAILS TO OPEN MOV V023/CB FTC/RELAY FTC	1.41E-02	RN23MOD5
5	2.57E-10	5.77	MEDIUM LOCA INITIATING EVENT OCCURS	4.36E-04	IEV-MLOCA
			CCF OF 2 SQUIB VALVES TO OPERATE	5.90E-05	ADX-EV-SA2
			CASK LOADING PIT UNAVAILABLE DUE TO FUEL UNLOADING OPERATIONS	1.00E-02	CLP-UNAVAILABLE
6	1.84E-10	4.13	MEDIUM LOCA INITIATING EVENT OCCURS	4.36E-04	IEV-MLOCA
			DUE TO CCF OF 4TH STAGE ADS SQUIB VALVES TO OPERATE	3.00E-05	ADX-EV-SA
			MECHANICAL FAILURE OF RNS MOV V055	1.41E-02	RN55MOD1
7	1.84E-10	4.13	MEDIUM LOCA INITIATING EVENT OCCURS	4.36E-04	IEV-MLOCA
			DUE TO CCF OF 4TH STAGE ADS SQUIB VALVES TO OPERATE	3.00E-05	ADX-EV-SA
			HARDWARE FAILURE OF ISOLATION MOV 011	1.41E-02	RN11MOD3
8	1.84E-10	4.13	MEDIUM LOCA INITIATING EVENT OCCURS	4.36E-04	IEV-MLOCA
			DUE TO CCF OF 4TH STAGE ADS SQUIB VALVES TO OPERATE	3.00E-05	ADX-EV-SA
			HARDWARE FAILS TO OPEN MOV V022/CB FTC/RELAY FTC	1.41E-02	RN22MOD4
9	1.84E-10	4.13	MEDIUM LOCA INITIATING EVENT OCCURS	4.36E-04	IEV-MLOCA
			DUE TO CCF OF 4TH STAGE ADS SQUIB VALVES TO OPERATE	3.00E-05	ADX-EV-SA
			HARDWARE FAILS TO OPEN MOV V023/CB FTC/RELAY FTC	1.41E-02	RN23MOD5
10	1.31E-10	2.94	MEDIUM LOCA INITIATING EVENT OCCURS	4.36E-04	IEV-MLOCA
			DUE TO CCF OF 4TH STAGE ADS SQUIB VALVES TO OPERATE	3.00E-05	ADX-EV-SA
			CASK LOADING PIT UNAVAILABLE DUE TO FUEL UNLOADING OPERATIONS	1.00E-02	CLP-UNAVAILABLE

(Sheet 2 of 3)

SEQUENCE 9 – MEDIUM LOCA DOMINANT CUTSETS (MLOCA-12)

NUMBER	CUTSET PROB.	PERCENTAGE	BASIC EVENT NAME		
11	1.26E-10	2.83	MEDIUM LOCA INITIATING EVENT OCCURS	4.36E-04	IEV-MLOCA
			CCF OF 2 SQUIB VALVES TO OPERATE	5.90E-05	ADX-EV-SA2
			CCF OF STOP CHECK VALVES V015A/B TO OPEN	4.90E-03	RNX-KV1-GO
12	7.46E-11	1.67	MEDIUM LOCA INITIATING EVENT OCCURS	4.36E-04	IEV-MLOCA
			CCF OF 2 SQUIB VALVES TO OPERATE	5.90E-05	ADX-EV-SA2
			OPERATOR FAILS TO ALIGN AND ACTUATE THE RNS	2.90E-03	RHN-MAN01
13	6.95E-11	1.56	MEDIUM LOCA INITIATING EVENT OCCURS	4.36E-04	IEV-MLOCA
			CCF OF 2 SQUIB VALVES TO OPERATE	5.90E-05	ADX-EV-SA2
			UNAVAILABILITY OF BUS ECS ES 1 DUE TO UNSCHEDULED MAINTENANCE	2.70E-03	EC1BS001TM
14	6.95E-11	1.56	MEDIUM LOCA INITIATING EVENT OCCURS	4.36E-04	IEV-MLOCA
			CCF OF 2 SQUIB VALVES TO OPERATE	5.90E-05	ADX-EV-SA2
			BUS UNAVAILABLE DUE TO UNSCHEDULED MAINTENANCE	2.70E-03	EC1BS012TM
15	6.95E-11	1.56	MEDIUM LOCA INITIATING EVENT OCCURS	4.36E-04	IEV-MLOCA
			CCF OF 2 SQUIB VALVES TO OPERATE	5.90E-05	ADX-EV-SA2
			BUS UNAVAILABLE DUE TO UNSCHEDULED MAINTENANCE	2.70E-03	EC1BS122TM
16	6.61E-11	1.48	MEDIUM LOCA INITIATING EVENT OCCURS	4.36E-04	IEV-MLOCA
			CCF OF 2 SQUIB VALVES TO OPERATE	5.90E-05	ADX-EV-SA2
			HARDWARE FAILURE OF VALVES ON DVI LINE A (V015A & 017)	5.07E-02	RNAMOD09
			HARDWARE FAILURE OF VALVES ON DVI LINE B (V015B & 017)	5.07E-02	RNBMOD10
17	6.41E-11	1.44	MEDIUM LOCA INITIATING EVENT OCCURS	4.36E-04	IEV-MLOCA
			DUE TO CCF OF 4TH STAGE ADS SQUIB VALVES TO OPERATE	3.00E-05	ADX-EV-SA
			CCF OF STOP CHECK VALVES V015A/B TO OPEN	4.90E-03	RNX-KV1-GO
18	5.53E-11	1.24	MEDIUM LOCA INITIATING EVENT OCCURS	4.36E-04	IEV-MLOCA
			COMMON CAUSE FAILURE OF THE BATTERIES IDSA-DB-1A/1B	4.70E-05	CCX-BY-PN
			UNAVAILABILITY OF BUS ECS ES 2 DUE TO UNSCHEDULED MAINTENANCE	2.70E-03	EC2BS002TM
19	5.53E-11	1.24	MEDIUM LOCA INITIATING EVENT OCCURS	4.36E-04	IEV-MLOCA
			COMMON CAUSE FAILURE OF THE BATTERIES IDSA-DB-1A/1B	4.70E-05	CCX-BY-PN
			BUS UNAVAILABLE DUE TO UNSCHEDULED MAINTENANCE	2.70E-03	EC2BS022TM

(Sheet 3 of 3)

SEQUENCE 9 – MEDIUM LOCA DOMINANT CUTSETS (MLOCA-12)

NUMBER	CUTSET PROB.	PERCENTAGE	BASIC EVENT NAME		
20	5.53E-11	1.24	MEDIUM LOCA INITIATING EVENT OCCURS	4.36E-04	IEV-MLOCA
			COMMON CAUSE FAILURE OF THE BATTERIES IDSA-DB-1A/1B	4.70E-05	CCX-BY-PN
			BUS UNAVAILABLE DUE TO UNSCHEDULED MAINTENANCE	2.70E-03	EC2BS221TM
21	5.53E-11	1.24	MEDIUM LOCA INITIATING EVENT OCCURS	4.36E-04	IEV-MLOCA
			COMMON CAUSE FAILURE OF THE BATTERIES IDSA-DB-1A/1B	4.70E-05	CCX-BY-PN
			UNAVAILABILITY OF BUS ECS ES 1 DUE TO UNSCHEDULED MAINTENANCE	2.70E-03	EC1BS001TM
22	5.53E-11	1.24	MEDIUM LOCA INITIATING EVENT OCCURS	4.36E-04	IEV-MLOCA
			COMMON CAUSE FAILURE OF THE BATTERIES IDSA-DB-1A/1B	4.70E-05	CCX-BY-PN
			BUS UNAVAILABLE DUE TO UNSCHEDULED MAINTENANCE	2.70E-03	EC1BS012TM
23	5.53E-11	1.24	MEDIUM LOCA INITIATING EVENT OCCURS	4.36E-04	IEV-MLOCA
			COMMON CAUSE FAILURE OF THE BATTERIES IDSA-DB-1A/1B	4.70E-05	CCX-BY-PN
			BUS UNAVAILABLE DUE TO UNSCHEDULED MAINTENANCE	2.70E-03	EC1BS121TM
24	4.50E-11	1.01	MEDIUM LOCA INITIATING EVENT OCCURS	4.36E-04	IEV-MLOCA
			CCF OF 2 SQUIB VALVES TO OPERATE	5.90E-05	ADX-EV-SA2
			CHECK VALVE V013 FAILURE TO OPEN	1.75E-03	RNNCV013GO
25	3.92E-11	.88	MEDIUM LOCA INITIATING EVENT OCCURS	4.36E-04	IEV-MLOCA
			BUS UNAVAILABLE DUE TO TEST OR CORRECTIVE MAINTENANCE	3.00E-04	IDDBSDS1TM
			BUS UNAVAILABLE DUE TO TEST OR CORRECTIVE MAINTENANCE	3.00E-04	IDBBSDS1TM

(Sheet 1 of 3)

SEQUENCE 10 – SPURIOUS ADS ACTUATION DOMINANT CUTSETS (SPADS-09)

NUMBER	CUTSET PROB.	PERCENTAGE	BASIC EVENT NAME		
1	2.75E-09	73.90	SPURIOUS ADS INITIATING EVENT OCCURS	5.40E-05	IEV-SPADS
			COMMON CAUSE FAILURE OF 2 ACCUMULATOR CHECK VALVES	5.10E-05	ACX-CV-GO
2	1.65E-10	4.43	SPURIOUS ADS INITIATING EVENT OCCURS	5.40E-05	IEV-SPADS
			CHECK VALVE 029B FAILS TO OPEN	1.75E-03	ACBCV029GO
			CHECK VALVE 029A FAILS TO OPEN	1.75E-03	ACACV029GO
3	1.65E-10	4.43	SPURIOUS ADS INITIATING EVENT OCCURS	5.40E-05	IEV-SPADS
			CHECK VALVE 029B FAILS TO OPEN	1.75E-03	ACBCV029GO
			CHECK VALVE 028A FAILS TO OPEN	1.75E-03	ACACV028GO
4	1.65E-10	4.43	SPURIOUS ADS INITIATING EVENT OCCURS	5.40E-05	IEV-SPADS
			CHECK VALVE 028B FAILS TO OPEN	1.75E-03	ACBCV028GO
			CHECK VALVE 029A FAILS TO OPEN	1.75E-03	ACACV029GO
5	1.65E-10	4.43	SPURIOUS ADS INITIATING EVENT OCCURS	5.40E-05	IEV-SPADS
			CHECK VALVE 028B FAILS TO OPEN	1.75E-03	ACBCV028GO
			CHECK VALVE 028A FAILS TO OPEN	1.75E-03	ACACV028GO
6	6.87E-11	1.85	SPURIOUS ADS INITIATING EVENT OCCURS	5.40E-05	IEV-SPADS
			FLOW TUNING ORIFICE PLUGS	7.27E-04	ACBOR001SP
			CHECK VALVE 029A FAILS TO OPEN	1.75E-03	ACACV029GO
7	6.87E-11	1.85	SPURIOUS ADS INITIATING EVENT OCCURS	5.40E-05	IEV-SPADS
			FLOW TUNING ORIFICE PLUGS	7.27E-04	ACBOR001SP
			CHECK VALVE 028A FAILS TO OPEN	1.75E-03	ACACV028GO
8	6.87E-11	1.85	SPURIOUS ADS INITIATING EVENT OCCURS	5.40E-05	IEV-SPADS
			CHECK VALVE 029B FAILS TO OPEN	1.75E-03	ACBCV029GO
			FLOW TUNING ORIFICE PLUGS	7.27E-04	ACAOR001SP
9	6.87E-11	1.85	SPURIOUS ADS INITIATING EVENT OCCURS	5.40E-05	IEV-SPADS
			CHECK VALVE 028B FAILS TO OPEN	1.75E-03	ACBCV028GO
			FLOW TUNING ORIFICE PLUGS	7.27E-04	ACAOR001SP
10	2.85E-11	.77	SPURIOUS ADS INITIATING EVENT OCCURS	5.40E-05	IEV-SPADS
			FLOW TUNING ORIFICE PLUGS	7.27E-04	ACBOR001SP
			FLOW TUNING ORIFICE PLUGS	7.27E-04	ACAOR001SP

(Sheet 2 of 3)

SEQUENCE 10 – SPURIOUS ADS ACTUATION DOMINANT CUTSETS (SPADS-09)

NUMBER	CUTSET PROB.	PERCENTAGE	BASIC EVENT NAME		
11	6.48E-12	.17	SPURIOUS ADS INITIATING EVENT OCCURS	5.40E-05	IEV-SPADS
			COMMON CAUSE FAILURE OF ACCUMULATOR TANKS	1.20E-07	ACX-TK-AF
12	2.27E-13	.01	SPURIOUS ADS INITIATING EVENT OCCURS	5.40E-05	IEV-SPADS
			ACCUMULATOR TANK B (T001B) RUPTURES	2.40E-06	ACBTK001AF
			CHECK VALVE 029A FAILS TO OPEN	1.75E-03	ACACV029GO
13	2.27E-13	.01	SPURIOUS ADS INITIATING EVENT OCCURS	5.40E-05	IEV-SPADS
			ACCUMULATOR TANK B (T001B) RUPTURES	2.40E-06	ACBTK001AF
			CHECK VALVE 028A FAILS TO OPEN	1.75E-03	ACACV028GO
14	2.27E-13	.01	SPURIOUS ADS INITIATING EVENT OCCURS	5.40E-05	IEV-SPADS
			CHECK VALVE 029B FAILS TO OPEN	1.75E-03	ACBCV029GO
			ACCUMULATOR TANK A (T001A) RUPTURES	2.40E-06	ACATK001AF
15	2.27E-13	.01	SPURIOUS ADS INITIATING EVENT OCCURS	5.40E-05	IEV-SPADS
			CHECK VALVE 028B FAILS TO OPEN	1.75E-03	ACBCV028GO
			ACCUMULATOR TANK A (T001A) RUPTURES	2.40E-06	ACATK001AF
16	9.42E-14	.00	SPURIOUS ADS INITIATING EVENT OCCURS	5.40E-05	IEV-SPADS
			ACCUMULATOR TANK B (T001B) RUPTURES	2.40E-06	ACBTK001AF
			FLOW TUNING ORIFICE PLUGS	7.27E-04	ACAOR001SP
17	9.42E-14	.00	SPURIOUS ADS INITIATING EVENT OCCURS	5.40E-05	IEV-SPADS
			FLOW TUNING ORIFICE PLUGS	7.27E-04	ACBOR001SP
			ACCUMULATOR TANK A (T001A) RUPTURES	2.40E-06	ACATK001AF
18	6.80E-14	.00	SPURIOUS ADS INITIATING EVENT OCCURS	5.40E-05	IEV-SPADS
			FLOW TUNING ORIFICE RUPTURE	7.20E-07	ACBOR001EB
			CHECK VALVE 029A FAILS TO OPEN	1.75E-03	ACACV029GO
19	6.80E-14	.00	SPURIOUS ADS INITIATING EVENT OCCURS	5.40E-05	IEV-SPADS
			FLOW TUNING ORIFICE RUPTURE	7.20E-07	ACBOR001EB
			CHECK VALVE 028A FAILS TO OPEN	1.75E-03	ACACV028GO
20	6.80E-14	.00	SPURIOUS ADS INITIATING EVENT OCCURS	5.40E-05	IEV-SPADS
			CHECK VALVE 029B FAILS TO OPEN	1.75E-03	ACBCV029GO
			FLOW TUNING ORIFICE RUPTURE	7.20E-07	ACAOR001EB

(Sheet 3 of 3)

SEQUENCE 10 – SPURIOUS ADS ACTUATION DOMINANT CUTSETS (SPADS-09)

NUMBER	CUTSET PROB.	PERCENTAGE	BASIC EVENT NAME		
21	6.80E-14	.00	SPURIOUS ADS INITIATING EVENT OCCURS	5.40E-05	IEV-SPADS
			CHECK VALVE 028B FAILS TO OPEN	1.75E-03	ACBCV028GO
			FLOW TUNING ORIFICE RUPTURE	7.20E-07	ACAOR001EB
22	2.83E-14	.00	SPURIOUS ADS INITIATING EVENT OCCURS	5.40E-05	IEV-SPADS
			FLOW TUNING ORIFICE RUPTURE	7.20E-07	ACBOR001EB
			FLOW TUNING ORIFICE PLUGS	7.27E-04	ACAOR001SP
23	2.83E-14	.00	SPURIOUS ADS INITIATING EVENT OCCURS	5.40E-05	IEV-SPADS
			FLOW TUNING ORIFICE PLUGS	7.27E-04	ACBOR001SP
			FLOW TUNING ORIFICE RUPTURE	7.20E-07	ACAOR001EB

APPENDIX 4: COMPARISON BETWEEN MELCOR AND RELAP RESULTS IN THE SIMULATION OF A SGTR IN AP1000

Steady state

The present paragraph evidences the main results obtained in the comparison between the ANSALDO RELAP 5 Nodalization (taken as model) results for a DBA and those obtained with the AP1000 MELCOR Nodalization for the same accident. Aim of these analyses is to validate the AP1000 MELCOR Nodalization in order to predict the possible behaviour of AP1000 during an accident.

The results of ANSALDO AP1000 Nodalization, during the steady-state and a DBA accident phase, are useful in order to verify the correctness of the MELCOR nodalization and its compliance to the design specifications. Unfortunately, the absence of experimental data to compare with the results of the calculation precludes a better validation of the calculation model.

The steady-state study is a combination of the calculation results by MELCOR and by RELAP5 and the Plant Description Document and references. The main results are summarized in Table 0.1. It is interesting to see that the differences are quite small, particularly taking into account the roughness of MELCOR nodalization, especially for the order of magnitude of each Control Volume.

Quantity	Unit	AP1000 Design Data	RELAP 5.3.2	MELCOR 1.8.5	Error
Core thermal power	MWth	3415	3415	3415	0.00%
Core pressure loss	Pa	-	318000	318726	0.2%
Core inlet temperature	°K	553.9	552.87	552.3	0.3%
Core outlet temperature	°K	594.3	595.47	593.7	0.1%
Core bypass flow rate	kg/s	380.7	380.94	396.00	4.0%

PS total mass inventory	kg	-	200700	200756	0.04%
PRZ pressure	Mpa	15.5	15.52	15.49	0.06%
PS total coolant flow rate	kg/s	15250	15094	15249	0.01%
MCP head	Pa	835000	835000	835000	0.00%
SG SS mass inventory	kg	-	82800	83180	0.46%
SG thermal power	MWth	1707	1702.8	1707.8	0.05%
SG exit pressure	MPa	5.76	5.76	5.76	0.00%
SG F–W temperature	°K	499.8	499.8	499.8	0.00%
SG F–W mass flow rate	kg/s	943.12	943.12	943.12	0.00%
SG steam mass flow rate	kg/s	943.12	943.2	943.2	0.01%
PRZ liquid level	m	6.72	Not given	6.65	1.04%
SG pressure loss	Pa	-	255000	258700	1.45%

Data inserted as initial/boundary condition *Data obtained from the code*

Table 0.1 Comparison between MELCOR, RELAP and Reference Data

SGTR MELCOR simulation and comparison with RELAP5 results

The assumption of a complete tube severance is conservative because the steam generator tube material (Inconel 690 TT) is a corrosion-resistant and ductile material. The more probable mode of tube failure is one or more smaller leaks of undetermined origin. Radioactivity in the secondary side is subject to continual surveillance, and an accumulation of such leaks, which exceeds the limits established in the Technical Specifications, is not permitted during operation.

Following a SGTR event, single or multiple, the pressurizer water level and primary system pressure will decrease, due to the leakage of reactor coolant into the secondary side of the steam generator.

Pressurizer Low Pressure and Low Level alarms will be actuated and the Chemical and Volume Control System (CVCS) makeup pump starts or increases its flow in the attempt to maintain the pressurizer level. In the secondary side, the feed water flow rate to the affected Steam Generator will be reduced, because of the break flow which is supplied to that steam generator from the primary side.

The condenser air removal discharge radiation monitor, steam generator blow-down radiation monitor, and/or main steam line radiation monitor alarm, indicate an increase of radioactivity in the secondary system. The continued loss of primary inventory leads to the reactor trip, on Low Pressurizer Pressure or Over Temperature ΔT signal, in the time frame from few hundred of seconds, for a multiple SGTR, to about 1000 s for a single tube rupture event.

The reactor trip automatically trips the turbine and, if offsite power is available, the steam dump valves open, permitting steam dump to the condenser. In the event of a coincident loss of offsite power or loss of the condenser, the steam dump valves automatically close to protect the condenser. In this case, the steam generator pressure rapidly increases resulting in steam discharge to the atmosphere through the steam generator power operated relief valves (PORVs) or the safety valves.

The resultant plant cool-down following the reactor trip leads to a rapid decrease in reactor coolant system pressure and pressurizer level. Soon after the reactor trip, a safeguard "S" signal that causes Core Makeup Tank (CMT) actuation is initiated by Low – 1 Pressurizer Pressure or Low – 2 Pressurizer Level. CMT actuation trips the reactor coolant pumps.

The "S" signal automatically terminates the normal feed-water supply, and actuates the Passive Residual Heat Removal System (PRHR) to provide the requested heat sink.

The PRHR heat exchangers transfer core decay heat to the In-containment Refueling Water Storage Tank (IRWST) and initiate a cool-down (and consequentially depressurization) of the RCS. Startup feed-water is initiated on Low SG Narrow Range Level signal and controls the steam generator levels to the narrow range low level set point. In the post trip phase the PRHR operation the CMT flow rate and, if available, the CVCS flow rate provide the required heat sink to absorb the decay heat.

With the decay heat removal by the PRHR heat exchangers, steam generator steaming through the Steam Generators PORVs or Safety Valves ceases. This drastically reduces the amount of steam released to the atmosphere.

The balance between the coolant shrinkage caused by PRHR and CMT operation and the flow rate injection from CVCS stabilizes RCS pressure and level. The RCS pressure tends to an equilibrium value where the total injected flow rate by the CVCS equals the break flow rate. The break flow rate will continue until the CVCS will be isolated by the Overfilling Protection Logic that automatically trips the CVCS pumps and isolates Startup Feed-water. Isolation of the CVCS pumps avoids the repressurization of the RCS. This allows RCS pressure to equilibrate with the secondary pressure, which almost terminates the break flow. Since the CMTs continue to inject cold borated water (CMTs work in recirculation mode, i.e.: hot water from the balance line replaces relatively cold borated water in the CMT) in the RCS, isolating the CVCS pumps does not present a safety concern. On the other side, the moderate swelling of the CMT water inventory up to the time PRHR HX matches the decay heat, results in a moderate break flow. In the long term, since the RCS is cooled down by the PRHR, RCS pressure will drop below SG pressure and a limited reverse flow will occur.

Successful Steam Generator overfilling protection, along with the successful actuation of passive residual heat removal, terminates the event independently from the number of ruptured tubes. These protection systems maintain offsite radiation doses within the allowable values for a design basis SGTR. The operator may take actions that would provide a more rapid mitigation of the consequences of an SGTR. Because of the series of alarms described above, the operator can readily determine when an SGTR occurs, identify and isolate the faulted steam generator, and complete the required recovery actions to stabilize the plant and terminate the primary-to-secondary break flow. The recovery procedures are completed on a time scale that terminates break flow to the secondary system before steam generator overfill occurs and limits the offsite doses to acceptable levels without actuation of the ADS. Adequate indications and controls are provided to enable the operator to carry out these functions.

The comparison between RELAP and MELCOR time sequences is summarized in Tab 0.2. The delays in the timing of various events are due to the difference of the models and also to the difference of the Nodalizations. For example, the MELCOR AP1000 Nodalization has a little lower inertia than RELAP Nodalization, due to the assumption used to describe the input as similar as possible to the RELAP Nodalization. Practically the MELCOR models are more simplified than RELAP ones, especially with respect to the accuracy of the thermo-hydraulic elements. RELAP uses more elements in order to perform a more precise analysis of some important thermodynamic

variables. MELCOR in fact does not need the accuracy of the RELAP, being mainly devoted to predict the melt behaviour, aerosol release and transport, etc.

.

EVENT	TIME (s)	
	RELAP	MELCOR
Reactor trip	0	0
PRZ heaters on	0	0
CVS on	0	0
RCPs off	0	0
Turbine trip	0	0
SG PORVs modulate to maintain pressure	60	20
Low SG NR mass set-point reached	1176	987
PRHR valves fully open	1233	1057
Affected SG PORV closure	1900	1870
Low PRZ level set-point reached	1731	1788
CMT injection valves fully open	1743	1800
Low Tcold set-point reached	1973	1948
S signal	1973	1865
Affected SG PORV spurious opening	1973	1900
PRZ heaters off (on S signal)	1973	1865
PRZ voided	1900	1865
MSIV fully closed	1985	1948
Low PRZ pressure set-point reached	2087	1865
Low Steam line pressure set-point reached	2511	3043
Affected SG PORV block valves closure	2511	3043
CVCS off (Hi SG level + Hi SG pressure + S signal)	25000	25000
End of calculation		

Table 0.2: Comparison between MELCOR and RELAP sequences of major events.

The following figures show some main points of the comparison. It is important to evidence that all MELCOR results are an overestimation of the RELAP results.

Due to the less inertia in the MELCOR calculation, the CVCS closes later than RELAP with consequently a peak in the primary circuit mass at 11000 seconds. The primary and secondary masses and pressures for this reason are overestimated, but the shapes of these thermo-hydraulic variables are taken (Figure 0.1).

The most important differences are in the behaviour of the SG in intact loop. In fact the MELCOR calculation evidences a lower depressurization than RELAP one (Figure 0.2), which justifies the temperature behaviour and flow rate in the intact side (Figures 0.4 and 0.8). Some other causes or consequences of that are the differences of temperature and mass of SG 2 (Figure 0.6 and Figure 0.20).

Also the break flow rate, in particular from the cold side (Figure 0.12), suffers of the CVCS closure delay, as the primary mass (Figure 0.19), but without significant shape changes of the curves. The PRHR is reasonably well modelled, as shown in Figures 0.13 and 0.18, as for CMT flow-rate (Figure 0.15).

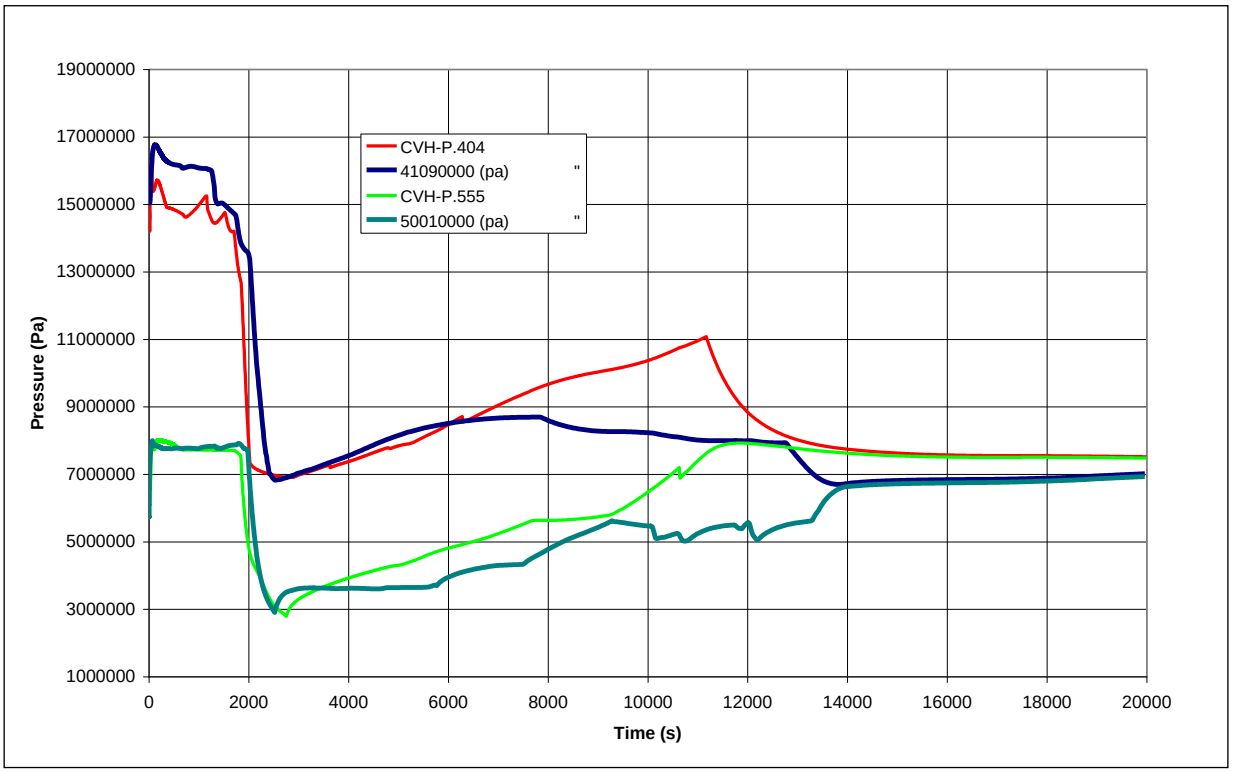

Figure 0.1 Primary and Secondary Pressure

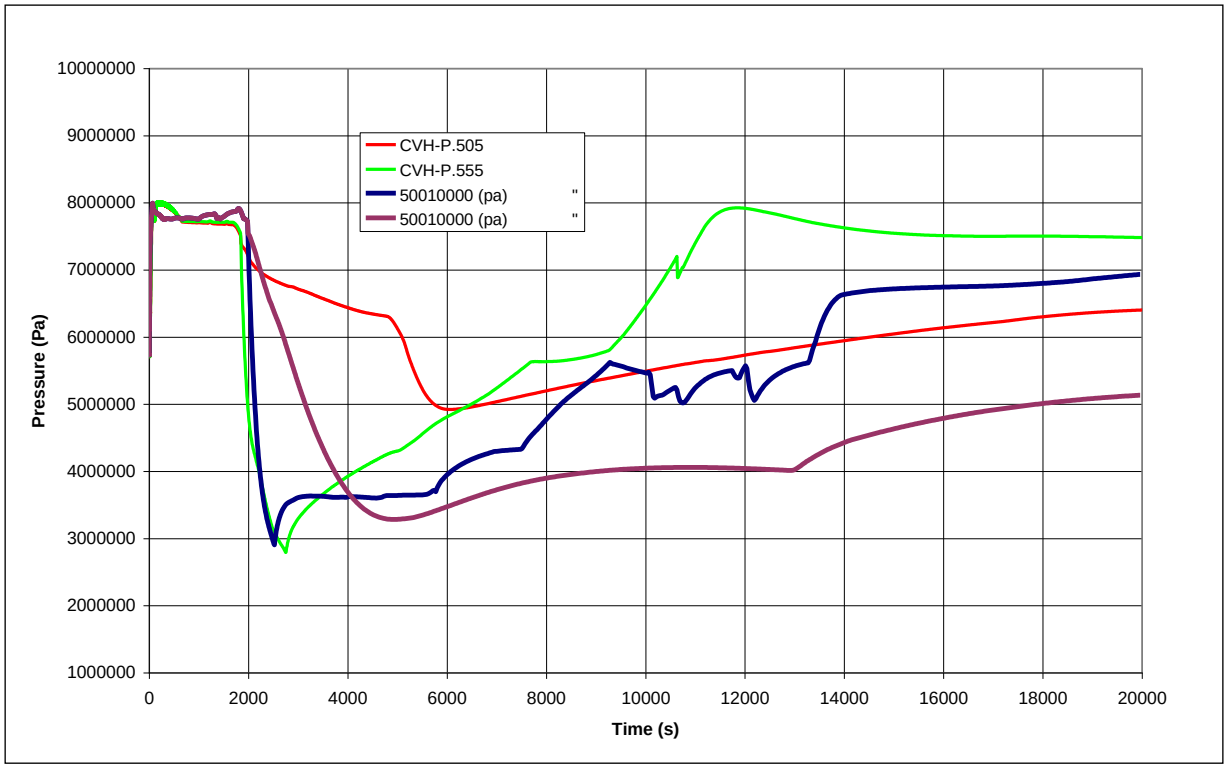

Figure 0.2 Secondary Side Pressure

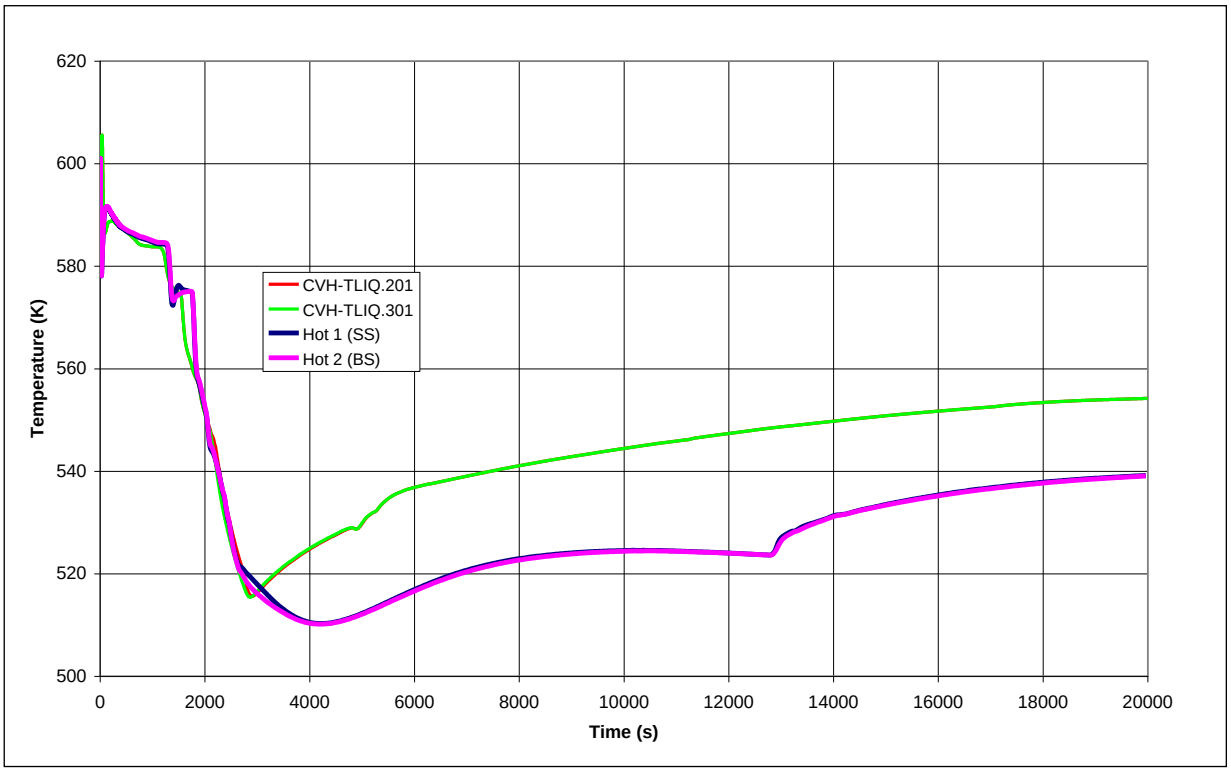

Figure 0.3 Hot-leg Temperature

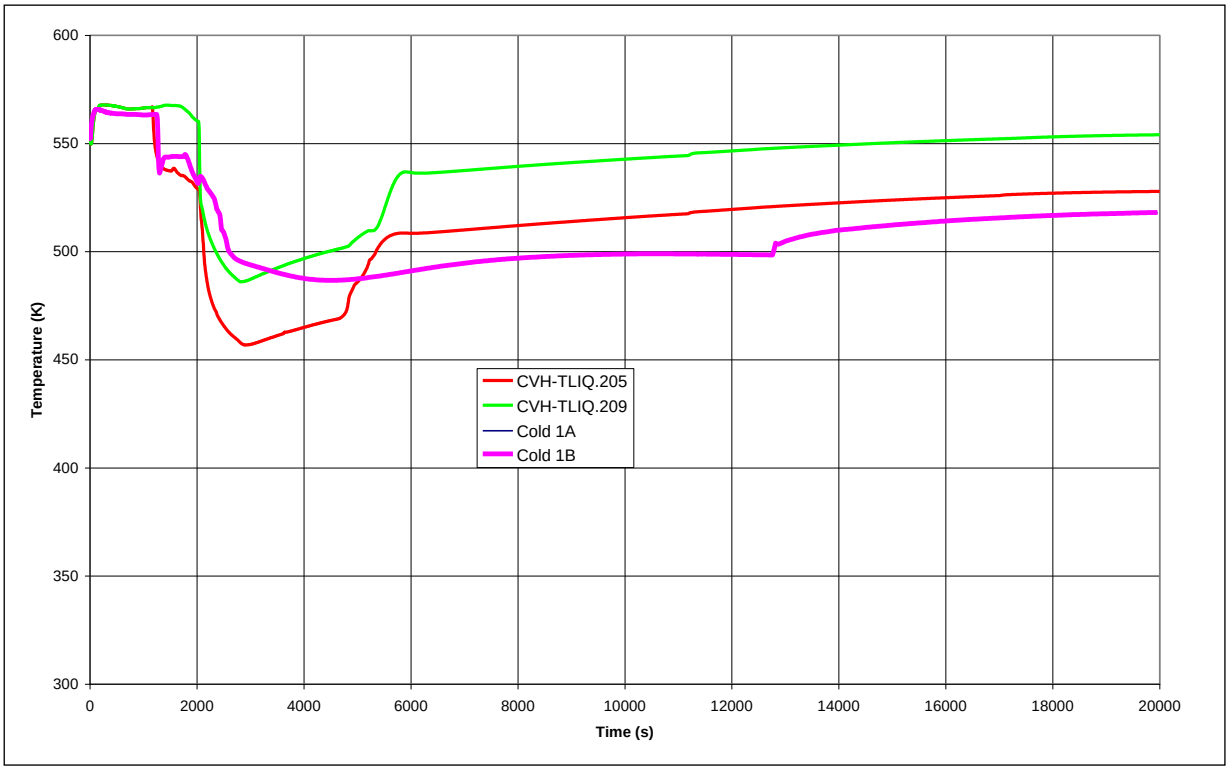

Figure 0.4 Cold-leg Intact Side Temperatures

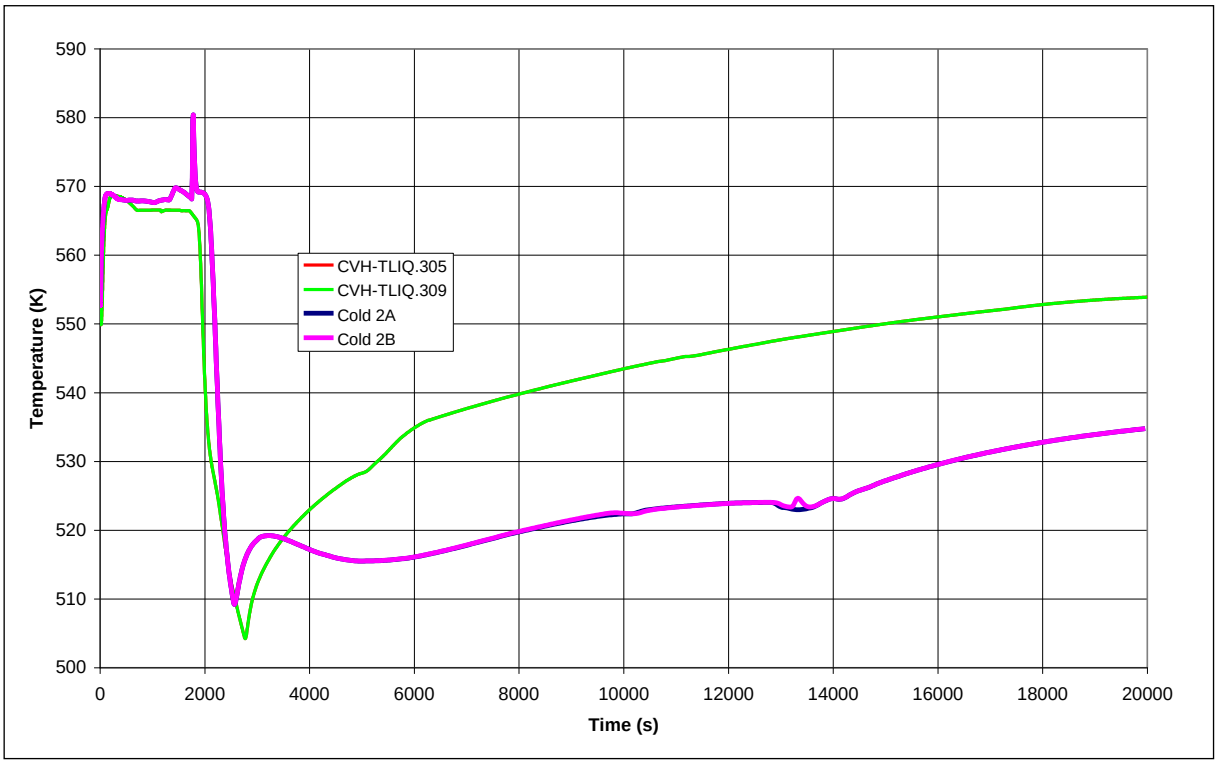

Figure 0.5 Cold-leg Break Side Temperatures

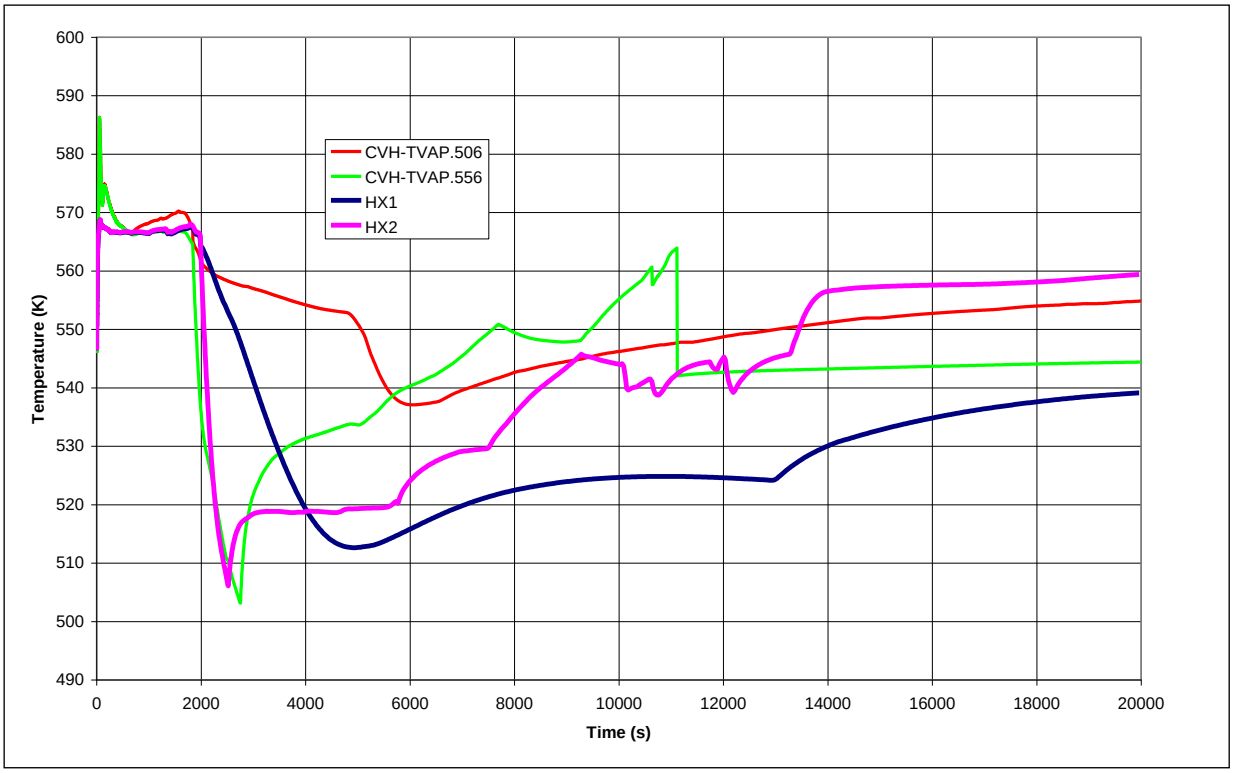

Figure 0.6 Secondary Temperatures

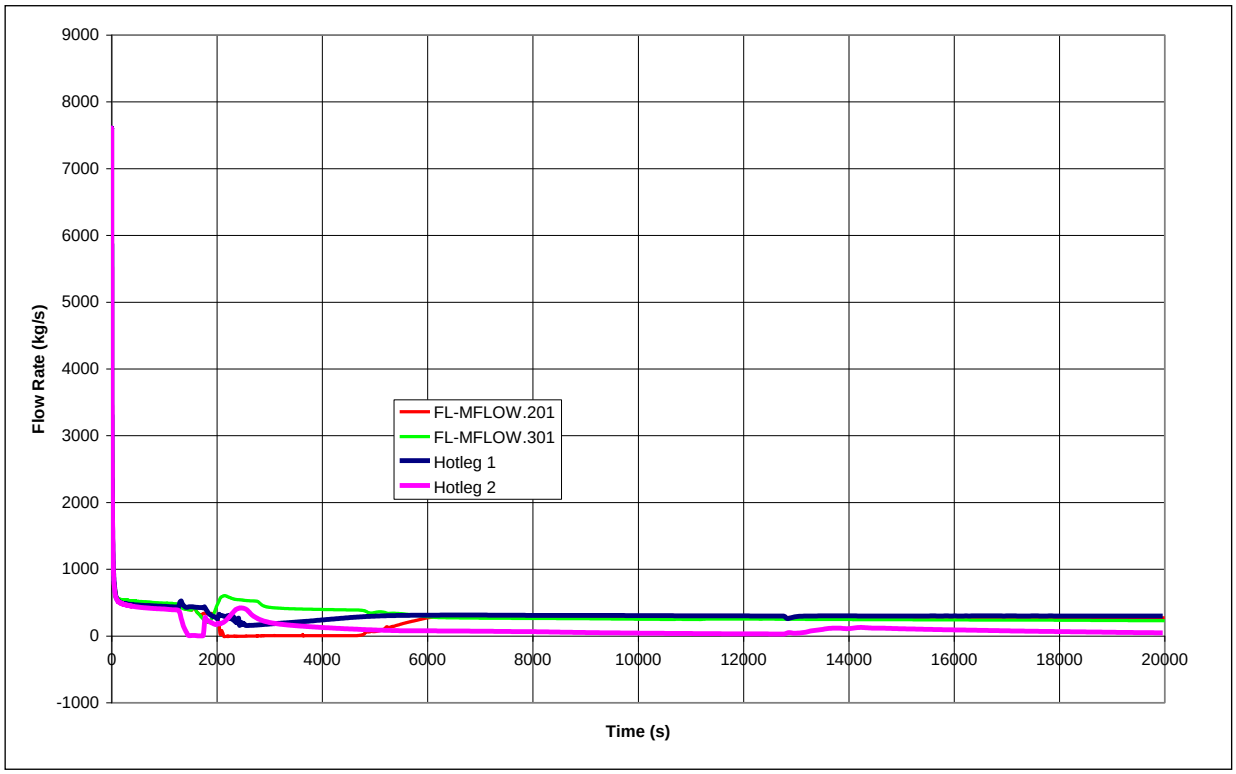

Figure 0.7 Hot-legs Flow Rates

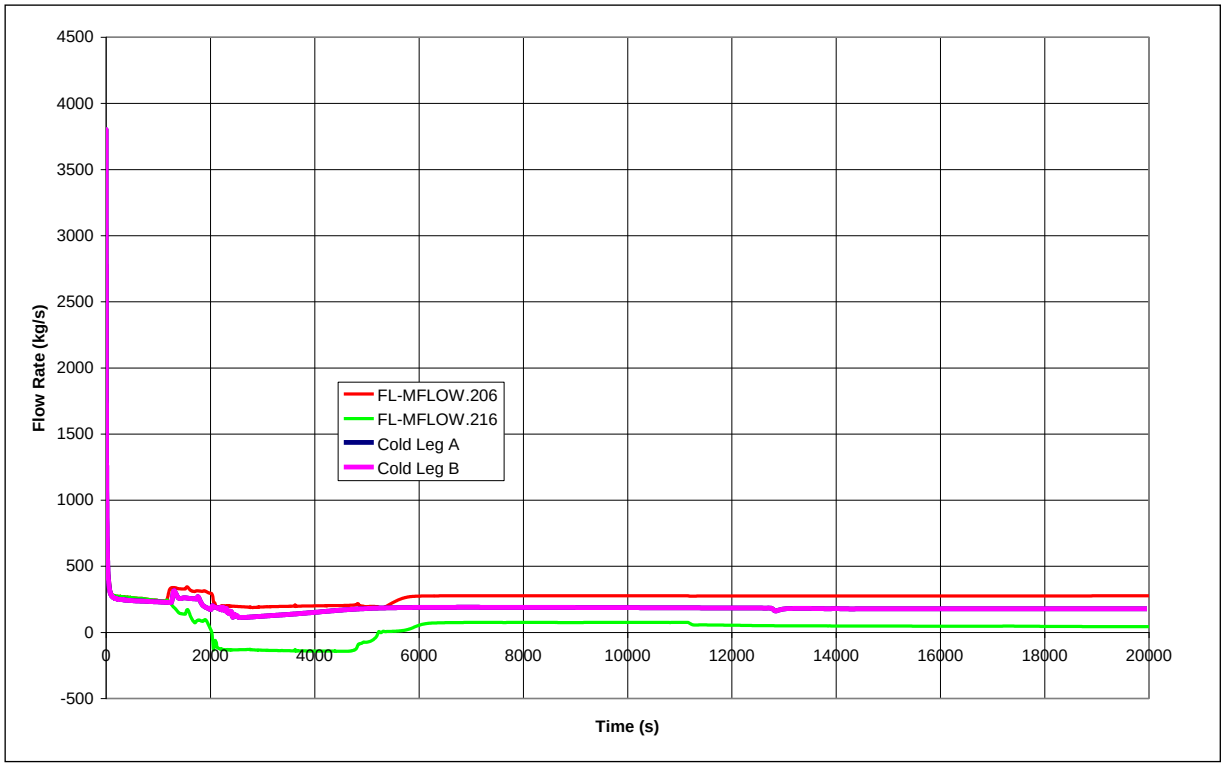

Figure 0.8 Cold-legs Intact Side Flow Rate

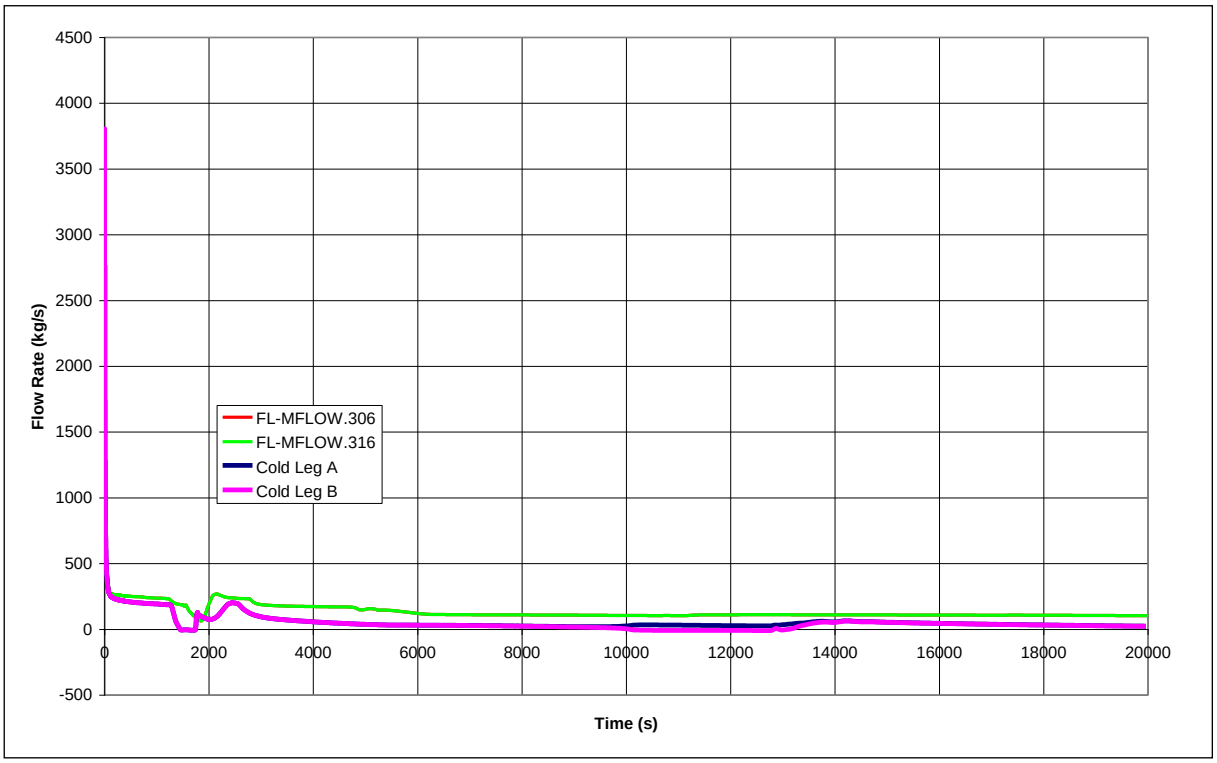

Figure 0.9 Cold-legs Break Side Flow Rates

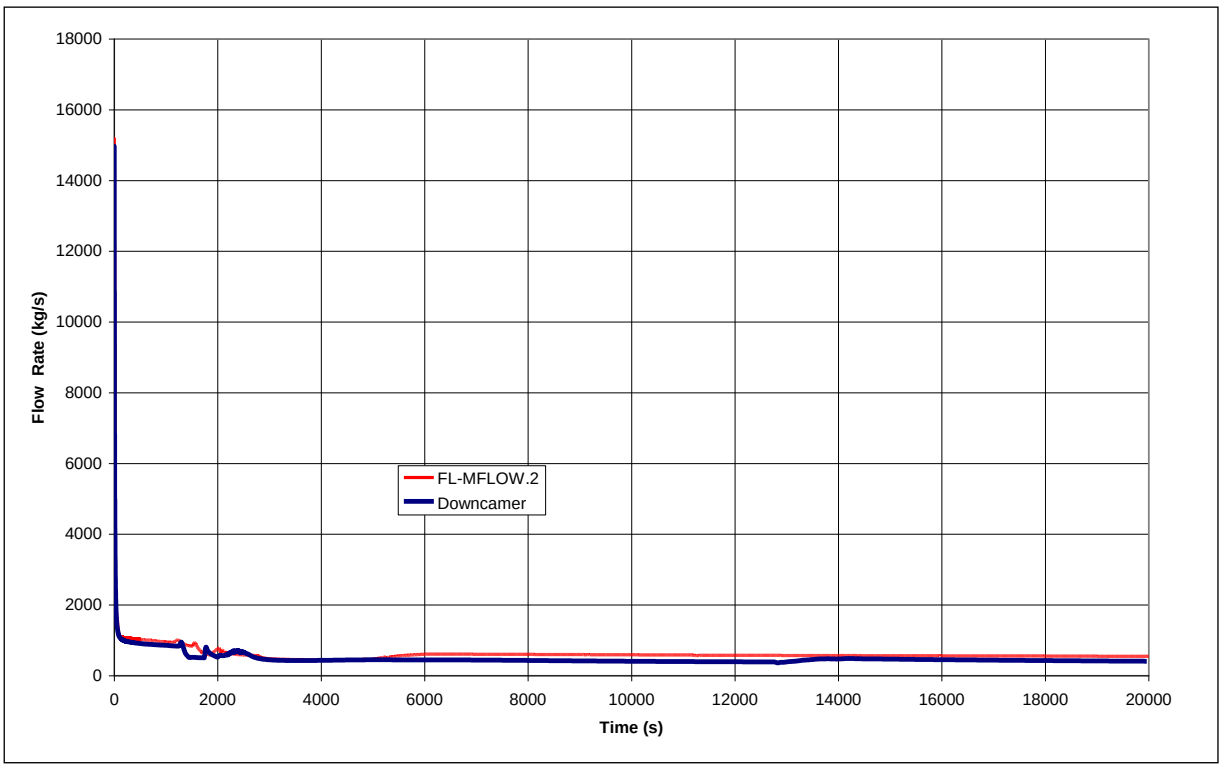

Figure 0.10 Down-comer Flow Rate

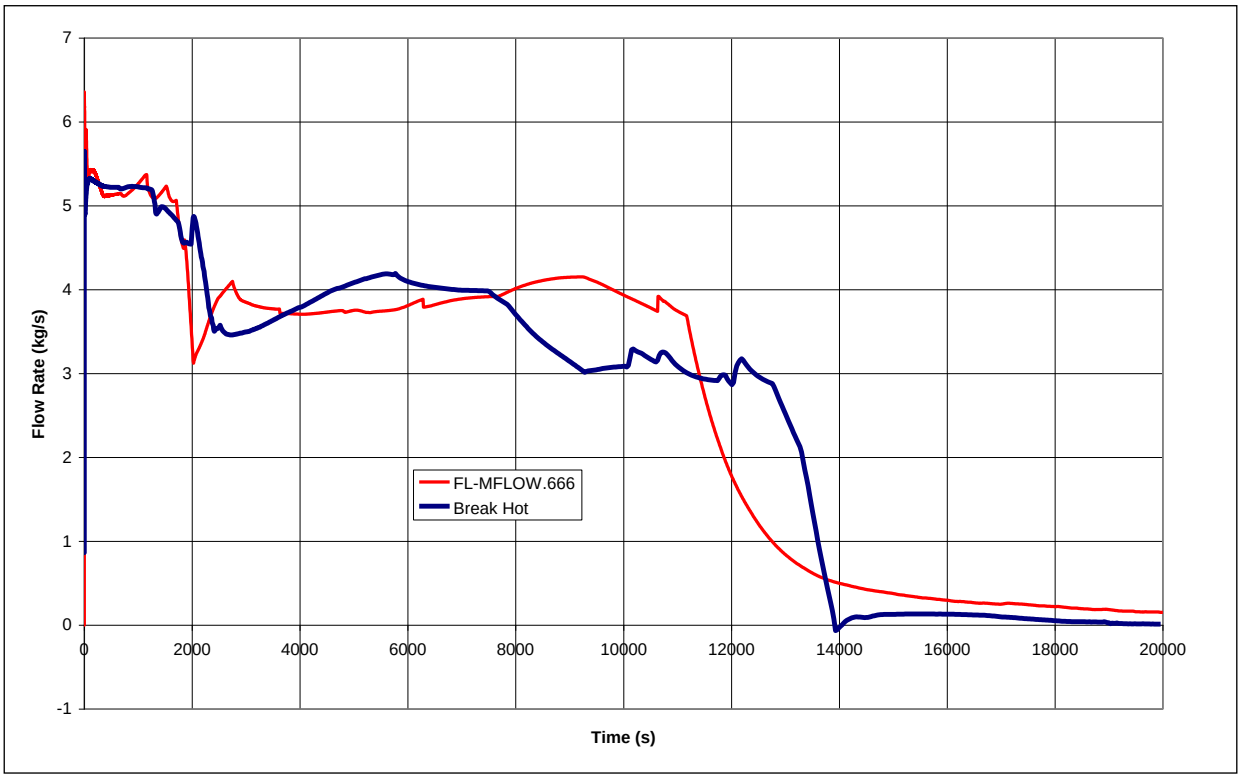

Figure 0.11 Break Hot Side Flow Rate

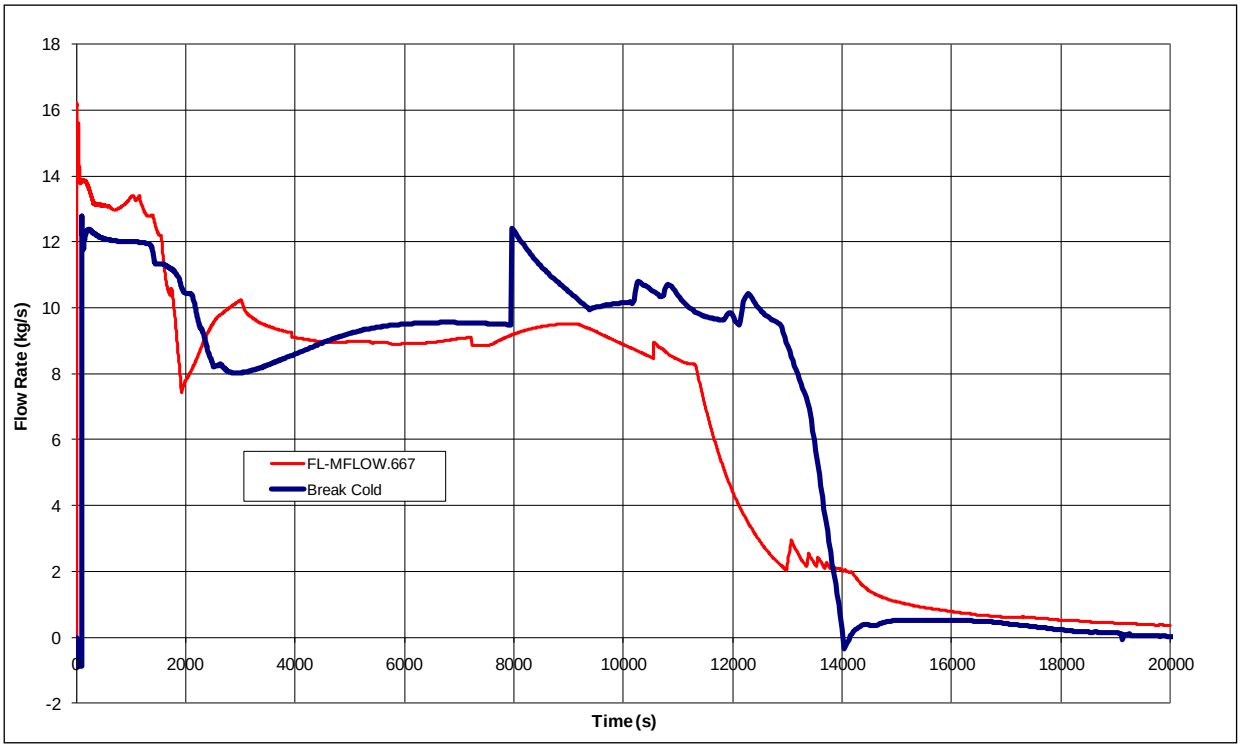

Figure 0.12 Break Cold Side Flow Rate

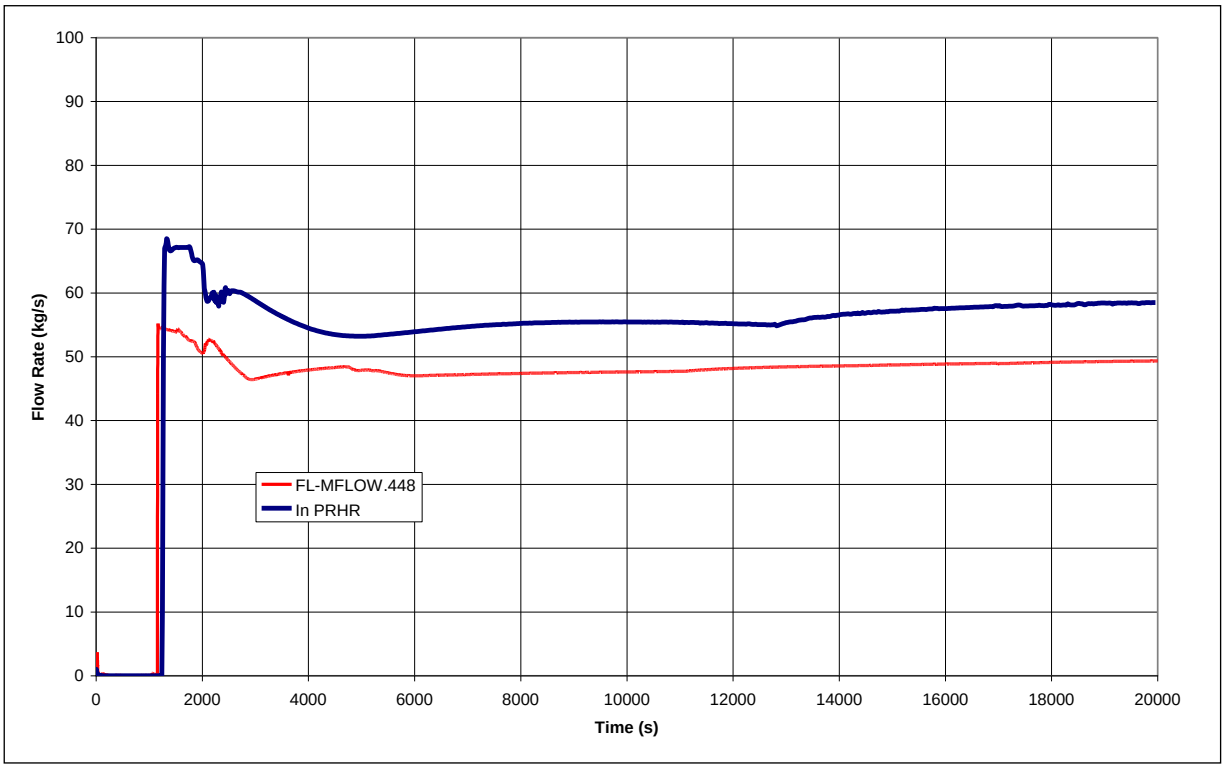

Figure 0.13 PRHR Flow Rate

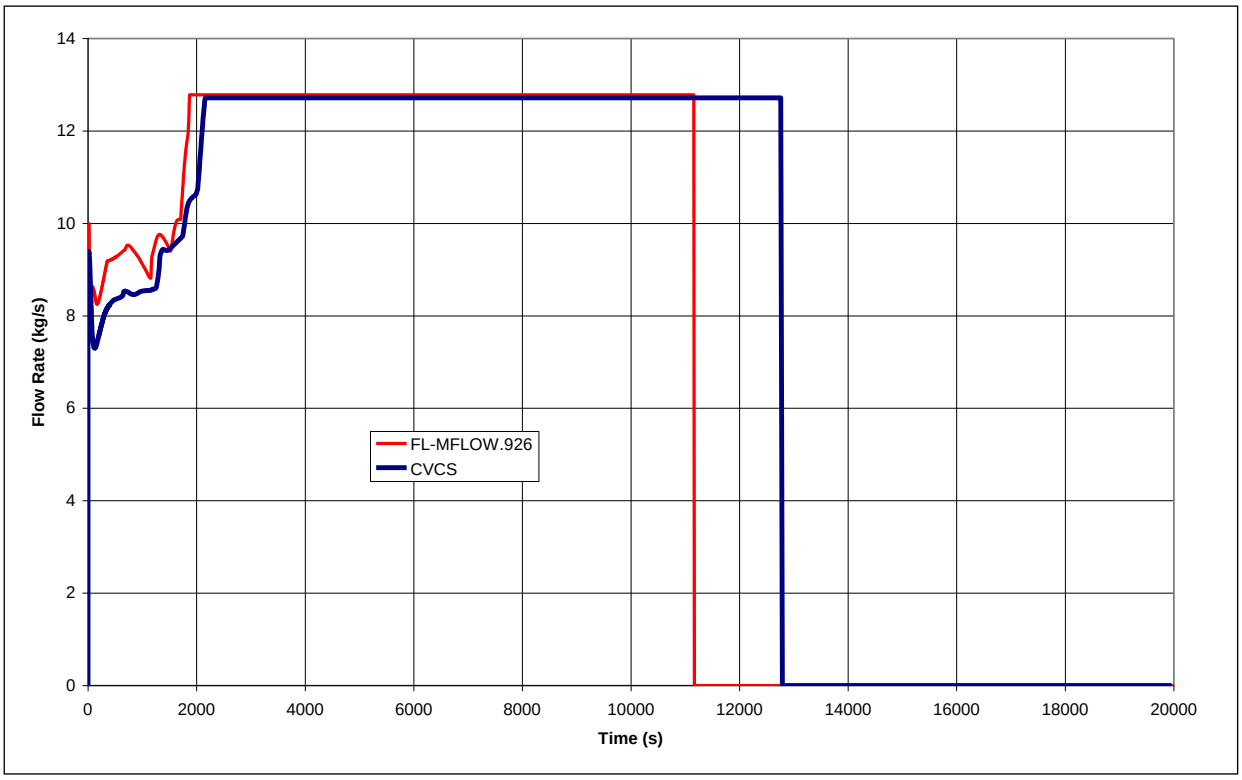

Figure 0.14 CVCS Flow Rate

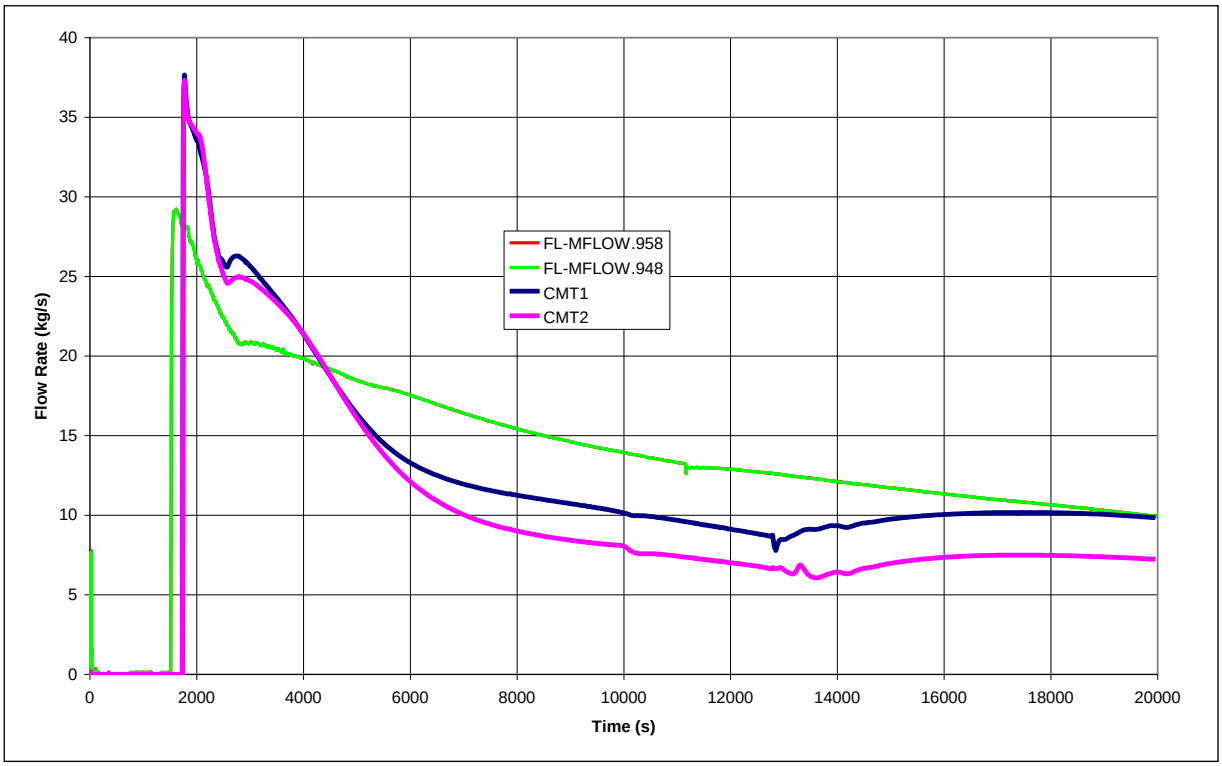

Figure 0.15 CMTs Flow Rates

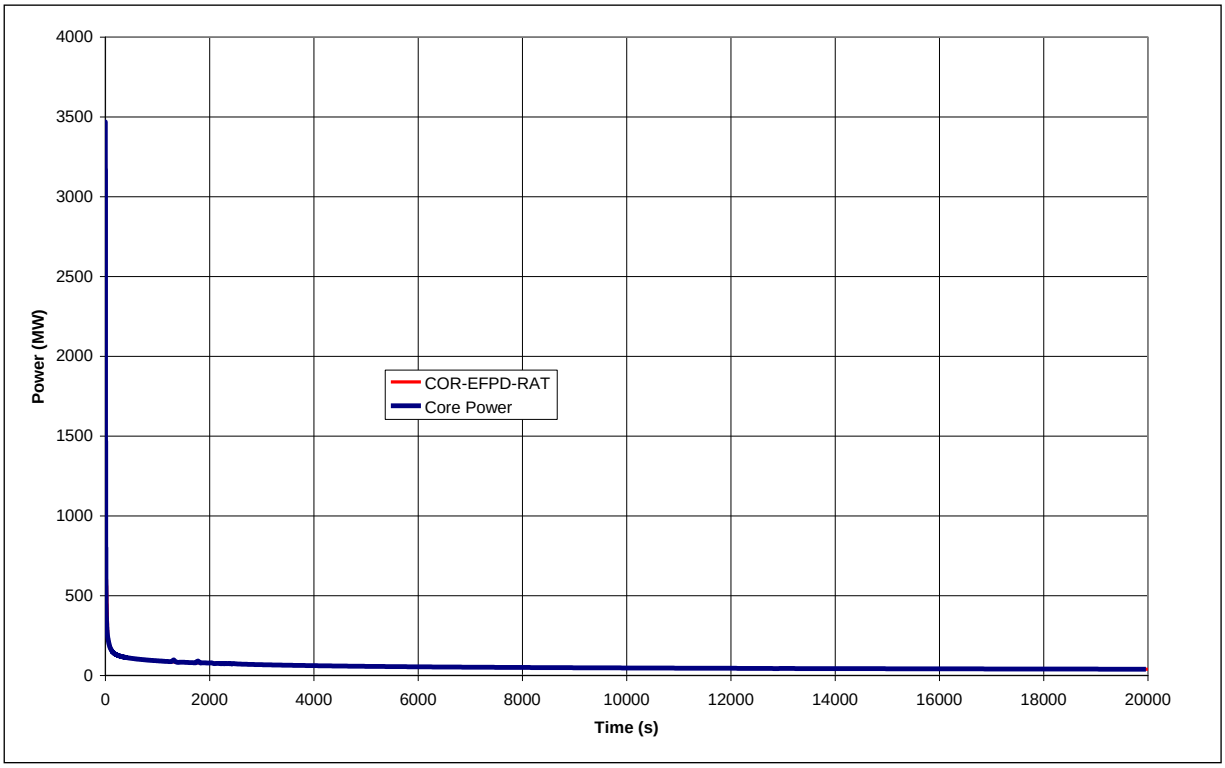

Figure 0.16 Core Power

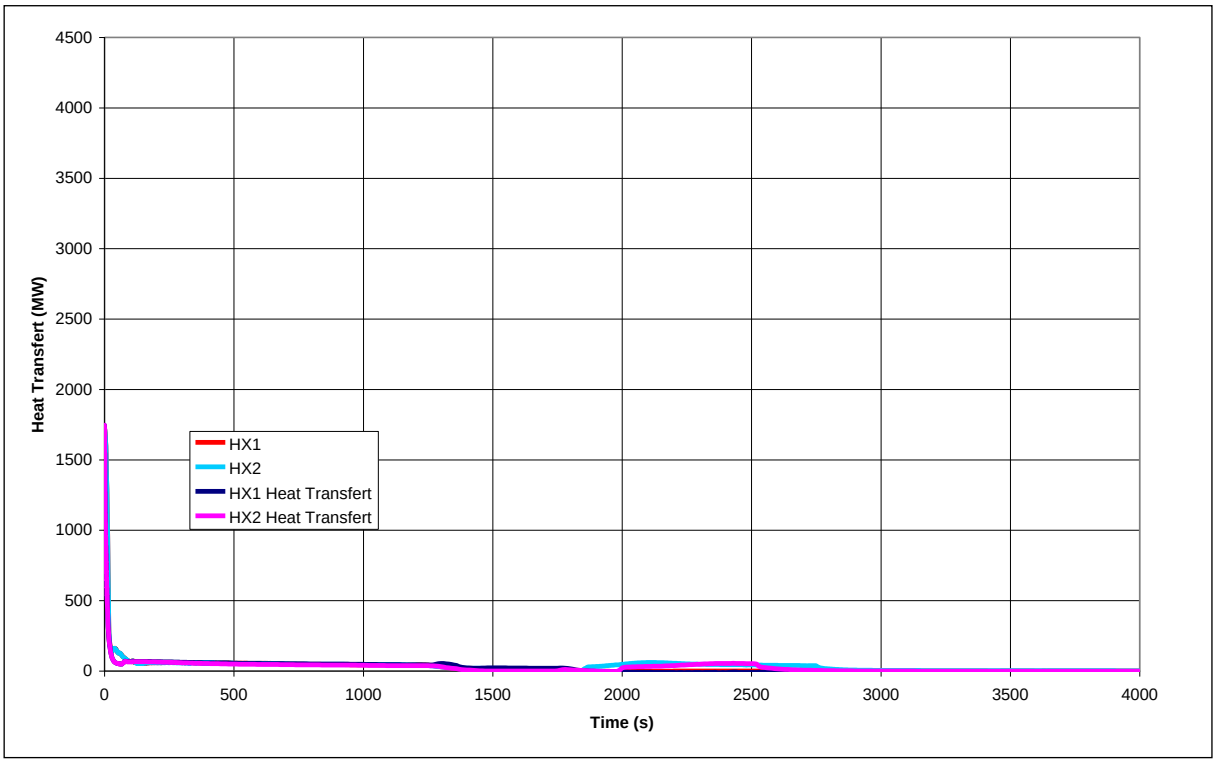

Figure 0.17 Steam Generator Heat Transfer

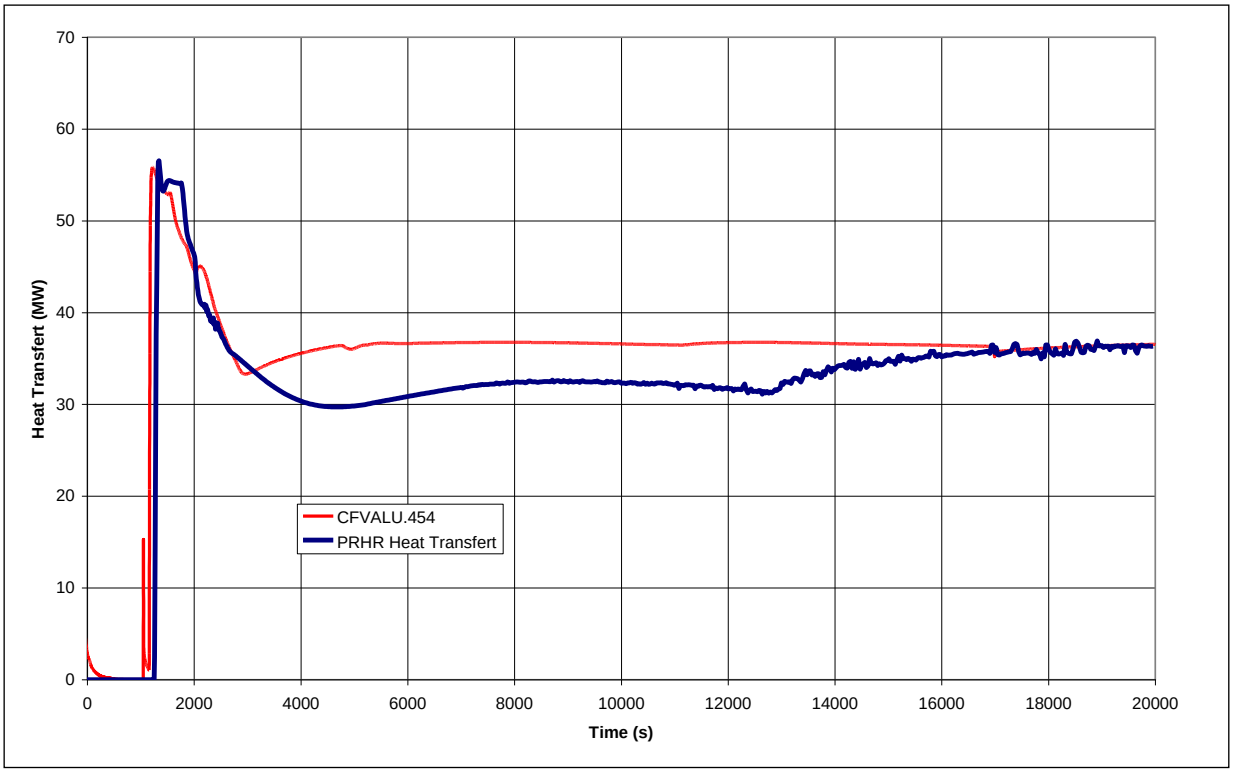

Figure 0.18 PRHR Heat Transfer

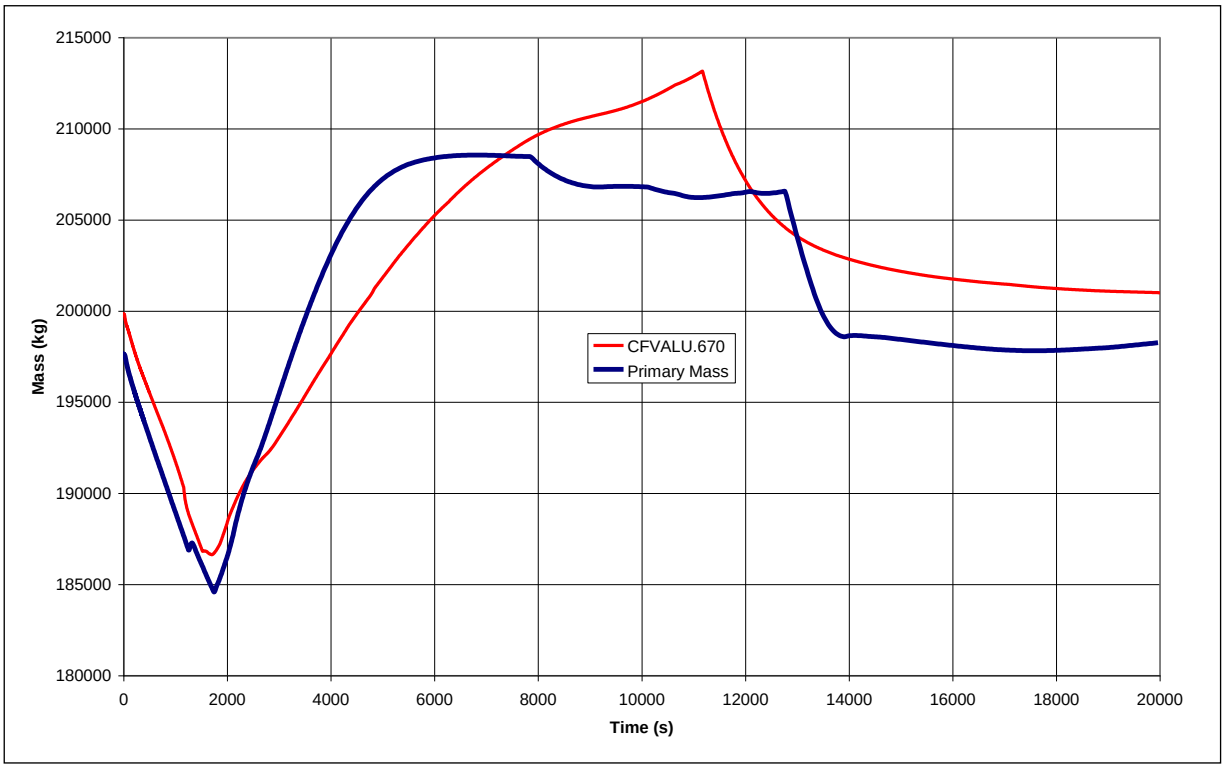

Figure 0.19 Primary Mass

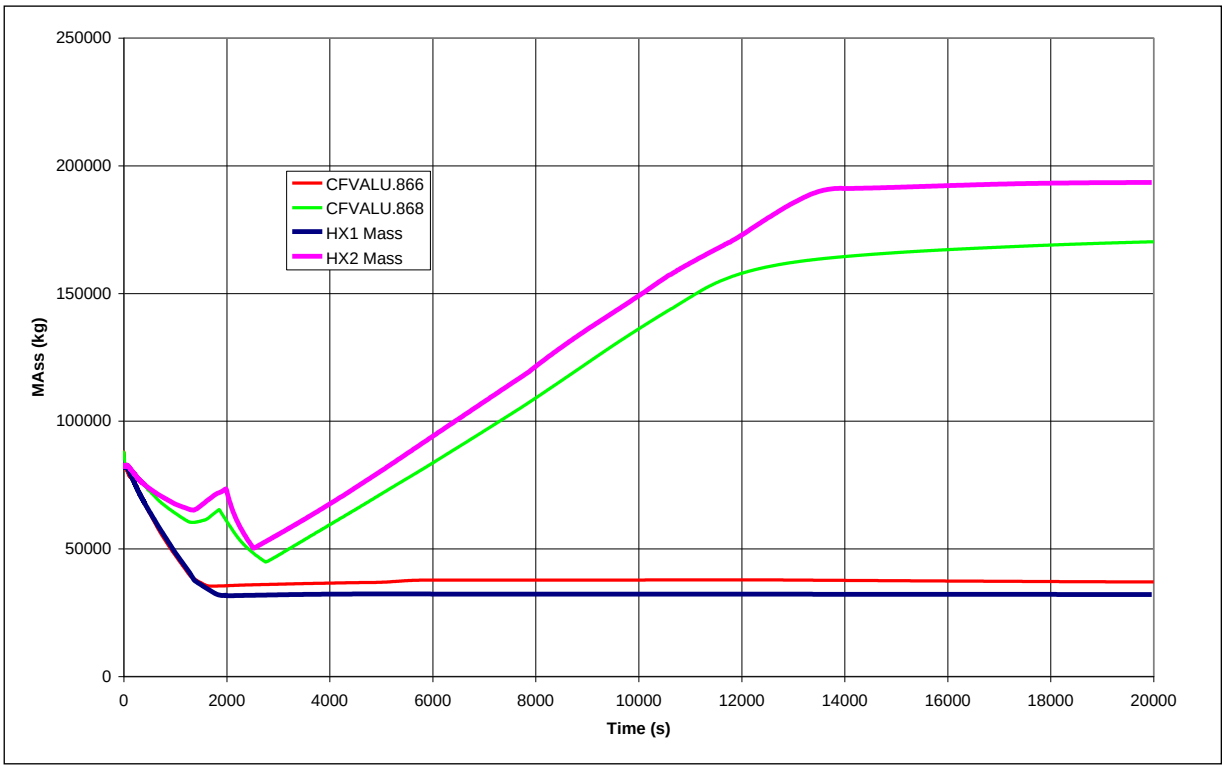

Figure 0.20 Secondary Mass